BIOHYDROGEN SYNTHESIS FROM FOOD WASTE: PROCESS DEVELOPMENT, OPTIMIZATION AND INTENSIFICATION

A Thesis Submitted in Partial Fulfilment of the Requirements for the Degree of

DOCTOR OF PHILOSOPHY

Avinash Anand

(Roll no. 206107101)

Department of Chemical Engineering
Indian Institute of Technology Guwahati
Guwahati– 781039, Assam, India

June 2025

Dedicated

to

Almighty, my Family & my mentor

INDIAN INSTITUTE OF TECHNOLOGY GUWAHATI
Department of Chemical Engineering

STATEMENT

I do hereby declare that the content embodied in this thesis titled **"*Biohydrogen Synthesis from Food Waste: Process Development, Optimization and Intensification*"** is the result of investigations carried out by me in the Department of Chemical Engineering, Indian Institute of Technology Guwahati, Guwahati, India, under the supervision of **Prof. Vijayanand Suryakant Moholkar**. In keeping with the general practice of reporting scientific observation, due acknowledgements have been made wherever the work described is based on the findings of other investigators.

Avinash Anand

June 2025 (Roll No: 206107101)

INDIAN INSTITUTE OF TECHNOLOGY GUWAHATI
Department of Chemical Engineering

SUPERVISION CERTIFICATE

This is to certify that **Mr. Avinash Anand** (Roll No.: 206107101) has conducted her doctoral thesis research under our supervision since December 2020. His thesis titled **"*Biohydrogen Synthesis from Food Waste: Process Development, Optimization and Intensification*"** is hereby submitted for the award of the Doctor of Philosophy degree. We affirm that Mr. Avinash Anand has successfully completed all requirements for the Doctor of Philosophy program as set forth by the regulations of the Indian Institute of Technology Guwahati. We further confirm that the research presented in her thesis is original and has not been submitted for a degree at any other institution.

Date:

Prof. Vijayanand S. Moholkar
(*PhD, CEng, FIChemE, FRSC*)
Professor (HAG) and Former Head,
Department of Chemical engineering,
School of Energy Science and Engineering,
Indian Institute of Technology Guwahati,
Guwahati - 781039, Assam, India.

ACKNOWLEDGEMENTS

This thesis marks the end of my cherished memories as a research scholar at IITG. It gives me immense pleasure to express my deepest gratitude to each and every one of you who made this thesis possible and constantly encouraged me during my research work.

My first and foremost appreciation goes to my supervisor, ***Prof. Vijayanand S. Moholkar***, for encouragement and relentless support throughout my research. I want to thank him for sharing his technical thoughts, which have always motivated me to progress towards new aspects. I am fortunate that he took me under his wing and considered me to work under his esteemed guidance. I have thoroughly enjoyed working with him, and I firmly believe he has brought out the best in me in every aspect. His profound knowledge has helped me to understand the mechanistic features of research work.

I want to acknowledge my sincere gratitude to my doctoral committee members, ***Prof. Kaustubha Mohanty, Prof. G. Paugazhenthi***, and ***Prof. S. Senthilkumar*** (Department of Bioscience and Bioengineering), for their insightful advice and suggestions throughout the research that led to the successful completion of the thesis.

My sincere thanks go to the Chemical Engineering Department faculty members for their continuous inspiration and valuable suggestions. I want to acknowledge ***the Department of Chemical Engineering, School of Energy Science and Engineering, Biofuel Laboratory, Param Ishan Supercomputing Facility, and Central Instruments Facilities (CIF)*** for providing various analytical facilities to conduct my research. I am also thankful to the Indian Institute of Technology Guwahati for providing me with the state of the art infrastructure for advanced research.

I am immensely thankful to my seniors, Dr. Shyamali Sarma, Dr. Kuldeep Roy, Dr. Kaustubh Chandrakant Khaire, Dr. Kajal Igntipi, Dr Bhaskarjyoti, Dr. Karan Kumar, Dr. Aradhana and research group members Pushpita, Rishiraj, Komal, Harshendra, Umesh, Arjita, Rahul, Ananya, Divyansh, Gurleen and Joyita. I am highly thankful to my friends, Chandan Mahata, Santosh Yadav, Govind Dubey, Pramod, Ajay, Pooja, Jhanki, Ramanuj, Debarshi, Prince, Shweta, for their love and support.

I want to thank my wife ***Mrs. Riya Nandi***, my son ***Tusharanshu Dutta***, my parents ***Mr. Dinesh Chandra Dutta*** & ***Mrs. Maya Devi***, my brothers ***Manish Dutta and Deepak Dutta*** and my family for showering their endless love, care, and support throughout my life. I owe my gratitude to all of them.

Last, I express my deepest gratitude to ***the Almighty God*** for blessing me and giving me the strength to complete this research work.

Avinash Anand

Abstract

This thesis has addressed the issue of the production of biohydrogen (bioH_2) from food waste. More specifically, the main objectives of the present thesis are: (1) optimization of food waste hydrolysis and its intensification using sonication, (2) mechanistic analysis of the ultrasound-induced food waste hydrolysis using molecular simulations, (3) optimization of dark fermentation of food waste hydrolysate using statistical design of experiments and artificial intelligence tools of artificial neural network coupled with genetic algorithm, and (4) intensification of dark fermentation using sonication and its metabolic flux analysis. The investigations carried out as per these objectives and the major results obtained are described in various chapters of the thesis as given below.

Chapter 1 presents a general introduction to the main theme of this dissertation, i.e. synthesis of biohydrogen from food waste using dark fermentation. **Chapter 2** presents a review and analysis of recent literature in the area of biohydrogen synthesis from various sustainable resources, including food waste hydrolysate.

Chapter 3 reports investigations in food waste hydrolysis. Initial optimization of hydrolysis parameters (Box–Behnken design) resulted in total reducing sugar yield of 263.4 mg/g biomass in 42 h. Sonication of the hydrolysis mixture at 35 kHz at 20% duty cycle yielded a 4× reduction in hydrolysis time with a 22% enhancement in TRS yield (320 mg/g biomass). Analysis of the glucoamylase enzyme's secondary structure through FTIR spectra deconvolution revealed significant changes induced by sonication. Sonication led to a reduction in α-helix and an increase in random coil content. Molecular dynamics simulations unveiled the majority of amino acid residues associated with the enzyme binding pocket in α-helix and random coil regions. Consequently, sonication widened the binding pockets, facilitating the easier transport of substrate and product. This effect translated into faster kinetics of enzymatic food waste hydrolysis.

Chapter 4 presents investigations into the optimization of the dark fermentation process from food waste hydrolysate using *Clostridium pasteurianum*. The optimization of fermentation parameters using response surface methodology (RSM) with central composite design (CCD) resulted in bioH_2 yield = 1039 mL/L (1.58 mol/mol hexose sugars) for the conditions: pH = 6.5, temperature = 36 °C, TRS concentration = 10 g/L. An artificial neural network coupled with a genetic algorithm (ANN-GA) predicted the optimum parameter set as pH = 6.7, temperature = 36.8 °C, TRS concentration = 10.85 g/L. A bioH_2 yield of 1108 mL/L (1.73

mol/mol hexose sugar) was obtained for these conditions. The modified Gompertz model revealed a maximum bioH_2 production rate of 185.34 mL/L·h for ANN-GA conditions as compared to 153.74 mL/L·h for RSM-CCD predicted conditions. Fermentation at ANN-GA-predicted conditions revealed a greater shift of metabolic intermediates towards the acetic acid/ butyric acid pathway, resulting in higher bioH_2 production. The ratio of acetic to butyric acid increased from 0.9 to 0.94, indicating a metabolic shift favoring bioH_2 production. These results demonstrate the superiority of the ANN-GA technique for simulating the behavior of a nonlinear system like the metabolic pathway of *C. pasteurianum.*

Chapter 5 presents studies in ultrasound-assisted dark fermentation of food waste hydrolysate using metabolic flux analysis (MFA). A metabolic flux model was devised to determine fluxes of intracellular metabolites using the concentrations of extracellular metabolites. This analysis revealed the effect of sonication on intracellular metabolic fluxes in test experiments. Hexose sugar uptake increased from 3.77 mmol/L·h to 5.55 mmol/L·h (~ 47% rise) with sonication, while butyrate and acetate fluxes at the acetyl-CoA node rose from 2.31 mmol/L·h to 2.5 mmol/L·h and 2.12 mmol/L·h to 4.12 mmol/L·h (i.e., a rise of ~9% and ~94%, respectively). Sonication improved bioH_2 yield by ~22%, and the acetate-to-butyrate (A/B) ratio by ~37%. These results pointed out that bioH_2 production is linked to carbon flux at the acetyl-CoA node. Higher flux towards the acetate route (than the butyrate route) enhances the hydrogen yield. A hypothetical MFA analysis was also conducted under sonication conditions for two situations, viz., complete redirection of carbon flux at acetyl-CoA node to acetate route and, secondly, doubling the uptake flux of hexose sugars. For the first case, bioH_2 enhanced from 4.13 mmol/L·h to 6.47 mmol/L·h, while for the second case, a bioH_2 flux of 14.53 mmol/L·h was predicted by the MFA model.

To summarize, the net bioH_2 yield from 1 kg of food waste under statistically optimized conditions was 5.1 g per kg of food waste, which further improved to 5.73 g per kg of food waste under sonication. In essence, this thesis has addressed three Sustainability Development Goals of the United Nations, viz., SDG 7 (Affordable and clean energy), SDG 12 (Responsible consumption and production patterns or circular economy) and SDG 13 (Climate action).

CONTENTS

LIST OF TABLES

LIST OF FIGURES

Chapter 1

Chapter 4

Chapter 5

ABBREVIATIONS

AA/AC	Acetic acid
AI	Artificial Intelligence
ANN	Artificial Neural Network
ATCC	American Type culture collection
ATP	Adenosine triphosphate
ATR	Auto thermal reforming
BA	Butyric acid
BBD	Box Behnken Design
$BioH_2$	Biohydrogen
C.	*Clostridium*
CCD	Central Composite Design
CHP	Cumulative hydrogen production
DNA	Deoxyribonucleic acid
DoE	Design of experiments
DTG	Derivative Thermogravimetry
EMP	Entner doudoroff pathway
Eq.	Equation
FADPH	Reduced form of flavin adenine dinucleotide
FW	Food Waste
GA	Genetic Algorithm
GHG	Greenhouse gas
Glc	Hexose sugar or reducing sugar
GLCM	Glucoamylase or Amyloglucosidase
HPLC	High Performance Liquid Chromatography
HRT	Hydraulic retention time
hyd	Hydrogenase
LA	Lactic acid
MD	Molecular dynamics
MFA	Metabolic Flux Analysis
MNA	Metabolic Network Analysis

MTCC	Microbial type culture collection
NAD	Nicotinamide adenine dinucleotide
NADH	Nicotinamide adenine dinucleotide
NADPH	Nicotinamide adenine dinucleotide phosphate
OVAT	One variable at a time
PDB	Protein data bank
PFL	Pyruvate formate lyase
POX	Partial oxidation
RCB	Reinforced Clostridium Broth
RCM	Reinforced Clostridium Medium
RMSD	Root Mean Square Deviation
RMSE	Root mean square error
RSM	Response Surface Methodology
SA	Succinic acid
SCO	Standard cubic metre
SDGs	Sustainable development goals
SMR	Steam methane reforming
SR	Steam reforming
TCA	Tricarboxylic acid
TFA	Trifluro acetic acid
TGA	Thermogravimetric Analysis
TRS	Total reducing sugar
UNEP	United Nations Environment Programme
US	Ultrasound
VMD	Visual Molecular Dynamics
XRD	X-ray Diffraction

NOTATIONS

%	Percentage
MJ/kg	Mega joule per kilogram
mL/g	Millilitre per gram
VSS/h	Volatile suspended solids per hour
kHz	Kilo Hertz
kJ/g	Kilo Joule per gram
mg/g	Milligram per gram
w/v	weight per volume
v/v	volume per volume
g/L	Gram per Litre
mL/L	Millilitre per litre
mmol/L/h	Millimole per litre per hour
kPa	Kilo Pascal
°C	Degree Celsius
kDa	Kilo Dalton
h	Hour
mL/min	Millilitre per minute
kJ/g	Kilojoule per gram
M	Molar
3D	Three Dimensional
°K	Degree Kelvin

CHAPTER 1

General Introduction

Declaration: This chapter of the thesis has been published online as two chapters in the book:
Carlos R. Soccol, Satunder Kaur Brar, K. Permaul, K. Pakshirajan, Julio Cesar de Carvalho (Eds.), *Biohydrogen – Advances and Processes* (Springer series: Biofuel and Biorefinery Technologies, Vol. 13), Springer Nature, 2024. Doi: 10.1007/978-3-031-49818-3
ISBN: 978-3-031-49817-6

The details of the chapters are as follows:
Anand, A., Kumar, K., Moholkar, V.S. Various Routes for Hydrogen Production and Its Utilization for Sustainable Economy. https://doi.org/10.1007/978-3-031-49818-3_20

Kumar, K., Anand, A., Moholkar, V.S. Molecular Hydrogen (H_2) Metabolism in Microbes: A Special Focus on Biohydrogen Production. https://doi.org/10.1007/978-3-031-49818-3_2

1.1 Introduction

The continuous combustion of fossil fuels in equipment like furnaces, boilers, and IC engines of vehicles and other machinery releases very harmful greenhouse gases (GHG) into the atmosphere, posing a significant threat to the global environment and resulting in climate change. Concerns about climate change and dwindling petroleum reserves are fuelling a resurgence in the search for alternatives, viz., renewable fuels. Hydrogen is one such possible substitute, and it is also regarded as the cleanest fuel, with only water as the only combustion product. It has a high energy content (or heat of combustion) of 142 MJ/kg, which is approximately 3× greater than that of the conventional hydrocarbon fuels like gasoline (46 MJ/kg) and diesel (43 MJ/kg) [1]. The main issue with using hydrogen as an alternate fuel is its scarcity in nature, as well as the necessity for low-cost manufacturing technologies. Present technologies for hydrogen production can be distinguished into two categories: conventional and renewable. The process of pyrolysis and hydrocarbon reforming is included in the first category, which is based on fossil fuels. SR (steam reforming), POX (partial oxidation), and ATR (auto thermal reforming) are the hydrocarbon-based processes used in hydrogen production [2]. Despite the fact that hydrogen produced through this route has demonstrated its capacity to be used as a clean energy resource, only a small fraction is presently used for this purpose. Most of the hydrogen has been used in the culinary, metallurgical, petrochemical, and electronics processing sectors as feedstock [3]. According to published statistics [4], roughly 49% of the hydrogen generated through hydrocarbon reforming is utilised in ammonia (NH_3) manufacture, followed by 8% in methyl alcohol (CH_3OH) production, 37% in petroleum refining, and 6% in other miscellaneous applications. H_2 storage has become the primary impediment to its use as a vehicle fuel due to the low density of hydrogen. Steam methane reforming (SMR) is the most cost-effective and widely used method for generating hydrogen from natural gas. A typical SMR hydrogen plant with a capacity of one million m^3 of hydrogen

per day is said to emit roughly 0.3-0.4 million SCO (standard cubic metres) of CO_2 into the atmosphere per day. [5]. It has been stipulated that CO_2 capture imposes approximately 25-30% additional cost to the SMR hydrogen production [3]. The technologies that manufacture hydrogen from renewable resources, such as biomass or water, fall in the second group. The technologies based on biomass as a feedstock may be split into two categories: thermochemical and biological processes [6]. Nowadays, most H_2 is produced by steam reforming natural gas [7]. Although prototype hydrogen vehicles have been developed, there is presently no extensive infrastructure for hydrogen production as a transportation fuel, and in–vehicle storage capacity remains a problem. Furthermore, hydrogen fuel cells are costly to manufacture, fragile, and have a short service life. Biohydrogen ($bioH_2$) production from carbohydrate-rich organic wastes and industrial wastewater has been recognized as one of the most encouraging and sustainable alternatives to fossil fuels, and it can also address the issue of reduction in GHG emissions. Biological methods such as direct and indirect biophotolysis, dark fermentation, and photo fermentation can all produce $bioH_2$ [8]. Among these, dark fermentation is an important method due to its higher rate of $bioH_2$ generation as well as the flexibility of the organic substrates used. However, the primary constraint of this method is the low yield of $bioH_2$ per mole of organic substrate consumed. Fermentative processes generally yield higher rates than photosynthetic hydrogen production, do not require light, use a variety of renewable sources, use less energy, and are technically much simpler and more stable, which seems to have more potential for practical applications [9]. $BioH_2$ generation from organic waste and residues has enormous potential to meet future energy needs. To date, the majority of $bioH_2$ production research has been done on a lab scale. Only a few pilot-scale research studies have been recorded, and no investigation on industrial-scale $bioH_2$ production has been reported to our knowledge [10]. The sustainability of the $bioH_2$ production process has to be accompanied by the potential for efficient scale-up at commercial levels. Despite encouraging results on lab-

scale research, significant R&D effort is required for bioH_2 production through biological routes on a commercial scale. In addition, material and energy analyses are necessary to assess the process performance.

Global warming has caused a steep rise in global temperatures in the last few years. As per the "Climate change: Global Temperature" reports, the global records for the warmest year were tracked since 1850, and 2023 was found to be the warmest of all [11,12]. The rate of warming is 0.20 °C per decade, which is more than three times faster since 1982. The reports from NASA further confirm this by stating that "Earth was about 2.45 °F (or about 1.36°C) warmer in 2023 than in the late 19th century (1850-1900) preindustrial average". This situation is particularly alarming and has raised urgent needs for protective measures to safeguard the Earth's atmosphere. The United Nations has established several Sustainable Development Goals (SDGs) focused on finding solutions to daunting issues of environmental pollution and energy security across the globe. The 17 SDGs have been shown in Fig. 1.1.

Figure 1.1: The 17 Sustainable Development Goals (SDGs) as laid down by the United Nations as part of the 2030 Agenda for Sustainable Development for peace and prosperity for people and the planet, now and into the future. (Reproduced from: https://commons.wikimedia.org/wiki/File:Sustainable_Development_Goals.png)

Hydrogen is regarded as the cleanest fuel on the basis of the combustion product of water. However, this is not actually the case, as the technique or method of bulk hydrogen production may release significant quantities of greenhouse gases. There are three potential technologies for bulk production of hydrogen to be used as transportation fuel, viz.: (1) coal gasification followed by water gas shift reaction, (2) steam reforming of methane followed by water gas shift reaction, (3) electrolysis of water. The key factor in all these technologies is the effective sequestration and storage of the CO_2, without release into the atmosphere. In order to distinguish between the above methodologies, hydrogen has been given a color code. This color code is explained as follows:

(1) **Green hydrogen:** This is produced through electrolysis of water, where electricity produced through renewable sources is utilized. This process is essentially "green" as it causes no emissions of carbon dioxide to the atmosphere. Hence, the hydrogen produced through this process is also designated green.

(2) **Blue hydrogen:** This is produced using conventional or fossil hydrocarbons as substrates (either through steam reforming or partial oxidation). The carbon dioxide produced in this process is sequestrated and stored underground.

(3) **Gray hydrogen:** This is produced from the combined process of steam methane reforming (SMR) and water gas shift reaction using natural gas as the feedstock. However, the CO_2 produced in the process is directly released to the atmosphere.

(4) **White hydrogen:** It is naturally available hydrogen in the atmosphere.

(5) **Red hydrogen:** This is produced by high-temperature catalytic cracking of water, in which the required energy is produced using nuclear power heating.

(6) **Pink hydrogen:** Pink hydrogen is essentially a product of electrolysis of water, where a nuclear power station provides the required electricity.

(7) **Purple hydrogen:** This is produced through water-splitting by chemo-thermal electrolysis using energy supplied by the nuclear power station.

(8) **Turquoise hydrogen:** This is a relatively novel technology based on thermal cracking or pyrolysis of methane. A peculiarity of this process is that it removes carbon in the form of a solid rather than CO_2.

(9) **Black or brown hydrogen:** This is the most conventional technique for hydrogen production. This is based on coal gasification to produce carbon monoxide, which is later converted to hydrogen through the water gas shift reaction. Depending on the coal utilized for gasification – either bituminous (black) or lignite (brown) – the hydrogen produced is assigned the black or brown colour. However, coal gasification produced large quantities of CO_2 (along with CO), which is released into the atmosphere. Thus, this process has the least prospects for the production of hydrogen as a clean fuel.

According to the statistics available in the literature, over 90% of hydrogen production comes from fossil energy sources: natural gas (40%), heavy oils and naphtha (30%), coal (18%), and electrolysis (4%). Hydrogen production via biomass stands at ~ 1% of the total production [13,14]. There is a growing focus on producing hydrogen from renewable sources to ensure the sustainable development of a hydrogen-based society and reduce greenhouse gas emissions. Dark fermentation is the conventional route for hydrogen production. Dark fermentation is a biological process that can occur under anaerobic conditions and uses low-cost substrates to produce hydrogen. It offers several advantages, including mild reaction conditions, high potential environmental benefits, and the utilization of readily available and inexpensive feedstocks [15]. Promoting the development and implementation of renewable hydrogen production methods like dark fermentation makes it possible to enhance sustainability and reduce the environmental impact of hydrogen as an energy resource [16]. The use of organic waste materials for dark fermentation offers the additional benefit of

effective valorization of organic waste. Hydrogen production from various sources in the present scenario is shown in Fig. 1.2 [15,17].

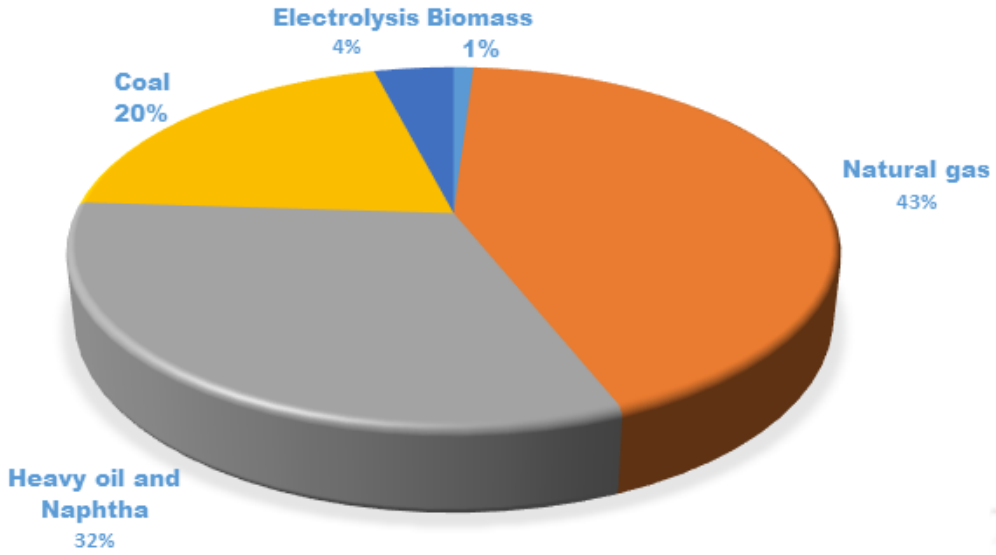

Fig. 1.2. Hydrogen (H_2) production from various sources [15]

1.2 Hydrogen production from biological processes

During bioH_2 production, some anaerobes are used as a matrix. These microbes are degrading organic waste to produce bioH_2 gas. Anaerobic photosynthetic bioH_2 production and anaerobic fermentation bioH_2 production are two types of biological hydrogen production methods. H_2-producing microbes are classified into two categories: (i) photosynthetic organisms, including cyanobacteria or green algae and photosynthetic bacteria; (ii) compatible and specific anaerobic H_2-producing bacteria, such as *Escherichia coli* (*E. coli*), Clostridial species, and *Enterobacter aerogenes*. Research on lab-scale bioH_2 production from biomass routes has given promising results, which demonstrate the potential of the sustainable hydrogen economy. Recent literature reports a number of studies on the conversion of waste to energy. Fermentative bioH_2 from various cheap feedstocks such as forest or agricultural residue [18], waste water [19], municipal solid waste [21], and food waste [18] has been reported [19]. The

amount of bioH_2 production from sucrose is influenced by various metabolites and metabolic pathways [20]. Acetic acid and butyric acid are important metabolites that are formed during bioH_2 production. Typically, one mole of glucose acetate fermentation yields 4 moles of bioH_2, while one mole of butyrate fermentation yields 2 moles of bioH_2 [21]. Transition metals like zinc (Zn), cadmium (Cd), chromium (Cr), copper (Cu), nickel (Ni), and lead (Pb) have been reported to inhibit anaerobic fermentation to produce bioH_2 [22].

There is a growing focus on producing bioH_2 from renewable sources to ensure the sustainable development of a hydrogen-based society and reduce greenhouse gas emissions. Dark fermentation is the conventional route for bioH_2 production. Dark fermentation is a biological process that can occur under anaerobic conditions and uses low-cost substrates to produce bioH_2. It offers several advantages, including mild reaction conditions, high potential environmental benefits, and the utilization of readily available and inexpensive feedstocks [15]. Promoting the development and implementation of renewable bioH_2 production methods like dark fermentation makes it possible to enhance sustainability and reduce the environmental impact of hydrogen as an energy resource [16]. Use of waste organic materials for dark fermentation offers the additional benefit of waste treatment.

Based on the synthesis route, bioH_2 generation can be classified as photo-independent (dark fermentation) and photo-dependent (photo fermentation and biophotolysis). Fig. 1.3 presents a summary of different routes for biological H_2 production. Apart from all these biological methods, we focus on bioH_2 production from microbial fermentation of organic waste. The dark fermentative method is widely used for the fermentation of organic waste. Biological H_2 production at ambient temperature and pressure is an alternative to chemical approaches. These H_2 generation techniques are more eco-friendly, require less energy, and also facilitate effective waste recycling [15]. Biological hydrogen production is categorized as photofermentation and anaerobic fermentation [23]. Hydrogen production by anaerobic

fermentation has merits over other biological processes, such as low cost, a rapid rate of cell growth, and the absence of oxygen constraint concerns. The limitations of the anaerobic approach for commercial-scale hydrogen generation are smaller productivity and yields [24], and reactor instability during large-scale operation [9,10].

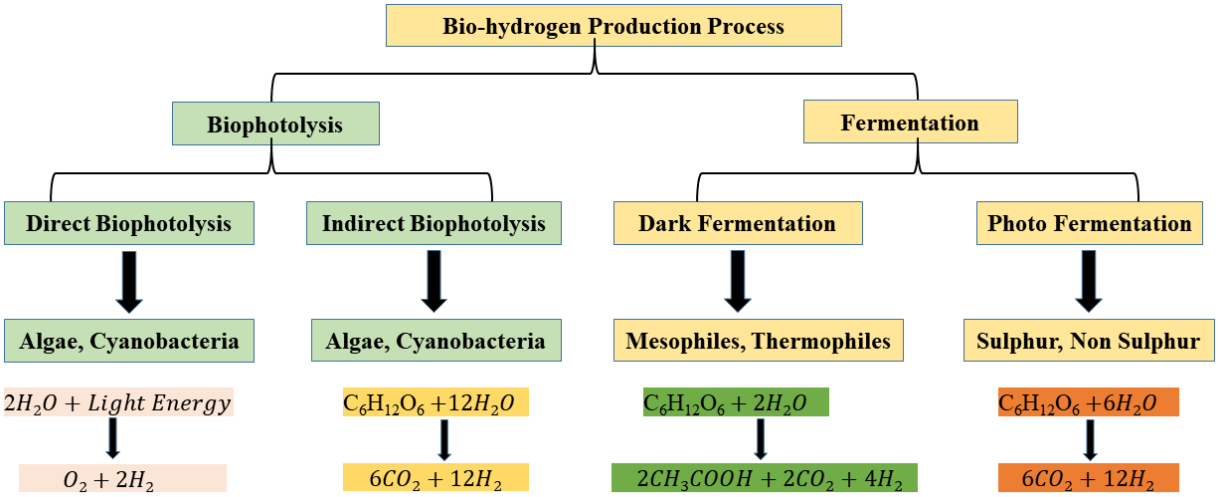

Fig. 1.3. Schematic summary of the biological hydrogen production process [25]

1.3 Biochemistry and physiology of H_2 metabolism

The atmosphere of prebiotic Earth was hydrogen-rich. Therefore, the theory regarding the existence of early biotic species that can metabolize H_2 is reasonable. This theory was first validated in the late 19th century [26]. In the year 1931, the enzyme responsible for H_2 metabolism was discovered and identified as *hyd* by two scientists, Stephenson and Stickland [27]. The key H_2 metabolising enzyme, *hyd*, catalyses the most fundamental reversible reaction, which is the reductive formation of hydrogen from protons and electrons (Eq. 1.1).

$$H_2 \leftrightharpoons [H^+ + H^-] \leftrightharpoons 2H^+ + 2e^- \quad (1.1)$$

Regardless of the simplicity of the reaction given in equation 1.1, the *hyd* enzyme has a highly complex structure and catalytic mechanism [28]. The direction of the reaction predominantly depends on the redox nature of the interacting substrates with the *hyd* enzyme.

In the availability of the electron acceptor, the *hyd* uptakes the H_2, while the availability of the electron donor makes *hyd* a H_2 producer [29]. The reaction that takes up H_2 results in the generation of protons and electrons, which are essential for the generation of ATP and reducing power. At the same time, the reactions that produce H_2 involve the reduction of protons by low oxidation electrons generated during fermentation [30]. Under cellular conditions, the H_2 oxidation is kinetically challenging but thermodynamically favourable. The generation of an ion gradient during reaction is crucial for effective enzyme catalysis [31]. Microbes tackle this problem with the help of two different classes of metal-*hyd* enzymes, viz., the [NiFe]-*hyd* and [FeFe]-*hyd*. In most microbes, the metal-hyd is responsible for H_2 consumption and generation during their life cycle [32,33]. The catalytic centre of this class of *hyd* enzymes consists of two metals, which are responsible for coordinating H_2 and catalysing its heterolytic cleavage (i.e., by increasing the acidity in the presence of the base) into a $H^+ and\ H^-$ anion. The H^+ is released and accepted by a base present in the catalytic center and is successively transferred to the aqueous exterior through a series of amino acids present in the structure of the *hyd* enzyme. The fate of the hydride anion is, however, different from that of the proton. The H^-consists of $2e^-$ that are relayed through the [FeS] cluster to the downstream acceptor of the chain (e.g., cytochromes), and the resultant H^+ is also released from the catalytic site of the enzyme. Several *hyd* during this reversible catalytic mechanism reduce the H^+ to molecular H_2. The ultimate direction of *the hyd* catalysed reaction is governed by the intrinsic redox potential of the interacting molecules with *hyd*. Three techniques have been utilized to study the biochemical and structural features of *hyd*, viz., crystallography, biochemical, molecular, or genetic. During the second half of the 20th century, multiple types of *hyd* enzymes were isolated, purified, and characterized. With the emergence of recombinant DNA technology in the late 20th century, the process of *hyd* classification on the basis of its genome sequence prevailed, which streamlined numerous studies on identifying features of *hyd* enzymes. The

understanding of genome sequences in the late 20th century paved the way for a structural engineering approach for *hyd* and associated genes for their maturation in cells. During the 1990s, Higuchi et al. [34] were able to develop the first crystal structure of [NiFe]-*hyd* isolated from *Desulfovibrio vulgaris* (*D. vulgaris*). Out of the prevalently found *hyd* enzymes, viz. [NiFe] and [FeFe], the double iron *hyd* is known to be present exclusively in a few green algae, facultative and obligate anaerobic bacteria. Though up till now [FeFe] type *hyd* has not been identified in Archaea, they are present in lower eukaryotes such as green algae and protozoa. In eukaryotes, they have been found in their subcellular organelles, e.g., chloroplasts of green algae and hydrogenosomes of protozoa. Initially, the classification of *hyd* was made based on the presence of specific electron donors and acceptors in their core catalytic sites, viz., coenzyme F_{420} (EC1.12.99.1), NAD (*hyd* of EC 1.12.1.12), ferredoxins (EC 1.18.99.1), or cytochromes (EC 1.12.2.1). As discussed above, the major *hyd* found in nature are iron-sulphur enzymes consisting of either two Fe atoms (in case of [FeFe]-*hyd* class) or a Ni atom and an Fe atom (in case of [NiFe]-*hyd* class). Apart from these, scientists have also discovered a third type of *hyd* in a few bacteria capable of gas fermentation, e.g., methanogens. The principle of this *hyd* is similar to H_2-producing bacteria commonly known as methylene-tetra-hydromethanopterin dehydrogenase (Hmd, EC 1.12.99.4). The Hmd class does not contain any metal apart from the Fe-S cluster. Therefore, it is also called iron-sulphur-cluster-free *hyd* or [Fe]-*hyd* (previously known as "metal-free dehydrogenase").

1.3.1 Enzymes essential for H_2 metabolism

Presently, the sequences of altogether more than 650 *hyd* enzymes are available in the protein database [35,36]. It is well observed that despite *hyd* are conspicuously diverse in many respects (e.g., size, electron donors and acceptors, quaternary structure), they consist of three phylogenetically distinct classes, the [NiFe], the [FeFe]-, and the [Fe]-*hyd*s, each characterized by a distinctive functional core that is conserved within each class [37–39]. The functional core consists of the subunits or domains that accommodate the catalytic site, which are minimally required for structure and function [40]. Metal content and sequence similarity are thus reliable classification criteria. Since, the presence of [Fe]-*hyd* or Hmd [38] are only restricted to some methane metabolising microbes (*aka*., methanogens), we have not adequately discussed their phylogenetic relationships, and therefore, only the *hyd* from [FeFe]- and [NiFe]- family are discussed in this chapter. Fig.1.4 shows a schematic representation of the classification, source, and role of the hydrogenase enzyme commonly found in microbes. As per the KEGG database, Table 1.1 represents the involvement of molecular hydrogen in chemical reactions existing in nature.

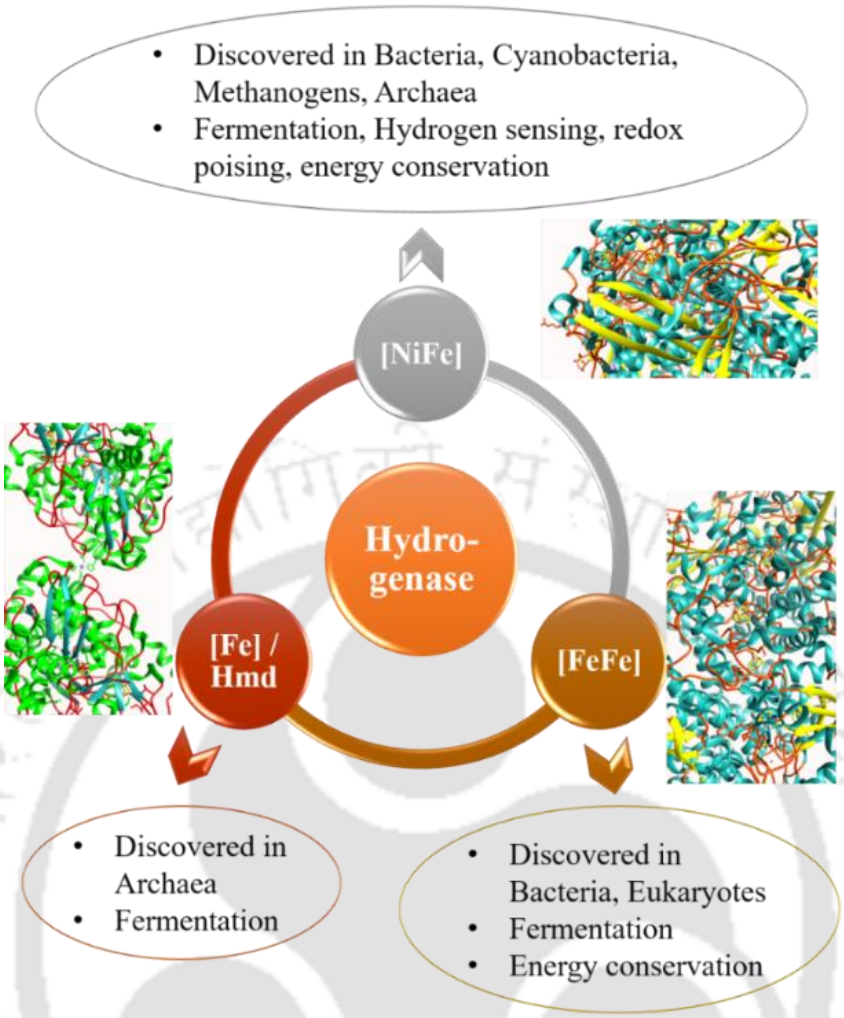

Fig. 1.4: Schematic representation of classification, source, and role of the hydrogenase enzyme commonly found in microbes

.

Table 1.1 Involvement of molecular hydrogen in chemical reactions existing in nature (as per KEGG database)

Reaction name	Reaction ID	Enzyme ID	Chemical equation
Hydrogen: ferredoxin oxidoreductase	R00019	EC 1.12.7.2	2 Reduced ferredoxin + 2 H^+ <==> H_2 + 2 Oxidized ferredoxin
Reduced ferredoxin: dinitrogen oxidoreductase	R00067	EC 1.18.6.1	2 e^- + 2 H^+ <==> H_2
Hydrogen: NAD^+ oxidoreductase	R00700	EC 1.12.1.2; EC 1.12.1.5	H_2 + NAD^+ <==> NADH + H^+
Hydrogen: quinone oxidoreductase	R02965	EC 1.12.5.1	Menaquinone + H_2 <==> Menaquinol
Hydrogen: coenzyme F_{420} oxidoreductase	R03025	EC 1.12.98.1	Coenzyme F420 + H_2 <==> Reduced coenzyme F_{420}
Hydrogen: ferricytochrome-c3 oxidoreductase	R04015	EC 1.12.2.1	2 Ferricytochrome c3 + H_2 <==> 2 Ferrocytochrome c3 + 2 H^+
Hydrogen : N5, N10-methenyltetraydro-methanopterin oxidoreductase	R04455	EC 1.12.98.2	5,10-Methenyltetrahydromethanopterin + H_2 <==> 5,10-Methylenetetrahydromethanopterin + H^+
Reduced ferredoxin: dinitrogen oxidoreductase (ATP-hydrolysing)	R05185	EC 1.18.6.1	16 ATP + N_2 + 8 Reduced ferredoxin + 8 H^+ + 16 H_2O <=> 16 Orthophosphate + 16 ADP + 8 Oxidized ferredoxin + 2 NH_3 + H_2
Reduced flavodoxin: dinitrogen oxidoreductase (ATP-hydrolysing)	R05186	EC 1.19.6.1	16 ATP + N_2 + 4 Reduced flavodoxin + 16 H_2O <==> 16 Orthophosphate + 16 ADP + 4 Oxidized flavodoxin + 2 NH_3 + H_2

Table 1.1 (*continued*…….)

Reaction name	Reaction ID	Enzyme ID	Chemical equation
Hydrogen: $NADP^+$ oxidoreductase	R07181	EC 1.12.1.3; EC 1.12.1.5	H_2 + NADP+ <==> NADPH + H^+
Hydrogen : (acceptor) oxidoreductase	R07182	EC 1.12.99.6	H_2 + Acceptor <==> Reduced acceptor
Hydrogen : 2-(2,3-dihydropentaprenyloxy) phenazine oxidoreductase	R09095	EC 1.12.98.3	Methanophenazine + H_2 <==> Dihydromethanophenazine
Ferredoxin oxidoreductase	R09508	EC 1.12.1.4	2 H_2 + NAD^+ + 2 Oxidized ferredoxin <=> 5 H^+ + NADH + 2 Reduced ferredoxin
H_2: polysulfide oxidoreductase	R10390	EC 1.12.98.4	H_2 + Polysulfide(n) <==> H_2S + Polysulfide(n-1)
Ferredoxin : H_2 oxidoreductase	R11943	EC 1.8.98.5	Coenzyme B + Coenzyme M + 2 Reduced ferredoxin + 2 H^+ <=> Coenzyme M 7-mercapto-heptanoylthreonine-phosphate heterodisulfide + 2 Oxidized ferredoxin + 2 H_2
Ferredoxin : dinitrogen oxidoreductase	R12084	EC 1.18.6.2	12 Reduced ferredoxin + 12 H^+ + N_2 + 40 ATP + 40 H_2O <=> 12 Oxidized ferredoxin + 3 H_2 + 2 NH_3 + 40 ADP + 40 Orthophosphate
CO_2 + Hydrogen <=> formate	R12754	EC 1.17.98.-	CO_2 + H_2 <=> Formate

[Fe]-*hyd* or Hmd: The very first Hmd enzyme was discovered in *Methanothermobacter marburgensis*, which has been studied extensively among the *hyd* of this type [13,41]. Hmd catalyzes the reversible reduction of methenyltetrahydromethanopterin (methenyl-H_4MPT^+) with H_2 to methylene-H_4MPT and H^+, which is an intermediate step in CO_2 reduction with H_2 to methane [42–44]. The function of these enzymes is essentially limited to the presence of nickel under growth conditions. Otherwise, the F_{420}-reducing [NiFe]-*hyd* will no longer be synthesized. [Fe]-*hyd* is comprised of the two identical subunits of 38 kDa, which is encoded by a monocistronic gene, and consists of two iron atoms per homodimer without an iron-sulfur cluster [29,38,45]. The presence of this enzyme has been marked in a dozen species from the methanogenic microbial family. Initially, it was wrongly thought that Hmd functions as a pure organic catalyst, but it has now been found that its catalytic activity heavily depends on a cofactor containing iron in its core [28,38]. The crystal structure of Hmd apoenzyme has been recently published and is available in protein databases [36,46]. In summary, the [Fe]-*hyd* is very different from the other two types of *hyd*, viz. [FeFe]- and [NiFe]-*hyd* not only on the basis of their structures, but also on the grounds of their catalytic mechanism [38,39,41,45]. The iron, which is required for enzyme activity in [Fe]-*hyd*, is not redox active. Therefore, their catalytic properties are different from those of the other two *hyd* of the [NiFe]- and [FeFe]-classes; hence, Hmd enzymes do not catalyze the reversible H_2 production reaction:

$$2H^+ + 2e^- \leftrightarrow H_2 \qquad (1.2)$$

The three-dimensional structures of Hmd or only [Fe]-*hydrogenase* from *Desulfovibrio vulgaris* (PDB ID: 1HFE) are given in Fig. 1.5. The binding mode and interactions of catalytic amino acid residues with ligands, cofactors, and ions bounds with the crystal structure of 1HFE are shown in Fig. 1.5 (b), (c).

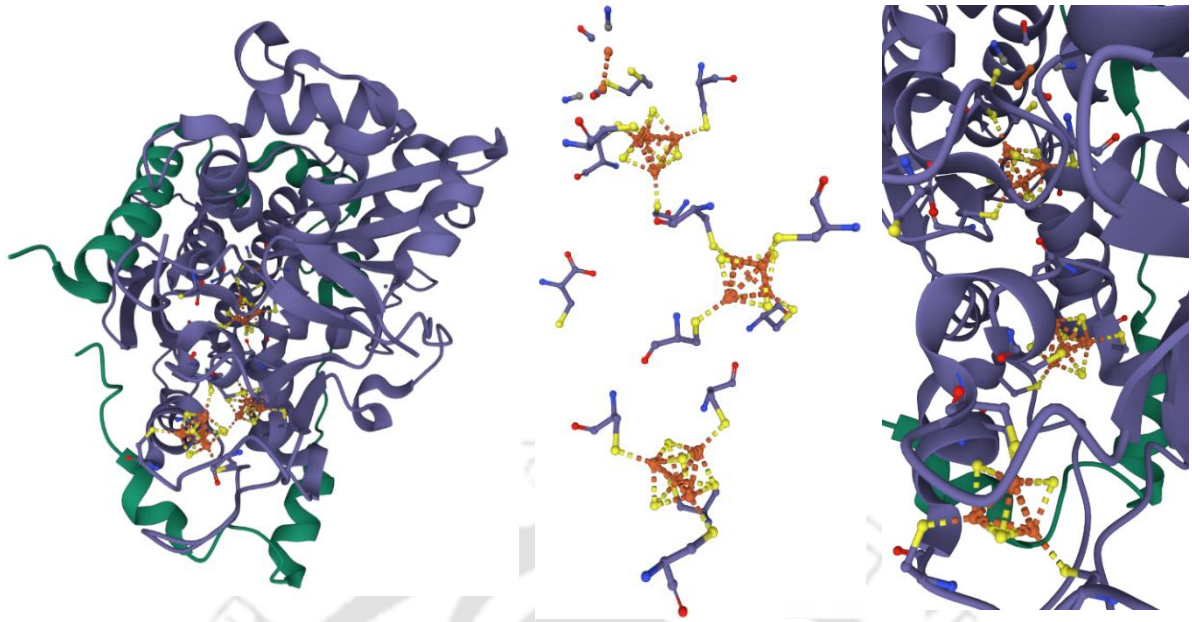

(a) (b) (c)

Fig. 1.5: 3-dimensional (3D) structures of [Fe]-hydrogenase from *Desulfovibrio vulgaris* (PDB ID: 1HFE). (a) Complete 3D structure of 1HFE visualized in Chimera, (b) interaction of active site amino acid residue with all types of ligands present in 1HFE without showing polymer chain, and (c) interaction of active site amino acid residue with ligand present in 1HFE with polymer chain.

[NiFe]-*hyd*: The *hyd* enzymes of this class are most abundant and extensively studied among all types of *hyd* enzymes from the bacterial domain [47]. The core [NiFe]-*hyd* is composed of an $\alpha\beta$ heterodimer with the α-subunit of 60 kDa (larger subunit) holding the bimetallic active site, and the β-subunit (smaller subunit) of 30 kDa holding the iron-sulfur clusters (Fig. 1.6a). Interesting point to note is that the size of the α- and β-subunits is smaller in multimeric *hyd*. Much has been understood regarding the general fold and the nature of the binuclear NiFe active site with the availability of crystal structures of *hyd* from *Desulfovibrio* [31,48]. The crystal structure of [NiFe]-*hyd* from *Desulfovibrio desulfuricans* ATCC 27774 (PDB ID: 1E3D) has revealed that the two subunits interact extensively via a huge contact surface, which folds into a globular heterodimer (shown in Fig. 1.6a). The catalytic centre (bimetallic nickel-iron) is profoundly buried in the larger subunit and is coordinated to the *hyd* by four cysteine

amino acid residues. The FTIR analysis suggested the presence of three non-proteinous docked ligands, one CO and three CN^-, bound to the Fe atom or SO, CO and CN^-. The FTIR and EPR properties revealed the presence of two additional CN^- ligands, with one CN^- attached to nickel, so that the structure of the active site may be $Ni(CN)Fe(CN)_3(CO)$ of the cytoplasmic NAD-reducing *hyd* of *Ralstonia eutropha* (formerly *Alcaligenes eutrophus* now renamed *Cupriavidus necator*). The β-subunit consists of up to three cubane iron-sulfur clusters of the [4Fe-4S] type arranged linearly. This conducts electrons between the H_2-activating center and the physiological electron acceptor (or donor) of *hyd*. It has been discovered in the crystal structure of *D. desulfuricans* ATCC 27774 [NiFe]-*hyd* (PDB ID: 1E3D) that the [4Fe-4S] cluster is nearest to the bimetallic center. This bimetallic center has been modified by the loss of one S atom and the inclusion of three O_2 atoms [4Fe-3S-3O]. Fig. 1.6 represents the 3-dimensional (3D) structures of [NiFe]-hydrogenase of *Desulfovibrio desulfuricans* ATCC 27774 (PDB ID: 1E3D).

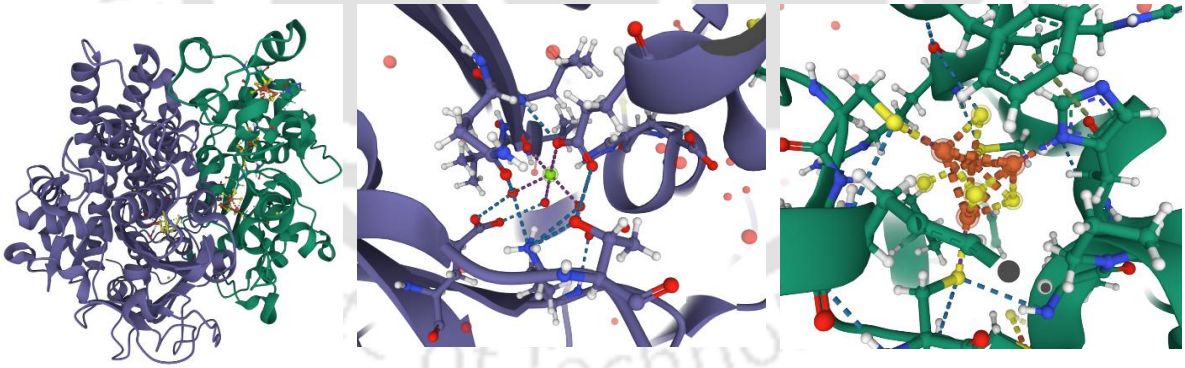

(a) (b) (c)

Fig. 1.6: 3-dimensional (3D) structures of [NiFe]-hydrogenase from *Desulfovibrio desulfuricans* ATCC 27774 (PDB ID: 1E3D). (a) Complete 3D structure of 1E3D visualized in Chimera, (b) interaction of active site amino acid residue with Mg^{2+} ion present in 1E3D, and (c) interaction of active site amino acid residue with iron-sulfur ([4Fe-3S]) cluster present in 1E3D.

[FeFe]-Hydrogenases: In contrast to [NiFe]-*hyd*, which is composed of not less than two subunits, several [FeFe]-*hyd* comprise only a catalytic subunit and are monomeric structures [45,49], though dimeric, trimeric, and tetrameric *hyd* structures are also known. The tiniest [FeFe]-*hyd*, having a molecular weight of 45-48 kDa has been discovered in green algae [50]. *Hyd* of this category are also found in anaerobic microbes, such as lower eukaryotes, sulfate-reducing bacteria, and *clostridia*. The [FeFe]-*hyd* is an exclusive *hyd* type to be found in eukaryotes, and they are found only in organelles, that is, in hydrogenosomes or in chloroplasts [39,49]. In contrast to [NiFe] bimetallic *hyd* enzymes, the catalytic subunits of [FeFe]-*hyd* differ significantly in size. In spite of the presence of the active site (H-cluster) that consists of conserved domains, these enzymes often consist of additional catalytic domains, which accommodate iron-sulfur clusters. In those, the H-clusters comprise a binuclear [FeFe] center, which is bound to a [4Fe-4S] cluster through a bridging cysteine of the [FeFe]-*hyd*. Non-protein components, such as CN^- and CO, are bound to the Fe atoms of the center. The iron atoms also share two bridging sulfur ligands of a small five-atom molecule, possibly a di(thiomethyl)amine molecule, HN(CH_2-S^-)$_2$. The Fe^{2+} atom is distal to the [Fe4-S4] cluster, and consists of an unoccupied coordination site, which is occupied by a competitive inhibitor (CO). Therefore, in the CO-inhibited form of the enzyme, it is thought to be the position where H_2 or H^- binds during enzyme turnover. A single hydrophobic channel that runs from the molecular surface to the active site and points at Fe^{2+} was detected in the structures of the [FeFe]-*hyd* from *D. desulfuricans* ATCC 775764 and the *hyd* I from *Clostridium pasteurianum*. In the same way as [NiFe]-*hyd*, a conceivable H^+ pathway has been proposed for [FeFe]-*hyd*. The 3-D structures of [FeFe]-*hyd* from *Clostridium pasteurianum* ATCC 6013 (PDB ID: 4XDD) and *Hyd*-1 from *Escherichia coli* (PDB ID: 5LMM) are given in Fig. 1.7. This image also provides the detailed information of ligands and co-factors bound to the active sites of 4XDD and 5LMM.

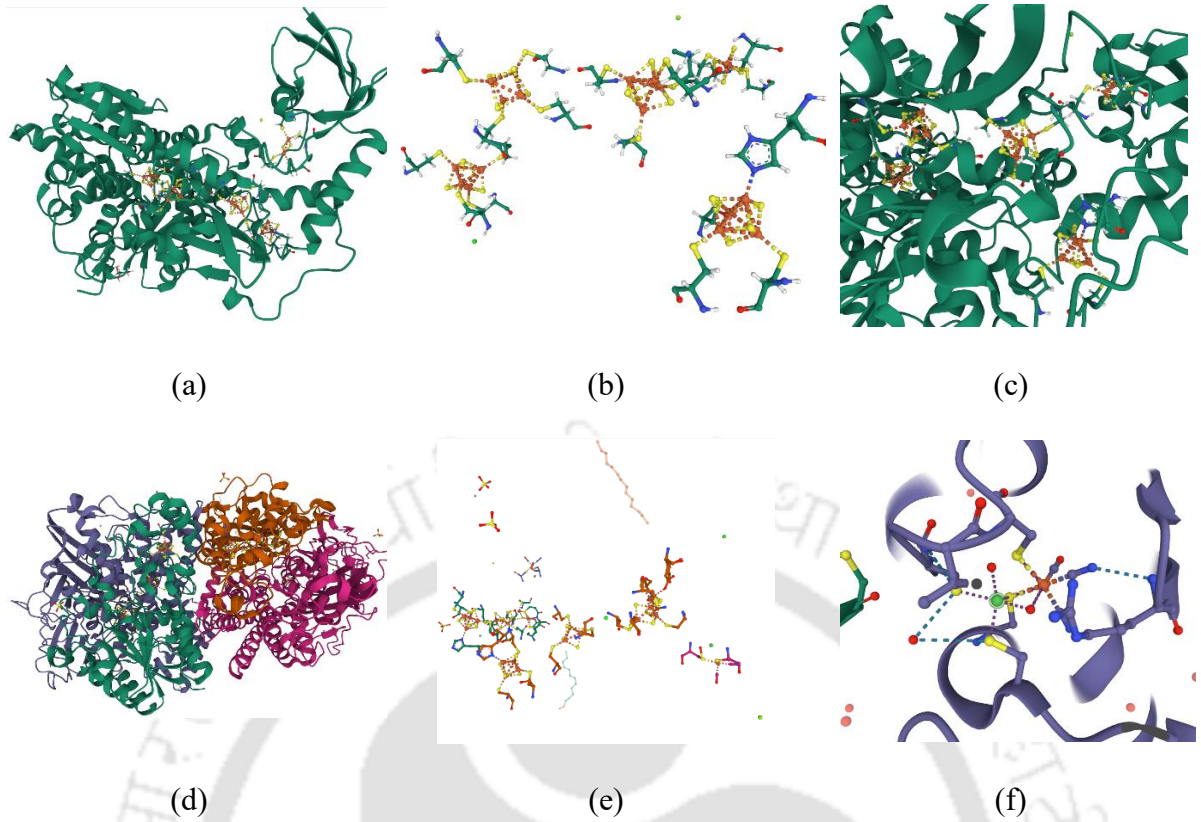

Fig. 1.7: 3-dimensional (3D) structures of [FeFe]-hydrogenase from *Clostridium pasteurianum* ATCC 6013 (PDB ID: 4XDD) and Hydrogenase-1 from *Escherichia coli* (PDB ID: 5LMM). (a) Complete 3D structure of 4XDD visualized in Chimera, (b) interaction of the active site amino acid residue all types of ligands present in 4XDD without showing polymer chain, (c) interaction of the active site amino acid residue with iron-sulfur ([4Fe-3S]) cluster present in 4XDD, (d) Complete 3D structure of 5LMM visualized in Chimera, (e) interaction of the active site amino acid residue with all types of ligands present in 5LMM without showing polymer chain, and (f) interaction of the active site amino acid residue with Ni^{+} ion present in 5LMM.

1.4 Microbiology of dark fermentative bacteria

Anaerobic conditions are favourable for most microorganisms present in the environment for biohydrogen production. Hydrogen is primarily produced by a process called "dark fermentation". Dark fermentative microorganisms are frequently called hydrogen producers in these processes [51]. These bacteria are characterized on the basis of the oxygen requirement and optimum temperature for growth. Obligate anaerobes are microorganisms that cannot survive in a more oxygenated environment [52]. Facultative anaerobes are the microbes that can grow in both aerobic and anaerobic conditions [24]. Compared to obligate anaerobes,

facultative bacteria are more amenable to laboratory conditions, making them more suitable for experimental work. Based on temperature needs, they are classified into mesophiles and thermophiles. Mesophiles and thermophiles are adapted to average and higher temperatures for their growth, respectively. Thermophiles have a big problem: they require a lot of energy to survive. However, it can overcome the thermodynamic barrier and produce hydrogen at a rate closer to the theoretical yield. BioH_2 can be produced in the environment by pure or mixed culture microbes. The application of organisms for fermentation mainly depends upon the type of fermentable substrate used [53].

1.4.1 Obligate anaerobic bacteria

The wide range of organic substrates can be degraded by strict anaerobes during fermentation, resulting in biohydrogen production. The organisms of the genus *Clostridia*, such as *C. pasteurianum, C. paraputrificumM-21*, *C. bifermentants*, C. *tyrobutyricum*, *C. beijerinckii*, *C. saccharoperbutylacetonicum*, *C. thermocellum*, *C. thermolactium*, and *C. butyricum*. These are obligate anaerobes and spore-forming microorganisms [54]. They produce bioH_2 at a higher rate. BioH_2 is produced during the exponential growth phase of *Clostridium* species, in addition to acids or metabolites. The shift in metabolism from the acidogenesis to the solventogenesis phase occurs in the stationary phase [55]. Approximately bioH_2 production in the range of 1.47-2.81 mol/mol glucose was reported previously by different *Clostridium* species [56].

1.4.2 Facultative anaerobic bacteria

The term "facultative" means that these organisms can switch between aerobic respiration (using oxygen) and anaerobic respiration (without oxygen), depending on oxygen availability in their environment. Facultative anaerobes possess metabolic pathways that generate energy through aerobic and anaerobic processes [57]. Aerobic respiration produces energy in the form

of adenosine triphosphate (ATP). During aerobic respiration, facultative anaerobes break down organic molecules (such as glucose) through enzymatic reactions, producing carbon dioxide and water as byproducts. However, when oxygen is limited or absent, facultative anaerobes can shift their metabolic strategy and employ anaerobic respiration [9,16]. Anaerobic respiration involves breaking organic molecules without oxygen, producing energy and metabolic byproducts. The final electron acceptor in anaerobic respiration can vary depending on the microorganism. For example, some facultative anaerobes may utilize nitrate, sulfate, or even carbon dioxide as alternative electron acceptors without oxygen. ATP can be generated by anaerobic fermentation in facultative anaerobes. The *Enterobacteriaceae* family is a widespread group of anaerobes capable of hydrogen production without oxygen [58]. There has been substantial research on two *Enterobacteriaceae* strains - identified as *Enterobacter aerogenes E.82005* and *Enterobacter cloacae IIT-BT 08* [59]. Hydrogen yield by *E. aerogenes E.82005* under anaerobic batch cultivation was 1.0 mol H_2/mol glucose at a productivity of 21 mmol/liter/h [60]. Molasses was used as the substrate for studies conducted in continuous mode of operation. Cellobiose, glucose and sucrose yielded 5.4, 2.2, 6.0 mol H_2 per mole of the substrate, respectively. The highest H_2 production rate with sucrose was 35 mmol/liter/h [61]. Fig. 1.8 shows a schematic representation of the diversity and classification of microorganisms capable of fermentative biohydrogen production.

1.4.3 Thermophiles

Thermophiles, often obligate anaerobes, can be found in various geothermally heated environments, including deep-sea hydrothermal vents and hot springs. A more significant concentration of sodium chloride is needed for growth and hydrogen generation media for deep-sea volcano isolates [62]. In comparison, a higher concentration of sulphur is required for volcanic vent isolates. The medium for obligate anaerobes needs reducing agents like L-cystine

HCl for the removal of even lesser amounts of oxygen. Thermophiles can utilize many substrates, viz. biomass (with pectin content), cellulose, and hemicellulose [63]. *Thermoanaerobacter, Caldicellulosiuptor,* and *Thermotoga* are some examples of the genera in this group [54]. All are highly thermophilic, Gram-positive, and cellulolytic. The species of the genus *Caldicellulosiruptor* can effectively degrade cellulose at temperatures up to 80 °C. It produces lactate, ethanol, and acetate as primary end metabolites along with the H_2 production process [62,64]. In contrast, Thermotogales bacteria have a sheath-like structure surrounding the cells called a toga; they are Gram-negative, anaerobic, thermophilic, and heterotrophic. All the species in this genus can ferment sugars and proteins to produce hydrogen.

1.4.4 Mixed culture

Natural environments such as sludge, soil and sediments are teeming with hydrogen-producing microorganisms. These substances may serve as sources of enrichment for hydrogen production. Hydrogen producers mostly use anaerobic sludge. For complex substrates like sewage sludge or cane molasses, co-cultures or mixed consortia are typically used for hydrogen production. Two essential functions are provided by the mixed cultures or consortia [65,66]. First, consortium members exchange metabolites or molecular signals for dividing labour for the decomposition of the complex substrates. The usage of consortia may improve substrate utilization. Using complex substrates, mixed consortia are superior to pure culture in several research studies [67]. The inoculum plays a crucial role in hydrogen generation. Current research suggests that waste-activated sludge is the most effective method for producing hydrogen, followed by animal compost, buried soil, and fermentation using native microbes [68].

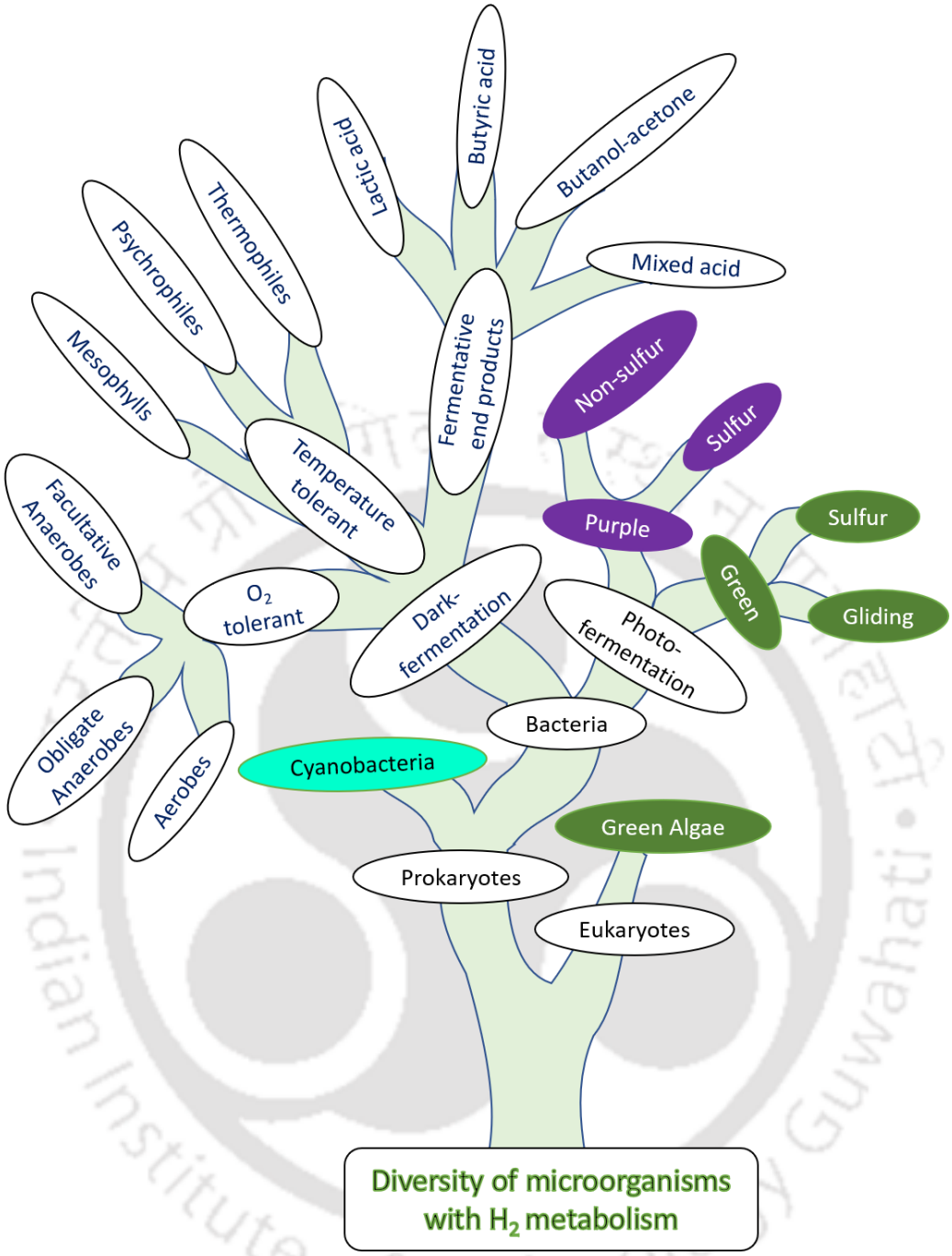

Fig. 1.8. Schematic representation for diversity and classification of microorganisms capable of fermentative biohydrogen production.

1.5 Biochemistry of dark fermentation

Anaerobic fermentation is a metabolic process that replenishes the cell's "currency" (ATP) energy. Moreover, tricarboxylic acid (TCA) gets blocked under anaerobic conditions. To eliminate the extracellular reductant, fermentation produces reduced metabolic byproducts

such as acids and alcohol [69]. Similarly, H_2 is produced during metabolism to maintain the cellular redox potential of carbohydrates. Glucose is the preferred carbon source for fermentation that results in butyric and acetic acids and H_2 gas as end products [70]. Initially, complex organic substrates are hydrolysed to glucose. Next, pyruvate is produced from glucose via the glycolytic pathway to regenerate ATP. Therefore, pyruvate might play a role in two distinct metabolic events resulting in hydrogen production. The obligate anaerobes like *Clostridia* further oxidize pyruvate to acetyl coenzyme A (Acetyl-CoA) by pyruvate ferredoxin oxidoreductase. Production of ATP and acetate is accompanied by the conversion of acetyl-CoA to acetyl phosphate. Reduction of ferredoxin (Fd) is required for the conversion of pyruvate to acetyl-CoA. [Fe-Fe] hydrogenase catalyzes the production of hydrogen by oxidizing reduced Fd. Eqs. 1.3 and 1.4 depict the overall reactions [52].

$$Pyruvate + CoA + 2Fd(ox) \rightarrow AcetylCoA + 2Fd(red) + CO_2$$
$$2H^+ + Fd(red) \rightarrow H_2 + Fd(ox) \qquad \text{(Eqs. 1.3 \& 1.4)}$$

Pyruvate oxidation to acetate results in the production of H_2 at a rate of 4 mol/mol of glucose. Pyruvate oxidation to butyrate produces 2 moles of H_2/mole of glucose. Thus, a larger A/B ratio is required for higher H_2 production in microorganisms with a mixed acid route. Both acetic and butyric acid are metabolic byproducts of the more general biological reaction depicted by Eqs. 1.5 and 1.6.

$$C_6H_{12}O_6 + 2H_2O \rightarrow 2CH_3COOH + 2CO_2 + 4H_2$$
$$C_6H_{12}O_6 \rightarrow CH_3CH_2CH_2COOH + 2CO_2 + 2H_2 \qquad \text{(Eqs. 1.5 \& 1.6)}$$

In some facultative anaerobes like *Escherichia coli*, the pyruvate is oxidized to acetyl-CoA and formate. The enzyme pyruvate formate lyase catalyzes the reaction. Subsequently, formate is cleaved by FHL (formate hydrogenlyase) to produce carbon dioxide and hydrogen [71].

$$Pyruvate + CoA \rightarrow AcetylCoA + formate$$
$$HCOOH \rightarrow CO_2 + H_2$$ (Eqs. 1.7 & 1.8)

The oxidation of pyruvate to lactate occurs immediately in lactic acid fermentation. No hydrogen is produced when the sole metabolic end product is ethanol, lactic, or propionic acid [24].

Moreover, Enteric bacteria are facultative anaerobes that can undergo anaerobic respiration (instead of fermentation) using terminal electron acceptors like nitrate or fumarate. Anaerobic respiration may hinder hydrogen generation. Thus, media exclusive of electron acceptors is required for hydrogen generation. Photo-fermentation bacteria can use organic acids produced during dark fermentation as substrate, which are oxidized to CO_2 and H_2 [72]. Hence, coupling of 2-stage dark fermentation with photo-fermentation can yield higher hydrogen production, viz. 12 mol of H_2/mol of glucose as per stoichiometry [72].

1.5.1 Metabolic pathway and molecular biology of the [Fe-Fe] hydrogenase enzyme

Dark fermentation produces molecular hydrogen to effectively disperse its abundant reducing chemicals (NADPH and FADH) as a diffuse gas [73]. The majority of current research on the synthesis of biohydrogen uses a dark fermentation process involving numerous unique microorganisms. The dark fermentation process involves obligate anaerobic bacteria (*Clostridium butyricum*, *Clostridium paraputrificum*, *Clostridium beijerinckii*, *Ruminococcus albus*, etc.) and facultative (*Escherichia coli*, *Citrobacter intermedius*, *Enterobacter aerogenes vb*., and *E. cloacae*) for biohydrogen production [64].

Glycolysis is the primary metabolic route by which pyruvate, a crucial metabolic intermediate, can be produced from a substrate. All dark fermentation methods produce molecular hydrogen from pyruvate under anaerobic conditions. However, they also produce various volatile fatty acids and alcohols [73,74]. Fig. 1.9 shows a schematic representation of the metabolic pathway in dark fermentation.

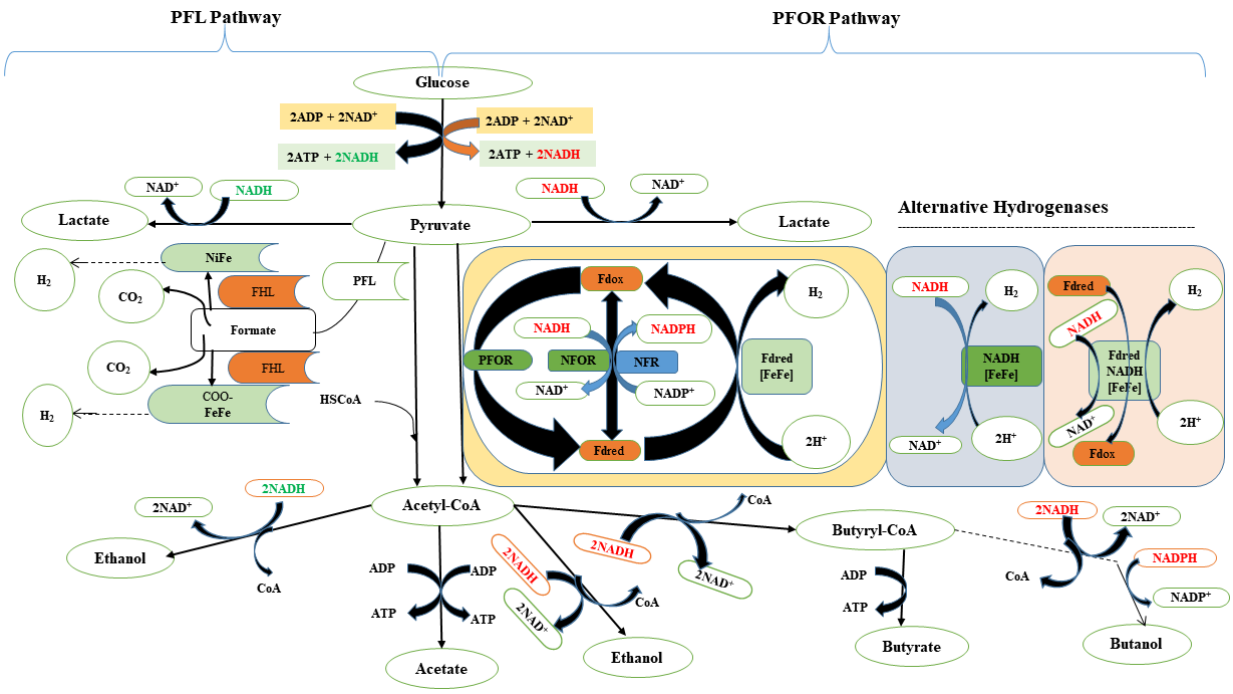

Fig. 1.9. Metabolic pathways of molecular hydrogen generation from glucose using dark fermentation. Anaerobic degradation of pyruvate by using the PFL: pyruvate-formate-lyase pathway and PFOR: pyruvate-ferredoxin-oxidoreductase pathway (adopted from Tapia-Venegas et al.[74]).

Hydrogen production from organic waste mainly involves two types of pathways. (1) synthesis of pyruvate from glucose through the glycolysis pathway, and (2) anaerobic degradation of pyruvate by using the pyruvate-formate-lyase (PFL) pathway and pyruvate ferredoxin oxidoreductase (PFOR) pathways. Two main routes are known for the anaerobic degradation of pyruvate in biohydrogen production. One is the PFOR pathway, and the other is the PFL pathway; both are involved in the dark fermentation of pyruvate for molecular hydrogen production [64,76]. In both pathways, pyruvate is initially synthesized from glucose and converted into acetyl-CoA. Next, reduced formate or ferredoxin is obtained. Molecular hydrogen production through the PFOR pathway and obligate anaerobes such as Clostridia use

the enzyme pyruvate-ferredoxin (Fd) oxidoreductase to convert pyruvate to acetyl-CoA during glycolysis.

Acetate and ATP are then produced via acetyl-CoA. By oxidizing reduced ferredoxin (Fdred) with a ferredoxin-dependent hydrogenase (Fd-[FeFe]), pyruvate is converted to acetyl-CoA. The reduced Fd is subsequently oxidized by [FeFe]-hydrogenase to produce molecular hydrogen (shown in Fig. 1.10. A) [23,77,78]. For every mole of glucose converted from pyruvate to acetate, 4 moles of H_2 are generated. Pyruvate is converted to butyrate, which produces 2 mol H_2/mol glucose [79]. Because of this, the acetate/butyrate ratio plays a vital role in producing molecular hydrogen in microorganisms that use the mixed acid route [78].

In the second metabolic PFL pathway, using the formate lyase activity of facultative anaerobes such as *Enterobacter*, the PFL pathway catalyzes the conversion of pyruvic acid to acetyl-CoA and formic acid. Formate is converted into CO_2 and molecular hydrogen by a formate hydrogen lyase (FHL) complex, including a [NiFe] hydrogenase (Fig.1.10. B). This process might occur with either [NiFe] hydrogenase or [FeFe] hydrogenase activity, based on the organism. Microorganisms with only the PFL pathway cannot access NADH to produce molecular hydrogen. Theoretically, it is restricted to 2 moles of molecular hydrogen for every mole of glucose [78].

Two critical enzymes are essential in producing molecular hydrogen in the dark fermentation process. One is [FeFe] hydrogenase and the other is formate hydrogen lyase (FHL). Microorganisms produce molecular hydrogen by utilizing these two enzymes [80]. In facultative anaerobic bacteria, the multi-enzyme complex known as the FHL system is involved in the synthesis of hydrogen. The formate hydrogen lyase complex produces hydrogen and CO_2 in anaerobic respiration due to the enzymatic decomposition of formate. Phylogenetically unrelated hydrogenases share some characteristics, such as including CO and Fe in their active site as a ligand for the Fe atom. Fe ions are found in the centers of [NiFe] and [FeFe]

hydrogenases. Only methanogenic archaea carry [Fe] hydrogenases, which have a single Fe^{3+} ion utilized for the hydrogen-dependent reduction of 5,10-methylene tetrahydromethanopterin during methanogenesis. Hydrogen oxidation is mostly catalyzed by [NiFe] hydrogenases. But when hydrogen is produced in the hydrogen lyase reaction, formate is implicated in the Hyd-3 of *E. coli*. Unlike [NiFe] hydrogenases, which are broadly distributed in nature, [FeFe] hydrogenases have far more constrained distributions. However, [FeFe] hydrogenases are known to play the most dominant role in hydrogen-generation among these three hydrogenases. They are typically present in anaerobic bacteria (*Thermotoga, Clostridia*). Compared to [NiFe] hydrogenase, these are 10-100-times more active in generating molecular hydrogen [80–82]. As per the KEGG database, Table 1.2 represents list of metabolic pathways in microorganism for H_2 metabolism.

Table 1.2. List of metabolic pathways in microorganisms for H_2 metabolism (as per KEGG database)

Pathway name	Chemical equation	Enzymes involved	Microbial genus family	Type of metabolism
Ferredoxin	$Fd_{rd} \rightarrow Fd_{ox} + H_2$	[FeFe]-*hyd* group A1 and B	Firmicutes, Bacteroidetes, Fusobacteria, Eukaryotes	Production
Bifurcation	$Fd_{rd} + NADH \rightarrow Fd_{ox} + NAD^+ + H_2$	[FeFe]-*hyd* group A3 and A4	Firmicutes, Bacteroidetes, Fusobacteria	
Formate	$Formate \rightarrow CO_2 + H_2$	[NiFe]-*hyd* group 4a and 4f	γ-proteobacteria and ε-proteobacteria	
Nicotinamide	$NAD(P)H \rightarrow NAD(P)^+ + H_2$	[NiFe]-*hyd* group 3b and 3c	Actinobacteria	
Acetogenesis	$CO_2 + H_2 \rightarrow Acetate$	[FeFe]-*hyd* group A3 and A4	Firmicutes	Consumption
Methanogenesis	$CO_2 + H_2 \rightarrow Methane$	[NiFe]-*hyd* group 3b, 3c, 4h, and 4i and [Fe]-*hyd*	Euryarchaeota	
Aerobic respiration	$O_2 + 2H_2 \rightarrow 2H_2O$	[NiFe]-*hyd* group 1b, 1d, 1f, 1h, and 2a	γ-proteobacteria, ε-proteobacteria and Actinobacteria	
Fumarate respiration	$Fumarate + H_2 \rightarrow Succinate$	[NiFe]-*hyd* group 1b, 1c, and 1d	γ-proteobacteria and ε-proteobacteria	
Sulfate respiration	$SO_4^{2-} + H_2 \rightarrow H_2S$	[NiFe]-*hyd* group 1a and 1b	δ-proteobacteria	

1.5.2 The structure of [FeFe] hydrogenase

The hydA gene encodes the [FeFe] hydrogenase enzyme's catalytic center. The distribution of [FeFe] hydrogenase is investigated using the hydA gene as a functional biomarker. The [FeFe] hydrogenase enzyme is thought to mature when the hydA gene contains the hydE, hydF, and hydG genes. According to previous literature, the number and variety of [FeFe] hydrogenases in the environment are low [79]. Mulder et al. [83] reported limited similarities in the [FeFe] hydrogenase sequence, with only ten multiple alignments found among more than one billion base pairs. This scarcity underscores the importance of investigating the distribution and presence of hydA sequences for studying [FeFe] hydrogenase diversity. However, it has been observed that some organisms possess hydA without the accompanying hydE, hydF, and hydG genes. The significance of these orphan hydA sequences or the role of an unrecognized maturation system remains unknown [83].

Compared to [NiFe] hydrogenases, [FeFe] has a narrower distribution and exhibits a modular structure with variations. The distribution of [FeFe] hydrogenase, relative to the hydA gene, is commonly found in Gram-positive *Clostridia* species and Gram-negative γ-proteobacteria such as *Desulfovibrio*. To gain a comprehensive understanding of the distribution range of [FeFe] hydrogenases, it is crucial to conduct detailed studies of genome sequences containing hydA, as well as homologs of hydE, hydF, and hydG [84,85].

1.5.3 H-clusters and active site

The active site of two iron ions is assumed to be present in all [FeFe] hydrogenases. Even though little is known about the synthesis of this active H-cluster, research in recent years has significantly increased our understanding. A [4Fe4S] subset of the H-cluster binds to the 2Fe subset that has been modified with ligands CO and CN using a cysteine thiolate. The CO ligand, primarily inorganic and poisonous, is essential to the active sites of hydrogenases (FeFe, NiFe,

and Fe). Compared to CN^- ligands, CO ligands bind less firmly. In catalytic reactions, it can also change between various configuration states. [NiFe] and [FeFe] hydrogenases require CN^- ligands. The 2FeH site is stabilized in the protein medium and is stabilized in low oxidation states via an H-bond to CN^- ligands [86]. The type of ligand, which acts as a link between the two Fe atoms, also typically regulates how the two Fe sites rotate. The kinetic parameters of enzyme catalysis are also strongly affected by changes in the electrostatic interaction pattern between the polypeptide environment and the CO and CN^- ligands. In light of this, it is highly intriguing to learn how these ligands are created by cellular metabolism and positioned in intricate metal centres [87]. The enzyme-linked thiocyanate (generated from carbamoyl phosphate in the CN^- ligand component) inhibits free cyanide, which acts as an intermediate in the active site of [NiFe] hydrogenase. In [FeFe] hydrogenase, the CN^- ligand in the active site is derived from the cleavage of S-adenosylmethionine by the hydG. This cleavage produces β-cresol and cyanide, with the free cyanide immediately transferred to hydF. hydF contains a di-iron cluster bonded to both CO and CN^-. hydF synthesizes guanosine-50-triphosphate, which is a crucial step in the H-cluster synthesis. This process requires the involvement of hydE and hydG [88]. hydE, hydF, and hydG primarily add the 2Fe subset to hydA (which already contains a [4Fe4S] cluster) by synthesizing it with CN^- and CO^- ligands. Studies have shown that the [4Fe4S] subset of the active site can be formed through biochemical processes and the generalized host cell mechanism without hydE, F, and G. However, adding the 2Fe subset by these maturation proteins is crucial for the complete assembly of the H-cluster [89]. hydG, as a multifunctional enzyme, plays a vital role in producing the CN^- and CO^- ligands necessary for the H-cluster synthesis. It is also involved in synthesizing dithiomethylamine, which serves as a bridging ligand for the 2Fe subset. In summary, these are the basic steps involved in the H-cluster synthesis of [FeFe] hydrogenase. The functions of maturation proteins hydE, hydF, and hydG in the synthesis of the H-cluster have provided valuable insights into this enzyme,

which plays a critical role in hydrogen production. The catalytic mechanism of the hydrogenase enzyme is shown in Figs. 1.10 (made by PyMol) and 1.11 (made by LigPlot) [90–92].

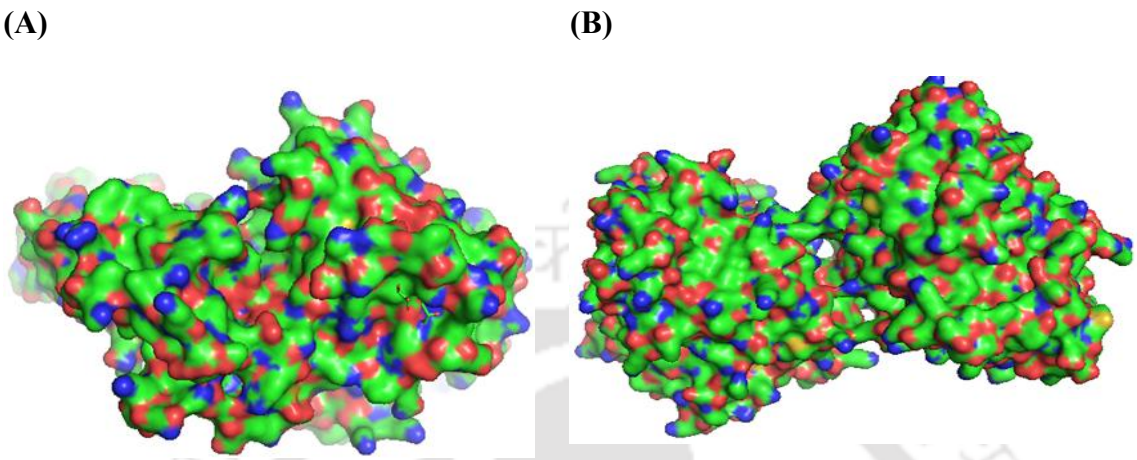

Fig. 1.10. Structure and active site residue of [FeFe] hydrogenase. **(A)** Surface model of CpI (PDB ID: 3C8Y) and (B) DdH (PDB ID: 1HFE) protein

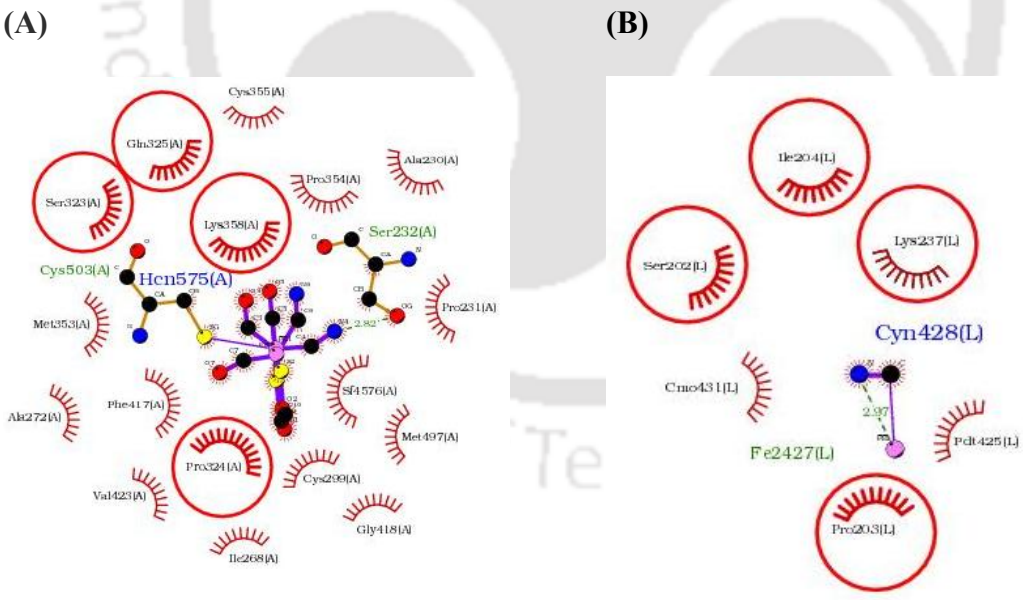

Fig. 1.11. H-bonds and hydrophobic interactions among the amino acid residues near the active site of hydrogenase (A). CpI (PDB ID: 3C8Y) and (B). DdH (PDB ID: 1HFE) enzymes with CN^- ligand.
Note: CpI: [FeFe]-hydrogenase-1 from *Clostridium pasteurianum*
DdH: periplasmic [FeFe] hydrogenase from *Desulfovibrio desulfuricans*

1.6 Overview

BioH_2 production holds significant potential as a sustainable and renewable energy source, though several technical and operational challenges remain. Current research emphasizes improving microbial systems, as stable and efficient anaerobic microbes are crucial for consistent hydrogen yields. Disruptions in microbial balance can alter gas composition, and while genetic modifications have shown promise in enhancing hydrogen production, scaling these solutions remains complex. The glycolytic pathway in microorganisms can achieve recovery of ~40% of the substrate energy as bioH_2, it can be enhanced by coupling biomethane production from left-over volatile fatty acids. Such integrated bioprocesses can have a negative carbon footprint.

Biowaste pretreatment and utilization are also critical areas, with studies exploring the conversion of agro-industrial and municipal residues such as food waste, sugarcane vinasse and palm oil mill effluent. Due to the variable composition of residues, pretreatment methods like drying, size reduction and hydrolysis, along with substrate-specific process optimization, are necessary to improve efficiency. Another vital aspect is the optimization of fermentation conditions, including pH, temperature, and medium composition, tailored to different residues. Recent advancements highlight the role of nanoparticle additives and pressure manipulation in enhancing hydrogen solubility and overall yields. The nanoparticle additives such as iron-based nanoparticles or nanobiochar can enhance electron transfer that can affect the metabolic pathways for hydrogen production.

For the transition from laboratory to industrial application, intermediate-scale pilot plants are essential to address process stability, microbial succession, and downstream processing challenges such as gas purification, insulation, and storage. Techno-economic and life cycle analyses play a critical role in assessing the viability of bioH_2 systems, which typically have low capital costs but must prove both economically and environmentally competitive with

other green energy options. Key concerns in this regard include reliance on fossil fuels for biomass transportation and processing, and alternative methane emissions from residues, which influence the overall carbon footprint of the process. In parallel, the integration of bioH_2 into biogas systems presents additional opportunities. The production of biomethane and its thermochemical conversion into turquoise hydrogen, alongside the formation of biohythane (a mixture of methane and hydrogen (10-30%), offers advantages in terms of fuel properties and transport. Future perspectives in the field focus on developing enzyme immobilization techniques, dark fermentation processes, and biohydrogen pathways from biomass residues. The primary goals moving forward with research and development in bioH_2 production, and its commercialization involve:

1. Use of cheap and waste materials as substrates for bioH_2 fermentation
2. Investigation into the fundamental aspects of biomass pretreatment and dark fermentation for optimization and scale-up pilot plant processes
3. Refining microbial ecology knowledge and development of genetically modified bacteria
4. Intensification of dark fermentation for faster bioH_2 production with higher yields
5. Integrating biohydrogen production into larger bio-refinery operations for a sustainable hydrogen economy.

The present thesis has attempted to address some of these goals.

References

[1] J. Appel, R. Schulz, Hydrogen metabolism in organisms with oxygenic photosynthesis: hydrogenases as important regulatory devices for a proper redox poising?, Journal of Photochemistry and Photobiology B: Biology 47 (1998) 1–11. https://doi.org/10.1016/S1011-1344(98)00179-1.

[2] P. Nikolaidis, A. Poullikkas, A comparative overview of hydrogen production processes, Renewable and Sustainable Energy Reviews 67 (2017) 597–611. https://doi.org/10.1016/j.rser.2016.09.044.

[3] N. Muradov, How to produce hydrogen from fossil fuels without CO2 emission, International Journal of Hydrogen Energy 18 (1993) 211–215. https://doi.org/10.1016/0360-3199(93)90021-2.

[4] H. Balat, E. Kırtay, Hydrogen from biomass – Present scenario and future prospects, International Journal of Hydrogen Energy 35 (2010) 7416–7426. https://doi.org/10.1016/j.ijhydene.2010.04.137.

[5] N. Muradov, T. Vezirolu, From hydrocarbon to hydrogen?carbon to hydrogen economy, International Journal of Hydrogen Energy 30 (2005) 225–237. https://doi.org/10.1016/j.ijhydene.2004.03.033.

[6] R. Kothari, A critical review on factors influencing fermentative hydrogen production, Front Biosci 22 (2017) 1195–1220. https://doi.org/10.2741/4542.

[7] S.E. Hosseini, M.A. Wahid, Hydrogen production from renewable and sustainable energy resources: Promising green energy carrier for clean development, Renewable and Sustainable Energy Reviews 57 (2016) 850–866. https://doi.org/10.1016/j.rser.2015.12.112.

[8] A. Gadhe, S.S. Sonawane, M.N. Varma, Optimization of conditions for hydrogen production from complex dairy wastewater by anaerobic sludge using desirability function approach, International Journal of Hydrogen Energy 38 (2013) 6607–6617. https://doi.org/10.1016/j.ijhydene.2013.03.078.

[9] D. Das, Hydrogen production by biological processes: a survey of literature, International Journal of Hydrogen Energy 26 (2001) 13–28. https://doi.org/10.1016/S0360-3199(00)00058-6.

[10] G. Balachandar, J.L. Varanasi, V. Singh, H. Singh, D. Das, Biological hydrogen production via dark fermentation: A holistic approach from lab-scale to pilot-scale,

International Journal of Hydrogen Energy 45 (2020) 5202–5215. https://doi.org/10.1016/j.ijhydene.2019.09.006.

[11] P. Friedlingstein, M. O'Sullivan, M.W. Jones, R.M. Andrew, Global Carbon Budget 2023, Earth System Science Data 15 (2023) 5301–5369. https://doi.org/10.5194/essd-15-5301-2023.

[12] P. Friedlingstein, M. O'Sullivan, M.W. Jones, R.M. Andrew, J. Zeng, Global Carbon Budget 2024, Earth System Science Data Discussions (2024) 1–133. https://doi.org/10.5194/essd-2024-519.

[13] K.-A. Adamson, P. Pearson, Hydrogen and methanol: a comparison of safety, economics, efficiencies and emissions, Journal of Power Sources 86 (2000) 548–555. https://doi.org/10.1016/S0378-7753(99)00404-8.

[14] A. Demirbas, Biohydrogen Generation from Organic Waste, Energy Sources, Part A: Recovery, Utilization, and Environmental Effects 30 (2008) 475–482. https://doi.org/10.1080/15567030600828909.

[15] G. Balachandar, N. Khanna, D. Das, Biohydrogen Production from Organic Wastes by Dark Fermentation, in: Biohydrogen, Elsevier, 2013: pp. 103–144. https://doi.org/10.1016/B978-0-444-59555-3.00006-4.

[16] H. El Bari, N. Lahboubi, S. Habchi, S. Rachidi, O. Bayssi, N. Nabil, Y. Mortezaei, R. Villa, Biohydrogen production from fermentation of organic waste, storage and applications, Cleaner Waste Systems 3 (2022) 100043. https://doi.org/10.1016/j.clwas.2022.100043.

[17] O. Elsharnouby, H. Hafez, G. Nakhla, M.H. El Naggar, A critical literature review on biohydrogen production by pure cultures, International Journal of Hydrogen Energy 38 (2013) 4945–4966. https://doi.org/10.1016/j.ijhydene.2013.02.032.

[18] W. Han, Y. Yan, Y. Shi, J. Gu, J. Tang, H. Zhao, Biohydrogen production from enzymatic hydrolysis of food waste in batch and continuous systems, Sci Rep 6 (2016) 38395. https://doi.org/10.1038/srep38395.

[19] T.Y. Wu, J.X.W. Hay, L.B. Kong, J.C. Juan, J.Md. Jahim, Recent advances in reuse of waste material as substrate to produce biohydrogen by purple non-sulfur (PNS) bacteria, Renewable and Sustainable Energy Reviews 16 (2012) 3117–3122. https://doi.org/10.1016/j.rser.2012.02.002.

[20] N. Ren, A. Wang, L. Gao, L. Xin, D.-J. Lee, A. Su, Bioaugmented hydrogen production from carboxymethyl cellulose and partially delignified corn stalks using

isolated cultures, International Journal of Hydrogen Energy 33 (2008) 5250–5255. https://doi.org/10.1016/j.ijhydene.2008.05.020.

[21] S. O-Thong, P. Prasertsan, D. Karakashev, I. Angelidaki, Thermophilic fermentative hydrogen production by the newly isolated Thermoanaerobacterium thermosaccharolyticum PSU-2, International Journal of Hydrogen Energy 33 (2008) 1204–1214. https://doi.org/10.1016/j.ijhydene.2007.12.015.

[22] A. Mudhoo, S. Kumar, Effects of heavy metals as stress factors on anaerobic digestion processes and biogas production from biomass, Int. J. Environ. Sci. Technol. 10 (2013) 1383–1398. https://doi.org/10.1007/s13762-012-0167-y.

[23] B. Gopalakrishnan, N. Khanna, D. Das, Dark-Fermentative Biohydrogen Production, in: Biohydrogen, Elsevier, 2019: pp. 79–122. https://doi.org/10.1016/B978-0-444-64203-5.00004-6.

[24] D. Das, Advances in biohydrogen production processes: An approach towards commercialization, International Journal of Hydrogen Energy 34 (2009) 7349–7357. https://doi.org/10.1016/j.ijhydene.2008.12.013.

[25] A.I. Osman, T.J. Deka, D.C. Baruah, D.W. Rooney, Critical challenges in biohydrogen production processes from the organic feedstocks, Biomass Conv. Bioref. (2020). https://doi.org/10.1007/s13399-020-00965-x.

[26] F. Tian, O.B. Toon, A.A. Pavlov, H. De Sterck, A Hydrogen-Rich Early Earth Atmosphere, Science 308 (2005) 1014–1017. https://doi.org/10.1126/science.1106983.

[27] M.A. Harris, C.A. Reddy, Hydrogenase Activity and the H2-Fumarate Electron Transport System in Bacteroides fragilis, Journal of Bacteriology 131 (1977) 922–928. https://doi.org/10.1128/jb.131.3.922-928.1977.

[28] K. Schuchmann, V. Müller, A Bacterial Electron-bifurcating Hydrogenase *, Journal of Biological Chemistry 287 (2012) 31165–31171. https://doi.org/10.1074/jbc.M112.395038.

[29] L. Bowman, L. Flanagan, P.K. Fyfe, A. Parkin, W.N. Hunter, F. Sargent, How the structure of the large subunit controls function in an oxygen-tolerant [NiFe]-hydrogenase, Biochemical Journal 458 (2014) 449–458. https://doi.org/10.1042/BJ20131520.

[30] M.M. Amin, E. Taheri, A. Fatehizadeh, M. Rezakazemi, T.M. Aminabhavi, Anaerobic membrane bioreactor for the production of bioH2: Electron flow, fouling modeling and kinetic study, Chemical Engineering Journal 426 (2021) 130716. https://doi.org/10.1016/j.cej.2021.130716.

[31] A. Volbeda, P. Amara, C. Darnault, J.-M. Mouesca, A. Parkin, M.M. Roessler, F.A. Armstrong, J.C. Fontecilla-Camps, X-ray crystallographic and computational studies of the O2-tolerant [NiFe]-hydrogenase 1 from Escherichia coli, Proceedings of the National Academy of Sciences 109 (2012) 5305–5310. https://doi.org/10.1073/pnas.1119806109.

[32] L.K. Meredith, D. Rao, T. Bosak, V. Klepac-Ceraj, K.R. Tada, C.M. Hansel, S. Ono, R.G. Prinn, Consumption of atmospheric hydrogen during the life cycle of soil-dwelling actinobacteria, Environmental Microbiology Reports 6 (2014) 226–238. https://doi.org/10.1111/1758-2229.12116.

[33] E.M. Doğan-Güner, H. Koku, Analysis of the carbon metabolism of Rhodopseudomonas palustris for biohydrogen production, Biotech Studies 31 (2022) 1–9. https://doi.org/10.38042/biotechstudies.1062792.

[34] Y. Higuchi, K. Inaka, N. Yasuoka, T. Yagi, Isolation and crystallization of high molecular weight cytochrome from *Desulfovibrio valgaris* Hildenborough, Biochimica et Biophysica Acta (BBA) - Protein Structure and Molecular Enzymology 911 (1987) 341–348. https://doi.org/10.1016/0167-4838(87)90075-6.

[35] B. Fc, K. Tf, W. Gj, M. Ef, B. Md, R. Jr, K. O, S. T, T. M, The Protein Data Bank: a computer-based archival file for macromolecular structures, Journal of Molecular Biology 112 (1977). https://doi.org/10.1016/s0022-2836(77)80200-3.

[36] H.M. Berman, J. Westbrook, Z. Feng, G. Gilliland, T.N. Bhat, H. Weissig, I.N. Shindyalov, P.E. Bourne, The Protein Data Bank, Nucleic Acids Research 28 (2000) 235–242. https://doi.org/10.1093/nar/28.1.235.

[37] P.M. Vignais, B. Billoud, J. Meyer, Classification and phylogeny of hydrogenases1, FEMS Microbiology Reviews 25 (2001) 455–501. https://doi.org/10.1111/j.1574-6976.2001.tb00587.x.

[38] S. Shima, R.K. Thauer, A third type of hydrogenase catalyzing H2 activation, The Chemical Record 7 (2007) 37–46. https://doi.org/10.1002/tcr.20111.

[39] J. Meyer, [FeFe] hydrogenases and their evolution: a genomic perspective, Cell. Mol. Life Sci. 64 (2007) 1063. https://doi.org/10.1007/s00018-007-6477-4.

[40] P.M. Vignais, B. Billoud, Occurrence, Classification, and Biological Function of Hydrogenases: An Overview, Chem. Rev. 107 (2007) 4206–4272. https://doi.org/10.1021/cr050196r.

[41] J.S. McDowall, B.J. Murphy, M. Haumann, T. Palmer, F.A. Armstrong, F. Sargent, Bacterial formate hydrogenlyase complex, Proceedings of the National Academy of Sciences 111 (2014) E3948–E3956. https://doi.org/10.1073/pnas.1407927111.

[42] B. Xie, J. Cheng, J. Zhou, W. Song, K. Cen, Cogeneration of hydrogen and methane from glucose to improve energy conversion efficiency, International Journal of Hydrogen Energy 33 (2008) 5006–5011. https://doi.org/10.1016/j.ijhydene.2008.07.048.

[43] A.M. Amin, E. Croiset, W. Epling, Review of methane catalytic cracking for hydrogen production, International Journal of Hydrogen Energy 36 (2011) 2904–2935. https://doi.org/10.1016/j.ijhydene.2010.11.035.

[44] A. Galadima, O. Muraza, From synthesis gas production to methanol synthesis and potential upgrade to gasoline range hydrocarbons: A review, Journal of Natural Gas Science and Engineering 25 (2015) 303–316. https://doi.org/10.1016/j.jngse.2015.05.012.

[45] M. Berney, C. Greening, K. Hards, D. Collins, G.M. Cook, Three different [NiFe] hydrogenases confer metabolic flexibility in the obligate aerobe Mycobacterium smegmatis, Environmental Microbiology 16 (2014) 318–330. https://doi.org/10.1111/1462-2920.12320.

[46] A.S. Rose, A.R. Bradley, Y. Valasatava, J.M. Duarte, A. Prlic, P.W. Rose, NGL viewer: web-based molecular graphics for large complexes, Bioinformatics 34 (2018) 3755–3758. https://doi.org/10.1093/bioinformatics/bty419.

[47] M. Brugna-Guiral, P. Tron, W. Nitschke, K.-O. Stetter, B. Burlat, B. Guigliarelli, M. Bruschi, M.T. Giudici-Orticoni, [NiFe] hydrogenases from the hyperthermophilic bacterium Aquifex aeolicus: properties, function, and phylogenetics, Extremophiles 7 (2003) 145–157. https://doi.org/10.1007/s00792-002-0306-3.

[48] D.M. Arias, E. Ortíz-Sánchez, P.U. Okoye, H. Rodríguez-Rangel, A. Balbuena Ortega, A. Longoria, R. Domínguez-Espíndola, P.J. Sebastian, A review on cyanobacteria cultivation for carbohydrate-based biofuels: Cultivation aspects, polysaccharides accumulation strategies, and biofuels production scenarios, Science of The Total Environment 794 (2021) 148636. https://doi.org/10.1016/j.scitotenv.2021.148636.

[49] K. Schuchmann, N.P. Chowdhury, V. Müller, Complex Multimeric [FeFe] Hydrogenases: Biochemistry, Physiology and New Opportunities for the Hydrogen Economy, Frontiers in Microbiology 9 (2018). https://www.frontiersin.org/article/10.3389/fmicb.2018.02911 (accessed March 31, 2022).

[50] N. Fakhimi, D. Gonzalez-Ballester, E. Fernández, A. Galván, A. Dubini, Algae-Bacteria Consortia as a Strategy to Enhance H2 Production, Cells 9 (2020) 1353. https://doi.org/10.3390/cells9061353.

[51] D. Das, N. Khanna, N. Veziroğlu, Recent developments in biological hydrogen production processes, CI&CEQ 14 (2008) 57–67. https://doi.org/10.2298/CICEQ0802057D.

[52] D. Das, N. Khanna, C.N. Dasgupta, Biohydrogen production: fundamentals and technology advances, CRC press, Boca Raton, 2014.

[53] P. Sampath, Brijesh, K.R. Reddy, C.V. Reddy, N.P. Shetti, R.V. Kulkarni, A.V. Raghu, Biohydrogen Production from Organic Waste – A Review, Chem. Eng. Technol. 43 (2020) 1240–1248. https://doi.org/10.1002/ceat.201900400.

[54] H. Shin, Hydrogen production from food waste in anaerobic mesophilic and thermophilic acidogenesis, International Journal of Hydrogen Energy 29 (2004) 1355–1363. https://doi.org/10.1016/j.ijhydene.2003.09.011.

[55] W. Han, X. Wang, L. Ye, J. Huang, J. Tang, Y. Li, N. Ren, Fermentative hydrogen production using wheat flour hydrolysate by mixed culture, International Journal of Hydrogen Energy 40 (2015) 4474–4480. https://doi.org/10.1016/j.ijhydene.2015.02.016.

[56] C. Lin, Fermentative hydrogen production at ambient temperature, International Journal of Hydrogen Energy 29 (2004) 715–720. https://doi.org/10.1016/j.ijhydene.2003.09.002.

[57] Y. Nakashimada, M.A. Rachman, T. Kakizono, N. Nishio, Hydrogen production of Enterobacter aerogenes altered by extracellular and intracellular redox states, International Journal of Hydrogen Energy 27 (2002) 1399–1405. https://doi.org/10.1016/S0360-3199(02)00128-3.

[58] S. Tanisho, Y. Suzuki, N. Wakao, Fermentative hydrogen evolution by Enterobacter aerogenes strain E.82005, International Journal of Hydrogen Energy 12 (1987) 623–627. https://doi.org/10.1016/0360-3199(87)90003-6.

[59] S. Tanisho, N. Wakao, Y. Kosako, Biological hydrogen production by Enterobacter aerogenes., J. Chem. Eng. Japan / JCEJ 16 (1983) 529–530. https://doi.org/10.1252/jcej.16.529.

[60] N. Kumar, D. Das, Continuous hydrogen production by immobilized Enterobacter cloacae IIT-BT 08 using lignocellulosic materials as solid matrices, Enzyme and

Microbial Technology 29 (2001) 280–287. https://doi.org/10.1016/S0141-0229(01)00394-5.

[61] N. Kumar, D. Das, Enhancement of hydrogen production by Enterobacter cloacae IIT-BT 08, Process Biochemistry 35 (2000) 589–593. https://doi.org/10.1016/S0032-9592(99)00109-0.

[62] E.W.J. Van Niel, P.A.M. Claassen, A.J.M. Stams, Substrate and product inhibition of hydrogen production by the extreme thermophile,Caldicellulosiruptor saccharolyticus, Biotechnol. Bioeng. 81 (2003) 255–262. https://doi.org/10.1002/bit.10463.

[63] S.A. Van Ooteghem, S.K. Beer, P.C. Yue, Hydrogen Production by the Thermophilic Bacterium Thermotoga neapolitana, in: M. Finkelstein, J.D. McMillan, B.H. Davison (Eds.), Biotechnology for Fuels and Chemicals, Humana Press, Totowa, NJ, 2002: pp. 177–189. https://doi.org/10.1007/978-1-4612-0119-9_14.

[64] M. Abo-Hashesh, P.C. Hallenbeck, Fermentative Hydrogen Production, in: P.C. Hallenbeck (Ed.), Microbial Technologies in Advanced Biofuels Production, Springer US, Boston, MA, 2012: pp. 77–92. https://doi.org/10.1007/978-1-4614-1208-3_5.

[65] H.H.P. Fang, H. Liu, Effect of pH on hydrogen production from glucose by a mixed culture, Bioresource Technology 82 (2002) 87–93. https://doi.org/10.1016/S0960-8524(01)00110-9.

[66] C. Lin, C. Cheng, Fermentative hydrogen production from xylose using anaerobic mixed microflora, International Journal of Hydrogen Energy 31 (2006) 832–840. https://doi.org/10.1016/j.ijhydene.2005.08.010.

[67] S. Roy, S. Ghosh, D. Das, Improvement of hydrogen production with thermophilic mixed culture from rice spent wash of distillery industry, International Journal of Hydrogen Energy 37 (2012) 15867–15874. https://doi.org/10.1016/j.ijhydene.2012.08.016.

[68] L. Zhang, J. Li, Q. Ban, J.H. and A.K. Jha, Metabolic Pathways of Hydrogen Production in Fermentative Acidogenic Microflora, 22 (2012) 668–673. https://doi.org/10.4014/jmb.1110.10076.

[69] S. Chen, K. Lee, Y. Lo, W. Chen, J. Wu, C. Lin, J. Chang, Batch and continuous biohydrogen production from starch hydrolysate by Clostridium species, International Journal of Hydrogen Energy 33 (2008) 1803–1812. https://doi.org/10.1016/j.ijhydene.2008.01.028.

[70] C.C.J. Leung, A.S.Y. Cheung, A.Y.-Z. Zhang, K.F. Lam, C.S.K. Lin, Utilisation of waste bread for fermentative succinic acid production, Biochemical Engineering Journal 65 (2012) 10–15. https://doi.org/10.1016/j.bej.2012.03.010.

[71] A. Pandey, J.-S. Chang, P.C. Hallenbeck, C. Larroche, Biohydrogen, 1st. edition, Elsevier, Amsterdam Boston, 2013.

[72] K. Nath, D. Das, Effect of light intensity and initial pH during hydrogen production by an integrated dark and photofermentation process, International Journal of Hydrogen Energy 34 (2009) 7497–7501. https://doi.org/10.1016/j.ijhydene.2008.11.065.

[73] L. Cabrol, A. Marone, E. Tapia-Venegas, J.-P. Steyer, G. Ruiz-Filippi, E. Trably, Microbial ecology of fermentative hydrogen producing bioprocesses: useful insights for driving the ecosystem function, FEMS Microbiology Reviews 41 (2017) 158–181. https://doi.org/10.1093/femsre/fuw043.

[74] K. Chandrasekhar, Y.-J. Lee, D.-W. Lee, Biohydrogen Production: Strategies to Improve Process Efficiency through Microbial Routes, IJMS 16 (2015) 8266–8293. https://doi.org/10.3390/ijms16048266.

[75] E. Tapia-Venegas, J.E. Ramirez-Morales, F. Silva-Illanes, J. Toledo-Alarcón, F. Paillet, R. Escudie, C.-H. Lay, C.-Y. Chu, H.-J. Leu, A. Marone, C.-Y. Lin, D.-H. Kim, E. Trably, G. Ruiz-Filippi, Biohydrogen production by dark fermentation: scaling-up and technologies integration for a sustainable system, Rev Environ Sci Biotechnol 14 (2015) 761–785. https://doi.org/10.1007/s11157-015-9383-5.

[76] P.C. Hallenbeck, Fundamentals of the fermentative production of hydrogen, Water Science and Technology 52 (2005) 21–29. https://doi.org/10.2166/wst.2005.0494.

[77] P.C. Hallenbeck, D. Ghosh, Advances in fermentative biohydrogen production: the way forward?, Trends in Biotechnology 27 (2009) 287–297. https://doi.org/10.1016/j.tibtech.2009.02.004.

[78] S. Mohanraj, A. Pandey, S. Venkata Mohan, K. Anbalagan, S. Kodhaiyolii, V. Pugalenthi, Metabolic Engineering and Molecular Biotechnology of Biohydrogen Production, in: Biohydrogen, Elsevier, 2019: pp. 413–434. https://doi.org/10.1016/B978-0-444-64203-5.00017-4.

[79] P. Hallenbeck, Biological hydrogen production; fundamentals and limiting processes, International Journal of Hydrogen Energy 27 (2002) 1185–1193. https://doi.org/10.1016/S0360-3199(02)00131-3.

[80] P. Rai, A. Pandey, A. Pandey, In-silico-mining of small sequence repeats in hydrogenase maturation subunits of E. coli, clostridium, and Rhodobacter,

International Journal of Hydrogen Energy 44 (2019) 17813–17822. https://doi.org/10.1016/j.ijhydene.2019.05.057.

[81] M. Winkler, J. Esselborn, T. Happe, Molecular basis of [FeFe]-hydrogenase function, Biochimica et Biophysica Acta (BBA) - Bioenergetics 1827 (2013) 974–985. https://doi.org/10.1016/j.bbabio.2013.03.004.

[82] X. Zhao, Z. Wang, X. Zhou, N. Qi, F. Chen, D. Li, X. Li, Full length obtains of hydA and phylogenetic analysis of bio-hydrogen production new species of Clostridium based on efficient hydA degenerate primers, International Journal of Hydrogen Energy 44 (2019) 29493–29499. https://doi.org/10.1016/j.ijhydene.2019.05.050.

[83] D.W. Mulder, E.S. Boyd, R. Sarma, R.K. Lange, J.A. Endrizzi, J.B. Broderick, J.W. Peters, Stepwise [FeFe]-hydrogenase H-cluster assembly revealed in the structure of HydAΔEFG, Nature 465 (2010) 248–251. https://doi.org/10.1038/nature08993.

[84] Y. Asada, Y. Koike, J. Schnackenberg, M. Miyake, I. Uemura, J. Miyake, Heterologous expression of clostridial hydrogenase in the cyanobacterium Synechococcus PCC7942, Biochimica et Biophysica Acta (BBA) - Gene Structure and Expression 1490 (2000) 269–278. https://doi.org/10.1016/S0167-4781(00)00010-5.

[85] P. Berto, S. D'Adamo, E. Bergantino, F. Vallese, G.M. Giacometti, P. Costantini, The cyanobacterium Synechocystis sp. PCC 6803 is able to express an active [FeFe]-hydrogenase without additional maturation proteins, Biochemical and Biophysical Research Communications 405 (2011) 678–683. https://doi.org/10.1016/j.bbrc.2011.01.095.

[86] S. Reissmann, E. Hochleitner, H. Wang, A. Paschos, F. Lottspeich, R.S. Glass, A. Böck, Taming of a Poison: Biosynthesis of the NiFe-Hydrogenase Cyanide Ligands, Science 299 (2003) 1067–1070. https://doi.org/10.1126/science.1080972.

[87] M. Bruschi, C. Greco, L. Bertini, P. Fantucci, U. Ryde, L.D. Gioia, Functionally Relevant Interplay between the Fe_4S_4 Cluster and CN^- Ligands in the Active Site of [FeFe]-Hydrogenases, J. Am. Chem. Soc. 132 (2010) 4992–4993. https://doi.org/10.1021/ja1008773.

[88] J.M. Kuchenreuther, J.A. Stapleton, J.R. Swartz, Tyrosine, Cysteine, and S-Adenosyl Methionine Stimulate In Vitro [FeFe] Hydrogenase Activation, PLoS ONE 4 (2009) e7565. https://doi.org/10.1371/journal.pone.0007565.

[89] S.E. McGlynn, E.M. Shepard, M.A. Winslow, A.V. Naumov, K.S. Duschene, M.C. Posewitz, W.E. Broderick, J.B. Broderick, J.W. Peters, HydF as a scaffold protein in [FeFe] hydrogenase H-cluster biosynthesis, FEBS Letters 582 (2008) 2183–2187. https://doi.org/10.1016/j.febslet.2008.04.063.

[90] Y. Nicolet, C. Piras, P. Legrand, C.E. Hatchikian, J.C. Fontecilla-Camps, Desulfovibrio desulfuricans iron hydrogenase: the structure shows unusual coordination to an active site Fe binuclear center, Structure 7 (1999) 13–23. https://doi.org/10.1016/S0969-2126(99)80005-7.

[91] Y. Nicolet, C. Cavazza, J.C. Fontecilla-Camps, Fe-only hydrogenases: structure, function and evolution, Journal of Inorganic Biochemistry 91 (2002) 1–8. https://doi.org/10.1016/S0162-0134(02)00392-6.

[92] A.S. Pandey, T.V. Harris, L.J. Giles, J.W. Peters, R.K. Szilagyi, Dithiomethylether as a Ligand in the Hydrogenase H-Cluster, J. Am. Chem. Soc. 130 (2008) 4533–4540. https://doi.org/10.1021/ja711187e.

CHAPTER 2

LITERATURE REVIEW

Declaration: Some part of this chapter has been published in the following book chapters:

Anand, A., Kumar, K., Moholkar, V.S. (2024). Various Routes for Hydrogen Production and Its Utilization for Sustainable Economy. In: Soccol, C.R., Brar, S.K., Permaul, K., Pakshirajan, K., de Carvalho, J.C. (Eds.) *Biohydrogen - Advances and Processes. Biofuel and Biorefinery Technologies*, vol 13. Springer, Cham. https://doi.org/10.1007/978-3-031-49818-3_20

Anand A, Umesh, Moholkar VS (2024) Chapter 3: Biohydrogen production from microbial fermentation of organic wastes. In: Nanda S, Dalai AK, Goud VV (Eds.) *Emerging Biofuels*. Elsevier, pp. 27–52 https://doi.org/10.1016/B978-0-323-99547-4.00011-3

2.1 Introduction

As noted in the previous chapter, bioH_2 produced through the fermentative route from cheap substrates like lignocellulosic biomass, dairy waste, food waste etc. holds high potential as a clean and sustainable fuel. However, large-scale production and commercialization of bioH_2 requires significant research and development efforts to overcome the bottlenecks. Both kinetics and yields of dark fermentation need to be improved to meet the requirements for commercial implementation. Different physical and biological parameters affect the yields of the dark fermentation process. The nature of the effects of these parameters on the fermentation process and interactions among them need to be properly identified. Optimization of the process parameters using the conventional statistical design of experiments (DoE) techniques is a versatile tool. Moreover, the use of modern-day tools of artificial intelligence can further help in the selection of the best combination of process parameters for the highest bioH_2 yield in a given system. Secondly, the pretreatment of the substrates prior to fermentation for their conversion to monomeric sugars is also an important step. Enhancing the kinetics and energy efficiency of this process is vital for the economy of large-scale bioH_2 production.

The yield and kinetics of dark fermentation can also be enhanced using biological routes such as synthetic biology and metabolic engineering. Understanding and analysis of the metabolic pathways of the microorganisms and the enzymes involved is also crucial for enhancing the bioH_2 yields with minimization of the formation of other metabolites. Metabolic flux analysis is a useful tool for understanding the complex metabolic pathways and genetic modifications (selection of specific genes for deletion) for enhancing bioH_2 production.

This thesis is aimed at investigating the process engineering as well as fundamental (metabolic) aspects of bioH_2 production through dark fermentation using food waste as substrate. Significant literature has already been published addressing these issues. In this chapter, we have reviewed the previous literature and have tried to present a critical analysis of the same. On the basis of this analysis, we have decided on the major objectives and methodologies of the thesis.

2.2 Routes of biohydrogen production in dark fermentation

The glycolysis pathway converts glucose to pyruvic acid (pyruvate) during anaerobic fermentation. Pyruvate is then transformed to acetyl-CoA, which may serve as feed for anaerobic bacteria, such as *C. butyricum*, to produce H_2 and CO_2. Alternatively, several microbes may convert acetyl-CoA to alcohols (e.g., ethyl alcohol) and acids (e.g., acetate and butyrate) under distinct circumstances. Butyric acid and acetic acid are made from NADH. Excess NADH is converted to NADP, which releases H_2. Hydrogen fermentation may be classified into three forms based on the content of the final product: (i) H_2 fermentation with butyric acid and acetic acid (mixed acid route), (ii) H_2 fermentation with propionic acid, and (iii) ethanol-type H_2 fermentation.

H_2 fermentation with butyric acid and acetic acid: Some *Clostridium* species, e.g., *C. pasteurianum*, *C. butyricum*, and *C. acetobutylicum*, carry out this form of H_2 fermentation under anaerobic conditions. During H_2 fermentation with butyrate formation, simple carbohydrates (e.g., hexose, sucrose, starch) are being metabolized to form CO_2, H_2, butyrate, acetate, and a very small amount of propionate as end-products. The main reactions are:

$$C_6H_{12}O_6 + 2\,H_2O \rightarrow 2\,CH_3COOH + 2\,CO_2 + 4\,H_2 \quad (2.1)$$

$$C_6H_{12}O_6 \rightarrow C_4H_9COOH + CO_2 + 2\,H_2 \quad (2.2)$$

Propionic acid-type fermentation: Fermentation of this type takes place during the anaerobic treatment of sewage, which contains more nitrogenous compounds (e.g., gelatin, beef extract, and yeast extract). Complex carbohydrates that are difficult to break down (e.g., cellulose) frequently undergo H_2 fermentation with propionic acid production in the absence of oxygen. The most commonly used bacteria for this sort of fermentation are *Propionibacterium*. Another essential feature of these bacteria is that they do not have the hydrogenase enzyme. As a result, in

propionic acid-type fermentation, no hydrogen is produced. This type of fermentation produces propionate and acetate as end-products.

Ethanol type H_2 fermentation: In this fermentation method, carbohydrates are first converted to pyruvic acid by *Saccharomyces cerevisiae*. The pyruvic acid is transformed to acetaldehyde and eventually ethanol or ethyl alcohol via the EMP or Entner–Doudoroff pathway. However, the principal end-products of ethyl alcohol type H_2 fermentation are ethanol, acetic acid, H_2, CO_2, and a small amount of succinic acid and butyric acid. Table 2.1 presents a summary of the literature on different substrates utilized in the dark fermentative biohydrogen production process.

Table 2.1. Substrates used for the dark fermentative biohydrogen production

Substrate	Inoculum	Substrate concentration		Yield (mol/mol)	Reference
		Range	Optimal		
Xylose	*Municipal sewage sludge*	10-100 g/L	20 g/L	2.25	[1]
	Clostridium butyricum CGS5	6-35 g/L	20 g/L	-----	[2]
Glucose	*Seed sludge*	0-295 g/L	-----	2.2	[3]
	Digested sludge	1.1-300 g/L	2.1 g/L	3.2	[4]
	Ruminococcus albus	-----	------	2.5	[5]
	Enterobacter cloacae IIT-BT 08	----	-----	2	[6]
Sucrose	*C.butyricum CGS5*	5-35 g/L	20 g/L	2.8	[2]
	Thermoanaero-bacter Thermosaccharo-lyticum PSU-2	5.6-60 g/L	20 g/L	2.5	[7]
	E. cloacae IIT-BT 08	0-1 g/L	----	6	[8]
Starch	*Anaerobic sludge*	5-55 g/L	20 g/L	2.2	[9]
	Thermococcus kodakarensis KODI	2-12 g/L	----	1.9	[10]
	Municipal digester sludge	8-35 g/L	32 g/L	1.8	[11]

Non-fat dry milk	*Anaerobic digester sludge*	0-100 g COD/L	4 g-COD/L	0.005	[1]
Rice slurry	*Anaerobic digester sludge*	2.9-24 g-COD/L	5.9 g COD/L	346	[4]
Food waste	*Anaerobic sludge*	3.2-10 g-COD/L	6.4 g COD/L	1.8	[12]
	Anaerobic digester sludge	0-32 g COD/L	4.6 g COD/L	101	[13]
Beer less biomass	*Mixed culture from cow dung*	0-50 g/L	20 g/L	0.0003	[14]
Corn stalk wastes	*Mixed culture*	5-20 g/L	15 g/L	0.007	[15]
	Clostridium sp. X9	0-20 g/L	-----	0.006	[16]
	Mixed culture	-----	-----	0.005	[11]
Wheat straw	*Mixed culture from cow dung*	0-15 g/L	-----	0.003	[17]

2.3 Factors affecting biohydrogen production

2.3.1 Temperature

The efficiency of dark fermentation is a strong function of the temperature. Essentially, the growth and metabolic activities of the microorganisms involved in H_2 production are influenced by temperature. Depending on the type of microbial cultures, dark fermentation is carried out at varying temperature ranges as follows: 25-40°C for mesophilic cultures, 40-65°C for thermophilic cultures, 65-80 °C for extreme thermophilic cultures, and > 80°C for hyperthermophilic cultures [18]. Obviously, the optimum temperatures for dark fermentation are a function of specific organisms and substrates employed. However, the temperature range commonly considered favourable for hydrogen is between 25° to 45 °C [9]. At lower temperatures below the optimum range, the metabolic activity of the microorganism decreases, leading to reduced hydrogen production rates. The lower activity can be attributed to decreased enzyme activity and slower substrate degradation.

The microbial community may also experience reduced biomass production, resulting in lower hydrogen yields. Conversely, microorganisms' activity can also be negatively affected at higher temperatures, above the optimum range [5]. Excessive heat can lead to the denaturation of

enzymes and other proteins, inhibiting their functionality. This can result in decreased substrate utilization and hydrogen production. Additionally, high temperatures can favour the growth of competing microorganisms that are inefficient in hydrogen production, reducing the overall hydrogen yield [19]. The temperature also affects the composition of the microbial community involved in dark fermentative hydrogen production. Different temperature ranges can be selected for other microbial species; as certain microorganisms have optimal growth conditions at specific temperatures. Temperature changes can influence the dominance of certain microbial populations, affecting hydrogen production efficiency. Therefore, the temperature impacts the metabolic activity of microorganisms directly involved in hydrogen production and indirectly influences the system's microbial ecology. The temperature sensitivity of hydrogen production may vary depending on the specific microorganisms and substrates used. Some organisms are more resilient to temperature fluctuations and adapt to a broader temperature range.

In contrast, others may be more sensitive and have more specific temperature conditions for optimal performance. To optimize hydrogen production through dark fermentation, it is crucial to identify the temperature range that maximizes hydrogen yield for a given set of microorganisms and substrates. In conclusion, temperature is a critical factor influencing dark fermentative hydrogen production [20]. The optimal temperature range promotes the metabolic activity of microorganisms, enhances enzyme functionality, and facilitates efficient substrate utilization, leading to increased hydrogen production rates. However, deviations from the optimum temperature range can negatively impact microbial activity, enzyme functionality, and microbial community composition, reducing hydrogen yields. Therefore, careful temperature control and optimization are essential for maximizing dark fermentative hydrogen production efficiency [21,22].

2.3.2 pH

pH affects the metabolism of microbial cells and, thus, the hydrogen output. Glycolysis by facultative anaerobes produces hydrogen. Hydrogen output depends on the pyruvate breakdown metabolites. All enzymes have optimal activity at a specific pH range. Hydrogenase, a crucial enzyme, modulates its activity by pH [23]. Studies have reported that hydrogen production has been found to switch from an acidogenic to a solventogenic phase when the concentration of dissociated acids increases. This is because of the increased ionic strength of the medium [24]. At acidic pH, nonpolar undissociated acids in the media can cause inhibition via diffusion through cell membranes. Additionally, pH adjustment becomes crucial when mixed consortia or sludge is utilized as the inoculum to control the activity of hydrogen-consuming methanogens [99]. Due to the increased generation of acidic metabolites, hydrogen production decreases at low pH (below 5.0), which limits the cell's ability to maintain internal pH [26]. It reduces ATP production within the cell, which in turn reduces glucose uptake. Multiple investigations have indicated relatively higher hydrogen output at a media pH between 5 and 7 [27,28]. These investigations also report a reduction in hydrogen production at non-optimum pH levels. Therefore, it is crucial to regulate the pH to maximize hydrogen output.

2.3.3 Partial pressure of hydrogen

The partial pressure of hydrogen in the headspace above the fermentation mixture strongly affects hydrogen generation pathways. Hydrogen accumulation in the reactor headspace, as the fermentation proceeds, raises the hydrogen partial pressure. Le Chatelier postulated that an accumulation of hydrogen above the fermentation mixture would impede the forward reaction [29,30]. Thus, hydrogen production varies inversely with the hydrogen partial pressure in the fermenter. Concurrently, higher production of reduced metabolites (viz. butanol, lactate, acetone, and ethanol) is seen through changed metabolic pathways [15].

Biohydrogen production is influenced by hydrogen partial pressure by the following ways:

(1) ***Hydrogen solubility*:** As the partial pressure of H_2 increases, more H_2 molecules dissolve in water, making it available for microorganisms to utilize. This can enhance the biohydrogen production rate.

(2) ***Substrate availability*:** Microorganisms employ sugars or wastewater as carbon sources for biohydrogen generation. Hydrogen partial pressure impacts substrate availability. Higher hydrogen partial pressures block microbial processes, lowering metabolic activity and substrate utilization [31].

(3) ***Enzyme activity*:** Different enzymes are used by microorganisms to produce hydrogen gas. The activity of these enzymes can be affected by hydrogen partial pressure. High hydrogen partial pressures can decrease the biohydrogen production rate, limiting enzyme activity [32,33].

(4) ***Microbial competition*:** Multiple microbial species battle it out in biohydrogen production systems. The partial pressure of hydrogen can affect microbial community structure and dominance. A decrease in biohydrogen production could result from an increase in hydrogen-consuming bacteria due to a rise in the partial pressure of hydrogen [34].

(5) ***System design*:** The partial pressure of hydrogen can affect the design and operation of biohydrogen production systems. It influences factors like reactor configuration, gas-liquid mass transfer rates, and the selection of microbial strains. Optimization of these parameters is crucial to achieving efficient biohydrogen production [35].

2.3.4 Volatile fatty acids (VFAs)

Fermentative hydrogen production (and yield) is adversely affected by metabolic end products like ethanol, acetic acid, butyric acid, and propionic acid. As these end metabolites accumulate, they can impact the overall efficiency of biohydrogen production. The following factors contribute to this inhibitory effect [36,37]:

(1) ***Increase in ionic strength*:** Ionic strength of the medium increases with the concentration of soluble end metabolites. This increase in ionic strength can lead to cellular lysis. The lysis of

hydrogen-producing bacteria releases intracellular components into the medium, disrupting the balance within the system.

(2) ***Proton permeation*:** Protons can diffuse through the cell membrane of hydrogen-producing bacteria at higher concentrations of acidic metabolites. This proton influx interferes with the cell's physiological balance, affecting cellular functions and hydrogen production.

(3) ***Utilization of maintenance energy*:** Maintenance energy is utilized for the restoration of the physiological balance within the cell under inhibitory conditions. Maintenance energy refers to the energy required for essential cellular functions and survival. However, redirecting energy toward maintenance compromises bacterial growth and hydrogen production.

Previous authors have studied the inhibitory effect of VFAs and have reported that with the rise in VFA (acetic acid, propionic acid, butyric acid) concentration, the substrate degradation efficiency, rate of hydrogen production, and hydrogen yield are reduced significantly [38–40]. This suggests that higher concentrations of VFAs negatively impact the overall performance of the biohydrogen production system. It is important to note that these inhibitory effects can vary depending on the specific microorganisms and process conditions employed in fermentative hydrogen production.

2.3.5 Nutrients

Maintenance of sufficient quantities of phosphate, nitrogen, and other inorganic trace minerals is required while using carbohydrates as a substrate for H_2 production. Nitrogen is necessary for microorganism growth as it is a component of amino acids. Studies have shown that organic nitrogen sources are more suitable for hydrogen production than inorganic ones. For instance, supplementing starch with 0.1% (w/v) polypeptide resulted in 2.4 mol H_2/mol glucose hydrogen yield. However, using urea or other inorganic salts as nitrogen sources did not

significantly improve hydrogen production [41,42]. Notably, supplementation of the nitrogen source enhances H_2 yield, but also increases the production cost.

Consequently, researchers are exploring cheaper alternatives to substitute nitrogen sources in hydrogen production media, such as corn-steep liquor (produced during corn starch manufacturing), which is a cost-effective substitute for peptone as a nitrogen source [43].

2.3.6 Metal ions

(1) Metal ions, being cofactors for enzymes in hydrogen metabolism, play an important role in biohydrogen production. Here are some general effects of metal ions on biohydrogen production [44]. Cofactor for hydrogenase: Metal ions, such as iron (Fe) and nickel (Ni), act as cofactors for hydrogenase enzymes, which catalyze the conversion of protons to hydrogen gas. These metal ions are essential for the proper functioning and stability of hydrogenase enzymes, ensuring efficient hydrogen production [9,45].

(2) ***Electron transfer*:** Metal ions can participate in electron transfer reactions within the biohydrogen production pathway. They can facilitate the transfer of electrons between enzymes or from substrates to enzymes of the hydrogen metabolic pathway, thereby improving the overall efficiency of the process.

(3) ***Enzyme activity and stability*:** Metal ions can influence both the stability and activity of various enzymes involved in biohydrogen production. They can enhance the catalytic activity of enzymes by providing necessary cofactors and creating a favourable environment for enzyme-substrate interactions.

(4) ***Cellular transport processes*:** Metal ions are involved in cellular transport processes, including the uptake and transport of substrates and essential nutrients required for hydrogen

production. Proper availability and regulation of metal ions can ensure optimal metabolic activity and overall hydrogen yield.

(5) ***Redox reactions*:** Some metal ions, such as iron, can participate in redox reactions and act as electron carriers or mediators. They can facilitate electron transfer reactions between different redox-active species, contributing to the system's overall electron flow and hydrogen production. Supplementing suitable metal ions in the fermentation media is essential for any fermentative process. Metal ions play important role as enzyme cofactors and also in cellular transport processes. For example, the hydrogenase enzyme contains a bimetallic Fe-Fe centre encircled by FeS protein clusters. The previous authors have investigated the effect of Fe supplementation on biohydrogen production. Lee et al. [37] reported a positive influence of higher Fe ion concentrations on the system. With supplementation of 4000 mg/L $FeCl_2$, the maximum hydrogen production rate of 24 mL/g VSS/h was obtained.

Similarly, Mg^{2+} is an essential cofactor for many enzymes in glycolysis, such as phosphoglycerate kinase, hexokinase, and phosphofructokinase. Lay et al. [45] reported effect of various trace metals, viz. Zn, Na, Fe, K, Mg, I, Mn, Ni, Mo, and Ca, on hydrogen production using *C. pasteurianum*. Higher hydrogen production required suitable concentrations of Mg, Na, Zn, and Fe. These studies highlight the importance of metal ion supplementation, particularly iron and magnesium, in promoting efficient biohydrogen production.

2.3.7 Hydraulic Retention Time (HRT)

HRT influences the performance and efficiency of the bioreactor, and thus, is a critical factor in biohydrogen production. HRT refers to the duration for which the substrate or wastewater remains in the system. Here are the effects of HRT on H_2 production [15,46]:

(1) ***Hydrogen yield*:** HRT significantly impacts the hydrogen yield from the bioreactor. A longer HRT gives microorganisms more time to metabolize the organic substrates and convert

them into hydrogen gas. This prolonged contact time enhances the overall hydrogen production. The extended HRT allows microorganisms to utilize organic matter, producing higher hydrogen yields. However, it is essential to note that excessively long HRTs may lead to decreased yields due to the accumulation of inhibitory metabolic byproducts or substrate limitation.

(2) ***Substrate utilization*:** HRT affects the utilization of organic substrates for biohydrogen production. A longer HRT allows microorganisms to efficiently metabolize complex organic compounds and convert them into hydrogen gas. The extended contact time facilitates the complete breakdown of organic matter, ensuring optimal utilization and maximizing the hydrogen production potential. Conversely, shorter HRTs may limit substrate utilization as microorganisms have less time to convert the organic compounds. Incomplete substrate utilization can result in lower hydrogen yields.

(3) ***Microbial community dynamics*:** HRT influences the composition and dynamics of the microbial community involved in biohydrogen production. Different microorganisms have varying growth rates and metabolic activities. A longer HRT favours the growth and dominance of slower-growing hydrogen-producing microorganisms. These microorganisms have a better chance to compete for resources and establish themselves in the bioreactor, leading to increased hydrogen production. On the other hand, shorter HRTs may favour faster-growing microorganisms that produce other metabolic byproducts instead of hydrogen. This can alter the microbial community structure and reduce the hydrogen production potential [47].

(4) ***Scale-up considerations*:** HRT is a crucial parameter when scaling up biohydrogen production systems. Maintaining an appropriate HRT becomes even more critical as the system size increases. The HRT must be optimized for efficient substrate utilization, stable performance, and maximum hydrogen yield. The scale-up process requires careful adjustment of HRT to match the specific conditions and requirements of the more extensive system. Improper HRT management during scale-up can decrease hydrogen production efficiency and compromise system stability [35,48,49].

In conclusion, HRT significantly influences biohydrogen production. A longer HRT generally leads to higher hydrogen yields, better substrate utilization, and stable reactor performance. It allows microorganisms sufficient time to metabolize organic substrates and produce hydrogen gas. However, finding the optimal HRT requires careful consideration of substrate characteristics, microbial community dynamics, and system scalability. Balancing these factors will help maximize biohydrogen production efficiency and stability.

2.4 Biohydrogen production from different organic wastes

Biohydrogen production from organic waste is an innovative and sustainable approach that harnesses the power of microorganisms to convert organic materials into hydrogen gas. This process, known as microbial fermentation, offers numerous environmental and energy-related benefits. Organic waste, including agricultural residues, food waste, and wastewater, contains complex organic compounds that specific microorganisms can use as a carbon source. These microorganisms break down the organic matter without oxygen through anaerobic fermentation, producing hydrogen gas as a metabolic byproduct. One of the critical advantages of biohydrogen production from organic waste is its potential to mitigate environmental issues associated with waste disposal. Instead of ending up in landfills, where organic waste contributes to generating greenhouse gases and leachate, it can be diverted to biohydrogen production facilities. This reduces waste accumulation and decreases the release of harmful substances into the environment. Moreover, biohydrogen is considered a clean and renewable energy source. When combusted, hydrogen gas produces only water vapor as a byproduct, making it an environmentally friendly alternative to conventional fossil fuels. Utilizing organic waste for biohydrogen production can simultaneously address waste management challenges and contribute to the transition toward a greener and more sustainable energy system.

Efforts in R&D are focused on developing more effective biohydrogen production processes, increasing the yield of hydrogen gas, and investigating the viability of various forms

of organic waste as feedstocks. Opportunities have emerged due to developments in genetic engineering and biotechnology for improving the efficiency of hydrogen-producing microorganisms and developing specialized microbial communities.

2.4.1 Industrial waste

Waste products from many industries, especially the agricultural and food industries, have high starch and cellulose contents, which essentially are carbohydrates. These solid wastes can be used for hydrogen gas production. Acid and enzymatic hydrolysis of these wastes can produce monomeric fermentable sugars, which can be converted to organic acids and biohydrogen gas. The lignocellulosic agricultural waste requires additional pretreatment. Size reduction and chemical delignification of agricultural waste is necessary before fermentation. Such wastes contain cellulose and hemicellulose, which can be hydrolyzed to produce monomeric sugars, and which can be fermented to organic acid and hydrogen gas. The lignin content of biomass is known to adversely impact enzymatic hydrolysis [50]. A schematic of biohydrogen production from lignocellulosic agro wastes is shown in Fig. 2.1. Biohydrogen production yields from continuous and dark fermentation of carbohydrates reported in previous literature are summarized in Table 2.2.

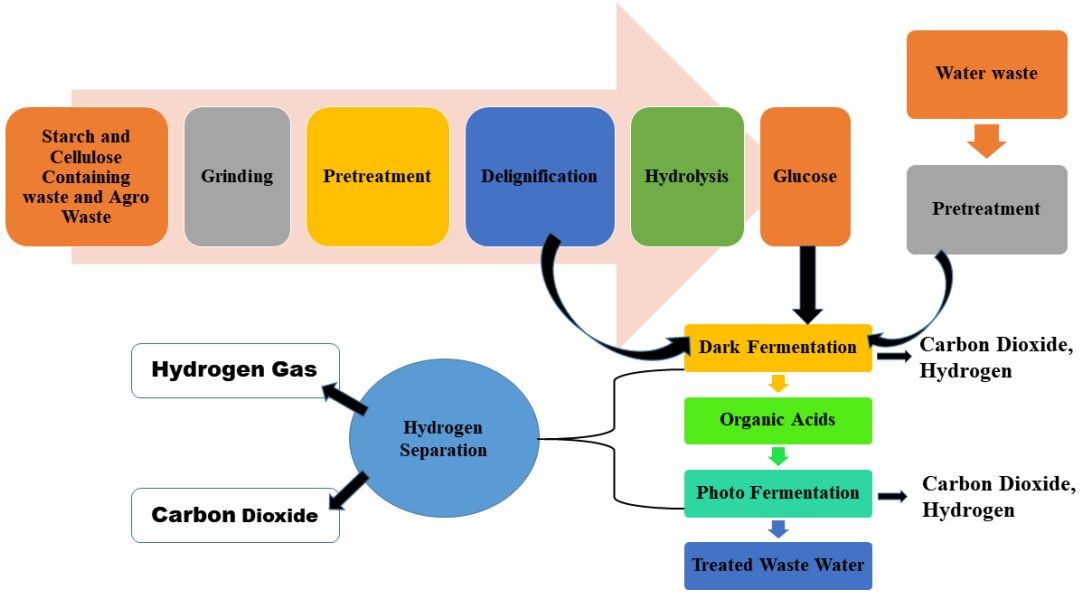

Fig. 2.1. A schematic of biohydrogen production from industrial wastes

Table 2.2: Biohydrogen production: continuous and batch dark fermentation of carbohydrates

Carbon source	Microorganism	Hydrogen yield	Reactor	References
Sugar beet juice	Mixed culture	1.7 mol/mol hexose	Batch	[10]
Glucose (13.7 g/L)	Mixed culture	1.2 mol/mol glucose	Trickling biofilter	[51]
Potato starch (1 g COD/L)	Mixed culture	0.59 mol/mol	Batch	[52]
Cellulose (5 g/L)	*Thermoanaerobacterium*	102	Batch	[53]
Starch (6 kg /m^3)	Mixed culture	1.29 L/g starch COD	CSTR	[45]
Starch (2%)	*E. aerogenes + C. butyricum*	2.6 mol/mol glucose	Immobilized	[54]
Lactose (29 mmol/L)	*C. termolacticum*	3 mol/mol lactose	CSTR	[55]
Starch (5 g/L)	*T. kodakaraensis KOD1*	3.33 mol/mol starch	Gas-lift Fermenter	[56]
Wheat starch (10 g/L)	Mixed culture	0.83 mol/mol starch	CSTR	[57]
Glucose	*C. acetobutyricum*	2 mol/mol glucose	Fed-batch	[58]
Microcristalline cellulose (25 g/L)	*Clostridium species*	2.18 mmol/g cellulose	Batch	[59]
Glucose (20 g COD/L)	*Clostridia sp.*	1.7 mol/mol glucose	CSTR	[9]
Sucrose (50 mM)	*Klebsiella oxytoca HP1*	3.6 mol/mol sucrose	CSTR	[60]

*CSTR (Continuous stirred tank reactor)

2.4.2 Sewage sludge

Wastewater treatment plant sludge contains a high quantity of carbohydrates and protein. When sludge was utilized as raw material for biohydrogen production, the yield was 0.6 mol/kg COD [61] and 1.2 mg H_2/g COD. The filtrate, however, produced larger biohydrogen yields (15 mg H_2/g COD) [62]. The soluble COD was raised in the pretreated sludge, which also boosted the hydrogen output (0.9 mmol/g dried sludge) [62]. Biohydrogen production yield from food industry wastewater is described in Table 2.3.

Table 2.3. Biohydrogen production from food industry waste: Photo-fermentation

Wastewater	Organism	Dilution (%)	Operation	Hydrogen Yield	References
Sugar refinery effluent with maleic acid	*R. sphaeroides* OU001	20	Batch	13.44 L/mol C	[63]
Tofu WW	*R. sphaeroides*	--	Immobilized	0.24 mL/mg Sugar	[64]
Sugar refinery effluent with maleic acid	*R. sphaeroides* OU001	20	Continuous	11.67 L/mol	[63]

2.4.3 Starch-based organic waste

Starch-based biomass, which includes crops like wheat, corn, rice, food waste, cassava, and potatoes, is abundant and rich in starch, a polysaccharide used by plants to store energy. Glucose molecules in starch are linked together by α (1→4) glycosidic bond, which can be hydrolyzed relatively easily than the β-1,4-glycosidic bonds in cellulose. Thus, starch-based biomass can be easily converted into fermentable monomeric sugars via enzymatic or acid saccharification [42]. The biodegradability of starch-based biomass makes it particularly suitable for anaerobic fermentation processes. Unlike cellulose-based biomass, starch-based biomass does not require extensive pretreatment and can undergo fermentation with milder processing. This characteristic makes it more favorable for biological applications and holds great potential for economic biofuel production, including biohydrogen [33,57]. Various types of starch, including wheat, rice, potato, cassava, cornstarch, and starch-rich residues like bread, sago, and brewery residues, have been

explored as potential feedstock for hydrogen production [65]. The utilization of starch-based biomass in hydrogen production offers several advantages. Starch can be easily broken down into fermentable sugars, which can then be converted into hydrogen gas through microbial processes. This renewable and sustainable approach holds promise for clean energy production. Overall, starch-based biomass presents opportunities for traditional biofuel production via fermentation, such as methane and ethanol, and emerging clean fuels like hydrogen production. Its abundance, biodegradability, and ease of conversion into simple sugars make it a preferred choice for economic and sustainable biofuel production.

2.5 Strategies for intensification of bioH_2 production

Previous research in intensification of organic waste fermentation for bioH_2 production has adopted several techniques: optimization of process parameters and media components, use of genetically modified microbial strain, efficient reactor design and better fermentation protocols etc. Each of these techniques are discussed below in detail.

2.5.1 *Process parameters optimization*

Until recently, no genetic tools were available for *C. pasteurianum*. Therefore, early research efforts were limited to culture optimization and the deployment of chemical mutagens as a means to isolate the strains with favorable phenotypes. Fermentative bioH_2 production is influenced by various factors such as substrate concentration, temperature, initial pH of media, media components, inoculum size, aeration and reactor type. These factors indirectly affect the activity of enzymes responsible for bioH_2 production, such as hydrogenase, pyruvate formate lyase, and formate hydrogen lyase. In this regard, previous literature exists on an increase or decrease in bioH_2 yield due to the above factors [66–68]. An optimum range is defined for all factors, such as an appropriate range of substrate concentration, which may enhance the bioH2 yield, while higher concentrations may inhibit or decrease the yield. Similarly, media components

such as nitrogen, phosphate, and metal ions, which are essential for the activity of enzymes responsible for bioH_2 production and the growth of bacteria, should also be maintained in the optimum range. Temperature and pH are critical factors that dramatically affect the bioH_2 production rate. An optimum range of pH and temperature is required for all enzymes and cofactors of bacteria to be active. Thus, optimization of parameters is a key technique to obtain maximum yields. The effect of various factors and their optimum range can be evaluated by experimental design methods including one factor at a time design, Taguchi design, full factorial design, Plackett-Burman design, Box-Behnken design (BBD), and central composite design (CCD). Many optimization studies have been reported for bioH_2 production using response surface methodology (RSM), which is a popular method to evaluate the individual effect of variables as well as interactive effects among the variables with minimum error [66]. In this process certain factors are selected and their individual effects are monitored as a response of interest, followed by the analysis of experimental results. Box-Behnken design (BBD) and central composite design (CCD) are used to estimate the relationship between response and the key factors and evaluate the optimum values based on a second-order polynomial. The second-order polynomial can be displayed as a contour plot or a surface plot. Based on the analysis of variance (ANOVA) of the model, we can determine the factors that have significant effects on the response.

Very few authors have dealt with bioH_2 production from food waste using *Clostridium* species [69,70]. Authors have adopted a non-statistical approach for optimization of bioH_2 production, and hence their study does not reveal the global optimum parameters for bioH_2 production from *Clostridium species*. Moreover, the relative influence (insignificant/significant) of each optimization parameter on bioH_2 production, and the interactions among the parameters are also not revealed in their study.

2.5.2 *Optimization by artificial intelligence*

Artificial Intelligence (AI) is a branch of computer science dedicated to creating intelligent machines that emulate human-like behavior and functionality. The production processes for bioH_2 are intricately complex, resulting in highly nonlinear relationships between dependent and independent variables. Numerous studies have emphasized that AI surpasses traditional statistical approaches when modeling biological processes [71,72]. AI-based modeling tools excel in articulating intricate relationships among variables and generating fitness functions that optimization tools can solve, ultimately leading to the identification of optimized conditions for bioH_2 production. AI offers diverse modeling tools, particularly emphasizing the effectiveness of artificial neural network (ANN) in modeling nonlinear systems [66,73].

2.5.3 Metabolic flux analysis

Metabolic flux analysis (MFA) is a technique for the assessment of intracellular metabolic fluxes in a biological system with central importance to maximize the product yield or to analyse in priori, the effect of targeted genetic modification on the product formation [74]. If the measured fluxes are not sufficient to determine all intracellular fluxes, optimization approaches are applied. This method was mainly established by Edwards et al [75] and was named flux balance analysis (FBA). The analysis of possible metabolic routes falls into metabolic network analysis (MNA). MFA technique has been applied to optimize the production of lysine [76], acetate [77], ethanol [78], biohydrogen [79] etc. In order to achieve high bioH_2 production yield, an extensive analysis and understanding of metabolic pathways in bioH_2 producing microorganisms is required, which may further aim to redesign or redirect metabolic pathways towards maximum product formation. The intracellular metabolic fluxes could be calculated by using mass balances across metabolites, stoichiometric reaction models as well as thermodynamics. MFA has been extensively applied in most research over the past decade in predicting changes in the fluxes and rate limiting steps of the specific pathway.

Although MFA has been applied to a few case studies of Clostridium species to study the effect of environmental conditions on bioH_2 yield [79], to the best of our knowledge, a detailed investigation of metabolic pathway fluxes of fermentative bioH_2 production using *Clostridium pasteurianum* from food waste hydrolysate was not found in the literature.

2.5.4 Intensification of fermentation: Role of ultrasound

Sonication or irradiation of fermentation with low to medium intensity ultrasound is a useful physical technique for intensification of the fermentation and other enzymatic reactions [79–81].

Ultrasound is a sound wave having a frequency higher than the upper limit of human hearing range (20 kHz). The frequency limit of ultrasound ranges from 20 kHz to 20 MHz. Ultrasonic waves are essentially longitudinal waves that propagate in a medium with alternating rarefaction and compression. Propagation of an ultrasound wave creates a variation in the bulk pressure in the medium. The secondary effect of sonication (or ultrasound wave irradiation) is cavitation. Cavitation phenomenon can be defined as nucleation, growth, oscillation, and implosive collapse of vapor or gas bubbles in the medium under the bulk pressure variation created due to sonication. Vapor bubbles are generated only under very high intensity of the ultrasound waves when the bulk pressure falls below the vapor pressure of the liquid medium. For low to mild intensities of ultrasound, the cavitation mainly occurs through gas nuclei present in the medium. These nuclei could be very small bubbles already present in the medium or these could be gas pockets trapped in the crevices of solid boundaries in the medium. These nuclei grow into cavitation bubbles under the influence of variation in the bulk pressure in the medium (the rarefaction half-cycle of ultrasound, when the bulk pressure is lowered below the static pressure).

The radial motion of the cavitation is influenced by the pressure amplitude or intensity of the ultrasound waves. If the pressure amplitude of the ultrasound is higher than the static pressure in the medium (which, in most cases, is the atmospheric pressure), the bubble grows to a size with its radius several times its original value in the rarefaction half cycle of ultrasound. Under these

conditions, the collapse of the bubble during the compression half cycle of ultrasound is dominated by the inertial forces. As the bubble contracts with rising static pressure, it creates a void around itself, in which the surrounding fluid elements gush in with high velocity and impart kinetic energy to the collapsing bubble. This phenomenon is essentially equivalent to adiabatic compression of a closed system comprising non-condensable gas on which work is done by the surrounding liquid. As a result, the bubble is compressed to a very small size, with a radius just a small fraction of the original value. The temperature and pressure inside the bubble reach very high – of the order of ~ 1000 bar and ~ 5000 K.

The expansion of the bubble during the rarefaction half cycle is also accompanied by evaporation of the liquid at the gas-liquid interface of the bubble. The vapor molecules diffuse towards the core of the bubble as the bubble keeps expanding. During the ensuing compression phase, the vapor molecules in the bubble diffuse backwards towards the gas-liquid interface or the bubble wall. However, the compression of the bubble is extremely fast (or transient), and not all vapor molecules can diffuse back and condense at the bubble wall. Some molecules get "entrapped" inside the bubble. These vapor molecules, along with the gas molecules (for example, nitrogen and oxygen molecules for an air bubble), are subjected to the extreme temperature and pressure generated in the bubble. At extreme temperatures and pressures, these molecules undergo thermal dissociation to generate radicals and other species inside the bubble. The bubble may get fragmented at the point of minimum radius (or maximum compression), which causes the release of these species into the bulk medium. The radical species generated during the transient collapse of a cavitation bubble induce and accelerate several chemical reactions in the medium. This phenomenon is popularly known as "sonochemical effect" and the chemical reactions induced by sonication (or transient cavitation) are called "sonochemistry".

Fig. 2.2 gives a schematic representation of the ultrasound wave propagation and transient cavitation phenomenon, as described above.

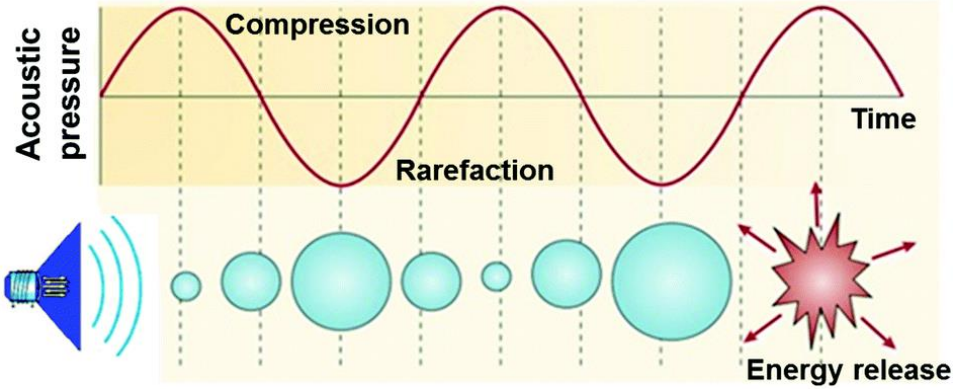

Fig 2.2: Bubble growth and collapse in a liquid irradiated with ultrasound, adopted from Sarma et al [68].

Physical effects of ultrasound and cavitation

The phenomena of ultrasound irradiation (or sonication) and cavitation also have various physical effects. The main manifestation of these physical effects is the generation of intense micro-convection and micromixing in the medium. A brief description of the physical effects of ultrasound and cavitation is given below [82].

Microstreaming: It can be defined as the small-amplitude oscillatory motion of fluid elements around a mean position, which is induced by the propagation of an ultrasound wave. For a typical ultrasound wave with a pressure amplitude of 120 kPa in water (ρ =1000 kg/m^3), C =1500 m/s), microstreaming velocity = 0.08 m/s.

Acoustic streaming: During the transmission of an ultrasound wave, the momentum of the wave is absorbed by the medium due to finite viscosity. This results in the setting up of low-velocity unidirectional currents of the fluid known as acoustic streaming [83].

***Microturbulence*:** The oscillatory motion of fluid induced due to volume oscillations of the cavitation bubble is called microturbulence. This phenomenon is explained as follows: in the expansion phase of the radial motion of a cavitation bubble, the liquid is displaced away from the bubble interface. During the collapse phase, the liquid is pulled towards the bubble as it fills the

vacuum in the liquid with size reduction of the bubble. The mean velocity of microturbulence depends on the amplitude of bubble oscillations.

Acoustic (shock) waves: As the cavitation bubble contracts during the compression phase of radial motion, void space is created in the liquid, and the fluid element spherically converges in this void space, and work is done on the bubble. For a cavitation bubble containing non-condensable gas such as air, the adiabatic compression results in the rapid rise of pressure inside the bubble. At the point of minimum radius (or maximum compression), the bubble wall comes to a sudden halt. In this instance, fluid elements converging towards the bubble are reflected from the interface. This reflection creates a high-pressure shock wave that propagates through the medium. The pressure exerted by the non-condensable gas inside the bubble causes the rebound of the bubble.

Microjets: As long as the motion of liquid in the vicinity of the cavitation bubble is symmetric and uniform. It maintains spherical geometry during radial motion driven by an ultrasound wave, and thus, there are no pressure gradients. If the bubble is located close to a phase boundary, either solid–liquid, gas–liquid, or liquid-liquid, the motion of liquid in its vicinity is hindered, resulting in the development of a pressure gradient around it. This non-uniformity of pressure results in the loss of spherical geometry of the bubble. During the asymmetric radial motion, the portion of the bubble exposed to higher pressure collapses faster than the rest of the bubble, which gives rise to the formation of a high-speed liquid jet directed towards the boundary. The velocity of these microjets has been estimated in the range of 120-150 m/s [84], and they cause severe damage at the point of impact (leading to effects like particle size reduction, microbial cell disruption, degradation of polymer chains etc.). In the case of metal surfaces, these micro jets can cause erosion of the surface.

A review of the literature indicates that the use of ultrasound directly during the fermentation process to enhance bioH_2 production is rare. Most studies focus on the application of ultrasonication as a pretreatment method, either for inoculum or for substrate, such as biomass. For example, ultrasonic pretreatment of palm oil mill effluent (POME) has been shown to increase hydrogen yield by 38% compared to non-sonicated treatments. To date, only few study, conducted by Hsia et al.[85] and Sarma et al.[79], had applied ultrasound to intensify fermentative bioH_2 production.

2.6 Research gaps in fermentative hydrogen production from food waste

BioH_2 production from food waste has been an active area of research for the past several years. However, there are several aspects of this process that have not been investigated in depth as yet. We have listed below some of these relatively less explored aspects.

(1) Multi-parametric statistical optimization of fermentation of food waste hydrolysate for the bioH_2 production that takes into account the interaction between process parameters.

(2) Advanced optimization of food waste hydrolysate fermentation using Artificial Intelligence (Artificial Neural Network) tools.

(3) Intensification of food waste hydrolysis using a suitable enzyme like α-glucoamylase and the fermentation of hydrolysate using the technique of sonication.

***Broad objectives of the present thesis*:** The present thesis has not only attempted to fill these research gaps, but has also tried to get a mechanistic insight into the influence of sonication on the kinetics of food waste hydrolysis and fermentation of hydrolysate. We have used molecular docking and dynamics simulation to investigate the biomechanics of ultrasound-assisted enzymatic hydrolysis, while for the ultrasound-assisted fermentation, we have employed metabolic flux analysis. In summary, this dissertation aims to provide both process engineering know-how and fundamental understanding of the beneficial effect of sonication on the synthesis of biohydrogen from food waste. The present thesis essentially addresses three Sustainability

Development Goals of the United Nations member states, viz., SDG 7 (Affordable and clean energy), SDG 12 (Responsible consumption and production patterns or circular economy) and SDG 13 (Climate action) by exploring hydrogen production through effective valorization of the food waste produced from different sources.

2.7 Outline of the present thesis

The present thesis comprises six chapters, the contents of which are summarized below:

Chapter 1 presents a general introduction to biohydrogen synthesis through microbial fermentation. In this chapter, general biochemistry, physiology, metabolic pathways, and enzymes involved in bioH_2 metabolism of microorganisms are discussed. Moreover, the docked structures of different hydrogenase enzymes in microbial cells are shown and discussed.

Chapter 2 includes a brief literature review on various aspects of hydrogen production by different microbial cultures and different optimization techniques for enhancing biohydrogen yield. The chapter concludes with research gaps, thesis outlines, and key highlights.

Chapter 3 presents studies in the hydrolysis of food waste using glucoamylase, which include statistical optimization of hydrolysis parameters using design of experiments, intensification of hydrolysis at optimum conditions using sonication, and mechanistic analysis of the ultrasound-induced enhancement of hydrolysis using molecular simulations.

Chapter 4 has addressed the optimization of biohydrogen synthesis from food waste hydrolysate. Initially, the optimization is carried out using statistical design of experiments (DoE). This is followed by further improvement of the bioH_2 yield in dark fermentation using an artificial neural network (ANN).

Chapter 5 presents studies on the intensification of dark fermentation of food waste hydrolysate using sonication. In addition to the experimental investigation, an attempt is also made to get mechanistic insight into the ultrasound-assisted dark fermentation using metabolic flux analysis

(MFA). Using the MFA model, some hypothetical cases of genetic modifications have also been analyzed for enhancing bioH_2 yield.

Chapter 6 presents an overview of the major results of the investigations presented in previous chapters. This chapter also presents a discussion on the utility of different investigations and their results presented in this thesis towards the design and upscaling of a biohydrogen production process from waste resources such as food waste. Moreover, some suggestions for further research in the area of biohydrogen production are also given.

References

[1] C. Lin, C. Cheng, Fermentative hydrogen production from xylose using anaerobic mixed microflora, International Journal of Hydrogen Energy 31 (2006) 832–840. https://doi.org/10.1016/j.ijhydene.2005.08.010.

[2] Y.-C. Lo, W.-M. Chen, C.-H. Hung, S.-D. Chen, J.-S. Chang, Dark H2 fermentation from sucrose and xylose using H2-producing indigenous bacteria: Feasibility and kinetic studies, Water Research 42 (2008) 827–842. https://doi.org/10.1016/j.watres.2007.08.023.

[3] H.H.P. Fang, H. Liu, Effect of pH on hydrogen production from glucose by a mixed culture, Bioresource Technology 82 (2002) 87–93. https://doi.org/10.1016/S0960-8524(01)00110-9.

[4] H. Fang, C. Li, T. Zhang, Acidophilic biohydrogen production from rice slurry, International Journal of Hydrogen Energy 31 (2006) 683–692. https://doi.org/10.1016/j.ijhydene.2005.07.005.

[5] I. Ntaikou, H.N. Gavala, G. Lyberatos, Modeling of fermentative hydrogen production from the bacterium Ruminococcus albus: Definition of metabolism and kinetics during growth on glucose, International Journal of Hydrogen Energy 34 (2009) 3697–3709. https://doi.org/10.1016/j.ijhydene.2009.02.057.

[6] N. Kumar, D. Das, Continuous hydrogen production by immobilized Enterobacter cloacae IIT-BT 08 using lignocellulosic materials as solid matrices, Enzyme and Microbial Technology 29 (2001) 280–287. https://doi.org/10.1016/S0141-0229(01)00394-5.

[7] S. O-Thong, P. Prasertsan, D. Karakashev, I. Angelidaki, Thermophilic fermentative hydrogen production by the newly isolated Thermoanaerobacterium thermosaccharolyticum PSU-2, International Journal of Hydrogen Energy 33 (2008) 1204–1214. https://doi.org/10.1016/j.ijhydene.2007.12.015.

[8] N. Kumar, D. Das, Enhancement of hydrogen production by Enterobacter cloacae IIT-BT 08, Process Biochemistry 35 (2000) 589–593. https://doi.org/10.1016/S0032-9592(99)00109-0.

[9] C. Lin, C. Chang, C. Hung, Fermentative hydrogen production from starch using natural mixed cultures, International Journal of Hydrogen Energy 33 (2008) 2445–2453. https://doi.org/10.1016/j.ijhydene.2008.02.069.

[10] I. Hussy, F. Hawkes, R. Dinsdale, D. Hawkes, Continuous fermentative hydrogen production from sucrose and sugarbeet, International Journal of Hydrogen Energy 30 (2005) 471–483. https://doi.org/10.1016/j.ijhydene.2004.04.003.

[11] K. Lee, Y. Hsu, Y. Lo, P. Lin, C. Lin, J. Chang, Exploring optimal environmental factors for fermentative hydrogen production from starch using mixed anaerobic microflora, International Journal of Hydrogen Energy 33 (2008) 1565–1572. https://doi.org/10.1016/j.ijhydene.2007.10.019.

[12] H. Shin, Hydrogen production from food waste in anaerobic mesophilic and thermophilic acidogenesis, International Journal of Hydrogen Energy 29 (2004) 1355–1363. https://doi.org/10.1016/j.ijhydene.2003.09.011.

[13] W. Chen, S. Chen, S. Kumarkhanal, S. Sung, Kinetic study of biological hydrogen production by anaerobic fermentation, International Journal of Hydrogen Energy 31 (2006) 2170–2178. https://doi.org/10.1016/j.ijhydene.2006.02.020.

[14] Y.-T. Fan, G.-S. Zhang, X.-Y. Guo, Y. Xing, M.-H. Fan, Biohydrogen-production from beer lees biomass by cow dung compost, Biomass and Bioenergy 30 (2006) 493–496. https://doi.org/10.1016/j.biombioe.2005.10.009.

[15] M.-L. Zhang, Y.-T. Fan, Y. Xing, C.-M. Pan, G.-S. Zhang, J.-J. Lay, Enhanced biohydrogen production from cornstalk wastes with acidification pretreatment by mixed anaerobic cultures, Biomass and Bioenergy 31 (2007) 250–254. https://doi.org/10.1016/j.biombioe.2006.08.004.

[16] Z. Zhang, J. Tay, K. Show, R. Yan, D. Teeliang, D. Lee, W. Jiang, Biohydrogen production in a granular activated carbon anaerobic fluidized bed reactor, International Journal of Hydrogen Energy 32 (2007) 185–191. https://doi.org/10.1016/j.ijhydene.2006.08.017.

[17] Y.-T. Fan, Y.-H. Zhang, S.-F. Zhang, H.-W. Hou, B.-Z. Ren, Efficient conversion of wheat straw wastes into biohydrogen gas by cow dung compost, Bioresource Technology 97 (2006) 500–505. https://doi.org/10.1016/j.biortech.2005.02.049.

[18] D. Levin, Biohydrogen production: prospects and limitations to practical application, International Journal of Hydrogen Energy 29 (2004) 173–185. https://doi.org/10.1016/S0360-3199(03)00094-6.

[19] J.P. Amend, E.L. Shock, Energetics of overall metabolic reactions of thermophilic and hyperthermophilic Archaea and Bacteria, FEMS Microbiol Rev 25 (2001) 175–243. https://doi.org/10.1111/j.1574-6976.2001.tb00576.x.

[20] A. Singh, S. Sevda, I. Abu Reesh, K. Vanbroekhoven, D. Rathore, D. Pant, Biohydrogen Production from Lignocellulosic Biomass: Technology and Sustainability, Energies 8 (2015) 13062–13080. https://doi.org/10.3390/en81112357.

[21] P. Hallenbeck, Biological hydrogen production; fundamentals and limiting processes, International Journal of Hydrogen Energy 27 (2002) 1185–1193. https://doi.org/10.1016/S0360-3199(02)00131-3.

[22] P.C. Hallenbeck, Fundamentals of the fermentative production of hydrogen, Water Science and Technology 52 (2005) 21–29. https://doi.org/10.2166/wst.2005.0494.

[23] M. Martino, C. Ruocco, E. Meloni, P. Pullumbi, V. Palma, Main Hydrogen Production Processes: An Overview, Catalysts 11 (2021) 547. https://doi.org/10.3390/catal11050547.

[24] S.W. Van Ginkel, B. Logan, Increased biological hydrogen production with reduced organic loading, Water Research 39 (2005) 3819–3826. https://doi.org/10.1016/j.watres.2005.07.021.

[25] D. Das, Hydrogen production by biological processes: a survey of literature, International Journal of Hydrogen Energy 26 (2001) 13–28. https://doi.org/10.1016/S0360-3199(00)00058-6.

[26] S. Bredholt, J. Sonne-Hansen, P. Nielsen, I.M. Mathrani, B.K. Ahring, Caldicellulosiruptor kristjanssonii sp. nov., a cellulolytic, extremely thermophilic, anaerobic bacterium, International Journal of Systematic and Evolutionary Microbiology 49 (1999) 991–996. https://doi.org/10.1099/00207713-49-3-991.

[27] K. Nath, D. Das, Effect of light intensity and initial pH during hydrogen production by an integrated dark and photofermentation process, International Journal of Hydrogen Energy 34 (2009) 7497–7501. https://doi.org/10.1016/j.ijhydene.2008.11.065.

[28] C. Mahata, S. Ray, D. Das, Optimization of dark fermentative hydrogen production from organic wastes using acidogenic mixed consortia, Energy Conversion and Management 219 (2020) 113047. https://doi.org/10.1016/j.enconman.2020.113047.

[29] F. Hawkes, I. Hussy, G. Kyazze, R. Dinsdale, D. Hawkes, Continuous dark fermentative hydrogen production by mesophilic microflora: Principles and progress, International Journal of Hydrogen Energy 32 (2007) 172–184. https://doi.org/10.1016/j.ijhydene.2006.08.014.

[30] J.S. Herring, J.E. O'Brien, C.M. Stoots, G.L. Hawkes, J.J. Hartvigsen, M. Shahnam, Progress in high-temperature electrolysis for hydrogen production using planar SOFC technology, International Journal of Hydrogen Energy 32 (2007) 440–450. https://doi.org/10.1016/j.ijhydene.2006.06.061.

[31] K.-A. Adamson, P. Pearson, Hydrogen and methanol: a comparison of safety, economics, efficiencies and emissions, Journal of Power Sources 86 (2000) 548–555. https://doi.org/10.1016/S0378-7753(99)00404-8.

[32] S. Tanisho, Y. Suzuki, N. Wakao, Fermentative hydrogen evolution by Enterobacter aerogenes strain E.82005, International Journal of Hydrogen Energy 12 (1987) 623–627. https://doi.org/10.1016/0360-3199(87)90003-6.

[33] S. Chen, K. Lee, Y. Lo, W. Chen, J. Wu, C. Lin, J. Chang, Batch and continuous biohydrogen production from starch hydrolysate by Clostridium species, International Journal of Hydrogen Energy 33 (2008) 1803–1812. https://doi.org/10.1016/j.ijhydene.2008.01.028.

[34] E.W.J. Van Niel, P.A.M. Claassen, A.J.M. Stams, Substrate and product inhibition of hydrogen production by the extreme thermophile,Caldicellulosiruptor saccharolyticus, Biotechnol. Bioeng. 81 (2003) 255–262. https://doi.org/10.1002/bit.10463.

[35] D. Das, N. Khanna, C.N. Dasgupta, Biohydrogen production: fundamentals and technology advances, CRC press, Boca Raton, 2014.

[36] D.T. Jones, D.R. Woods, Acetone-butanol fermentation revisited, Microbiol Rev 50 (1986) 484–524. https://doi.org/10.1128/mr.50.4.484-524.1986.

[37] Y.J. Lee, T. Miyahara, T. Noike, Effect of pH on microbial hydrogen fermentation, J. Chem. Technol. Biotechnol. 77 (2002) 694–698. https://doi.org/10.1002/jctb.623.

[38] K.T. Chung, Inhibitory effects of H2 on growth of Clostridium cellobioparum, Appl Environ Microbiol 31 (1976) 342–348. https://doi.org/10.1128/aem.31.3.342-348.1976.

[39] Y. Chen, Y. Yin, J. Wang, Recent advance in inhibition of dark fermentative hydrogen production, International Journal of Hydrogen Energy 46 (2021) 5053–5073. https://doi.org/10.1016/j.ijhydene.2020.11.096.

[40] S. Van Ginkel, B.E. Logan, Inhibition of Biohydrogen Production by Undissociated Acetic and Butyric Acids, Environ. Sci. Technol. 39 (2005) 9351–9356. https://doi.org/10.1021/es0510515.

[41] H. Yokoi, Y. Maeda, J. Hirose, S. Hayashi, Y. Takasaki, [No title found], Biotechnology Techniques 11 (1997) 431–433. https://doi.org/10.1023/A:1018429109020.

[42] H. Yokoi, A. Saitsu, H. Uchida, J. Hirose, S. Hayashi, Y. Takasaki, Microbial hydrogen production from sweet potato starch residue, Journal of Bioscience and Bioengineering 91 (2001) 58–63. https://doi.org/10.1016/S1389-1723(01)80112-2.

[43] J.-H. Wu, C.-Y. Lin, Biohydrogen production by mesophilic fermentation of food wastewater, Water Science and Technology 49 (2004) 223–228. https://doi.org/10.2166/wst.2004.0757.

[44] Y. Nicolet, C. Cavazza, J.C. Fontecilla-Camps, Fe-only hydrogenases: structure, function and evolution, Journal of Inorganic Biochemistry 91 (2002) 1–8. https://doi.org/10.1016/S0162-0134(02)00392-6.

[45] J.-J. Lay, Modeling and optimization of anaerobic digested sludge converting starch to hydrogen, Biotechnol. Bioeng. 68 (2000) 269–278. https://doi.org/10.1002/(SICI)1097-0290(20000505)68:3<269::AID-BIT5>3.0.CO;2-T.

[46] Y.-C. Lo, Y.-C. Su, C.-Y. Chen, W.-M. Chen, K.-S. Lee, J.-S. Chang, Biohydrogen production from cellulosic hydrolysate produced via temperature-shift-enhanced bacterial cellulose hydrolysis, Bioresource Technology 100 (2009) 5802–5807. https://doi.org/10.1016/j.biortech.2009.06.066.

[47] S. Zhang, Y. Lee, T.-H. Kim, S.-J. Hwang, Effects of OLRs and HRTs on hydrogen production from high salinity substrate by halophilic hydrogen producing bacterium (HHPB), Bioresource Technology 141 (2013) 227–232. https://doi.org/10.1016/j.biortech.2012.12.056.

[48] H. Spiller, A. Ernst, W. Kerfin, P. Böger, Increase and Stabilization of Photoproduction of Hydrogen in Nostoc muscorum by Photosynthetic Electron Transport Inhibitors, Zeitschrift Für Naturforschung C 33 (1978) 541–547. https://doi.org/10.1515/znc-1978-7-815.

[49] D. Das, Advances in biohydrogen production processes: An approach towards commercialization, International Journal of Hydrogen Energy 34 (2009) 7349–7357. https://doi.org/10.1016/j.ijhydene.2008.12.013.

[50] T. De Vrije, G.G. De Haas, G.B. Tan, E.R.P. Keijsers, P.A.M. Claassen, Pretreatment of Miscanthus for hydrogen production by Thermotoga elfii, International Journal of Hydrogen Energy 27 (2002) 1381–1390. https://doi.org/10.1016/S0360-3199(02)00124-6.

[51] Y.-K. Oh, S.H. Kim, M.-S. Kim, S. Park, Thermophilic biohydrogen production from glucose with trickling biofilter, Biotechnol. Bioeng. 88 (2004) 690–698. https://doi.org/10.1002/bit.20269.

[52] B.E. Logan, S.-E. Oh, I.S. Kim, S. Van Ginkel, Biological Hydrogen Production Measured in Batch Anaerobic Respirometers, Environ. Sci. Technol. 36 (2002) 2530–2535. https://doi.org/10.1021/es015783i.

[53] H. Liu, T. Zhang, H.H.P. Fang, [No title found], Biotechnology Letters 25 (2003) 365–369. https://doi.org/10.1023/A:1022341113774.

[54] H. Yokoi, T. Tokushige, J. Hirose, S. Hayashi, Y. Takasaki, [No title found], Biotechnology Letters 20 (1998) 143–147. https://doi.org/10.1023/A:1005372323248.

[55] C. Collet, Hydrogen production by Clostridium thermolacticum during continuous fermentation of lactose, International Journal of Hydrogen Energy 29 (2004) 1479–1485. https://doi.org/10.1016/j.ijhydene.2004.02.009.

[56] T. Kanai, H. Imanaka, A. Nakajima, K. Uwamori, Y. Omori, T. Fukui, H. Atomi, T. Imanaka, Continuous hydrogen production by the hyperthermophilic archaeon, Thermococcus kodakaraensis KOD1, Journal of Biotechnology 116 (2005) 271–282. https://doi.org/10.1016/j.jbiotec.2004.11.002.

[57] I. Hussy, F.R. Hawkes, R. Dinsdale, D.L. Hawkes, Continuous fermentative hydrogen production from a wheat starch co-product by mixed microflora, Biotechnol. Bioeng. 84 (2003) 619–626. https://doi.org/10.1002/bit.10785.

[58] H.-L. Chin, Z.-S. Chen, C.P. Chou, Fedbatch Operation Using Clostridium acetobutylicum Suspension Culture as Biocatalyst for Enhancing Hydrogen Production, Biotechnol. Prog. 19 (2003) 383–388. https://doi.org/10.1021/bp0200604.

[59] J.-J. Lay, Biohydrogen generation by mesophilic anaerobic fermentation of microcrystalline cellulose, Biotechnol. Bioeng. 74 (2001) 280–287. https://doi.org/10.1002/bit.1118.

[60] L. Minnan, H. Jinli, W. Xiaobin, X. Huijuan, C. Jinzao, L. Chuannan, Z. Fengzhang, X. Liangshu, Isolation and characterization of a high H2-producing strain Klebsiella oxytoca HP1 from a hot spring, Research in Microbiology 156 (2005) 76–81. https://doi.org/10.1016/j.resmic.2004.08.004.

[61] C. Wang, C. Chang, C. Chu, D. Lee, B.-V. Chang, C. Liao, Efficient production of hydrogen from wastewater sludge, J. Chem. Technol. Biotechnol. 79 (2004) 426–427. https://doi.org/10.1002/jctb.997.

[62] C.C. Wang, C.W. Chang, C.P. Chu, D.J. Lee, B.-V. Chang, C.S. Liao, J.H. Tay, Using filtrate of waste biosolids to effectively produce bio-hydrogen by anaerobic fermentation, Water Research 37 (2003) 2789–2793. https://doi.org/10.1016/S0043-1354(03)00004-6.

[63] M. Yetis, Photoproduction of hydrogen from sugar refinery wastewater by Rhodobacter sphaeroides O.U. 001, International Journal of Hydrogen Energy 25 (2000) 1035–1041. https://doi.org/10.1016/S0360-3199(00)00027-6.

[64] H. Zhu, T. Suzuki, A.A. Tsygankov, Y. Asada, J. Miyake, Hydrogen production from tofu wastewater by Rhodobacter sphaeroides immobilized in agar gels, International Journal of Hydrogen Energy 24 (1999) 305–310. https://doi.org/10.1016/S0360-3199(98)00081-0.

[65] T. Zhang, H. Liu, H.H.P. Fang, Biohydrogen production from starch in wastewater under thermophilic condition, Journal of Environmental Management 69 (2003) 149–156. https://doi.org/10.1016/S0301-4797(03)00141-5.

[66] C. Mahata, S. Dhar, S. Ray, D. Das, Effect of thermal pretreated organic wastes on the dark fermentative hydrogen production using mixed microbial consortia, Fuel 284 (2021) 119062. https://doi.org/10.1016/j.fuel.2020.119062.

[67] S. Yadav, V. Singh, C. Mahata, D. Das, Optimization for simultaneous enhancement of biobutanol and biohydrogen production, International Journal of Hydrogen Energy 46 (2021) 3726–3741. https://doi.org/10.1016/j.ijhydene.2020.10.267.

[68] S. Sarma, V.K. Dubey, V.S. Moholkar, Kinetic and thermodynamic analysis (with statistical optimization) of hydrogen production from crude glycerol using Clostridium pasteurianum, International Journal of Hydrogen Energy 41 (2016) 19972–19989. https://doi.org/10.1016/j.ijhydene.2016.08.204.

[69] W. Han, X. Wang, L. Ye, J. Huang, J. Tang, Y. Li, N. Ren, Fermentative hydrogen production using wheat flour hydrolysate by mixed culture, International Journal of Hydrogen Energy 40 (2015) 4474–4480. https://doi.org/10.1016/j.ijhydene.2015.02.016.

[70] S. Kanchanasuta, P. Prommeenate, N. Boonapatcharone, N. Pisutpaisal, Stability of *Clostridium butyricum* in biohydrogen production from non-sterile food waste, International Journal of Hydrogen Energy 42 (2017) 3454–3465. https://doi.org/10.1016/j.ijhydene.2016.09.111.

[71] S. Faizollahzadeh Ardabili, B. Najafi, S. Shamshirband, B. Minaei Bidgoli, R.C. Deo, K. Chau, Computational intelligence approach for modeling hydrogen production: a review, Engineering Applications of Computational Fluid Mechanics 12 (2018) 438–458. https://doi.org/10.1080/19942060.2018.1452296.

[72] P. Karthic, S. Joseph, N. Arun, S. Kumaravel, Optimization of biohydrogen production by *Enterobacter species* using artificial neural network and response surface methodology, Journal of Renewable and Sustainable Energy 5 (2013) 033104. https://doi.org/10.1063/1.4803746.

[73] L. Jia, W. Li, J. Qiao, An online adjusting RBF neural network for nonlinear system modeling, Appl Intell 53 (2023) 440–453. https://doi.org/10.1007/s10489-021-03106-7.

[74] G. Stephanopoulos, A.A. Aristidou, J. Nielsen, Metabolic Engineering: Principles and Methodologies, Elsevier, 1998.

[75] J.S. Edwards, M. Covert, B. Palsson, Metabolic modelling of microbes: the flux-balance approach., Environmental Microbiology 4 (2002). https://web.stanford.edu/group/covert/publicationpdfs/Edwards2002.pdf (accessed May 25, 2025).

[76] J.-Z. Xu, Z.-H. Wu, S.-J. Gao, W. Zhang, Rational modification of tricarboxylic acid cycle for improving l-lysine production in Corynebacterium glutamicum, Microb Cell Fact 17 (2018) 105. https://doi.org/10.1186/s12934-018-0958-z.

[77] X. Liu, D.E. Cooper, A.A. Cluntun, M.O. Warmoes, S. Zhao, M.A. Reid, J. Liu, P.J. Lund, M. Lopes, B.A. Garcia, K.E. Wellen, D.G. Kirsch, J.W. Locasale, Acetate production from glucose and coupling to mitochondrial metabolism in mammals, Cell 175 (2018) 502. https://doi.org/10.1016/j.cell.2018.08.040.

[78] Z. Li, J. Gu, J. Ding, N. Ren, D. Xing, Molecular mechanism of ethanol-H2 co-production fermentation in anaerobic acidogenesis: Challenges and perspectives, Biotechnology Advances 46 (2021) 107679. https://doi.org/10.1016/j.biotechadv.2020.107679.

[79] S. Sarma, A. Anand, V.K. Dubey, V.S. Moholkar, Metabolic flux network analysis of hydrogen production from crude glycerol by Clostridium pasteurianum, Bioresource Technology 242 (2017) 169–177. https://doi.org/10.1016/j.biortech.2017.03.168.

[80] F.C. Lunelli, P. Sfalcin, M. Souza, E. Zimmermann, V. Dal Prá, E.L. Foletto, S.L. Jahn, R.C. Kuhn, M.A. Mazutti, Ultrasound-assisted enzymatic hydrolysis of sugarcane bagasse for the production of fermentable sugars, Biosystems Engineering 124 (2014) 24–28. https://doi.org/10.1016/j.biosystemseng.2014.06.004.

[81] S. Singh, M. Agarwal, S. Sarma, A. Goyal, V.S. Moholkar, Mechanistic insight into ultrasound induced enhancement of simultaneous saccharification and fermentation of Parthenium hysterophorus for ethanol production, Ultrasonics Sonochemistry 26 (2015) 249–256. https://doi.org/10.1016/j.ultsonch.2015.02.011.

[82] V.S. Moholkar, M. Huitema, S. Rekveld, M.M.C.G. Warmoeskerken, Characterization of an ultrasonic system using wavelet transforms, Chemical Engineering Science 57 (2002) 617–629. https://doi.org/10.1016/S0009-2509(01)00397-9.

[83] R.S. Malani, S.B. Umriwad, K. Kumar, A. Goyal, V.S. Moholkar, Ultrasound–assisted enzymatic biodiesel production using blended feedstock of non–edible oils: Kinetic analysis, Energy Conversion and Management 188 (2019) 142–150. https://doi.org/10.1016/j.enconman.2019.03.052.

[84] T. Sivasankar, A.W. Paunikar, V.S. Moholkar, Mechanistic approach to enhancement of the yield of a sonochemical reaction, AIChE J. 53 (2007) 1132–1143. https://doi.org/10.1002/aic.11170.

[85] C.-L. Hsiao, J.-J. Chang, J.-H. Wu, W.-C. Chin, F.-S. Wen, C.-C. Huang, C.-C. Chen, C.-Y. Lin, Clostridium strain co-cultures for biohydrogen production enhancement from condensed molasses fermentation solubles, International Journal of Hydrogen Energy 34 (2009) 7173–7181. https://doi.org/10.1016/j.ijhydene.2009.06.028.

CHAPTER 3

Hydrolysis of Food Waste using Glucoamylase: Statistical Optimization, Ultrasound-assisted Intensification and Mechanistic Analysis with Molecular Simulations

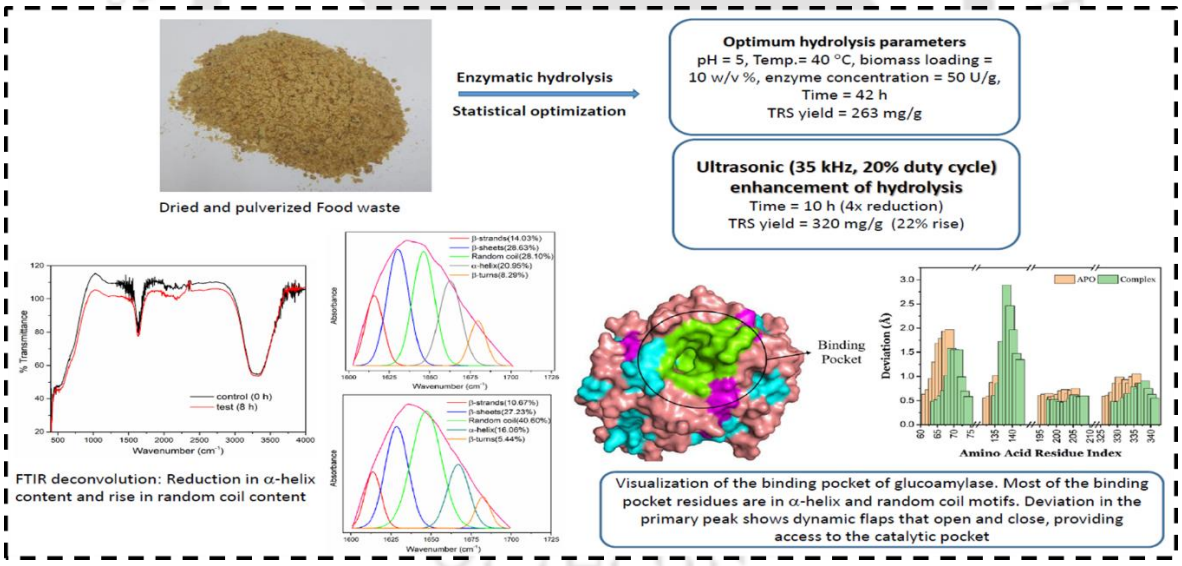

Online: Anand, A., Kumar, K., Khaire, K.C., Roy, K., Moholkar, V.S., 2024. Ultrasound-assisted hydrolysis of food waste using glucoamylase: Statistical optimization and mechanistic analysis with molecular simulations. *Bioresource Technology Reports* 27, 101932. https://doi.org/10.1016/j.biteb.2024.101932

3.1 Introduction

Food waste (FW) produced from diverse sources, including food processing plants, households, and commercial establishments like restaurants and cafeterias, has been investigated as a cheap and sustainable feedstock for the synthesis of value-added products [1,2] through the fermentation route. A summary of representative literature on the synthesis of value-added products from the fermentation of food waste is provided in the Appendix 3A at the end of this chapter (Table 3A.1). The typical sugar content of food waste varies from 40 to 70% (with starch content in the range of 25 to 45%) depending on the type and source [3]. The starch content in food waste needs to be hydrolyzed into monomeric sugars before fermentation [4]. Thus, hydrolysis or saccharification is one of the essential pretreatments in the fermentative synthesis of value-added products from food waste. Amyloglucosidase or glucoamylase (GLCM) has been a widely employed enzyme for the hydrolysis of starch in food waste. This enzyme exhibits a well-defined structure and function that make it indispensable for its biological activities. Structurally, GLCM is typically composed of a protein chain with a specific 3-D conformation, often organized into domains. These domains facilitate the recognition and binding of its substrate, which is typically starch or glycogen. Functionally, GLCM is primarily responsible for the hydrolysis of α-1,4-glycosidic linkages present in the polymeric chains of starch or glycogen, effectively breaking them down into smaller glucose units. This enzymatic cleavage results in the release of individual glucose molecules, which are readily absorbed and utilized by an organism as a source of energy. GLCM is widely employed in various industrial processes, including the production of high-fructose corn syrup and bioethanol, where its ability to convert starch into glucose efficiently is harnessed. In both biological and industrial contexts, the structure-function relationship of GLCM underscores its significance in facilitating the breakdown and utilization of complex carbohydrates. However, in addition to the high cost of enzymes, slow kinetics is a significant

limitation of the enzymatic hydrolysis or saccharification of food waste. Thus, intensifying the kinetics of hydrolysis by glucoamylase is crucial to the large-scale implementation of food waste-based processes for value-added products.

Sonication (or ultrasound irradiation) is known to enhance the kinetics of enzymatic processes [5,6]. Ultrasound and its secondary effect of cavitation (which essentially is nucleation, growth, and transient collapse of gas or vapor microbubbles) generate intense micro-turbulence in the liquid medium. This micro-turbulence induces changes in the secondary structures of the enzymes, which leads to a rise in the activity of the enzymes. Wang et al. [7] have studied the effect of sonication on the hydrolysis of starch by GLCM. The solubility of the starch improved by 136% with the application of 22 kHz sonication at an intensity of 7.2 W/mL for 10 min. Analysis of the ultrasound-exposed enzyme structure using circular dichroism revealed an increase in the random coil content of the enzyme with a concurrent reduction in α-helix and β-sheet contents. A rise in the random coil content made the structure of glucoamylase more flexible with the unfolding of proteins, which enhanced the catalytic efficiency. In another study, Meng et al. [8] studied the effect of ultrasound on the properties and conformation of glucoamylase. Moderate intensity sonication led to a rise in α-helix and random coil content of the enzyme by 17.8 and 12.4%, with a concurrent rise in the tryptophan and tyrosine population on the surface of the enzyme. These conformational changes increased the enzyme activity. High-intensity sonication, however, resulted in the deactivation of the enzyme.

The objectives of the present study are 3-fold: (1) statistical optimization of food waste hydrolysis using glucoamylase and intensification of the process at optimum conditions with sonication, (2) determination of changes in secondary structure of glucoamylase induced by sonication using deconvolution technique (FTIR), and (3) mechanistic investigation into the ultrasound-induced enhancement of glucoamylase activity with molecular docking and

dynamics simulations with a representative substrate of amylotriose. Concurrent analysis of the experimental and molecular simulation results has revealed interesting mechanistic features of the ultrasonic enhancement of the food waste hydrolysis by glucoamylase (GLCM).

The novelty of the study lies in its ternary integrative approach that combines statistical optimization of hydrolysis, ultrasound-assisted enhancement of the enzymatic hydrolysis, and molecular modeling that provides physical insight into the ultrasound-induced enhancement of hydrolysis. Statistical optimization of enzymatic hydrolysis using response surface methodology (RSM) refines process parameters, ensuring maximum enzyme activity and substrate conversion under optimal conditions. The use of ultrasound at optimum conditions obtained using RSM enhances the efficiency of glucoamylase in breaking down food waste into fermentable sugars, accelerating the process and improving glucose yield. Additionally, molecular simulations provide significant mechanistic insights into the interaction between ultrasound, enzyme, and substrate at a molecular level. These simulations reveal how ultrasound affects enzyme structure and activity, potentially uncovering new pathways for enhancing enzymatic reactions.

3.2 Materials and methods

3.2.1 Materials and initial processing of food waste

Food waste (a mixture of starchy foods such as rice, cereals and potatoes) was collected from the food outlets on the Indian Institute of Technology Guwahati campus. It was dried in a hot air oven at 60 °C for 72 h, followed by pulverization using a mixer grinder to a uniform particle size of 0.85 mm (Bajaj Pluto 500 W). This procedure helped preserve the quality of food waste and minimize microbial growth during storage. The pulverized, moisture-free food waste was sealed at 25°C in a red cap bottle for further use. Amyloglucosidase (glucoamylase) enzyme from *Aspergillus niger* was purchased from Sigma-Aldrich, USA. All other chemicals

and media components were procured from HiMedia Pvt. Ltd., India, and used as received without any pretreatment.

3.2.2 Characterization of food waste biomass

3.2.2.1 Determination of sugar content and composition of food waste biomass

Compositional analyses of food waste biomass were carried out by High-Performance Liquid Chromatography (HPLC) equipped with an autosampler (Shimadzu, UFLC, Prominence, Japan). The reaction mixture was prepared by adding 1 mL of 2 M trifluoroacetic acid (TFA) and 5 mg of food waste biomass to a 2 mL Eppendorf tube. The Eppendorf tube was placed in a water bath (80 °C) for two hours. Hydrolyzed food waste was centrifuged at 10,000 rpm for 15 min. The supernatant was transferred to a fresh 2 mL Eppendorf tube to evaporate the remaining TFA and dried for 12 h in a hot air oven at 80 °C. TFA hydrolyzed food waste biomass was suspended in 500 µL ultrapure water, followed by filtration through a syringe filter (polyvinylidene fluoride membrane) with a pore size of 0.22 µm. The monosaccharide content of TFA hydrolyzed food waste biomass was scrutinized by HPLC (Shimadzu, Model: DGU-20A5R, autosampler type) with a refractive index (RI) detector equipped with a photodiode analyzer (PDA). The HPLC employed a 300 mm × 7.8 mm Aminex@ HPX-87H column along with a guard column (catalog # 1250140, 50 mm × 7.8 mm). The reducing sugar content in hydrolyzed food waste was determined using a mobile phase of 0.05 mM H_2SO_4 at a flow rate of 0.6 mL/min with oven temperature maintained at 60ºC [9]. The actual sugar composition in food waste biomass was obtained using standards of five monomeric sugars, viz., maltose, glucose, galactose, arabinose, and xylose.

3.2.2.2 Functional group analysis of food waste biomass

The functional groups in the food waste biomass were analyzed using Fourier transform infrared (FTIR) spectroscopy (Perkin Elmer, Spectrum Two, USA). Food waste biomass was mixed with potassium bromide (1:100 w/w ratio) using a mortar and pestle, and the pellets

were created under a 15-ton hydraulic press [9]. The FTIR spectra of food samples were obtained in the wave number range of 4000 - 400 cm^{-1}.

3.2.2.3 *Surface morphology analysis of food waste biomass*

Field Emission Scanning Electron Microscopy (FE-SEM) examined the surface morphology of food waste biomass (Carl Zeiss, Model-Gemini 300, Germany). Before placing samples of food waste biomass on the carbon tape, the carbon tape was glued to the stab surface. To prevent biomass from gaining moisture, the samples on the stab were double-gold coated in the vacuum chamber. Images of the double gold-coated samples were captured using an FE-SEM analyzer at a 5 KX magnification for surface morphology investigation.

3.2.2.4 Thermal degradation analysis of food waste

Thermal degradation (or thermogravimetric analysis) of food waste was performed with a thermal analyzer (NETZSCH, Model: STA449F3A00). The thermogravimetric (TGA) and differential thermogravimetric (DTG) curves were obtained with respect to temperature. The sample was heated under an argon gas environment at 10 ºC min^{-1} from 30 to 1000 ºC.

3.2.3 Statistical optimization of the enzymatic hydrolysis of food waste

The physical parameters for enzymatic hydrolysis or saccharification of food waste biomass were optimized by using the statistical 2^{nd} order Box-Behnken design (BBD) (Design Expert 9.0.7.1 version, Stat-Ease) with total reducing sugar yield per unit mass of biomass as the objective function (or response variable). The parameters for optimization and their ranges were: temperature (30°-50°C), citrate phosphate buffer (pH 4-6), food waste biomass loading (5-15% w/v), time of hydrolysis (12-72 h), and amyloglucosidase concentration (20-80 U/g). All experiments were repeated in triplicate to assess the reproducibility of the results. The relationship between the objective function (TRS yield) and optimization parameters was established by fitting a 2^{nd}-order polynomial equation to the experimental data. Table 3.1 depicts the set of experiments in the Box Behnken design and their results. Experiments in the

statistical design were carried out in a 5 mL test tube with a 2 mL working volume. After completion of the specific period, the reaction was arrested by immersing the test tube in a boiling water bath. The reaction mixture was centrifuged at 10000 rpm (12298 *g*) for 5 min to remove traces of particulate impurities, and the hydrolysate was separated. The total reducing sugar released in the hydrolysate was estimated using the Nelson-Somogyi method [10], while the glucose content was measured using the GOD-POD method and HPLC analysis. Finally, a validation experiment was conducted to verify the total reducing sugar and glucose yield at the predicted optimum conditions.

Validation experiment*:* The validation experiment was carried out in a 500 mL Erlenmeyer flask with a reaction volume of 100 mL. The flask was placed in an incubator shaker (Orbitek, Scigenics Biotech) operated at 200 rpm. The resulting hydrolysate was analyzed for total reducing sugar content by the Nelson-Somogyi method and the glucose content by the GOD-POD method.

3.2.4 Intensification of enzymatic hydrolysis by ultrasound

In this case, the enzymatic hydrolysis experiment was conducted in an ultrasound bath (2L Sonorex Digitec, Elma, Germany) at optimum conditions obtained using the statistical experimental design. The bath dimensions were 25 cm × 15 cm × 10 cm. It operated at a frequency of 35 kHz with a power rating of 35 W. During the enzymatic hydrolysis reaction, sonication was performed at a duty cycle of 20%, translating to 2 minutes of sonication followed by 8 minutes of mechanical shaking every 10 minutes of the reaction. The reaction flask was positioned at the center of the bath, submerging approximately half of its height in the water. To maintain consistent acoustic intensity throughout the bath, the flask's position remained unchanged across all experiments. Bath water temperature was carefully controlled at 30 ± 2 °C. A control experiment involving only mechanical shaking was conducted, and 200 µL samples were periodically withdrawn from the reaction mixture to determine the

instantaneous total reducing sugar concentration. Control experiments continued for 42 h, ensuring that the difference in total reducing sugar content between successive samples was less than 5%. In contrast, test experiments (including sonication) were conducted for 10 h. Both control and test experiments were performed in triplicate.

3.2.5 Computational analysis of food waste hydrolysis by glucoamylase (GLCM)

3.2.5.1 Selection of glucoamylase structure for molecular docking

The model system for molecular simulations comprised glucoamylase (GLCM) enzyme with alpha-1,4-maltotriose (or amylotriose), the principal constituent of food waste, as the substrate. The catalytic mechanism of the GLCM enzyme was investigated using molecular docking protocols reported in our previous study [11,12]. The 3D coordinates of GLCM from *Aspergillus niger* complexed with tris and glycerol were imported from the Protein Data Bank (PDB) [13]. Among the seven crystal structures of GLCM from *Aspergillus niger* available in the RCSB-PDB database (PDB IDs: 1ACO, 1ACZ, 1KUL, 1KUM, 3EQA, 5GHL, and 6FRV; last accessed on May 19, 2024), 3EQA was selected. This structure was chosen due to its superior quality, as indicated by its Ramachandran scores, and its best resolution of 1.90 Å compared to the other available structures. The docking calculations were performed using AutoDock v1.5.7 [14] integrated in MGL Tools v1.5.7. The Gaussian 09 package [15] was used to draw and optimize the chemical geometry of amylotriose. The imported GLCM had chemical moieties attached to its chemical structure, such as MAN (α-D-mannopyranose), TRS (2-amino-2-hydroxymethyl-propane-1,3 diol), GOL (Glycerol), and crystal water, which were removed before performing docking simulations. Interactions present in the GLCM-amylotriose complex were analyzed in the PLIP tool (https:plip-tool.biotec.tu-dresden.de/plip-web/) and PyMOL™ v2.4.1 [16]. The docking simulations were reproduced by removing amylotriose from the GLCM-amylotriose complex, followed by redocking in GLCM to compare binding coordinates and affinities.

3.2.5.2 Prediction of the binding pocket and active site of glucoamylase (GLCM) enzyme

The molecular interactions between GLCM and amylotriose, i.e., the catalytic mechanism of GLCM, were investigated using molecular docking protocols as described in our previous studies [11,12]. The chemical structure of amylotriose was drawn and optimized using the Gaussian 09 package [15]. Ideally, docking simulations should be conducted around an experimentally predicted binding site. The binding site of 3EQA (ID: P69328; AMYG_ASPNG) for the D-glucose molecule has been identified in the UniProtKB database (https://www.uniprot.org/ uniprotkb/) as involving the active site residues W144, D200, and E203. Experimental studies have shown that amylotriose is a major constituent of the food waste examined in our study. Therefore, we attempted to predict a binding pocket for the representative substrate amylotriose using blind docking methods, constructing a grid box to cover the entire GLCM structure and substrate, along with site-specific docking. The binding pocket reported in the UniProtKB database may not be suitable for amylotriose due to its much larger size than D-glucose.

3.2.5.3 Molecular dynamics (MD) simulations and analysis

The MD simulation analysis for validating the docking results was performed using the GROMACS v2019.3 software package, and the analysis of MD trajectories was executed through VMD (Visual Molecular Dynamics) [17] software and its associated plugins. For detailed methodology and analysis, please refer to section 3A.1 in the Appendix 3A.

3.2.5.4 Analysis of the changes in the secondary structure of GLCM

We employed an FTIR-based method to explore modifications in the secondary structure of GLCM caused by sonication [18]. The secondary derivatives of peak frequencies ranging from 1600 to 1700 cm^{-1} were discerned and smoothed using a 20-point Savitzky-Golay algorithm [19]. Quantification of the multicomponent peak area under the amide-I bands of GLCM was

conducted through a Gaussian function fitting program in Origin 9.0. The determination of secondary structure fractions was achieved utilizing the deconvolution methodology for FTIR spectra, as documented in previous literature [12,20].

3.3 Results and Discussion

3.3.1 Characterization of food waste biomass

The monosaccharide composition analysis of food waste biomass by TFA hydrolysis showed only two reducing sugars: glucose and maltose. FE-SEM image of the surface morphology of food waste biomass is shown in Fig. 3A.1 (A) in Appendix 3A. The surface morphology of the biomass showed a smooth, compact, and exposed fibrous structure. Fig. 3A.1 (B) in Appendix 3A shows the FTIR spectra of food waste biomass. The peaks of starch mainly occurred in the wavenumber range 3600 - 2850 cm^{-1} and 1640 - 850 cm^{-1} [21,22]. The peaks observed within the range of 3600-2850 cm^{-1} are attributed to stretching fluctuations or vibrations involving C-H or O-H bonds within the food waste biomass [23]. The stretching vibrations of C-H bonds at 2894 cm^{-1} represent the overall hydrocarbon components present in the food waste biomass. Additionally, the more prominent peaks at 3331 and 3634 cm^{-1} correspond to intra- and intermolecular O-H bond stretching, respectively. These findings confirm the presence of starch in the food waste biomass [24].

Both DTG and TGA analyses were used to examine the thermal decomposition and stability of food waste (refer to Fig. 3A.1(C) in Appendix 3A). As per the TGA analysis, food waste biomass was stable up to 210 °C. The decomposition of food waste occurs in three stages. The first stage (75 ºC to 210 ºC) showed a 7% weight loss corresponding to moisture loss. The decomposition in the second step (240 ºC and 450 ºC) showed 58% weight loss due to the fragmentation of food waste into different organic compounds. In the last stage (above 450 ºC) of thermal degradation, residual food waste was converted into ash.

3.3.2 Results of statistical optimization of food waste hydrolysis

As noted earlier, the optimization parameters (or variables) for enzymatic hydrolysis of food waste biomass were biomass loading (%, w/v), amyloglucosidase enzyme loading (U/g), time (h), temperature (°C), and pH, with total reducing sugar yield as the response variable or objective function. The results of the Box-Behnken experimental design are shown in Table 3.1. The following 2nd order (quadratic) equation was fitted to the experimental data:

Reducing sugar yield (mg/g of food waste biomass) = -442.67 + 2.03·A + 30.95·B + 2.50·C + 10.55·D + 88.19·E – 0.003·A·B + 0.00052 A·C + 0.0016 A·D + 0.016·A·E + 0.0031·B·C + 0.0093·B·D + 0.093·B·E – 0.0016·C·D – 0.016·C·E – 0.047·D·E – 0.020·A^2 –1.66·B^2 – 0.028·C^2– 0.13·D^2 – 8.13·E^2

Various notations are: A = glucoamylase concentration (U/g), B = biomass loading (% w/v), C = time of hydrolysis (h), D = temperature (ºC), E = pH

The analysis of variance (ANOVA) of the quadratic model is given in Table 3.2. A large overall *F*-value (103.06) and *p*-value (< 0.0001) for the model show the significance of model terms with only a 0.01% chance of noise. The individual coefficients of the optimization variables have a *p*-value < 0.05, which indicates their significance. However, the coefficients of the interaction terms in the quadratic model have a *p*-value > 0.05, which indicates their insignificance. Physically, this result means that the optimization variables do not have any interaction among them, and their influence on enzymatic hydrolysis is essentially independent. *p*-values of model coefficients for squared variables (A^2, B^2, C^2 etc.) are < 0.05, which indicates their significance. The *p*-value of Lack-of-Fit is > 0.05 (insignificant), which shows that the model fits well with the experimental data. Finally, the regression coefficient of the model (R^2) = 0.9861 and the predicted R^2 = 0.9776 are in reasonable agreement with the adjusted R^2 = 0.9766, as shown in Table 3.2, and also show the best fit of the model. Response surfaces for the objective function of optimization (TRS yield) between pairs of optimization variables are

shown in the Appendix 3A (refer to Fig. 3A.2). The set of values of optimization variables for the highest TRS yield is pH = 5, temperature = 40 ºC, biomass loading = 10% w/v, enzyme loading = 50 U/g, and time = 42 h, TRS yield (model predicted) = 255.1 mg/g biomass.

Validation experiment: The validation experiment of food waste hydrolysis (as noted in the previous section) was conducted using the optimized set of parameters obtained using the statistical design of experiments. The validation experiment resulted in a total reducing sugar (TRS) yield of 263.4 mg/g (with glucose content of 245 mg/g). The yield of reducing sugars in the validation experiment was very close to the predictions of the quadratic model.

3.3.2.1 Results of ultrasound-assisted hydrolysis of food waste

The total reducing sugar (TRS) yield in 10 h ultrasound-assisted food waste hydrolysis at optimum temperature conditions, enzyme concentration, biomass loading, and pH was 320.43 ± 3.8 mg/g. As noted earlier, the sonication was applied at 20% duty cycle, which means that the sonication period during the total treatment of 10 hours was only 2 hours. We want to state that further treatment for 2 hours reduced the TRS concentration. For the 11-hour treatment, the TRS yield was reduced to 261.43 mg/g, and the 12-h treatment further reduced the yield to 203.59 mg/g. This result is probably a consequence of the oxidative degradation of the monomeric sugar molecules induced by the radicals generated by sonication. A comparison of the results of ultrasound-assisted experiments and the control experiment (TRS yield of 263.4 ± 2.2 mg/g in 42 h of treatment) reveals that the kinetics of enzymatic hydrolysis were enhanced ~ 4×. In addition, the total reducing sugar yield increased by approximately 22% with the sonication of the reaction mixture. Several previous authors have reported the enhancement effect of ultrasound on the enzymatic hydrolysis of various substrates. Waghmare and Rathod [25] have reported the enhancement of the hydrolysis of waste cooking oil using immobilized lipase and 22 kHz sonication. Singh et al. [26] have reported a 6-fold enhancement of the rate

of enzymatic hydrolysis of a cellulose-rich fraction of *Parthenium hysterophorus* using carboxymethyl cellulose, in addition to a 20% rise in the sugar yield in the presence of 35 kHz sonication. Sulaiman et al. [27] reported 85% enhancement in the rate of hydrolysis of soluble carboxymethyl cellulose (CMC) and insoluble cellulose using cellulase and 20 kHz ultrasound. Wang et al. [7] achieved faster hydrolysis and degradation of starch using glucoamylase in presence of 22 kHz sonication.

Table 3.1. Results of the statistical experimental design for optimization of food waste hydrolysis using glucoamylase

Run Order	Biomass loading (% w/v)	Enzyme loading (U/g)	Time (h)	Temperature (°C)	pH	Reducing sugar yield (model, mg/g)	Reducing sugar yield (expt, mg/g)
1	5	20	72	50	4	144.2	146.3 ± 3.0
2	15	20	72	30	6	151.3	151.6 ± 4.5
3	10	50	42	40	4	240.9	250.2 ± 3.1
4	5	20	72	50	6	152.7	145.4 ± 2.6
5	5	80	12	30	4	155.1	154.5 ± 4.2
6	10	50	42	40	5	255.1	250.0 ± 6.1
7	15	20	72	50	4	132.1	131.4 ± 1.0
8	5	20	12	50	6	149.2	152.2 ± 2.5
9	15	20	12	50	6	137.1	137.3 ± 3.6
10	5	20	12	30	4	145.9	144.4 ± 2.9
11	15	20	72	50	6	142.4	145.4 ± 3.2
12	15	80	72	50	6	155.3	155.5 ± 5.1
13	15	20	12	50	4	124.9	123.3 ± 3.0
14	5	20	72	30	6	163.5	166.5 ± 3.6
15	5	80	12	30	6	169.1	168.5 ± 6.5
16	15	80	72	30	6	162.3	161.7 ± 5.7
17	15	20	12	30	4	130.1	129.5 ± 5.5
18	10	50	42	40	5	255.1	270.0 ± 2.6
19	5	80	72	30	6	176.3	176.6 ± 2.9
20	5	80	72	50	6	167.4	170.4 ± 2.5
21	15	20	72	30	4	139.1	137.6 ± 2.5
22	10	50	12	40	5	226.9	229.1 ± 7.0
23	10	50	72	40	5	234.1	237.1 ± 2.0
24	5	20	12	50	4	138.9	138.2 ± 4.6
25	10	50	42	40	5	255.1	248.0 ± 4.6
26	15	80	12	30	6	153.3	153.6 ± 3.2
27	10	50	42	40	5	255.1	260.2 ± 6.0
28	15	80	12	30	4	137.3	139.6 ± 5.0
29	10	80	42	40	5	242.9	245.0 ± 3.0
30	5	20	72	30	4	153.1	152.4 ± 3.2
31	5	20	12	30	6	158.1	158.4 ± 6.1
32	15	80	12	50	4	134.0	133.5 ± 3.0
33	10	50	42	40	5	255.1	232.0 ± 7.2
34	10	50	42	30	5	245.2	247.3 ± 6.0
35	10	20	42	40	5	231.9	234.9 ± 8.9
36	10	50	42	40	5	255.1	268.0 ± 9.5
37	5	50	42	40	5	220.7	223.7 ± 10.7
38	15	80	72	30	4	148.2	147.7 ± 5.1
39	10	50	42	40	5	255.1	252.0 ± 5.6
40	15	20	12	30	6	144.1	143.5 ± 7.0
41	15	80	72	50	4	143.0	141.5 ± 6.7
42	5	80	72	50	4	157.1	156.4 ± 3.8
43	5	80	12	50	6	162.1	162.3 ± 5.5
44	15	80	12	50	6	148.1	147.5 ± 5.1
45	10	50	42	40	5	255.1	240.0 ± 4.4
46	5	80	12	50	4	149.9	148.3 ± 5.7
47	15	50	42	40	5	206.7	208.8 ± 4.1
48	10	50	42	40	6	253.1	249.0 ± 8.5
49	10	50	42	50	5	238.1	241.2 ± 4.2
50	5	80	72	30	4	164.1	162.6 ± 5.0

Table 3.2. ANOVA for the statistical design of experiments

Sources	Sum of squares	Degrees of Freedom	Mean square	*F*-value	*p*-value	Remark
Model	1.1×10^5	20	5473.14	103.06	< 0.0001	
A-Enzyme	1028.63	1	1028.63	19.37	0.0001	
B-Substrate	1668.57	1	1668.57	31.42	< 0.0001	Significant
C-Time	438.54	1	438.54	8.26	0.0075	
D-Temp.	422.12	1	422.12	7.95	0.0086	
E-pH	1271.36	1	271.36	23.94	< 0.0001	
AB	6.93	1	6.93	0.13	0.72	
AC	6.93	1	6.93	0.13	0.72	
AD	6.93	1	6.93	0.13	0.72	
AE	6.93	1	6.93	0.13	0.72	
BC	6.93	1	6.93	0.13	0.72	Insignificant
BD	6.93	1	6.93	0.13	0.72	
BE	6.93	1	6.93	0.13	0.72	
CD	6.93	1	6.93	0.13	0.72	
CE	6.93	1	6.93	0.13	0.72	
DE	6.93	1	781.43	14.71	0.72	
A^2	781.43	1	4250.36	80.03	0.0006	
B^2	4250.36	1	1502.77	28.30	< 0.0001	
C^2	1502.77	1	448.6	8.45	0.0069	Significant
D^2	448.60	1	163.35	3.08	0.09	
E^2	163.35	1	53.11			
Lack of fit	331.01	22	172.73			Insignificant
Model statistics: R^2 = 0.99, Adj R^2 = 0.98, Pred. R^2 = 0.98						

Table 3.3. Results of deconvolution of FTIR spectra for secondary structure analysis of GLCM

Experiment	α-Helix	β-sheets	β-strands	β-turns	Random coils	Total
Control	20.95	28.63	14.03	8.29	28.10	100
Test	16.06	27.23	10.67	5.44	40.60	100

3.3.3 Changes in the secondary structure of GLCM induced by sonication

The FTIR spectra of GLCM in control and test experiments are shown in Fig. 3.1A. The most sensitive region in these FTIR spectra, i.e., amide I band (1600−1690 cm^{-1}) [28], which is due to the C=O stretch vibration of the peptide linkage, was analyzed with multi-peak fitting Gaussian function. The wavenumber ranges corresponding to various secondary structures of GLCM used for deconvolution of FTIR spectra were: β-sheets (1638 ± 2.0 cm^{-1}), β-turns (1664 - 1690 cm^{-1}), random coils (1648 ± 2.0 cm^{-1}), α-helix (1656 ± 2.0 cm^{-1}), and β-strands (1627 ± 2.0 cm^{-1}) [28]. The deconvolution of the FTIR spectra of GLCM is shown in Figs. 3.1B and C. The percentages of different secondary structural motifs in GLCM determined from deconvolution analysis in control and test experiments are listed in Table 3.3.

The results presented in Table 3.3 reveal the significant impact of sonication on the secondary structure of GLCM. The primary change is an increase in random coil content from 28.10 % to 40.60 %, with a reduction in α-helix content from 20.95 % to 16.06 %. The content of β-sheets and β-turns also reduces with sonication. Similar conformational changes in the secondary structure of enzymes induced by sonication have been reported by previous authors [12,29].

Molecular insight into sonication-induced enhancement of food waste hydrolysis

3.3.3.1 *Molecular docking simulations of amylotriose with GLCM enzyme*

The optimized structure of amylotriose, obtained through DFT simulation, is shown in Fig. 3A.3 of the Appendix 3A. Molecular docking analysis, conducted as detailed in the methodology section, provided significant insights into the interaction between amylotriose, a representative food waste substrate, and GLCM.

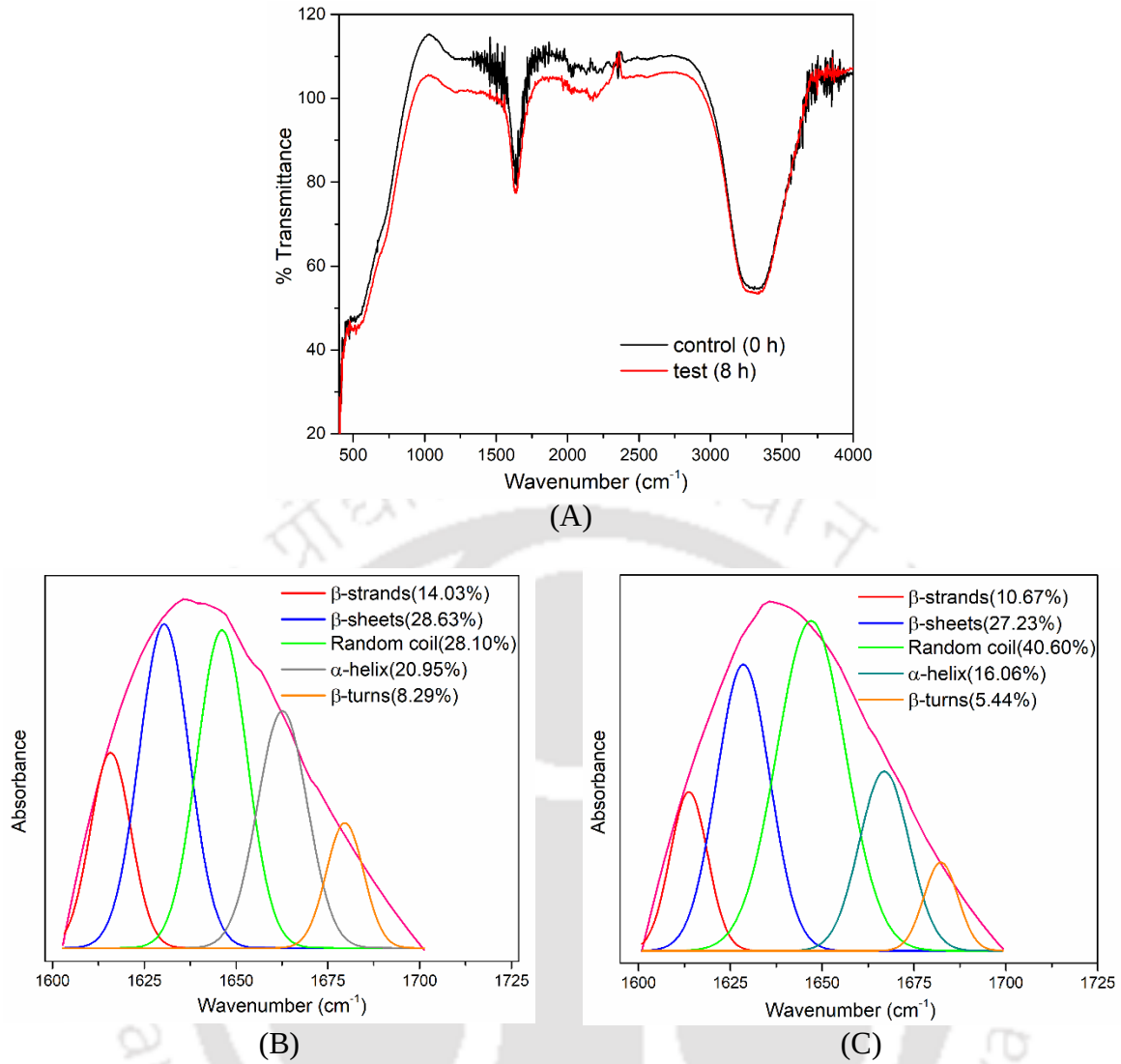

Figure 3.1. Assessing the impact of sonication on the secondary structure of glucoamylase (GLCM) enzyme. (A) FTIR spectra of the glucoamylase enzyme in control conditions (hydrolysis with mechanical agitation) and test conditions (hydrolysis with mechanical agitation and sonication at a 20% duty cycle). Deconvolution of the FTIR spectra within the amide I region (1600-1725 cm^{-1}) to estimate various secondary structural components of GLCM: (B) Control experiments. (C) Test experiments.

As noted in section 3.2.5.2, the binding pocket consisting of active site residues for the D-glucose molecule has been experimentally identified as TRP144, ASP200, and GLU203. Our attempts to predict a binding pocket for amylotriose using blind docking methods and site-specific docking (summarized in Table 3A.2 given in Appendix 3A) revealed that amylotriose does not fit into the glucose binding pocket reported in the UniProtKB database. The blind docking analysis showed a binding energy (ΔG) of -3.56 kcal/mol. This negative binding energy indicates a favorable and strong binding affinity between amylotriose and GLCM, suggesting potential efficiency in this interaction. Hydrogen bonding emerged as the primary interaction type, crucial for the stability of the enzyme-substrate complex. The PyMOL visualization (Fig. 3.2, Fig. 3.3) vividly illustrates this molecular interaction, highlighting critical residues: ASP71, GLU204, ARG329, TYR335, and TYR336. These residues are essential for the binding specificity and catalytic activity of GLCM, emphasizing their importance in the interaction with amylotriose.

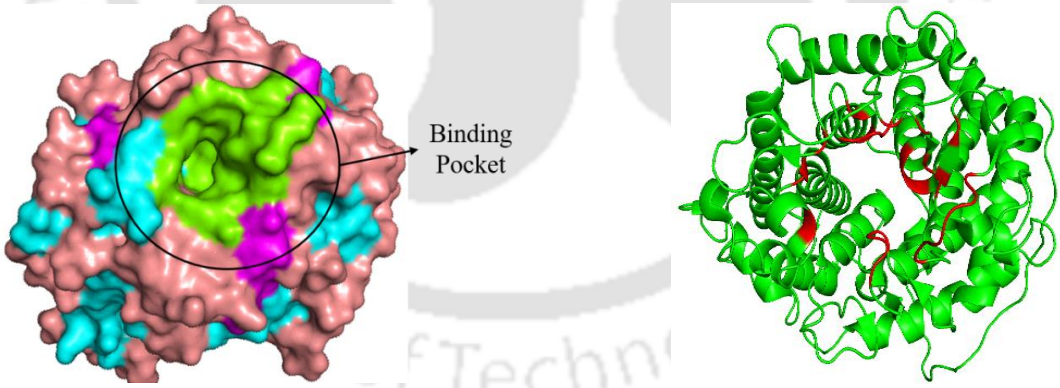

(A) (B)

Figure 3.2 Visualization of the binding pocket of GLCM using PyMOL. Green-colored residues in (A) show binding pocket residues and cavities, and red-colored residues in (B) are residues in the most probable binding pocket.

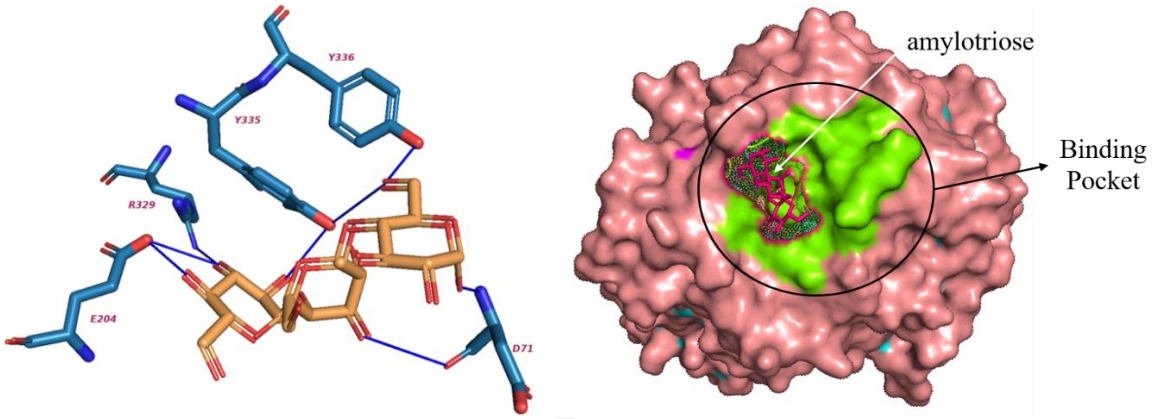

(A) (B)

Figure 3.3: PyMOL visualization of molecular docking of GLCM and amylotriose (A) interactions in the amylotriose-GLCM docked complex and (B) amylotriose in the binding pocket of GLCM

3.3.3.2 MD simulation of amylotriose with GLCM enzyme

To scrutinize the influence of substrates on enzyme dynamics, a Root Mean Square Deviation (RMSD) analysis was conducted on both MD trajectories. As illustrated in Fig. 3.4A, the protein RMSD values from representative trajectories for each system reveal similar flexibility of GLCM in the presence of amylotriose substrates. This observation aligns with the previous findings across various systems, encompassing glycoside hydrolases and other enzymes [30–33].

Principal component analysis (PCA) and enzyme dynamics interpretation: To shed light on the differential effects of the amylotriose on GLCM dynamics, PCA was employed, offering insights into large protein movements. As depicted in Fig. 3.4B, the involvement of each residue in the primary PCA normal mode for GLCM was assessed to be essential for enzyme dynamics. The selected mode, representing the most extensive amplitude, remained consistent in both the control simulation (APO - no substrate) and simulations with amylotriose (complex)

as the substrate. However, the corresponding PCA mode varied in amplitude in the complex. Fig. 3.4B indicates that this mode corresponds to the dynamic opening and closing of a cleft, which is crucial for substrate binding, release, and interaction with the catalytic center.

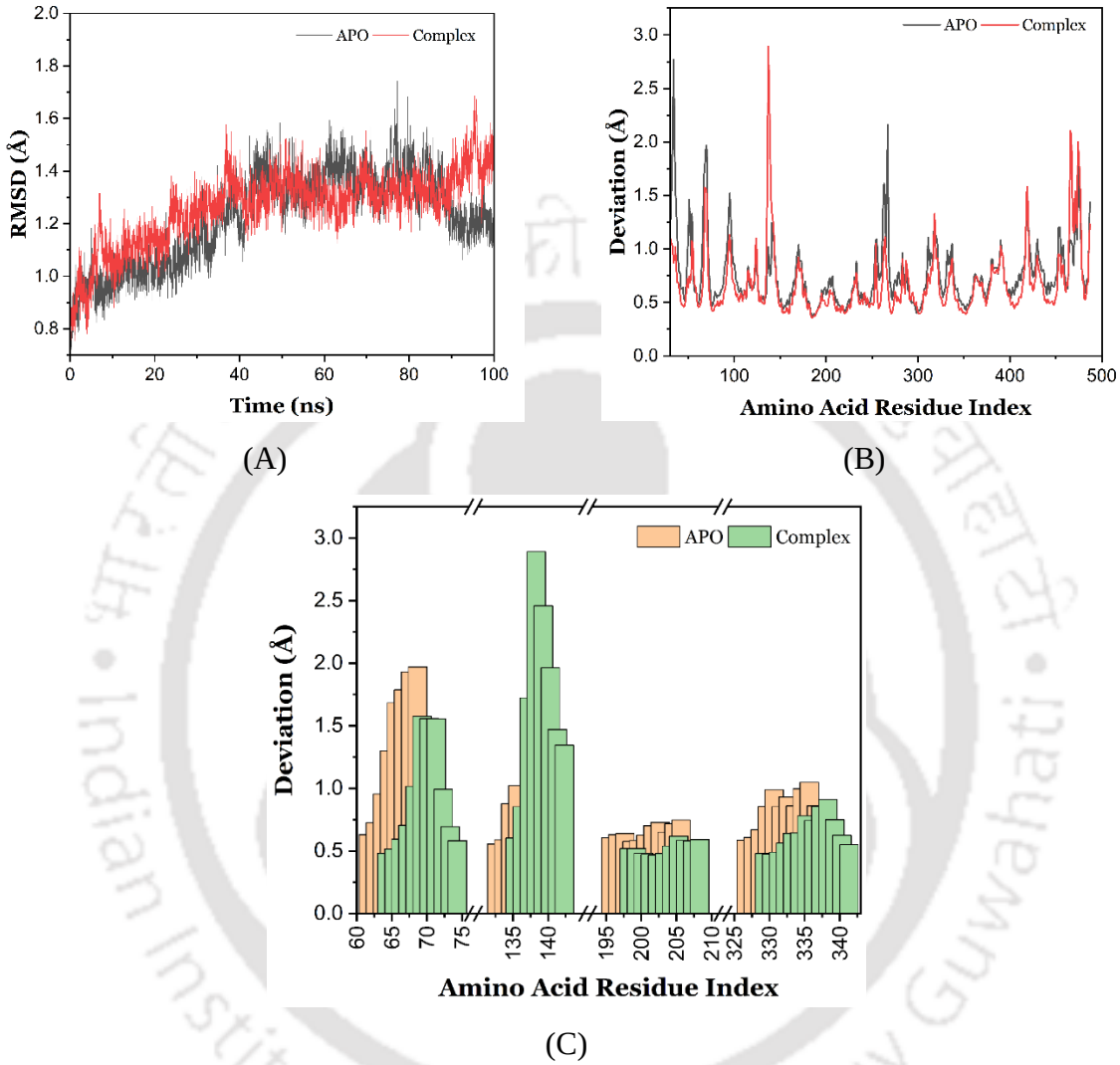

Figure 3.4: Molecular dynamics simulations and trajectory analysis of GLCM in apo form and complexed with amylotriose. (A) Analysis of Root Mean Squared Deviation (RMSD) depicting structural stability in GLCM without substrate (apo, black) and with amylotriose (complex, red); (B) Individual amino acid motional amplitudes in Principal Component Analysis (PCA) for GLCM without substrate (black) and with amylotriose (red); (C) Detailed view highlighting amplitude and deviation in the primary peak region in (B), corresponding to dynamic flaps that open and close, providing access to the catalytic pocket.

The observations derived from the PCA mode depicted in Fig. 3.4C imply a more substantial interaction between GLCM and amylotriose, potentially suggesting the opening of a binding pocket in the presence of amylotriose. Consequently, we interpret our PCA findings as

indicative of a notably slower opening and closing process of the clefts surrounding the enzyme's catalytic site when amylotriose is bound. Moreover, it is plausible that once amylotriose is bound, the anticipated opening of clefts may not occur. This dynamic movement is closely linked to catalysis, facilitating the entry of a new substrate and the release of products. Drawing from our MD simulations, this study proposes that a higher concentration of amylotriose may, in fact, inhibit enzymatic activity (substrate inhibition). This inhibition arises from the prolonged residence of the cleaved substrate within the catalytic pocket, hindering its timely departure and consequently impeding fresh substrate molecules from accessing the reaction site. Inefficient release of reaction products or the potential binding of a different substrate can lead to enzyme inhibition, thereby diminishing the efficiency of biomass conversion.

3.3.3.3 Correlation of docking analysis with modifications in the secondary structure of GLCM

As noted earlier, the deconvolution analysis of the FTIR spectrum of ultrasound-treated GLCM revealed a reduction in α-helix content with a concurrent rise in random coil content. As most of the amino acid residues associated with binding pockets are present in random coil and some residues are present in α-helix, the reduction in α-helix content and concurrent increment in random coil content has the following implications: (i) enzyme structure is relaxed due to unfolding of the proteins resulting in widening of the binding pockets. (ii) the relaxed enzyme structure provides easy accessibility of substrate to the binding pocket. Points (i) & (ii) essentially signify the stabilization of [E-S] or enzyme-substrate complex and improved efficiency of the enzyme, resulting in faster reaction kinetics. In Fig. 3.4C, the observed variation in amino acid residues within the binding pocket and catalytic residues (as depicted in Fig. 3.3A) indicates a dynamic response to the presence of amylotriose, implying the opening

of binding pockets. We propose that ultrasound serves to reinforce and stabilize this opening of the binding pocket, allowing a greater number of substrates, such as amylotriose, to bind more effectively to the desired site. This enhanced interaction between the enzyme and substrate is speculated to impact the reaction kinetics positively. The ultrasound-induced structural changes in GLCM, particularly the sustained opening of the binding pocket, facilitate increased accessibility of the substrate to the enzyme's active site. Consequently, this heightened accessibility contributes to an accelerated enzymatic reaction, resulting in faster kinetics during the hydrolysis of food waste. The interplay between ultrasound-induced structural modifications and the subsequent impact on substrate binding and enzyme activity underscores the multifaceted role of sonication in optimizing the efficiency of food waste hydrolysis processes.

In essence, this study has put forth an effective strategy for solid waste management, in terms of a process for faster enzymatic hydrolysis of food waste into fermentable sugars for producing value-added products. This study has also attempted to give physical insight into ultrasound-assisted enhancement using molecular docking and dynamics simulations. The major limitation of this study is the scale of the experiments. All experiments have been carried out on lab-scale, which may not fully translate to large-scale or commercial applications. Challenges for efficient scale-up include maintaining consistent sonication efficiency and enzyme activity. Moreover, the results of molecular simulations based on a specific food waste substrate (amylotriose) may not be applicable to the wide variations in food waste components in commercial-scale operations.

3.4 Conclusions

The present study has investigated three facets of food waste hydrolysis using glucoamylase: (1) statistical optimization of physical parameters, (2) enhancement of hydrolysis kinetics with sonication, and (3) mechanistic investigation in sonication-induced kinetics enhancement with molecular docking and dynamics simulations. Optimization of food waste hydrolysis resulted in the following optimized parameters for TRS yield of 263.4 mg/g: biomass loading = 10 % w/v, GLCM loading = 50 U/g, temperature = 40 ºC, pH = 5, time = 42 h. Application of 35 kHz sonication at 20 % duty cycle resulted in a marked (4×) reduction in hydrolysis time (10 h) with a 22 % rise in TRS yield (320 mg/g biomass). Deconvolution analysis of the FTIR spectrum of ultrasound–treated GLCM showed major modifications in the secondary structure of the enzyme, viz., reduction in alpha helix content and rise in random coil content. The molecular docking simulation of the binding of amylotriose (representative food waste component) with GLCM revealed the presence of a majority of amino acid residues associated with the binding pocket in α-helix and random coil content of GLCM. The sonication of the enzyme essentially widened the binding pocket of the enzyme, providing easier transport of substrate/product to/from the binding pocket, which was manifested in 4× faster hydrolysis with a significant rise in TRS yield.

CHAPTER 3: Appendix 3A

Table 3A.1: Value-added products from the fermentation of food waste

Type of waste	Pre-treatment	Reactor type	Inoculum	Type of Biofuel	References
Food waste	Heat	7.5L bioreactor with 3L working volume	*Seed sludge(SS)*	Biohydrogen	[34]
Apple pomace	Enzymatic	150 ml bioreactor with 100 ml working volume	*HSSS*	Biohydrogen	[35]
FW	Heat	CSTR,500 ml working volume	*HSSS*	Biohydrogen	[36]
FW	Alkaline	ASBR with 0.15 m^3 working volume	*HSSS*	Biohydrogen	[37]
FW	US with acid	Bottle with 200 ml working volume	*Seed sludge*	Biohydrogen	[38]
FW	Lactate fermentation	Bioreactor with 150 ml working volume	*Irradiated R. sphaeriods*	Biohydrogen	[37]
FW	Drying	SSF, 500 ml flask	*S.Cerevisiae*	Bioethanol	[39]
Waste bread	Drying	Separate,300 ml flask,80 g waste bread	*S.Cerevisiae*	Bioethanol	[40]
FW	LAB spraying	Separate, tower shaped reactor	*S.Cerevisiae KF-7*	Bioethanol	[41]
FW	LAB spraying	Continuous fermenter with 4.3 kg FW	*S.Cerevisiae KF-7*	Bioethanol	[42]
FW	Freeze drying of waste	Anaerobic seed sludge	Two-stage, UASB 8L working volume,	Methane	[43]
FW	Freeze drying	Anaerobic seed sludge	UASB, 2.7 L working volume	Methane	[44]
FW	Fungal hydrolysis by A.oryzae	Schizochytrium mangroveri	Smf 2 L bioreactor	Biodiesel	[45]
FW	Fungal hydrolysis by A. oryzae & A. awamori, autolysis	Chlorella pyrenoidosa	Smf 2 L bioreactor	Biodiesel	[45]

FW: food waste; ASBR: anaerobic sequencing batch reactor; SS: seed sludge; HSS: heat-shocked seed sludge; US: ultrasonication; LAB: lactic acid bacteria; SSF: simultaneous saccharification and fermentation; Smf: submerged fermentation.

Table 3A.2: Best binding energy (B. E.) comparison in blind and site-specific molecular docking for amylotriose as substrate

SI. No.	Blind docking				Site-specific docking (for the binding site reported in the UniProtKB database)			
	Rank	Run	B. E.	RMSD	Rank	Run	B. E.	RMSD
1	1	46	-3.56	26.32	1	27	+6.61	17.11
2	1	63	-0.10	27.41	1	32	+12.78	17.46
3	1	79	+0.75	27.20	1	48	+14.52	17.13
4	2	59	-2.14	35.60	1	9	+16.30	17.65
5	3	5	-1.99	27.37	1	36	+16.47	16.95
6	4	55	-1.49	11.50	1	11	+17.22	16.49
7	5	72	-1.39	27.17	1	22	+18.46	17.14
8	6	53	-1.32	18.41	1	86	+18.53	17.27
9	7	3	-1.21	26.11	1	30	+18.76	17.17
10	7	42	+0.08	25.12	1	44	+19.22	16.62

Section 3A.1: Molecular dynamics simulations and analysis

The study employed Molecular Dynamics (MD) simulations, employing the GROMACS v2019.3 software package for computational investigations [46]. In accordance with established methodologies, we utilized the CHARMM36-July2021 force field [47] to characterize the molecular systems under scrutiny. Employing periodic boundary conditions, we maintained the systems within the NVT ensemble, ensuring a constant temperature of 310 K, and the NPT ensemble, maintaining a pressure of 1 atm. To manage temperature, Langevin dynamics were applied. Short-range non-bonded interactions were subject to a distance cutoff of 11.0 Å, while the particle-mesh Ewald (PME) method [48] was employed to calculate long-range electrostatic interactions. Integration of the equations of motion followed the r-RESPA multiple-time-step scheme, with van der Waals interactions updated every two steps and electrostatic interactions every four steps. The integration time step was uniformly set to 2 fs for all simulations within the study. In the control simulation, lacking a substrate, we initiated a 2 ns equilibration phase by gradually raising the temperature from 0 K to 310 K. Backbone atom restraints were imposed during the initial equilibration period. For simulations involving substrates, a nuanced

equilibration procedure was undertaken, featuring 3 ns of backbone atom constraints followed by an additional 15 ns where backbone atoms within 5 Å of the substrate were constrained. Each system underwent rigorous MD simulations lasting 100 ns.

Trajectory analysis: The analysis of MD trajectories was executed through the utilization of VMD (Visual Molecular Dynamics) software and its associated plugins [17]. To assess structural stability, we computed the Root Mean Square Deviation (RMSD) for both the ligand and the protein. Hydrogen bonds were discerned based on specific criteria: the distance between acceptor and hydrogen atoms was required to be less than 3.0 Å, and the angle formed between the hydrogen-donor-acceptor trio needed to be smaller than 30 degrees for each trajectory frame. Employing the ProDy plugin [49], Principal Component Analysis (PCA) was conducted, affording insights into correlated atomic motions across the molecular dynamics trajectory. This analytical approach facilitated the investigation of slower motions within the enzyme's flexible regions.

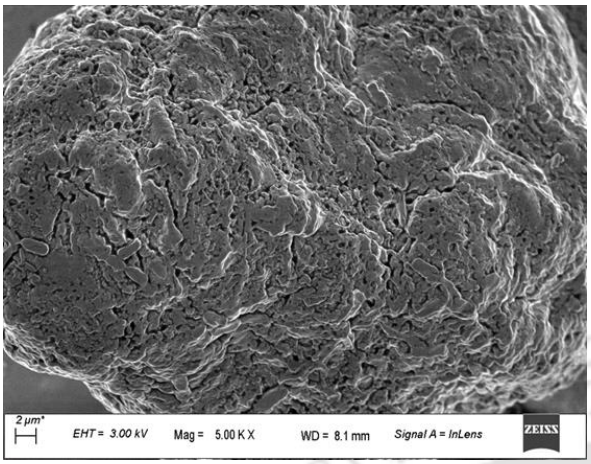

(A)

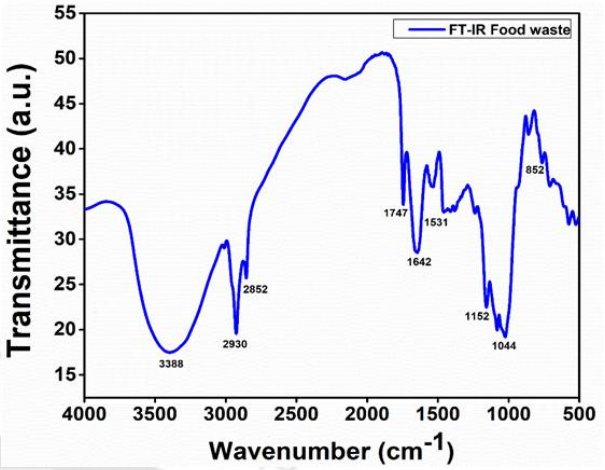

(B)

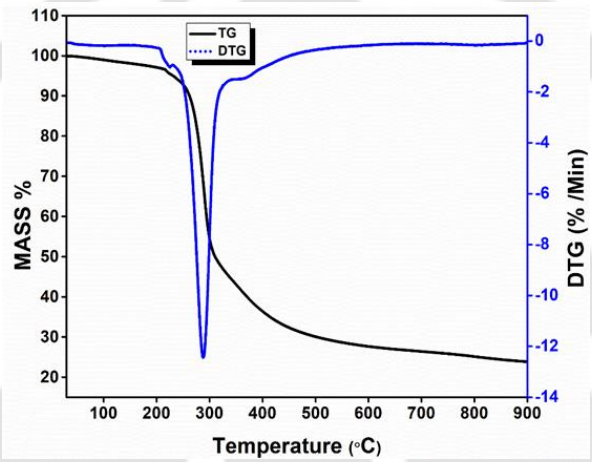

(C)

Figure 3A.1. Characterization of food waste biomass. (A) FE-SEM micrograph; (B) FTIR spectrum; (C) TGA and DTG curves

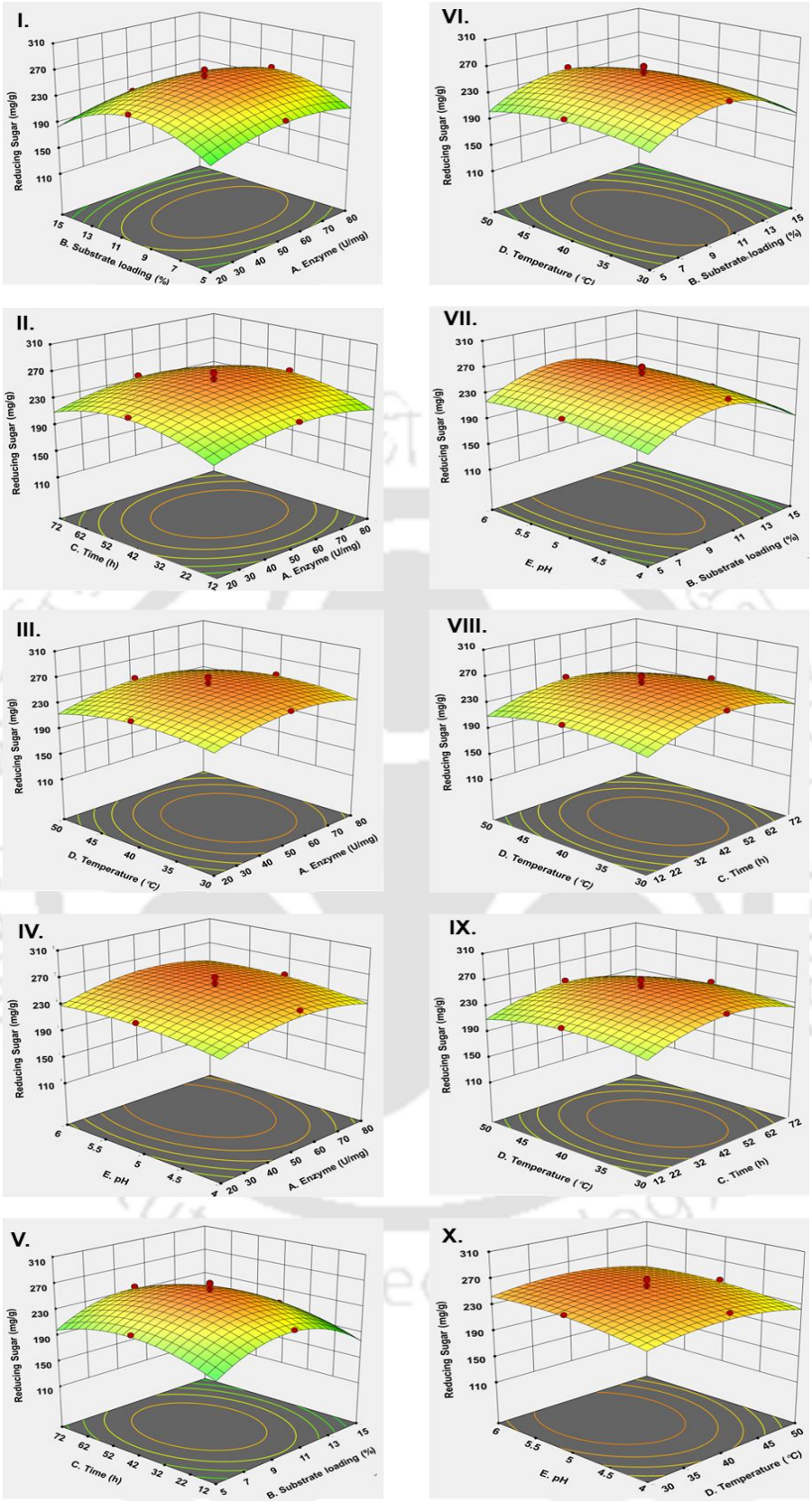

Figure 3A.2: 3-D surface graphs (the interactions between independent variables) of RSM based saccharification optimization of food waste biomass in terms of reducing sugar released (mg/g). I) Enzyme loading Vs Substrate loading, II) Enzyme loading Vs Time, III) Enzyme loading Vs Temperature, IV) Enzyme loading Vs pH, V) Substrate loading Vs Time, VI) Substrate loading Vs Temperature, VII) Substrate loading Vs pH, VIII) Time Vs Temperature, IX) Time Vs pH and X) Temperature Vs pH.

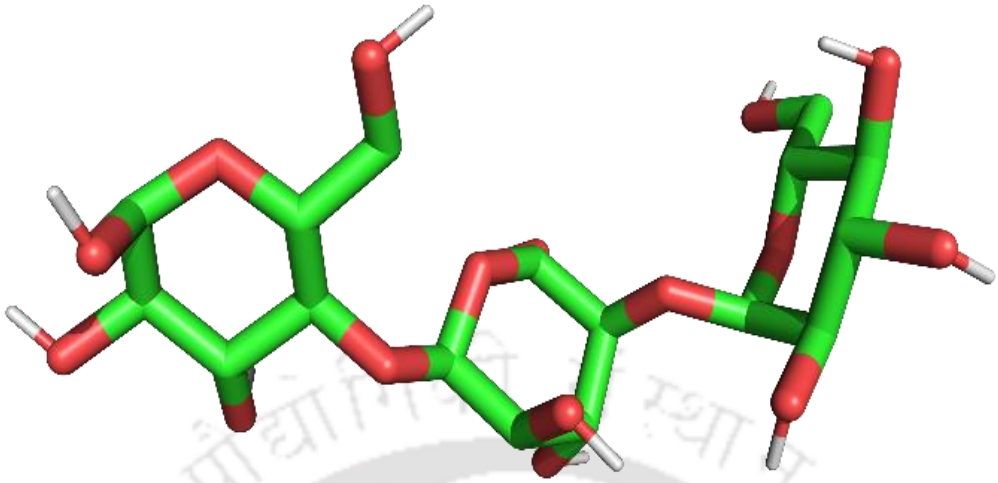

Figure 3A.3: Optimized structure of amylotriose

References

[1] C. Zhang, G. Xiao, L. Peng, H. Su, T. Tan, The anaerobic co-digestion of food waste and cattle manure, Bioresource Technology 129 (2013) 170–176. https://doi.org/10.1016/j.biortech.2012.10.138.

[2] C. Gong, A. Singh, P. Singh, A. Singh, Anaerobic Digestion of Agri-Food Wastes for Generating Biofuels, Indian J Microbiol 61 (2021) 427–440. https://doi.org/10.1007/s12088-021-00977-9.

[3] K. Paritosh, S.K. Kushwaha, M. Yadav, N. Pareek, A. Chawade, V. Vivekanand, Food Waste to Energy: An Overview of Sustainable Approaches for Food Waste Management and Nutrient Recycling, BioMed Research International 2017 (2017) 1–19. https://doi.org/10.1155/2017/2370927.

[4] N.H.M. Yasin, T. Mumtaz, M.A. Hassan, N. Abd Rahman, Food waste and food processing waste for biohydrogen production: A review, Journal of Environmental Management 130 (2013) 375–385. https://doi.org/10.1016/j.jenvman.2013.09.009.

[5] D. Wang, L. Yan, X. Ma, W. Wang, M. Zou, J. Zhong, T. Ding, X. Ye, D. Liu, Ultrasound promotes enzymatic reactions by acting on different targets: Enzymes, substrates and enzymatic reaction systems, International Journal of Biological Macromolecules 119 (2018) 453–461. https://doi.org/10.1016/j.ijbiomac.2018.07.133.

[6] Priya, P.R. Gogate, Ultrasound-Assisted Intensification of Activity of Free and Immobilized Enzymes: A Review, Ind. Eng. Chem. Res. 60 (2021) 9650–9668. https://doi.org/10.1021/acs.iecr.1c01217.

[7] D. Wang, X. Ma, L. Yan, T. Chantapakul, W. Wang, T. Ding, X. Ye, D. Liu, Ultrasound assisted enzymatic hydrolysis of starch catalyzed by glucoamylase: Investigation on starch properties and degradation kinetics, Carbohydrate Polymers 175 (2017) 47–54. https://doi.org/10.1016/j.carbpol.2017.06.093.

[8] H. Meng, D. Li, C. Zhu, The effect of ultrasound on the properties and conformation of glucoamylase, International Journal of Biological Macromolecules 113 (2018) 411–417. https://doi.org/10.1016/j.ijbiomac.2018.02.129.

[9] K. Chandrakant Khaire, V. Suryakant Moholkar, A. Goyal, Alkaline pretreatment and response surface methodology based recombinant enzymatic saccharification and fermentation of sugarcane tops, Bioresource Technology 341 (2021) 125837. https://doi.org/10.1016/j.biortech.2021.125837.

[10] N. Nelson, A PHOTOMETRIC ADAPTATION OF THE SOMOGYI METHOD FOR THE DETERMINATION OF GLUCOSE, Journal of Biological Chemistry 153 (1944) 375–380. https://doi.org/10.1016/S0021-9258(18)71980-7.

[11] K. Kumar, P. Patro, U. Raut, V. Yadav, L. Barbora, V.S. Moholkar, Elucidating the molecular mechanism of ultrasound-enhanced lipase-catalyzed biodiesel synthesis: a computational study, Biomass Conv. Bioref. (2023). https://doi.org/10.1007/s13399-023-04742-4.

[12] K. Kumar, K. Roy, V.S. Moholkar, Mechanistic investigations in sonoenzymatic synthesis of n-butyl levulinate, Process Biochemistry 111 (2021) 147–158. https://doi.org/10.1016/j.procbio.2021.09.005.

[13] C. Zardecki, S. Dutta, D.S. Goodsell, M. Voigt, S.K. Burley, RCSB Protein Data Bank: A Resource for Chemical, Biochemical, and Structural Explorations of Large and Small Biomolecules, J. Chem. Educ. 93 (2016) 569–575. https://doi.org/10.1021/acs.jchemed.5b00404.

[14] G.M. Morris, R. Huey, W. Lindstrom, M.F. Sanner, R.K. Belew, D.S. Goodsell, A.J. Olson, AutoDock4 and AutoDockTools4: Automated docking with selective receptor flexibility, J. Comput. Chem. 30 (2009) 2785–2791. https://doi.org/10.1002/jcc.21256.

[15] L.A. Curtiss, P.C. Redfern, K. Raghavachari, Gaussian-4 theory, The Journal of Chemical Physics 126 (2007) 084108. https://doi.org/10.1063/1.2436888.

[16] S. Yuan, H.C.S. Chan, Z. Hu, Using PyMOL as a platform for computational drug design, WIREs Comput Mol Sci 7 (2017). https://doi.org/10.1002/wcms.1298.

[17] W. Humphrey, A. Dalke, K. Schulten, VMD: Visual molecular dynamics, Journal of Molecular Graphics 14 (1996) 33–38. https://doi.org/10.1016/0263-7855(96)00018-5.

[18] C. Ortiz, M.L. Ferreira, O. Barbosa, J.C.S. Dos Santos, R.C. Rodrigues, Á. Berenguer-Murcia, L.E. Briand, R. Fernandez-Lafuente, Novozym 435: the “perfect” lipase immobilized biocatalyst?, Catal. Sci. Technol. 9 (2019) 2380–2420. https://doi.org/10.1039/C9CY00415G.

[19] J. Luo, K. Ying, J. Bai, Savitzky–Golay smoothing and differentiation filter for even number data, Signal Processing 85 (2005) 1429–1434. https://doi.org/10.1016/j.sigpro.2005.02.002.

[20] A.B. Muley, S.A. Chaudhari, S.B. Bankar, R.S. Singhal, Stabilization of cutinase by covalent attachment on magnetic nanoparticles and improvement of its catalytic activity by ultrasonication, Ultrasonics Sonochemistry 55 (2019) 174–185. https://doi.org/10.1016/j.ultsonch.2019.02.019.

[21] A.H.D. Abdullah, S. Chalimah, I. Primadona, M.H.G. Hanantyo, Physical and chemical properties of corn, cassava, and potato starchs, IOP Conf. Ser.: Earth Environ. Sci. 160 (2018) 012003. https://doi.org/10.1088/1755-1315/160/1/012003.

[22] K.C. Khaire, V.S. Moholkar, A. Goyal, Separation and characterization of cellulose from sugarcane tops and its saccharification by recombinant cellulolytic enzymes, Preparative Biochemistry & Biotechnology 51 (2021) 811–820. https://doi.org/10.1080/10826068.2020.1861011.

[23] W. Su, H. Ma, Q. Wang, J. Li, J. Ma, Thermal behavior and gaseous emission analysis during co-combustion of ethanol fermentation residue from food waste and coal using TG–FTIR, Journal of Analytical and Applied Pyrolysis 99 (2013) 79–84. https://doi.org/10.1016/j.jaap.2012.10.023.

[24] M.F. Tiappi Deumaga, N. Jacquet, C. Vanderghem, M. Aguedo, H.G. Thomas, P. Gerin, M. Deleu, A. Richel, Fractionation and Structural Characterization of Hemicellulose from Steam-Exploded Banana Rachis, Waste Biomass Valor 11 (2020) 2183–2192. https://doi.org/10.1007/s12649-018-0457-9.

[25] G.V. Waghmare, V.K. Rathod, Ultrasound assisted enzyme catalyzed hydrolysis of waste cooking oil under solvent free condition, Ultrasonics Sonochemistry 32 (2016) 60–67. https://doi.org/10.1016/j.ultsonch.2016.01.033.

[26] S. Singh, S. Sarma, M. Agarwal, A. Goyal, V.S. Moholkar, Ultrasound enhanced ethanol production from Parthenium hysterophorus: A mechanistic investigation, Bioresource Technology 188 (2015) 287–294. https://doi.org/10.1016/j.biortech.2014.12.038.

[27] A.Z. Sulaiman, A. Ajit, Y. Chisti, Ultrasound mediated enzymatic hydrolysis of cellulose and carboxymethyl cellulose, Biotechnol Progress 29 (2013) 1448–1457. https://doi.org/10.1002/btpr.1786.

[28] J. Kong, S. Yu, Fourier Transform Infrared Spectroscopic Analysis of Protein Secondary Structures, ABBS 39 (2007) 549–559. https://doi.org/10.1111/j.1745-7270.2007.00320.x.

[29] A.J. Borah, M. Agarwal, M. Poudyal, A. Goyal, V.S. Moholkar, Mechanistic investigation in ultrasound induced enhancement of enzymatic hydrolysis of invasive biomass species, Bioresource Technology 213 (2016) 342–349. https://doi.org/10.1016/j.biortech.2016.02.024.

[30] R.C. Bernardi, I. Cann, K. Schulten, Molecular dynamics study of enhanced Man5B enzymatic activity, Biotechnology for Biofuels 7 (2014) 83. https://doi.org/10.1186/1754-6834-7-83.

[31] C. Li, T. Tan, H. Zhang, W. Feng, Analysis of the conformational stability and activity of Candida antarctica lipase B in organic solvents: insight from molecular dynamics and quantum mechanics/simulations, J Biol Chem 285 (2010) 28434–28441. https://doi.org/10.1074/jbc.M110.136200.

[32] P.R. Batista, G. Pandey, P.G. Pascutti, P.M. Bisch, D. Perahia, C.H. Robert, Free Energy Profiles along Consensus Normal Modes Provide Insight into HIV-1 Protease Flap

Opening, J. Chem. Theory Comput. 7 (2011) 2348–2352. https://doi.org/10.1021/ct200237u.

[33] M.S. Sadeghi Googheri, M.R. Housaindokht, H. Sabzyan, Reaction mechanism and free energy profile for acylation of Candida Antarctica lipase B with methylcaprylate and acetylcholine: Density functional theory calculations, Journal of Molecular Graphics and Modelling 54 (2014) 131–140. https://doi.org/10.1016/j.jmgm.2014.10.001.

[34] J.K. Kim, B.R. Oh, Y.N. Chun, S.W. Kim, Effects of temperature and hydraulic retention time on anaerobic digestion of food waste, Journal of Bioscience and Bioengineering 102 (2006) 328–332. https://doi.org/10.1263/jbb.102.328.

[35] H. Wang, J. Wang, Z. Fang, X. Wang, H. Bu, Enhanced bio-hydrogen production by anaerobic fermentation of apple pomace with enzyme hydrolysis, International Journal of Hydrogen Energy 35 (2010) 8303–8309. https://doi.org/10.1016/j.ijhydene.2009.12.012.

[36] D.-Y. Lee, Y. Ebie, K.-Q. Xu, Y.-Y. Li, Y. Inamori, Continuous H2 and CH4 production from high-solid food waste in the two-stage thermophilic fermentation process with the recirculation of digester sludge, Bioresource Technology 101 (2010) S42–S47. https://doi.org/10.1016/j.biortech.2009.03.037.

[37] D.-H. Kim, S.-H. Kim, K.-Y. Kim, H.-S. Shin, Experience of a pilot-scale hydrogen-producing anaerobic sequencing batch reactor (ASBR) treating food waste, International Journal of Hydrogen Energy 35 (2010) 1590–1594. https://doi.org/10.1016/j.ijhydene.2009.12.041.

[38] E. Elbeshbishy, H. Hafez, B.R. Dhar, G. Nakhla, Single and combined effect of various pretreatment methods for biohydrogen production from food waste, International Journal of Hydrogen Energy 36 (2011) 11379–11387. https://doi.org/10.1016/j.ijhydene.2011.02.067.

[39] N. Sharma, K.L. Kalra, H.S. Oberoi, S. Bansal, Optimization of fermentation parameters for production of ethanol from kinnow waste and banana peels by simultaneous saccharification and fermentation, Indian J Microbiol 47 (2007) 310–316. https://doi.org/10.1007/s12088-007-0057-z.

[40] J. Kawa-Rygielska, W. Pietrzak, A. Czubaszek, Characterization of fermentation of waste wheat-rye bread mashes with the addition of complex enzymatic preparations, Biomass and Bioenergy 44 (2012) 17–22. https://doi.org/10.1016/j.biombioe.2012.04.016.

[41] Y.-Q. Tang, Y. Koike, K. Liu, M.-Z. An, S. Morimura, X.-L. Wu, K. Kida, Ethanol production from kitchen waste using the flocculating yeast Saccharomyces cerevisiae strain KF-7, Biomass and Bioenergy 32 (2008) 1037–1045. https://doi.org/10.1016/j.biombioe.2008.01.027.

[42] Y. Koike, M.-Z. An, Y.-Q. Tang, T. Syo, N. Osaka, S. Morimura, K. Kida, Production of fuel ethanol and methane from garbage by high-efficiency two-stage fermentation process,

Journal of Bioscience and Bioengineering 108 (2009) 508–512. https://doi.org/10.1016/j.jbiosc.2009.06.007.

[43] N.H. Heo, S.C. Park, H. Kang, Effects of Mixture Ratio and Hydraulic Retention Time on Single-Stage Anaerobic Co-digestion of Food Waste and Waste Activated Sludge, Journal of Environmental Science and Health, Part A 39 (2004) 1739–1756. https://doi.org/10.1081/ESE-120037874.

[44] A.P. Trzcinski, D.C. Stuckey, Parameters affecting the stability of the digestate from a two-stage anaerobic process treating the organic fraction of municipal solid waste, Waste Management 31 (2011) 1480–1487. https://doi.org/10.1016/j.wasman.2011.02.015.

[45] D. Pleissner, W.C. Lam, Z. Sun, C.S.K. Lin, Food waste as nutrient source in heterotrophic microalgae cultivation, Bioresource Technology 137 (2013) 139–146. https://doi.org/10.1016/j.biortech.2013.03.088.

[46] M.J. Abraham, T. Murtola, R. Schulz, S. Páll, J.C. Smith, B. Hess, E. Lindahl, GROMACS: High performance molecular simulations through multi-level parallelism from laptops to supercomputers, SoftwareX 1–2 (2015) 19–25. https://doi.org/10.1016/j.softx.2015.06.001.

[47] K. Vanommeslaeghe, E. Hatcher, C. Acharya, S. Kundu, S. Zhong, J. Shim, E. Darian, O. Guvench, P. Lopes, I. Vorobyov, A.D. Mackerell Jr., CHARMM general force field: A force field for drug-like molecules compatible with the CHARMM all-atom additive biological force fields, Journal of Computational Chemistry 31 (2010) 671–690. https://doi.org/10.1002/jcc.21367.

[48] A. Grzybowski, E. Gwóźdź, A. Bródka, Ewald summation of electrostatic interactions in molecular dynamics of a three-dimensional system with periodicity in two directions, Phys. Rev. B 61 (2000) 6706–6712. https://doi.org/10.1103/PhysRevB.61.6706.

[49] A. Bakan, L.M. Meireles, I. Bahar, ProDy: Protein Dynamics Inferred from Theory and Experiments, Bioinformatics 27 (2011) 1575–1577. https://doi.org/10.1093/bioinformatics/btr168.

भारतीय प्रौद्योगिकी संस्थान गुवाहाटी
Indian Institute of Technology Guwahati

CHAPTER 4

Optimization of biohydrogen synthesis using statistical design of experiments (DoE) and artificial neural network (ANN)

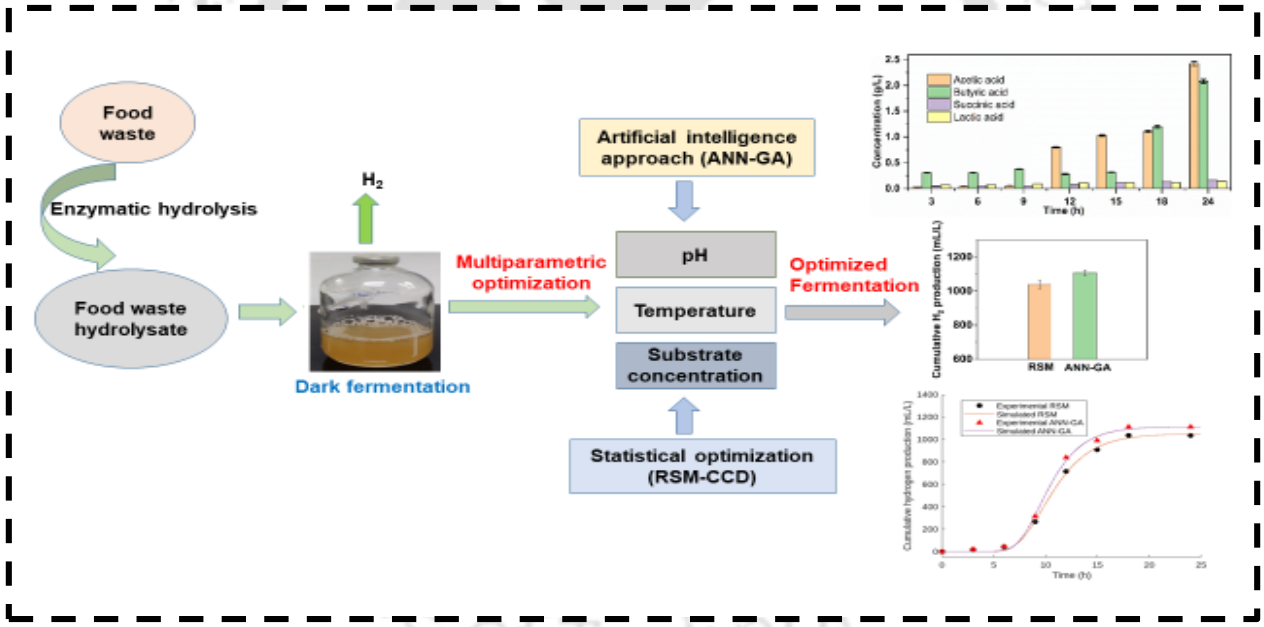

Online: Anand, A., Mahata, C., Moholkar, V.S., 2024. Biohydrogen synthesis from food waste hydrolysate: Optimization using statistical design of experiments (DoE) and artificial neural network (ANN). Biomass and Bioenergy 191, 107452. https://doi.org/10.1016/j.biombioe.2024.107452

4.1. Introduction

Environmental pollution and energy security concerns have triggered extensive global research on green (or renewable) energy over the last decade. Hydrogen is considered one of the promising energy sources because of its high energy density (142 kJ/g) and carbon neutrality [1]. Recently, biological processes have gained significant attention from researchers owing to their environmental sustainability. Dark fermentation is the most efficient process for biohydrogen ($bioH_2$) production because of its low energy requirements, ambient conditions of operation, and the option of using diverse waste feedstocks [2,3]. One of the alternative waste feedstocks for dark fermentation is food waste. The United Nations Environment Programme (UNEP) has reported that India's annual food waste generation amounts to 68.7 million tonnes (as per their food wastage index), whereas global production of food waste is estimated at 1.3 billion [4]. It also estimated that one third of the annual food production in India results in wastage [5]. On the other hand, solid food waste is a potential sustainable feedstock for $bioH_2$ production due to its high carbohydrate content in the form of starch and simple sugars [6]. However, direct utilization of food waste for $bioH_2$ production using fermentative microbes is challenging [7–10]. Hydrolysis of starch to convert carbohydrates into monomeric sugars is necessary prior to $bioH_2$ fermentation [11]. The enzymatic hydrolysis of food waste is a promising technology for sustainable bioenergy generation. Using glucoamylase enzyme for saccharification also has a significant advantage in that it eliminates the necessity for chemical-based pretreatment (employing acids or alkalis) of food waste biomass, which not only reduces the environmental impact of the process but also improves its economy [6,9].

$BioH_2$ production through dark fermentation involves acidogenesis phases. It is highly perceptive to optimize the operating conditions of the fermentation process, such as temperature, pH, inoculum size% (v/v), and total reducing sugar (TRS) concentrations [12,13]. The influence of these parameters on H_2 production has been reported by previous authors using an OVAT (one-variable-at-a-time) approach [2,14]. However, this approach does not account for the interactive

effects among the selected independent variables, and thus, would be insufficient for evaluating optimal conditions for the best fermentation operation [15]. The technique of statistical design of experiments, e.g., response surface methodology (RSM) coupled with central composite design (CCD), accounts for the interactive effects among parameters and accurately predicts the optimum fermentation conditions with minimum experimental runs [16]. Enhancement in bioH_2 production using RSM has been reported previously [17]. However, a significant limitation of RSM is that it cannot accurately model highly non-linear responses [18], which may yield inaccurate optimum sets of the independent variables.

Relatively new artificial intelligence (AI) techniques have emerged as a powerful tool for analyzing non-linear systems [15,19]. In recent years, the application of AI-based modeling methods such as artificial neural networks (ANN) coupled with genetic algorithms (GA) has received increased attention. Previous literature has clearly demonstrated the efficacy of the ANN technique (as compared to the statistical design of experiments) for the optimization of dark fermentative bioH_2 production [19–21].

The objective of the present study is parametric optimization of bioH_2 production from food waste hydrolysate by *Clostridium pasteurianum* using statistical experimental design, viz. RSM and ANN coupled with Genetic Algorithm (GA). Tix et al. [22] have recently reported bioH_2 production from organic waste using dark fermentation, in which a combination of hydrolyzing enzymes (cellulase, glucoamylase, amylase, pectinase, xylase) was used. Han et al. [6] have reported bioH_2 production from food waste using glucoamylase for food waste hydrolysis. Han et al. have used a one-variable-at-a-time (OVAT) approach for the optimization of bioH_2 production from food waste hydrolysate. The dark fermentation process is influenced by several parameters, with interactions among them. Therefore, the present study explores a strategic optimization of dark fermentative hydrogen production from food hydrolysate using statistical design of experiments (RSM–CCD) and ANN–GA techniques. These techniques can perform simultaneous optimization of all parameters for maximum bioH_2 production, and also deduce the nature of

interactions among these parameters. Furthermore, a kinetic study was performed using the data obtained from the validation experiment at optimum conditions obtained using RSM–CCD and ANN–GA techniques.

4.2 Materials and Methods

4.2.1 Pretreatment of food waste

Food waste was collected from different food outlets on the I.I.T. Guwahati campus. It was dried in a hot air oven at 60 °C for 72 h. Next, the food waste biomass was pulverized to a particle size of 0.85 mm in a mixer grinder (Bajaj Pluto 500 W) and stored at 25°C. *Clostridium pasteurianum* MTCC 116 culture was procured from the Microbial Type Culture Collection (MTCC), Chandigarh, India. Glucoamylase enzyme (GLCM) from *Aspergillus niger* was procured from Sigma-Aldrich. All other chemicals were supplied by HiMedia Pvt. Ltd., India. These chemicals were used directly, without any pretreatment.

4.2.2 Enzymatic hydrolysis of food waste

The hydrolysis of food waste using glucoamylase enzyme (GLCM) was carried out in an incubator shaker at the optimum conditions reported in the previous chapter (refer to section 3.2.3 of chapter 3). These optimum conditions obtained using statistical optimization were as follows: pH = 5, GLCM loading = 50 U/g, temperature = 40 ºC, biomass loading = 10% w/v, time = 42 h. The composition of the hydrolysate was: glucose = 245 mg/g food waste and maltose = 18.5 mg/g food waste. Thus, the hydrolysate comprised hexose sugars only and was used as substrate for bioH_2 production [23].

4.2.3 Inoculum preparation

Reinforced Clostridial Medium (RCM), also known as Reinforced Clostridial Broth (RCB), was used as the culture medium for *C. pasteurianum*. The RCM composition was: sodium chloride = 0.005 g/L, yeast extract = 0.005 g/L, beef extract = 0.01 g/L, peptone = 0.01 g/L, glucose = 0.005

g/L, starch = 0.001 g/L, sodium acetate = 0.003 g/L, L-cysteine hydrochloride = 0.0005 g/L, agar = 0.0005 g/L. 1 M NaOH was used to adjust the pH of the medium to 7. Using a Lab Companion SI-300R rotary incubator shaker, the medium was incubated for 24 hours at 180 rpm and 37 °C. After streaking the culture onto an agar plate containing 15 g/L of agar and the same medium composition, it was kept at 37°C in a desiccator equipped with an anaerobic gas pack. Once a month, the culture broth was subcultured and used as stock.

4.2.4 Batch fermentation

Before injection into anaerobic or oxygen-free environments, *C. pasteurianum* cells were cultured in fresh RCM. In a typical batch experiment, 60 mL RCM medium, 0.5 mL of 6% L-cysteine hydrogen chloride (% w/v, as reducing agent), and 5–20% v/v inoculum (mid-log phase of culture) were transferred to a 120 mL serum bottle. Reaszurin dye (0.1% w/v) was also added to the medium to indicate anaerobic conditions. The production media for bioH_2 with specified concentration (indicated in g/L) included: peptone (2), yeast extract (1), TRS concentration (2 – 15), sodium chloride (5), KH_2PO_4 (4), K_2HPO_4 (0.23), and sodium acetate (3). Additionally, 10 mL of each vitamin and trace element solution was added to the 1 L of production media. The vitamin solution composition (in g/L) was: folic acid (0.01), para–amino benzoic acid (0.01), citric acid (0.02), and riboflavin (0.025). The trace element solution comprised of following components with specified concentration (g/L): $CuCl_2 \cdot 6H_2O$ (0.05), $FeCl_3$ (0.1), $MgCl_2 \cdot 6H_2O$ (0.2), $CoCl_2 \cdot 6H_2O$ (0.2), Na_2MoO_4 (0.01), $ZnSO4 \cdot 7H_2O$ (0.05), $MnO_4 \cdot 7H_2O$ (0.01), H_3BO_3 (0.01), $N(CH_2COOH)_3$ (4.5). 1 M NaOH was used to adjust the pH of the medium to the desired level (5 – 10). Before sterilization, the medium was purged for 15 min with 99.99 % pure N_2. Serum bottles were autoclaved (121°C and 15 psi pressure) for 30 min. This was followed by inoculation (5 – 20% v/v) and incubation of the serum bottles at 30–42°C and 180 rpm. After an 18-hour incubation period, the total gas generated in the serum bottle was collected using the water

displacement method and then analyzed with gas chromatography (GC) [12,24]. To assess the reproducibility of the results, each experiment was conducted thrice.

Prior to the main experiments in the statistical design of experiments, we conducted preliminary experiments using one-variable-at-a-time (OVAT) for optimization of three independent parameters, viz. pH, temperature, and TRS concentration. In the OVAT approach, one parameter value was varied, keeping other parameters constant.

4.2.5 Statistical optimization of bioH_2 fermentation

The physicochemical parameters for bioH_2 production from food waste hydrolysate were optimized using the response surface methodology (RSM). A 5-level 3-factor CCD generated through Design Expert 13 version software was used to perform the RSM. Factors and their experimental design levels for CCD were obtained from the preliminary experiments (single parameter optimization) and summarized in Table 4A.1 (given in Appendix 4A). Cumulative hydrogen production (mL/L) (hydrogen produced /total broth volume) was the objective function of the statistical experimental design. The parameters chosen for optimization were pH, temperature, and TRS concentration. Previous studies showed that the effect of inoculum size was not a significant parameter for hydrogen production in dark fermentation [12,15]. Therefore, it was not considered for multiparameter optimization in the present investigation.

The general form of the 2nd-order polynomial regression model with three variables was used to elucidate the response behavior described in (Eq. 4.1).

$$Y = \alpha_0 + \sum_{i=1}^{k} \alpha_{ii} X_i + \sum_{i=1}^{k} \alpha_{ii} X_i^2 + \sum_{i \neq j} \sum_{i} \alpha_{ij} X_i X_j \qquad (4.1)$$

Notations used: Y = measured response variable (mL/L), α_0 = intercept or regression coefficient, α_{ii} = quadratic coefficient, α_{ij} = interaction coefficient, k = number of factors, X = uncoded level of the input variable. Solution of (Eq. 4.1) yields the optimum set of independent variables for maximum bioH_2 production. The fitness of the regression model was assessed using ANOVA,

whereas 2-D contour plots revealed the interactive effects among the independent variables. The complete set of 20 experiments in the RSM-CCD design is described in Table 4.1.

4.2.6 Artificial intelligence (AI) approach for bioH_2 fermentation

The dark fermentation process for bioH_2 is intricately complex, resulting in highly nonlinear relationships between dependent and independent variables. Numerous previous studies have reported better efficacy of AI (over conventional statistical optimization) for modeling and optimization of bioH_2 production [25–27]. In this context, we have used the AI approach for the optimization of dark fermentation with the artificial neural network (ANN) tool, which is advisable for modeling nonlinear systems. The algorithm followed in this study is given below.

4.2.6.1 Artificial neural network coupled with Genetic algorithm (ANN-GA)

By employing a mathematical depiction of interconnected neurons, the artificial neural network replicates the brain's learning process through a structured network architecture [28]. A standard neural network comprises three layers: input, hidden, and output [29]. The hidden layer links neurons to the input and output layers through adjustable weights. These weights enable the network to compute intricate relationships between input and output variables, facilitating complex information processing. An "activation function" is responsible for the non-linear transformation of the input signal within a neural network node into an output signal. This transformation occurs after the addition of weighted inputs to the neuron and the incorporation of bias, as outlined in (Eq. 4.2) [30]. The preferred activation function is the hyperbolic tangent, as depicted in (Eq. 4.3) [31].

In this study, the experimental data was acquired through CCD design, and the ANN model for bioH_2 production was established using Table 4.1. The data were divided into three sets, with 70% allocated for training, 15% for testing, and 15% for validation [32]. The training of the proposed ANN was carried out utilizing a "multilayer perceptron feed-forward neural network

with error back-propagation" (BP) employing the "Levenberg– Marquardt algorithm" in MATLAB version [16,17].

$$y_i = \sum_{i=1}^{n} x_i w_{ij} + \theta_j \quad (4.2)$$

$$f(y_i) = \frac{2}{1+\exp(-2y_i)} - 1 \quad (4.3)$$

where x_i = input parameters matrix, θ_j = bias matrix, y_i = weighted inputs and w_{ij} = connection weights matrix

After formulating the ANN model, it served as the objective function for further optimization using genetic algorithm (GA) as the tool. GA, a stochastic non-linear optimization method rooted in natural selection and belonging to the evolutionary algorithms class, is driven by AI. In this approach, solutions from a current population were leveraged to create a new population, with the requirement that the new population has improved quality [33]. At each step, the algorithm utilized three primary bio-inspired rules, viz. mutation, crossover, and selection, to create the next generation from the current population [34]. This iterative process was continued until an optimal solution was reached.

4.2.7 Analytical methods

The time profiles of hexose sugars and metabolites in the fermentation mixture were monitored using HPLC (Shimadzu, Model: DGU-20A5R) equipped with refractive index (RI) detector and photodiode analyzer (PDA). The column used in HPLC was 300 mm × 7.8 mm Aminex@ HPX-87H along with a 50 mm × 7.8 mm guard column. The mobile phase was 0.01 M H_2SO_4 in ultra–pure water with a flow rate of 0.6 mL/min [35]. The product gas was analyzed using a GC (Make: Thermo Scientific, Model: Ceres800 plus). The GC used Porapak Q (60/80 mesh) column and argon as carrier gas at a flow rate of 30 mL/min. The column oven in GC operated at 45 °C, and the injector and detector temperatures were maintained at 200 °C. Detailed protocol for analysis of H_2 gas content and soluble metabolites concentration is given in our

previous paper [11,23].

4.3 Results and Discussion

4.3.1 Preliminary experiments

Preliminary experiments were carried out to ascertain the impact of the following parameters on bioH_2 generation prior to the statistical design study: (1) initial pH of fermentation, (2) incubation temperature, (3) initial TRS concentration, and (4) inoculum size. The approach used in the preliminary experiments was "one variable at a time (OVAT)". The primary CCD experiments were designed using the findings of these experiments.

pH of fermentation medium: Experiments were carried out using serum bottles containing production media with initial pH levels ranging from 5 to 10. The initial pH of the medium was adjusted using 1 N ortho-phosphoric acid or 1 M NaOH. Cumulative hydrogen production (CHP) increased from 212 ± 3 mL/L (H_2 content in the product gas 12.4 ± 2% v/v) at an initial pH of 5, to 722 ± 7 ml/L (H_2 content 42 ± 2% v/v) at an initial pH of 7 (Fig. 4.1(A)). Further rise in initial pH led to a gradual reduction in H_2 production due to the inhibition of the hydrogenase enzyme, which is mainly responsible for hydrogen production. The maximum H_2 production was achieved at an initial pH of 7, which is consistent with the literature [36]. pH more than 7 refers to alkaline conditions; it has several effects on biochemical activity and reproduction, which could be harmful to normal cellular functions. For example, elevated pH might result in DNA denaturation, which can cause various undesirable physiological changes including the instability of the plasma membrane and cytosolic enzymes [37]. pH << 7, which refers to acidic conditions, is also detrimental to cell viability as it can cause DNA damage. Deviations from this optimum pH essentially result in low ATP levels within the cell, thereby hindering bacterial growth and enzyme activity, consequently reducing H_2 production [12,38].

Incubation temperature: While holding other parameters constant, the impact of temperature was examined in the range of 30 to 42 °C. Batch experiments with growth media were carried out at

different temperatures (30, 32, 35, 37, 40, and 42 °C) in order to assess the impact of temperature on H_2 production. The initial pH was set at 7, the total reducing sugar (TRS) concentration was 15 g/L, and the serum bottles were shaken at 180 rpm. As shown in Fig. 4.1(B), the maximum CHP of 705 ± 25 mL/L (H_2 content in the produced gas 38 ± 2% v/v) was recorded at 37 °C. This value progressively dropped to 312 ±12 mL/L (H_2 content 25 ± 2% v/v) at 42 °C. The optimum temperature for CHP was thus determined to be 37 °C, consistent with previous literature results [39]. Lower hydrogen production was observed at higher temperatures, which may be attributed to the thermal deactivation of the hydrogenase enzyme [40].

Initial concentration of food waste hydrolysate: Food waste hydrolysate obtained from enzymatic hydrolysis of food waste was used as the sole carbon source or substrate. The substrate (reducing sugar) concentration in the fermentation mixture was varied in the range of 0–15 g/L. The effects of TRS were conducted under the optimum experimental conditions obtained from previous experiments. Cumulative hydrogen production was found to increase with hydrolysate concentration (Fig. 4.1(C)). Maximum hydrogen production (790 ± 25 mL/L) was obtained at a hydrolysate concentration of 10 g/L and reduced thereafter. Furthermore, in the presence of high substrate concentration, the consumption of other essential nutrients in the media by the microbial cells may reduce, which results in lowering of metabolism rate and hydrogen yield [41,42] . These results might be attributed to the product inhibition (due to substrate inhibition effect) at high TRS concentration in the present study. Moreover, higher TRS concentration could result in more soluble metabolites and lower a pH, which could be detrimental to H_2 producing microbes [15].

Inoculum size: Batch studies were carried out using different inoculum sizes from a *C. pasteurianum* culture that was cultivated overnight. Using 15 g/L TRS as the substrate, freshly prepared anaerobic production media was inoculated with inoculum sizes of 5, 10, 15, and 20% v/v. After 18 hours of incubation at 37 °C and 180 rpm shaking in an incubator shaker, the gaseous phase was examined for the formation of hydrogen gas. When the inoculum size was 5%, the CHP increased to 313 ± 12 mL/L (18.5 ± 0.8% v/v), but when the inoculum size was 10% v/v, it grew

to 718 ± 15 mL/L (41 ± 2% v/v). Following that, a 20% v/v drop in inoculum size was seen in the H_2 production. The variations in the CHP with inoculum size are seen in Fig. 4.1(D). A plausible explanation for the decrease in H_2 generation with greater inoculum sizes is excessive substrate consumption, which causes the cells to proliferate and produce more metabolites such as lactate, butyrate, acetate, and succinate. The pH drops quickly as a result of the fermentation medium's formation of acidic byproducts. The results shown in Fig. 4.1(D) indicated that the ideal inoculum concentration for hydrogen generation was 10% v/v.

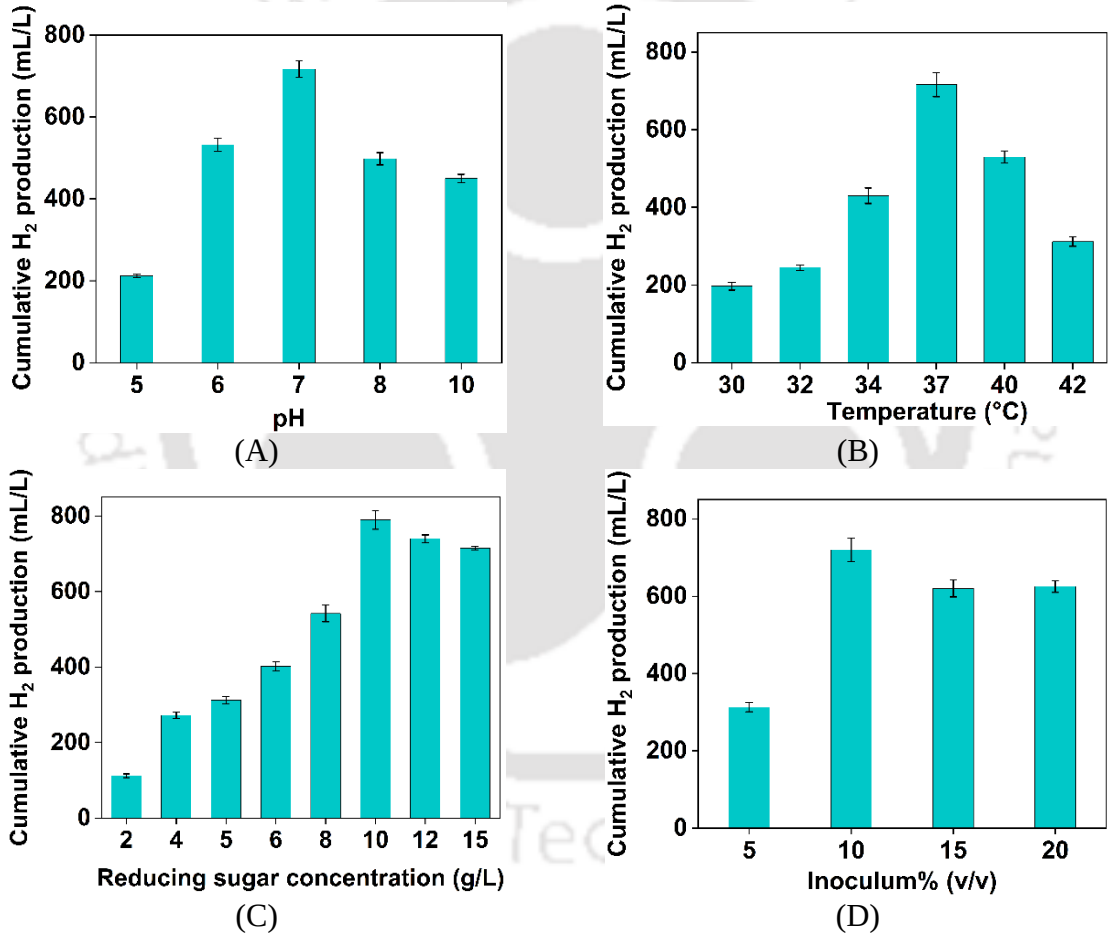

Fig. 4.1. Results of initial (or preliminary) experiments on cumulative hydrogen production (mL/L) in batch fermentation. Effect of (A) pH, (B) temperature (°C), (C) reducing sugar concentration (g/L), and (D) inoculum size% (v/v)

Table 4.1. CCD design and the response for bioH_2 production

Run	TRS Concentration (g/L) (Factor A)	pH (Factor B)	Temperature (°C) (Factor C)	CHP (actual) (mL/L)	CHP (ANN predicted) (mL/L)	CHP (RSM predicted) (mL/L)
1	10	6.5	36.0	1032.0	1026.2	1044.6
2	10	5.0	36.0	154.7	156.4	148.8
3	7	5.6	39.6	136.2	158.6	120.5
4	10	6.5	42.0	215.3	228.2	202.2
5	10	6.5	36.0	1032.0	1026.2	1044.6
6	10	6.5	30.0	130.5	120.6	117.9
7	5	6.5	36.0	528.0	511.4	542.7
8	13	7.4	32.4	304.1	324.6	337.8
9	7	7.4	32.4	409.6	434.9	391.1
10	10	6.5	36.0	1032.0	1026.2	1044.6
11	13	5.6	32.4	160.4	144.8	167.7
12	15	6.5	36.0	731.1	722.4	690.8
13	7	7.4	39.6	298.3	306.3	309.1
14	10	6.5	36.0	1044	1026.2	1044.6
15	7	5.6	32.4	244.6	235.6	257.8
16	10	8.0	36.0	450.2	482.7	440.5
17	13	5.6	39.6	313.6	313.0	350.1
18	13	7.4	39.6	570.6	557.8	575.5
19	10	6.5	36.0	1032.0	1026.2	1044.6
20	10	6.5	36.0	1032.0	1026.2	1044.6
					ANN-GA	RSM
R^2					0.9968	0.9960
RMSE					7.996	26.4558

4.3.2 Optimization of process parameters for enhanced bioH_2 production

4.3.2.1 Response surface methodology-based fermentation of food waste hydrolysate

BioH_2 production from food waste hydrolysate was optimized for the following variables by employing a CCD statistical design: pH, temperature (°C), and TRS (g/L). The optimization experiments were carried out in a 120 mL serum bottle with a shaking speed of 180 rpm in an incubator shaker. The results of the CCD design are shown in Table 4.1. The results were further analyzed by RSM to generate a second order polynomial equation to show hydrogen production as a function of process parameters. The 2nd order equation for the CCD design relating the response variable to optimization variables is given below:

Cumulative BioH_2 Production (mL/L) (cumulative volume of hydrogen produced/total volume of fermentation broth)

$$Y = 1044.67 + 44.05A + 89.63B + 25.09C + 9.20A\cdot B + 79.93A\cdot C + 13.82B\cdot C - 151.27A^2 - 266.92B^2 - 312.74C^2 \quad (4.4)$$

The above quadratic model (Eq. 4.4) of the response data of bioH_2 fits well, as revealed by the ANOVA analysis given in Table 4.2. A large overall *F*-value (274.82) for the model and *p*-value (< 0.0001) show the significance of model terms and had only a 0.01% chance of noise. *p*-values > 0.1 indicate non-significance of model terms. Individual parameters (A, B, and C) significantly influenced bioH_2 production (*p*-value < 0.0001). Among the parameters, pH (B) had the most substantial impact on bioH_2 production (*F*-value 106.09), followed by TRS concentration in food waste hydrolysate (A) (*F*-value 25.59) and temperature (*F*-value 8.30). Similar results was observed by Gawal et al. [43]. The model coefficients of the products of optimization variables (or the interaction parameters) (A·B and A·C) have a *p*-value < 0.05, which indicates their significance. In contrast, the product B·C has a *p*-value > 0.05, which

indicates its non-significance. In physical terms, this result suggests that some physical variables used in optimization independently influence the yield of bioH_2 production from food waste hydrolysate. On the other hand, the *p*-values of model coefficients for squared variables (A^2, B^2, C^2 etc.) are < 0.05, which indicates their significance [12]. The Lack-of-Fit has *p*-value > 0.05 (insignificant), which confirms the fitness of the model [15]. Finally, the regression coefficient of the model (R^2) = 0.996 and the predicted R^2 = 0.99 are in reasonable agreement with the adjusted R^2 = 0.9952 as shown in Table 4.2, and essentially show the best fit of the model.

Table 4.2. ANOVA analysis for bioH_2 production

Source	Sum of squares	df	Mean square	*F*-value	*p*-value	Remark
Model	3056.33	9	339.59	274.82	< 0.0001	significant
A – TRS concentration	34.41	1	34.41	25.59	< 0.0001	
B – pH	236.2	1	236.2	106.09	< 0.0001	
C –Temperature	18.38	1	18.38	8.30	0.0003	
AB	0.176	1	0.176	0.65	0.0191	
AC	106.14	1	106.14	49.35	< 0.0001	
BC	1.82	1	1.82	1.47	0.117	
A^2	254.99	1	254.99	318.46	< 0.0001	
B^2	1110.84	1	1110.84	991.58	< 0.0001	
C^2	1710.09	1	1710.09	1361.22	< 0.0001	
Residual	6.18	10	0.6177			
Lack of Fit	3.52	5	0.7035	1.34	0.3832	not significant
Pure Error	2.66	5	0.5319			
Cor Total	3062.5	19				
Fit statistics						
R^2 = 0.9960						
Adj. R^2 = 0.9952						
Pred R^2 = 0.9900						

Fig. 4A.1 (given in Appendix 4A) shows the 2-D contour plots that represent the mutual interaction among the input variables. Two independent variables were varied while the third variable was held fixed at zero coded value (or mean value) to create these plots. Significant interaction among any two independent parameters is indicated by the elliptical shape of the contour plot. In such a case, the maximum value of the response variable is achievable for the combination of values of two parameters within the smallest ellipse [27,43]. The contour plots between TRS concentration and pH (at temperature = 36 ºC), and between TRS concentration and temperature (at pH = 6.5) showed the maximum cumulative hydrogen production at the point of intersection of major and minor axes of the innermost ellipse, suggesting high correlation levels [12]. On the other hand, an insignificant interaction between pH and temperature was observed in the third contour plot, which was circular in type. Consequently, an insignificant *p*-value (Table 4.2) was observed for the interaction between pH and temperature in the regression equation (Eq. 4.4). However, the highest response region for all the contour plots was located in the plots themselves, which means the maximum H_2 production could be achieved inside the designed boundary [27,44]. Eventually, the optimum condition for obtaining maximum CHP was calculated by setting the partial derivative of (Eq. 4.4) to zero.

Appendix 4A includes a 3D response surface (Fig. 4A.2) for the objective function of optimization (CHP) between pairs of optimization variables. The combination of optimization variables for the highest yield of bioH_2 is as follows: pH = 6.5, temperature = 36 ºC, TRS concentration = 10 g/L. The predicted cumulative yield by the quadratic model for the optimum set of parameters is 1044.6 mL/L, which is in close consent or agreement with the model prediction.

A plausible explanation for the significance of interactions among TRS & pH and TRS & temperature, and the synergism between the parameters can be given as follows: TRS is the

substrate for dark fermentation. Therefore, the bioH_2 production increases with TRS concentration till the self-inhibition limit at high concentration levels. However, the maximum TRS concentration in the experimental design is 15 g/L, which is well below the self-inhibition levels (typically > 50 g/L).

The microorganisms involved in the fermentation process are sensitive to pH, which affects enzyme activity. Optimal pH conditions can enhance the activity of key enzymes that break down sugars, leading to a more efficient conversion of TRS into bioH_2. Maintaining an appropriate pH balance ensures that the microbial community remains healthy and active. Therefore, high TRS concentration (within the limits used in this study) in concurrence with optimum pH value results in enhanced bioH_2 production.

Temperature affects the rate of enzymatic reactions in the metabolic pathway. Within a certain range, an increase in temperature can lead to higher metabolic rates, thus speeding up the breakdown of TRS and enhancing bioH_2 production. The microbial culture used in this study, *Clostridium pasteurianum*, is a mesophilic bacterium with the best growth temperature range of 36-37°C. A higher TRS concentration, combined with the optimal temperature, can lead to a higher rate of bioH_2 production because the microbes are more metabolically active.

***Synergistic effect of TRS, pH, and temperature*:** The interaction between TRS concentration, pH, and temperature can create optimal conditions for specific metabolic pathways that favor hydrogen production. For example, some pathways might be more active at slightly acidic pH levels and moderate temperatures, leading to increased bioH_2 yield when TRS levels are sufficient. High TRS concentrations mean that the microbes have ample substrates for metabolism, and if the pH and temperature are also optimum, the conversion efficiency can be maximized. An optimum pH also helps minimize the production of inhibitory by-products (soluble metabolites) that can suppress hydrogen production. This ensures that the fermentation

process remains focused on bioH_2 production. This synergy ensures that the sugars are utilized efficiently, leading to higher hydrogen yields.

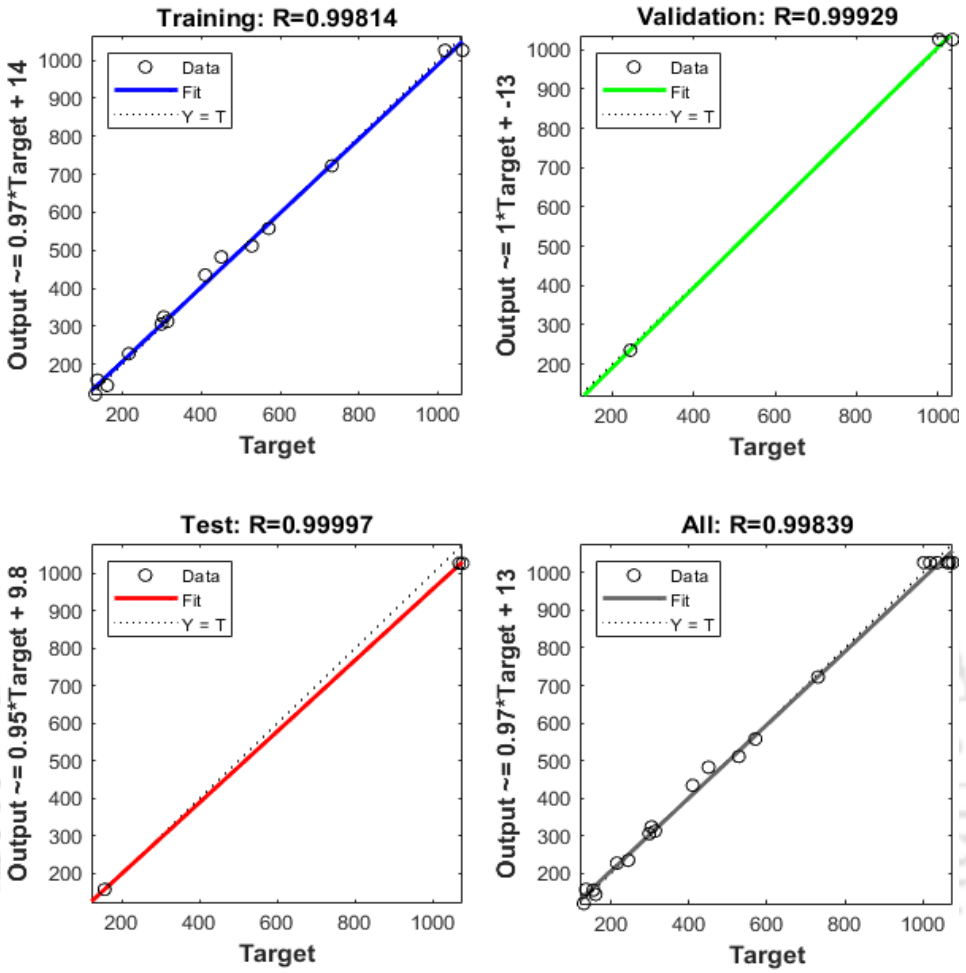

Fig. 4.2. Regression of the ANN-GA simulations

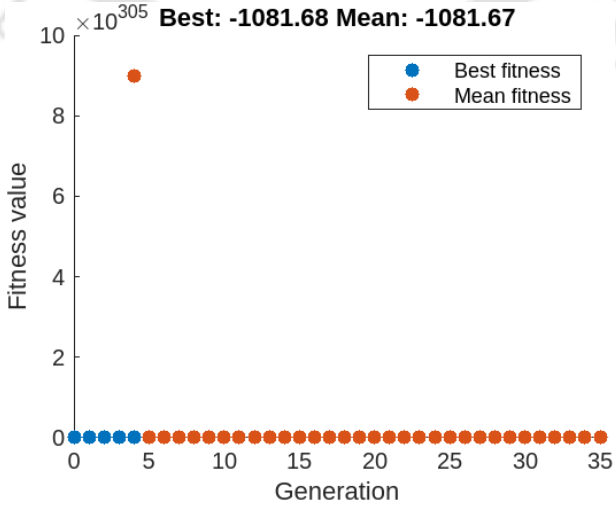

Fig. 4.3. Generation plot for global solutions in GA

4.3.2.2 Optimization using ANN–GA technique

The ANN model for bioH_2 production was developed using the experimental results in Table 4.1. The ANN model for bioH_2 production was trained at 3 epochs adopting a 3-9-1 network topology (refer to Fig. 4A.3 in Appendix 4A). R^2-value and RMSE were determined as 0.999 and 7.996, respectively. Lower RMSE and higher R^2-value indicated a good relationship between the target and predicted values. Regression of ANN-GA simulations plots are shown in Fig. 4.2. ANN architecture (Fig. 4A.3), ANN performance (Fig. 4A.4), ANN training site (Fig. 4A.5), and ANN error histogram (Fig. 4A.6) are provided in Appendix 4A. ANN model, after attaining the desired level of accuracy, was used as a fitness function in GA optimization algorithms to predict the optimum set of parameters for maximum bioH_2 production [45]. The parameters used in GA algorithms are selected based on the literature [46,47]. The generation plot shows that the global solution is reached after 5 iterations (refer to Fig. 4.3). Reaching a solution in fewer generations could indicate that the GA found promising results quickly. ANN-GA technique yielded the following set of optimum parameters: TRS concentration in food waste hydrolysate = 10.85 g/L, pH = 6.8, temperature = 36.82 ºC, and predicted CHP =1081.7 mL/L.

4.3.3 Comparison of prediction capability between RSM and ANN

To compare the predictive accuracy of the Response Surface Methodology (RSM) and Artificial Neural Network (ANN) models for bioH_2 production, two key metrics were used: the coefficient of determination (R^2) and the root mean square error (RMSE). These metrics were calculated using eqs. 4.5 and 4.6, respectively.

$$R^2 = 1 - \frac{\sum_{i=1}^{n}\left(z_i^{exp} - z_i^{pred}\right)^2}{\sum_{i=1}^{n}\left(z_i^{exp} - z^{mean}\right)^2} \qquad (4.5)$$

$$RMSE = \sqrt{\frac{\sum_{i=1}^{n}\left(z_i^{exp} - z_i^{pred}\right)^2}{n}} \quad (4.6)$$

where z_i^{pred} is the corresponding predicted data, z_i^{exp} is the experimental data, n is the number of experiments, and z^{mean} is the mean of experimental data.

The higher the R^2 value and the lower the RMSE value, the better the prediction accuracy of the model. As shown in Table 4.1, the R^2 values for the ANN and RSM models were 0.9968 and 0.9960, respectively, whereas the RMSE values were 7.996 and 26.45, respectively. Thus, the ANN model demonstrated superior predictive performance compared to the RSM model due to higher R^2 and lower RMSE values. While the RSM model relies on a 2nd-order polynomial, the improved prediction accuracy of the ANN model can be attributed to its ability to analyze more complex, higher-order nonlinear relationships. Previous studies have also reported superior generalization capability of the ANN model over the RSM model [15,17,48]. However, it is essential to note that the prediction capability of the ANN model is constrained by the range of process parameters used during training.

4.3.4 Validation studies

The predictability of developed RSM and ANN-GA models was ascertained by performing a validation fermentation experiment at the optimum conditions. As per the RSM technique (referring to Table 4.1), the predicted optimum parameters for maximum bioH_2 production were: temperature = 36 °C, pH = 6.5, TRS concentration = 10 g/L, with the predicted bioH_2 yield = 1044 mL/L. This is in accordance with the experimental response of 1039 mL/L (46 ± 2% H_2 content in product gas) with an error of 3.4%.

Table 4.3. Comparative study of bioH_2 production from different waste sources

Reactor type	Microorganism	Substrate	Cumulative hydrogen production (mL/L)	BioH_2 yield (mol/mol glucose or hexose sugar)	References
Batch	Anaerobic sludge	Food waste	982	–	[49]
Batch	Anaerobic sludge	Food waste	1014	–	[39]
Batch	Anaerobic digesters inocula	Food waste	380	–	[50]
Packed bed reactor	Mixed culture	Hydrolyzed waste wheat	834	–	[51]
Batch	Granular microbial preparation	Food waste	1400	–	[52]
CSTR	Anaerobic sludge	Wheat flour hydrolysate	1423	1.90	[53]
CSTR	Anaerobic sludge	Food waste hydrolysate	1500	1.97	[6]
Batch	*Clostridium beijerinckii KCTC 1785*	Food Waste	–	1.12	[54]
Batch	Anaerobic bacteria	lignocellulosic biomass	–	0.76	[55]
Batch	*E. harbinense*	Sugarcane molasses	–	1.58	[56]
Batch	*Clostridium pasteurianum*	Food waste hydrolysate	1108	1.73	Present study

In the case of the ANN–GA approach, the predicted optimum parameters for bioH_2 production were: temperature = 36.8 °C, pH = 6.7, TRS concentration = 10.85 g/L, with predicted bioH_2 yield = 1081 mL/L. This is in accordance with the experimental response of 1108 mL/L (52 ± 2% H_2 content in product gas) with an error of 1.5%. The bioH_2 yields in terms of reducing sugars in food waste hydrolysate at optimized parameters from RSM and ANN-GA were: 1.58 and 1.73 mol/mol hexose sugars, respectively. It's interesting to note that the ideal pH and temperature for maximizing the synthesis of bioH_2 from food waste hydrolysate are comparable to those needed for other substrates, such as groundnut de-oiled cake, glycerol, glucose, and palm oil effluent [27,57]. A comparison of the results of the present study with previous literature on bioH_2 production is given in Table 4.3. It can be seen from Table 4.3 that the bioH_2 yield in our study is at par or higher than the previous studies using either food waste or lignocellulosic biomass as substrate [54–56]. It should be, however, noted that the

experiments in the current study were carried out in serum bottles, while many previous studies have used a CSTR or similar bioreactor. The fermentation parameters in a reactor are much better controlled in a reactor, and higher yields could be expected than in lab-scale batch experiments.

The time profiles of cumulative bioH_2 production and various metabolites in the validation experiments conducted at optimized conditions obtained by RSM-CCD and ANN-GA techniques are shown in Figs. 4.4 and 4.5, respectively. Acetic acid (AA), butyric acid (BA), lactic acid (LA), and succinic acid (SA) were mainly four metabolites produced during the dark fermentation by *C. pasteurianum*. The metabolic pathways leading to AA and BA formation favor hydrogen production. Referring to Figs. 4.4 and 4.5, the concentrations of the metabolites AA and BA at 18 h are 1.11 and 1.19 g/L, respectively, for the optimum fermentation conditions obtained using the ANN technique, whereas for the fermentation conditions obtained using RSM, these concentrations are 1 and 1.1 g/L, respectively. These profiles of the metabolic intermediates clearly indicate that the metabolic pathway of *C. pasteurianum* shifts towards AA and BA, resulting in relatively higher H_2 production for the ANN-GA predicted fermentation conditions, as compared to the RSM-CCD predicted conditions. It may also be noted that approx. 70% substrate conversion or an average sugar consumption rate of 0.38 g/L h was obtained at the fermentation conditions predicted by the ANN-GA technique.

4.3.5 Kinetic model of bioH_2 production

Modified Gompertz (Eq. 4.7) model was used to analyze the hydrogen production in a batch system.

$$H(t) = P exp\{-exp[\frac{R_m e}{P}(\lambda - t) + 1]\} \quad (4.7)$$

Various notations are: H(t) = cumulative bioH_2 production (mL/L), P = hydrogen production potential (mL/L), R_m = maximum bioH_2 production rate (mL/L·h), e = 2.71828, λ is the lag

phase time (h), *t* is the cultivation time (h) [58]. In the present study, cumulative bioH_2 production data obtained in validation experiments was used to fit the modified Gompertz model using MATLAB 2023 (curve fitting toolbox version 1.1.7) software.

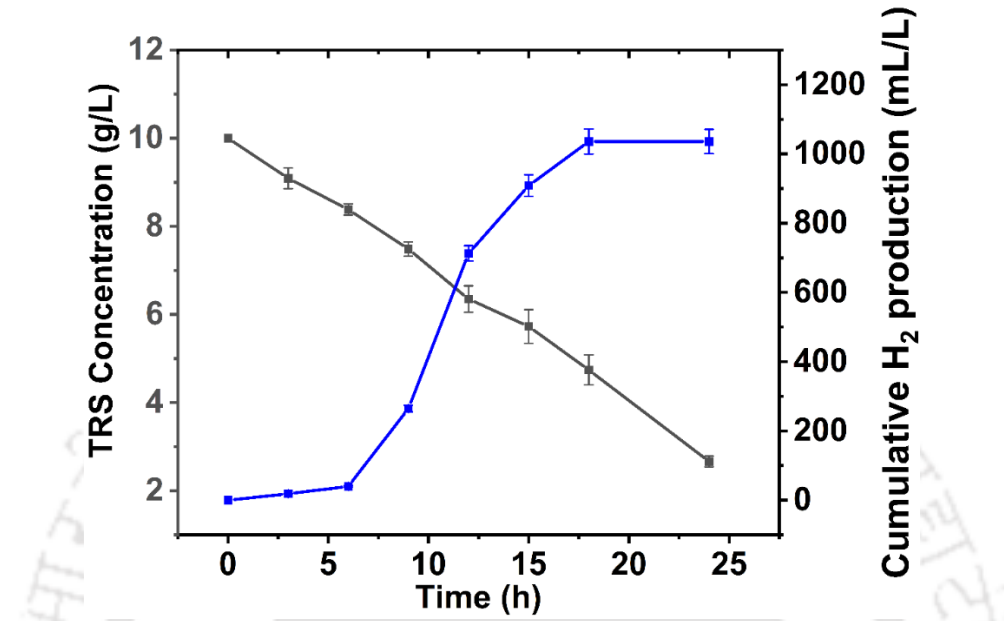

(A)

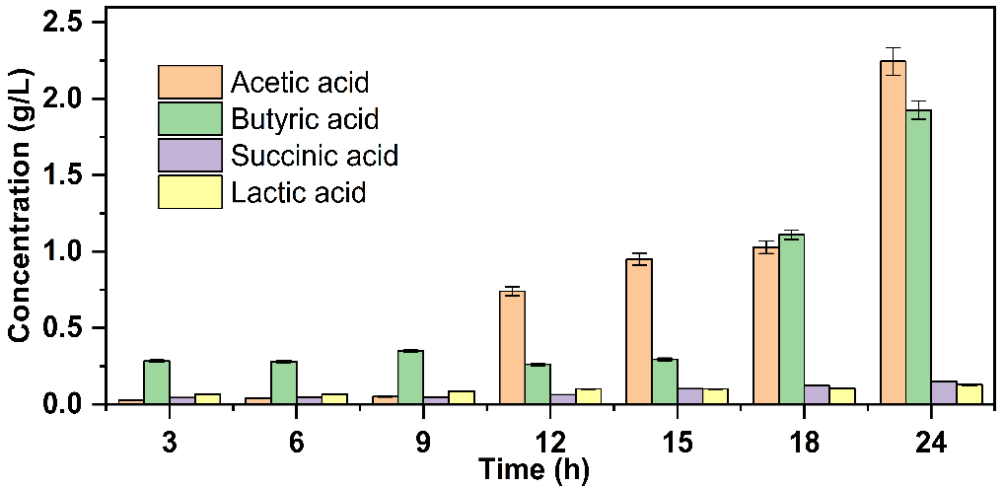

(B)

Fig. 4.4. Results of dark fermentation at optimum conditions obtained using RSM-CCD design. (A) Time profiles of TRS concentration and cumulative hydrogen production, (B) Time profile of the concentrations of different metabolites in the fermentation mixture

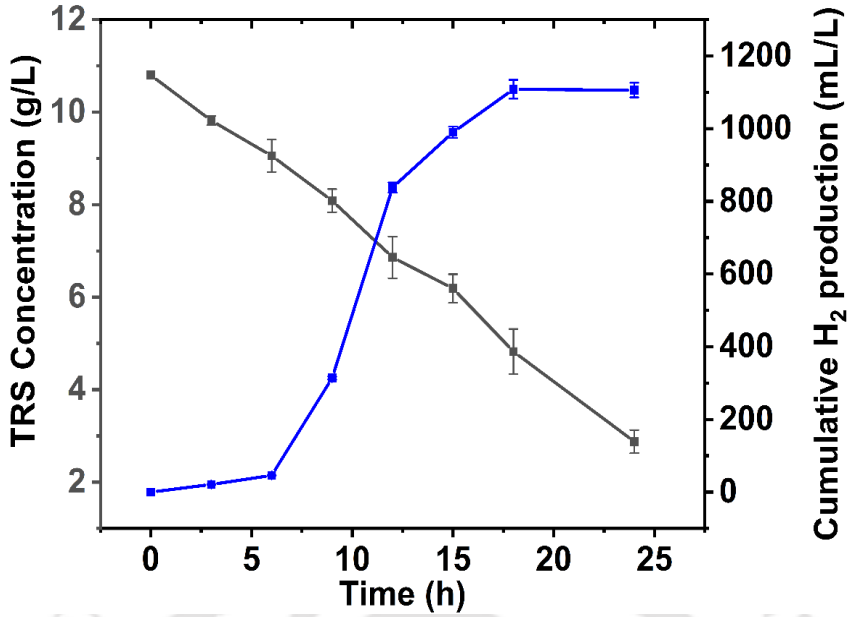

(A)

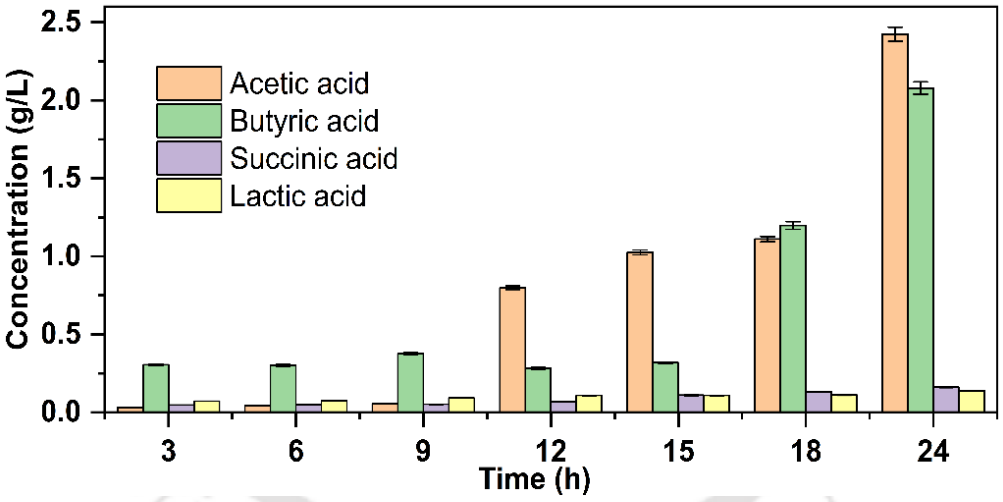

(B)

Fig. 4.5. Results of dark fermentation at optimum conditions obtained using ANN-GA technique. (A) Time profiles of TRS concentration and cumulative hydrogen production, (B) Time profile of the concentrations of different metabolites in the fermentation mixture

The kinetic parameters such as lag time (λ), maximum hydrogen production rate (R_m), and hydrogen production potential (P) were estimated, and these are summarized in Table 4. P represents the asymptotic maximum hydrogen production that can be achieved under the given conditions in the batch system. This is the total amount of hydrogen that will be produced when the process reaches completion. R_m is the fastest rate at which the microbes are converting substrates into hydrogen during the exponential phase of growth. λ represents the initial lag phase before significant hydrogen production begins; this period is also called the acclimatization phase. The term $\frac{R_m e}{P}(\lambda - t)$ describes how quickly the system transitions from the lag phase to the exponential production phase and then to the stationary phase [59]. The following trends can be interpreted from Eq. 4.7:

(1) Early phase ($t < \lambda$): During the lag phase, the term (λ - t) is positive, and the argument of the exponential function is large, resulting in H(t) being small; hydrogen production is minimal under this condition.

(2) Exponential growth phase ($t \sim \lambda$): As t approaches λ, the term (λ - t) approaches zero, and the exponential term decreases, leading to a rapid increase in H(t); this is the period of maximum hydrogen production rate.

(3) Stationary phase ($t > \lambda$): Eventually, as t increases further, the term (λ - t) becomes negative, and the exponential term stabilizes. The cumulative hydrogen production approaches P, indicating that the process is on the verge of completion.

The correlation coefficient (R^2) and RMSE values of both cases (RSM and ANN-GA) are shown in Table 4.4, which indicates a good match between experimental and model data. The experimental and simulated time profiles of bioH_2 production for the validation experiments conducted at optimum conditions predicted by RSM and ANN-GA techniques are shown in Fig. 4.6.

Table 4.4. Kinetic parameters of biohydrogen production

Parameters	RSM	ANN-GA
P (mL/L)	1051	1114
R_m (mL/L·h)	153.74	185.37
λ (h)	7.22	7.23
R^2	0.9984	0.9975
RMSE	22.28	29.71

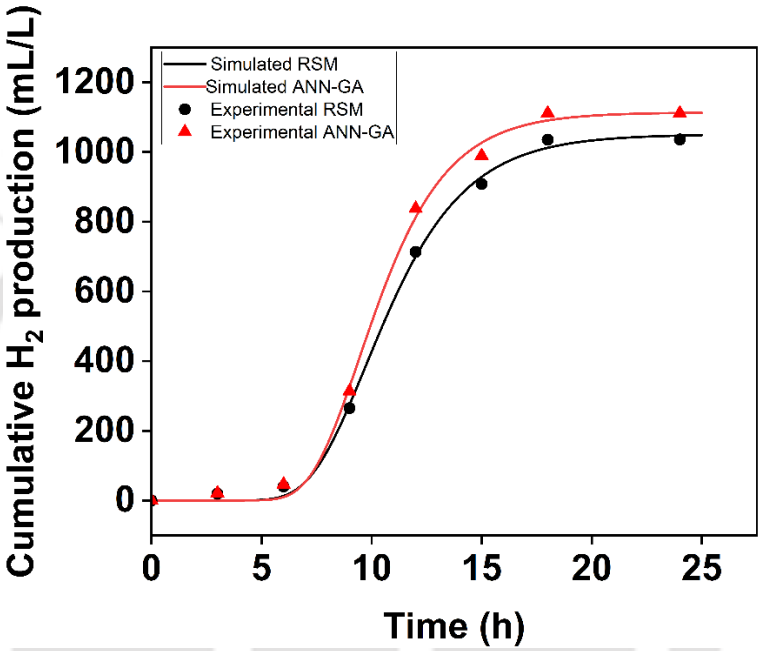

Fig. 4.6. Experimental and simulated bioH_2 production profiles in validation experiments conducted at optimum conditions obtained using RSM and ANN-GA techniques

4.4 Conclusions

The present study has addressed the matter of valorization of food waste to bioH_2 through dark fermentation using *Clostridium pasteurianum*. Optimization of fermentation parameters was done using a statistical design of experiments. Dark fermentation at the optimum parameters predicted by the statistical RSM-CCD method resulted in a bioH_2 yield of 1039 mL/L (1.58 mol/mol hexose sugars). The statistical experimental data were also analyzed using an artificial neural network coupled with genetic algorithm (ANN-GA). Dark fermentation at the optimum

conditions predicted by ANN-GA resulted in bioH_2 yield of 1108 mL/L (1.73 mol/mol hexose sugar). Analysis of bioH_2 profiles using a modified Gompertz model revealed higher H_2 production potential at ANN-GA-predicted fermentation conditions. The profiles of metabolic intermediates shifted towards the acetic acid/ butyric acid pathway at ANN-GA-predicted conditions, which resulted in higher H_2 production. These results demonstrate the superior efficacy of the ANN-GA methodology for simulating and predicting the behavior of a non-linear system like the metabolic pathway of *C. pasteurianum* in dark fermentation.

CHAPTER 4: Appendix 4A

Table 4A.1: Factors and their experimental design levels for CCD matrix

Factors	Levels	
	Low (-α)	High (+α)
B–pH	5	10
C–Temperature	30	42
A –Food waste hydrolysate	2	15

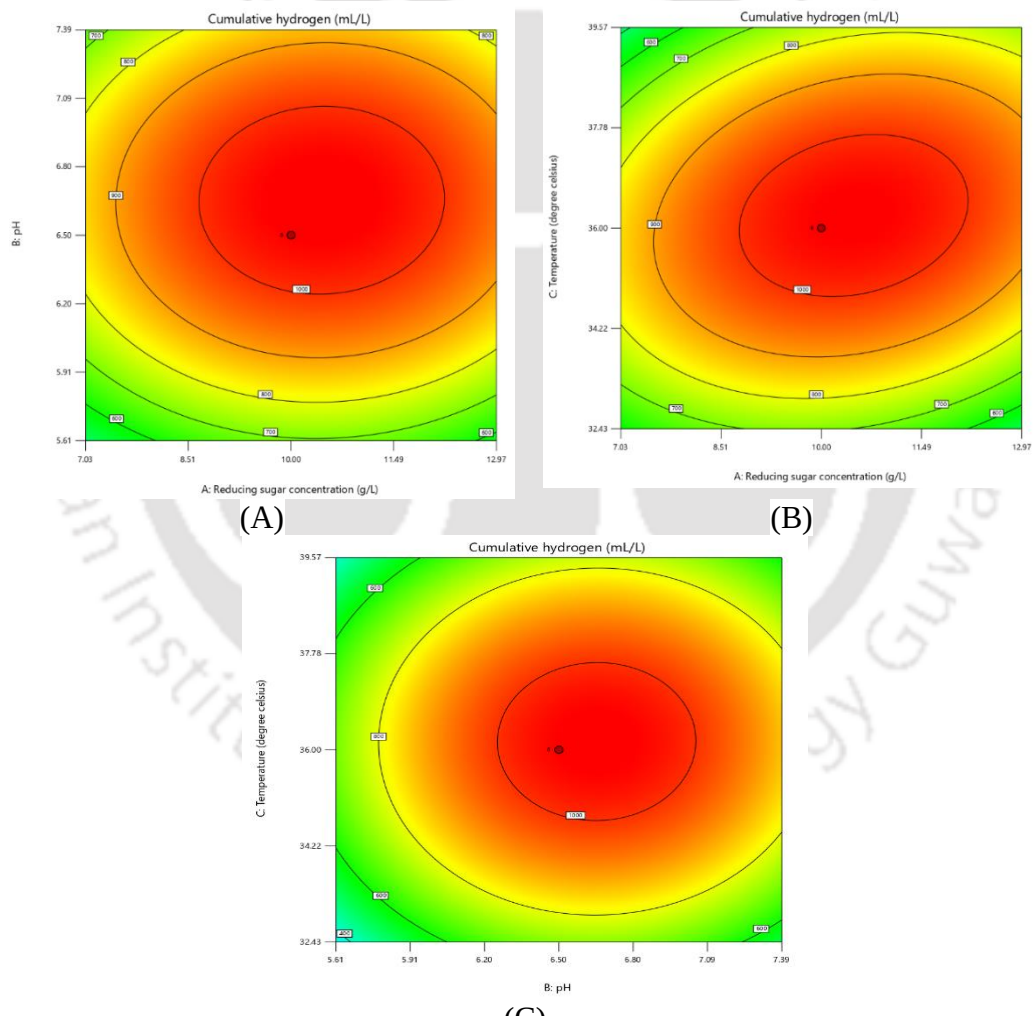

(A) (B)

(C)

Fig. 4A.1. Contour plots for interactive effects of different parameters on hydrogen production. (A) Food waste hydrolysate concentration vs pH (B) Food waste hydrolysate concentration vs temperature (C) pH and temperature.

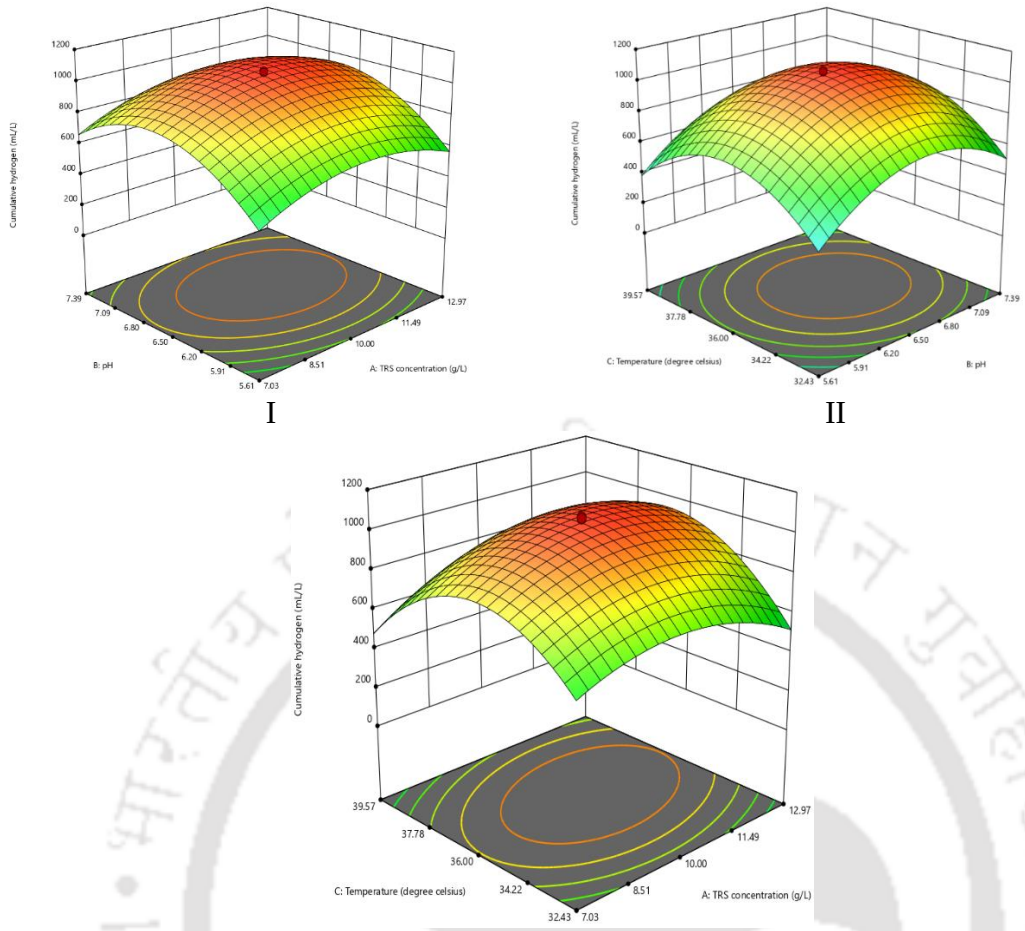

Fig. 4A.2: 3–D surface graphs (interaction between independent variables) of RSM-based optimization of biohydrogen production in terms of cumulative H_2 production (mL/L) (I) TRS concentration (g/L) vs pH (II) pH vs temperature (III) TRS concentration vs temperature

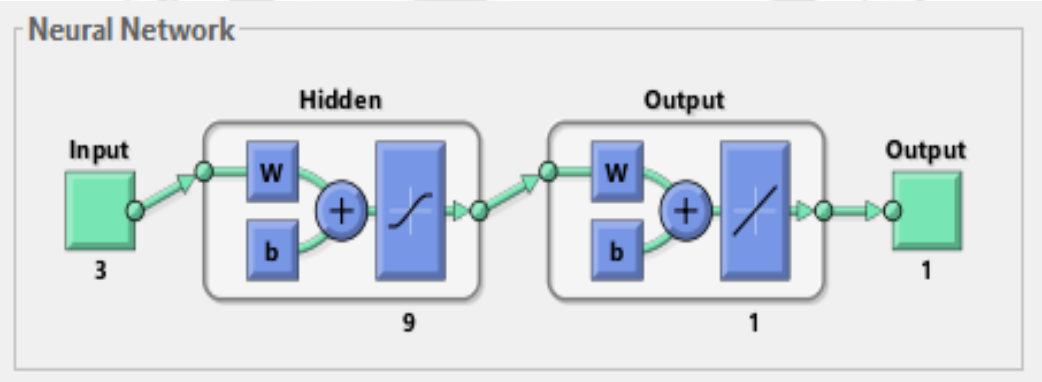

Fig. 4A.3. Artificial neural network (ANN) architecture

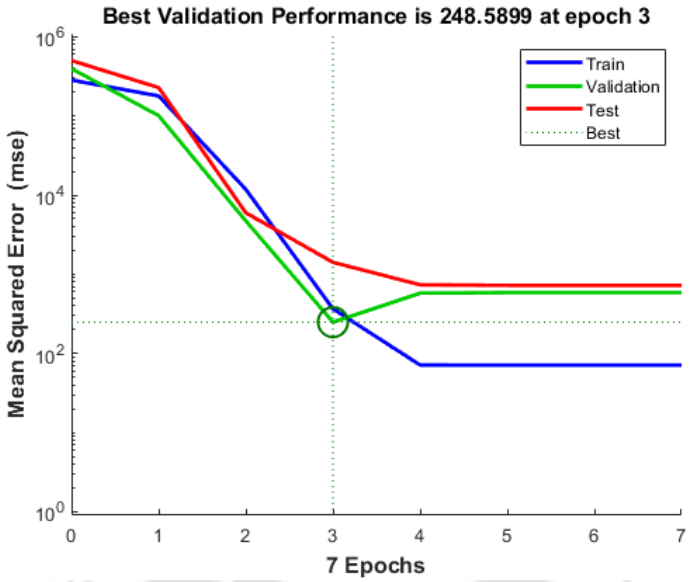

Fig. 4A.4. ANN performance

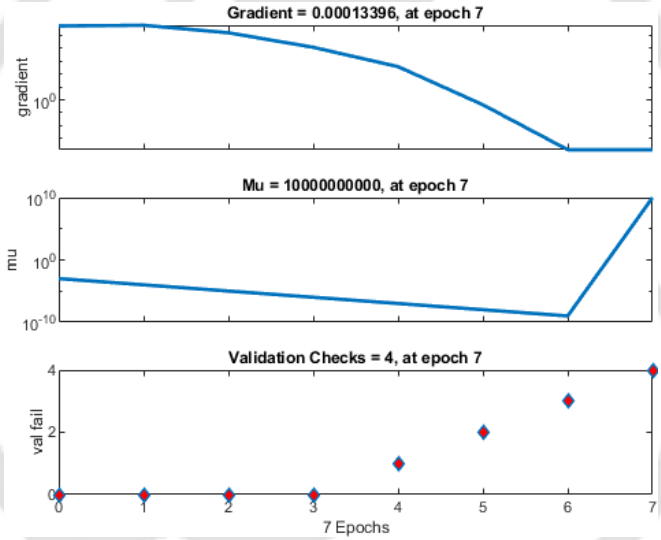

Fig. 4A.5. ANN training site

Fig. 4A.6. ANN error histogram

References

[1] J. Hu, Comparisons of biohydrogen production technologies and processes, in: Waste to Renewable Biohydrogen, Elsevier, 2021: pp. 71–107. https://doi.org/10.1016/B978-0-12-821659-0.00010-1.

[2] S. Kumari, D. Das, Improvement of biohydrogen production using acidogenic culture, International Journal of Hydrogen Energy 42 (2017) 4083–4094. https://doi.org/10.1016/j.ijhydene.2016.09.021.

[3] A. Anand, Umesh, V.S. Moholkar, Chapter 3 - Biohydrogen production from microbial fermentation of organic wastes, in: S. Nanda, A.K. Dalai, V.V. Goud (Eds.), Emerging Biofuels, Elsevier, 2024: pp. 27–52. https://doi.org/10.1016/B978-0-323-99547-4.00011-3.

[4] A. Sahoo, A. Dwivedi, P. Madheshiya, U. Kumar, R.K. Sharma, S. Tiwari, Insights into the management of food waste in developing countries: with special reference to India, Environ Sci Pollut Res 31 (2024) 17887–17913. https://doi.org/10.1007/s11356-023-27901-6.

[5] A. Das, M. Verma, V. Mishra, Food waste to resource recovery: a way of green advocacy, Environ Sci Pollut Res 31 (2024) 17874–17886. https://doi.org/10.1007/s11356-023-27193-w.

[6] W. Han, Y. Yan, Y. Shi, J. Gu, J. Tang, H. Zhao, Biohydrogen production from enzymatic hydrolysis of food waste in batch and continuous systems, Sci Rep 6 (2016) 38395. https://doi.org/10.1038/srep38395.

[7] V.E. Balderas-Hernandez, K.P. Landeros Maldonado, A. Sánchez, A. Smoliński, A. De Leon Rodriguez, Improvement of hydrogen production by metabolic engineering of Escherichia coli: Modification on both the PTS system and central carbon metabolism, International Journal of Hydrogen Energy 45 (2020) 5687–5696. https://doi.org/10.1016/j.ijhydene.2019.01.162.

[8] H. El Bari, N. Lahboubi, S. Habchi, S. Rachidi, O. Bayssi, N. Nabil, Y. Mortezaei, R. Villa, Biohydrogen production from fermentation of organic waste, storage and applications, Cleaner Waste Systems 3 (2022) 100043. https://doi.org/10.1016/j.clwas.2022.100043.

[9] W. Han, X. Wang, L. Ye, J. Huang, J. Tang, Y. Li, N. Ren, Fermentative hydrogen production using wheat flour hydrolysate by mixed culture, International Journal of Hydrogen Energy 40 (2015) 4474–4480. https://doi.org/10.1016/j.ijhydene.2015.02.016.

[10] S.G. Santiago, J.M. Morgan-Sagastume, O. Monroy, I. Moreno-Andrade, Biohydrogen production from organic solid waste in a sequencing batch reactor: An optimization of the hydraulic and solids retention time, International Journal of Hydrogen Energy 45 (2020) 25681–25688. https://doi.org/10.1016/j.ijhydene.2019.11.224.

[11] A. Anand, V.S. Moholkar, Analysis of Food Waste as Potential Substrate for Biohydrogen Production, in: V.S. Moholkar, K. Mohanty, V.V. Goud (Eds.), Sustainable Energy Generation and Storage, Springer Nature, Singapore, 2023: pp. 135–144. https://doi.org/10.1007/978-981-99-2088-4_11.

[12] S. Sarma, V.K. Dubey, V.S. Moholkar, Kinetic and thermodynamic analysis (with statistical optimization) of hydrogen production from crude glycerol using Clostridium pasteurianum, International Journal of Hydrogen Energy 41 (2016) 19972–19989. https://doi.org/10.1016/j.ijhydene.2016.08.204.

[13] K. Trchounian, H. Sargsyan, A. Trchounian, H2 production by Escherichia coli batch cultures during utilization of acetate and mixture of glycerol and acetate, International Journal of Hydrogen Energy 40 (2015) 12187–12192. https://doi.org/10.1016/j.ijhydene.2015.07.057.

[14] V. Singh, H. Singh, D. Das, Optimization of the medium composition for the improvement of hydrogen and butanol production using *Clostridium saccharoperbutylacetonicum* DSM 14923, International Journal of Hydrogen Energy 44 (2019) 26905–26919. https://doi.org/10.1016/j.ijhydene.2019.08.125.

[15] C. Mahata, S. Ray, D. Das, Optimization of dark fermentative hydrogen production from organic wastes using acidogenic mixed consortia, Energy Conversion and Management 219 (2020) 113047. https://doi.org/10.1016/j.enconman.2020.113047.

[16] M.A. Mohd Asrul, M.F. Atan, H. Abdul Halim Yun, J.C.H. Lai, A review of advanced optimization strategies for fermentative biohydrogen production processes, International Journal of Hydrogen Energy 47 (2022) 16785–16804. https://doi.org/10.1016/j.ijhydene.2022.03.197.

[17] G. Bilgiç, E. Bendeş, B. Öztürk, S. Atasever, Recent advances in artificial neural network research for modeling hydrogen production processes, International Journal of Hydrogen Energy 48 (2023) 18947–18977. https://doi.org/10.1016/j.ijhydene.2023.02.002.

[18] X. Zhang, Q. Zhang, Y. Li, H. Zhang, Modeling and optimization of photo-fermentation biohydrogen production from co-substrates basing on response surface methodology and artificial neural network integrated genetic algorithm, Bioresource Technology 374 (2023) 128789. https://doi.org/10.1016/j.biortech.2023.128789.

[19] S. Yadav, V. Singh, C. Mahata, D. Das, Optimization for simultaneous enhancement of biobutanol and biohydrogen production, International Journal of Hydrogen Energy 46 (2021) 3726–3741. https://doi.org/10.1016/j.ijhydene.2020.10.267.

[20] A.K. Pradhan, H. Goyal, P. Patel, P. Mondal, Bio-hydrogen production from crude glycerol: Optimisation through response surface methodology and artificial neural network approach, Biomass and Bioenergy 185 (2024) 107243. https://doi.org/10.1016/j.biombioe.2024.107243.

[21] Y. Wang, G. Yang, V. Sage, J. Xu, G. Sun, J. He, Y. Sun, Optimization of dark fermentation for biohydrogen production using a hybrid artificial neural network (ANN) and response surface methodology (RSM) approach, Environmental Progress & Sustainable Energy 40 (2021) e13485. https://doi.org/10.1002/ep.13485.

[22] J. Tix, F. Moll, S. Krafft, M. Betsch, N. Tippkötter, Hydrogen Production from Enzymatic Pretreated Organic Waste with Thermotoga neapolitana, Energies 17 (2024) 2938. https://doi.org/10.3390/en17122938.

[23] A. Anand, K. Kumar, K.C. Khaire, K. Roy, V.S. Moholkar, Ultrasound-assisted hydrolysis of food waste using glucoamylase: Statistical optimization and mechanistic analysis with molecular simulations, Bioresource Technology Reports 27 (2024) 101932. https://doi.org/10.1016/j.biteb.2024.101932.

[24] S. Singh, M. Agarwal, S. Sarma, A. Goyal, V.S. Moholkar, Mechanistic insight into ultrasound induced enhancement of simultaneous saccharification and fermentation of Parthenium hysterophorus for ethanol production, Ultrasonics Sonochemistry 26 (2015) 249–256. https://doi.org/10.1016/j.ultsonch.2015.02.011.

[25] S. Faizollahzadeh Ardabili, B. Najafi, S. Shamshirband, B. Minaei Bidgoli, R.C. Deo, K. Chau, Computational intelligence approach for modeling hydrogen production: a review, Engineering Applications of Computational Fluid Mechanics 12 (2018) 438–458. https://doi.org/10.1080/19942060.2018.1452296.

[26] P. Karthic, S. Joseph, N. Arun, S. Kumaravel, Optimization of biohydrogen production by *Enterobacter species* using artificial neural network and response surface methodology, Journal of Renewable and Sustainable Energy 5 (2013) 033104. https://doi.org/10.1063/1.4803746.

[27] C. Mahata, S. Dhar, S. Ray, D. Das, Effect of thermal pretreated organic wastes on the dark fermentative hydrogen production using mixed microbial consortia, Fuel 284 (2021) 119062. https://doi.org/10.1016/j.fuel.2020.119062.

[28] S. Schmidgall, R. Ziaei, J. Achterberg, L. Kirsch, S.P. Hajiseyedrazi, J. Eshraghian, Brain-inspired learning in artificial neural networks: A review, APL Machine Learning 2 (2024) 021501. https://doi.org/10.1063/5.0186054.

[29] H. Yu, Q. Zhao, Brain-inspired multisensory integration neural network for cross-modal recognition through spatiotemporal dynamics and deep learning, Cogn Neurodyn (2023). https://doi.org/10.1007/s11571-023-09932-4.

[30] Z. Liu, Y. Wang, X. Hua, Prediction and optimization of oscillating wave surge converter using machine learning techniques, Energy Conversion and Management 210 (2020) 112677. https://doi.org/10.1016/j.enconman.2020.112677.

[31] A.A. Alnaqi, H. Moayedi, A. Shahsavar, T.K. Nguyen, Prediction of energetic performance of a building integrated photovoltaic/thermal system thorough artificial neural network and hybrid particle swarm optimization models, Energy Conversion and Management 183 (2019) 137–148. https://doi.org/10.1016/j.enconman.2019.01.005.

[32] M. Ekpenyong, A. Asitok, S. Antai, B. Ekpo, R. Antigha, N. Ogarekpe, Statistical and Artificial Neural Network Approaches to Modeling and Optimization of Fermentation Conditions for Production of a Surface/Bioactive Glyco-lipo-peptide, Int J Pept Res Ther 27 (2021) 475–495. https://doi.org/10.1007/s10989-020-10094-8.

[33] A. Asfaram, M. Ghaedi, M.H. Ahmadi Azqhandi, A. Goudarzi, M. Dastkhoon, Statistical experimental design, least squares-support vector machine (LS-SVM) and artificial neural network (ANN) methods for modeling the facilitated adsorption of methylene blue dye, RSC Advances 6 (2016) 40502–40516. https://doi.org/10.1039/C6RA01874B.

[34] M. Mitchell, An Introduction to Genetic Algorithms, MIT Press, 1998.

[35] K. Kumar, S.M. Jadhav, V.S. Moholkar, Acetone-Butanol-Ethanol (ABE) fermentation with clostridial co-cultures for enhanced biobutanol production, Process Safety and Environmental Protection 185 (2024) 277–285. https://doi.org/10.1016/j.psep.2024.03.027.

[36] F. Ndayisenga, Z. Yu, J. Zheng, B. Wang, H. Liang, I.A. Phulpoto, T. Habiyakare, D. Zhou, Microbial electrohydrogenesis cell and dark fermentation integrated system enhances biohydrogen production from lignocellulosic agricultural wastes: Substrate pretreatment towards optimization, Renewable and Sustainable Energy Reviews 145 (2021) 111078. https://doi.org/10.1016/j.rser.2021.111078.

[37] S. Farmanbordar, A. Javid, H. Amiri, J.F.M. Denayer, K. Karimi, Enhanced biobutanol production with sustainable Co-substrates synergy from paper waste and garden waste

with municipal biowaste, Biomass and Bioenergy 186 (2024) 107262. https://doi.org/10.1016/j.biombioe.2024.107262.

[38] Y. Mu, X.-J. Zheng, H.-Q. Yu, determining optimum conditions for hydrogen production from glucose by an anaerobic culture using response surface methodology (RSM), International Journal of Hydrogen Energy 34 (2009) 7959–7963. https://doi.org/10.1016/j.ijhydene.2009.07.093.

[39] S.A. Alavi-Borazjani, L.A. da C. Tarelho, M.I. Capela, Parametric optimization of the dark fermentation process for enhanced biohydrogen production from the organic fraction of municipal solid waste using Taguchi method, International Journal of Hydrogen Energy 46 (2021) 21372–21382. https://doi.org/10.1016/j.ijhydene.2021.04.017.

[40] P. Dessì, E. Porca, A.-M. Lakaniemi, G. Collins, P.N.L. Lens, Temperature control as key factor for optimal biohydrogen production from thermomechanical pulping wastewater, Biochemical Engineering Journal 137 (2018) 214–221. https://doi.org/10.1016/j.bej.2018.05.027.

[41] Y. Li, Y. Qiu, X. Zhang, M. Zhu, W. Tan, Strain screening and optimization of biohydrogen production by Enterobacter aerogenes EB-06 from glycerol fermentation, Bioresour. Bioprocess. 6 (2019) 15. https://doi.org/10.1186/s40643-019-0250-z.

[42] D. Nagaiah, P. Srinivasa Rao, R.S. Prakasham, et al, High Biomass Sorghum as a Potential Raw Material for Biohydrogen Production: A Preliminary Evaluation, Current Trends in Biotechnology and Pharmacy 6 (2012) 183–189.

[43] P.M. Gawal, Cost-effective 2,3-BD separation: insights from aqueous two-phase extraction-assisted distillation, Biomass Conv. Bioref. (2024). https://doi.org/10.1007/s13399-024-05392-w.

[44] P. Mullai, M.K. Yogeswari, K. Sridevi, Optimisation and enhancement of biohydrogen production using nickel nanoparticles – A novel approach, Bioresource Technology 141 (2013) 212–219. https://doi.org/10.1016/j.biortech.2013.03.082.

[45] T. Shi, J. Zhou, Y. Ayub, S. Toniolo, J. Ren, Novel process optimization based on machine learning: A study on biohydrogen production from waste resources, Biomass and Bioenergy 185 (2024) 107222. https://doi.org/10.1016/j.biombioe.2024.107222.

[46] K.M. Desai, S.A. Survase, P.S. Saudagar, S.S. Lele, R.S. Singhal, Comparison of artificial neural network (ANN) and response surface methodology (RSM) in fermentation media optimization: Case study of fermentative production of scleroglucan, Biochemical Engineering Journal 41 (2008) 266–273. https://doi.org/10.1016/j.bej.2008.05.009.

[47] G. Dhanarajan, M. Mandal, R. Sen, A combined artificial neural network modeling–particle swarm optimization strategy for improved production of marine bacterial lipopeptide from food waste, Biochemical Engineering Journal 84 (2014) 59–65. https://doi.org/10.1016/j.bej.2014.01.002.

[48] S. Yadav, V. Singh, C. Mahata, D. Das, Optimization for simultaneous enhancement of biobutanol and biohydrogen production, International Journal of Hydrogen Energy 46 (2021) 3726–3741. https://doi.org/10.1016/j.ijhydene.2020.10.267.

[49] I. Moreno-Andrade, M.J. Berrocal-Bravo, I. Valdez-Vazquez, Biohydrogen production from food waste and waste activated sludge in codigestion: influence of organic loading rate and changes in microbial community, Journal of Chemical Technology & Biotechnology 98 (2023) 230–237. https://doi.org/10.1002/jctb.7238.

[50] R.F. Tiegam Tagne, P. Costa, S. Casella, L. Favaro, Optimization of biohydrogen production by dark fermentation of African food-processing waste streams, International Journal of Hydrogen Energy 49 (2024) 266–276. https://doi.org/10.1016/j.ijhydene.2023.07.348.

[51] F. Karaosmanoglu Gorgec, I. Karapinar, Biohydrogen production from hydrolyzed waste wheat by dark fermentation in a continuously operated packed bed reactor: The effect of hydraulic retention time, International Journal of Hydrogen Energy 44 (2019) 136–143. https://doi.org/10.1016/j.ijhydene.2018.08.155.

[52] V. Hovorukha, O. Havryliuk, G. Gladka, O. Tashyrev, A. Kalinichenko, M. Sporek, A. Dołhańczuk-Śródka, Hydrogen Dark Fermentation for Degradation of Solid and Liquid Food Waste, Energies 14 (2021) 1831. https://doi.org/10.3390/en14071831.

[53] W. Han, D.N. Liu, Y.W. Shi, J.H. Tang, Y.F. Li, N.Q. Ren, Biohydrogen production from food waste hydrolysate using continuous mixed immobilized sludge reactors, Bioresource Technology 180 (2015) 54–58. https://doi.org/10.1016/j.biortech.2014.12.067.

[54] J.K. Kim, L. Nhat, Y.N. Chun, S.W. Kim, Hydrogen production conditions from food waste by dark fermentation with Clostridium beijerinckii KCTC 1785, Biotechnol Bioproc E 13 (2008) 499–504. https://doi.org/10.1007/s12257-008-0142-0.

[55] C.-L. Cheng, Y.-C. Lo, K.-S. Lee, D.-J. Lee, C.-Y. Lin, J.-S. Chang, Biohydrogen production from lignocellulosic feedstock, Bioresource Technology 102 (2011) 8514–8523. https://doi.org/10.1016/j.biortech.2011.04.059.

[56] W. Li, C. Cheng, G. Cao, N. Ren, Enhanced biohydrogen production from sugarcane molasses by adding Ginkgo biloba leaves, Bioresour Technol 298 (2020) 122523. https://doi.org/10.1016/j.biortech.2019.122523.

[57] A. de A. Guilherme, P.V.F. Dantas, J.C.J. Soares, E.S. dos Santos, F.A.N. Fernandes, G.R. de Macedo, Pretreatments and enzymatic hydrolysis of sugarcane bagasse aiming at the enhancement of the yield of glucose and xylose, Braz. J. Chem. Eng. 34 (2017) 937–947. https://doi.org/10.1590/0104-6632.20170344s20160225.

[58] S. Kumari, D. Das, Biologically pretreated sugarcane top as a potential raw material for the enhancement of gaseous energy recovery by two stage biohythane process, Bioresource Technology 218 (2016) 1090–1097. https://doi.org/10.1016/j.biortech.2016.07.070.

[59] S.C. González, A. Possas, E. Carrasco, A. Valero, A. Bolívar, G.D. Posada-Izquierdo, R.M. García-Gimeno, G. Zurera, F. Pérez-Rodríguez, 'MicroHibro': A software tool for predictive microbiology and microbial risk assessment in foods, International Journal of Food Microbiology 290 (2019) 226–236. https://doi.org/10.1016/j.ijfoodmicro.2018.10.007.

भारतीय प्रौद्योगिकी संस्थान गुवाहाटी
Indian Institute of Technology Guwahati

CHAPTER 5

Ultrasound-assisted enhancement in biohydrogen production from food waste hydrolysate: A metabolic flux analysis

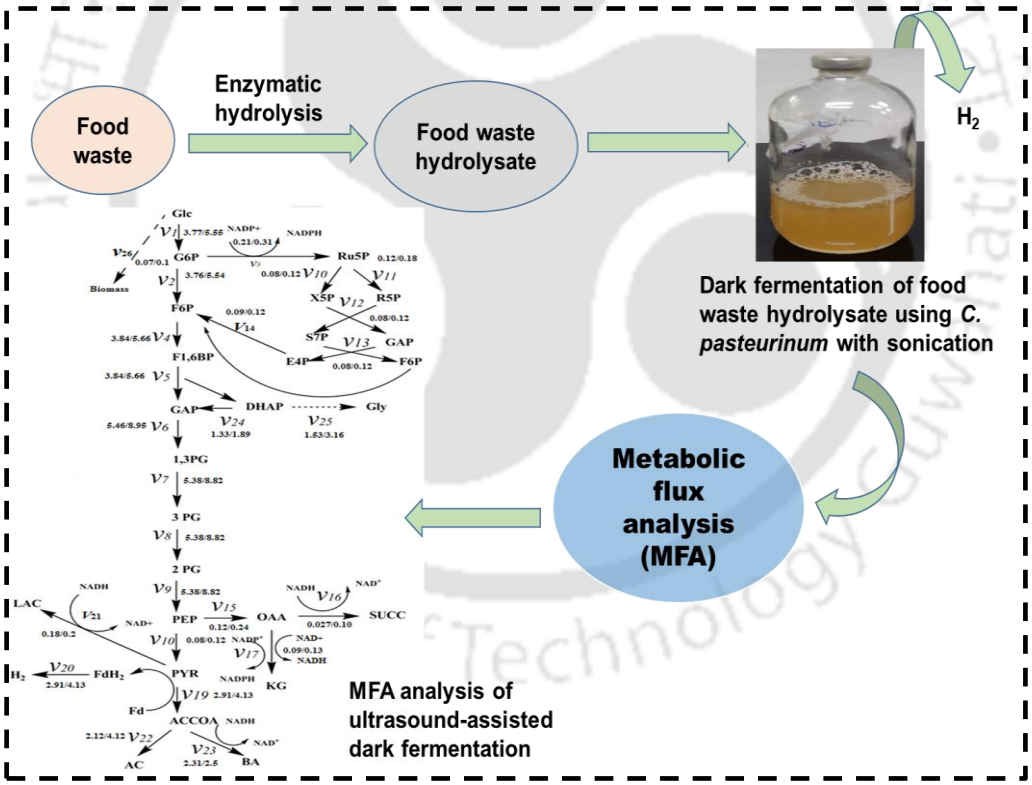

***Online*: A. Anand**, V.S. Moholkar, Ultrasound-assisted enhancement in biohydrogen production from food waste hydrolysate: a metabolic flux analysis, *Bioprocess Biosyst Eng* (2025). https://doi.org/10.1007/s00449-025-03265-8.

5.1 Introduction

Hydrogen has recently gained recognition as a promising and environmentally friendly alternative fuel for both the industrial and transportation sectors. Hydrogen-powered fuel cell vehicles are progressing toward commercial introduction in the automobile market within the next few years [1]. Traditionally, hydrogen production at an industrial scale has heavily relied on the energy-intensive process of steam reforming methane [2]. However, a potential green alternative route for hydrogen production is dark fermentation (DF). Hydrogen produced through biological (or biochemical) routes is known as biohydrogen (bioH_2). BioH_2 production has several merits over the conventional steam-methane reforming route, viz., low energy requirement, operation at ambient conditions - making it a safe and eco-friendly process, and substrate flexibility [3–5]. The conventional substrate for fermentative hydrogen production is lignocellulosic biomass, such as agro-residue [6–8]. This biomass requires significant pretreatment to convert the cellulose and hemicellulose into fermentable monomeric sugars. A potential sustainable alternative substrate for fermentative H_2 production is food waste. As per a report published by the United Nations Environment Program (UNEP), approximately 69 million tons of food waste is generated in India (estimate based on food wastage index) [9]. Food waste production on a global level is estimated at 1.3 billion [10, 11]. The food waste generated in domestic and industrial sectors is rich in nutrients (30-60% starch, 5-10% proteins, and 10-40% lipids) [12]. Unlike lignocellulosic biomass, which requires extensive multi-stage pretreatment, the starch in food waste can be easily hydrolyzed in a single-step process into fermentable sugars, mainly comprising glucose. The last decade has seen significant research on food waste hydrolysate as an alternative substrate for bioH_2 production [13–15].

Although bioH_2 production from food waste is a potential economical option that also promotes a circular bioeconomy, a major shortcoming of implementing fermentation processes on a large scale is the slow kinetics. However, the kinetics of fermentation can be significantly improved

through several methods. A conventional approach involves optimizing the process parameters, such as pH, temperature, and substrate concentration. Another strategy is the utilization of recombinant or genetically engineered microbial cultures [16, 17]. A relatively novel technique for enhancing fermentation kinetics is the application of mild-intensity ultrasound irradiation or sonication to the fermentation mixture [18–23]. Sonication introduces energy into the fermentation medium on an extremely small temporal and spatial scale, which has a remarkable effect on the physical and chemical transformations occurring within the system. Several mechanistic investigations into sonication-induced enhancement in fermentation kinetics reveal enhanced cellular (or transmembrane) transport of substrates and products, as well as conformational changes in the secondary structure of cellular enzymes, which boost metabolism [24, 25]. In our previous papers, we have demonstrated the effective use of ultrasound for enhancing the yield of *Clostridial* glycerol fermentation to 1,3-propanediol and butanol [26, 27]. A few previous studies have also reported the use of ultrasound for improving feedstock pretreatment and enhancing biohydrogen yield from dark fermentation [28–31].

Food waste hydrolysate is comprised mostly of hexose sugars (glucose and maltose). Hexose sugar fermentation by many *Clostridial* species consists of two phases: acidogenesis and solventogenesis. It may, however, be noted that not all *Clostridial* species exhibit the solventogenesis phase during fermentation. A recent study by Li et al. [32] on the effect of butyrate and acetate on hydrogen production has shown that the strain *Clostridium tyrobutyricum* does not exhibit the solventogenesis phase. In another study, Mermejo et al. [33] demonstrated that the strain of *Clostridium beijerinckii* Br21 does not exhibit the solventogenesis phase during glycerol fermentation to 1,3-propanediol. The initial steps involve the enzyme dehydrogenase converting glucose into glucose-6-phosphate (G6P), which is further transformed into PEP and eventually pyruvate (2 moles per mole of glucose) along with 2 NADH and 2 H^+ species. As per the core metabolic pathway of anaerobic fermentation

reported by Yu et al. [34], pyruvate can undergo two simultaneous conversions: it can form lactate, catalysed by lactate dehydrogenase, or it can form acetyl-CoA and CO_2 through the action of pyruvate–ferredoxin (Fd) oxidoreductase. Simultaneously, ferredoxin (Fd) undergoes reduction. The enzyme hydrogenase reduces Fd, resulting in the generation of bioH_2. The acetyl-CoA can be converted into either acetate (catalysed by phosphotransacetylase and acetate kinase) or butyrate through another intermediate of butyryl-CoA (catalysed by phosphotransbutyrylase and butyrate kinase). NADH generated during the conversion of glucose to pyruvate also undergoes oxidation to yield 2 moles of H_2. Consequently, bioH_2 production is linked to the formation of pyruvate and acetyl-CoA. According to the Thauer limit, the maximum bioH_2 yield per mole of glucose in *Clostridial* fermentation is 4 moles of H_2/ mole of glucose, where acetate is the primary product of the metabolic pathway, and all available electrons are utilized for H_2 production [16, 35]. However, the actual production of bioH_2 from hexose sugar fermentation is smaller than the theoretical yield due to the formation of soluble metabolites and other solvents. To increase the bioH_2 yield, it is crucial to investigate the involvement of other pathways in cellular functions and metabolic processes. Metabolic flux analysis (MFA) is a valuable technique for determining these pathways in cell metabolism. It also serves as an effective tool for understanding how microorganisms regulate their metabolism and overall physiology, as shown in previous studies [36, 37]. A summary of the literature on MFA related to bioH_2 production by various microbial strains is provided in the Appendix 5A (Table 5A.1).

This study addresses the issue of ultrasound-assisted fermentation of hexose sugar hydrolysate obtained from the enzymatic hydrolysis of food waste using the microbial strain *Clostridium pasteurianum*. It should be noted that the strain of *Clostridium pasteurianum* has several distinct merits for bioH_2 production, which include: (1) NADH-dependent hydrogenase system, which enables direct utilization of NADH from glycolysis for H_2 production, (2)

tolerance to low pH (acidic) environments and flexible switching between acidogenesis (H_2 producing) and solventogenesis (butanol-producing) phase, (3) genetic accessibility that allows metabolic engineering to knockout competing pathways and overexpress hydrogenase genes, and (4) good internal redox balance management and efficient NAD^+ recycling through multiple pathways for NAD^+ regeneration. In *Clostridium pasteurianum*, NADH competition is a critical factor affecting bioH_2 production as multiple metabolic pathways compete for the same pool of NADH. The extent to which NADH is diverted away from hydrogen production influences the hydrogen yield. In addition to these merits, *Clostridium pasteurianum* also offers opportunities for enhancing bioH_2 production through genetic interventions, such as knocking out NADH-consuming pathways (for example, ethanol and butanol production through alcohol dehydrogenase), overexpressing NADH-dependent hydrogenases, and enhancing substrate uptake, which leads to higher NADH generation.

As noted earlier, several previous authors have reported the beneficial effect of sonication on dark fermentation for bioH_2 production. However, most of these studies employ a "black box" approach, focusing on the observed enhancement in bioH_2 productivity and yield rather than the mechanism by which ultrasound affects cellular metabolism. The present study aims to investigate the effect of ultrasound on the metabolic network of *Clostridium pasteurianum* during the dark fermentation of food waste hydrolysate, and to elucidate the underlying mechanism using metabolic flux analysis (MFA). Two cases were examined in this study: a control system (employing mechanical agitation during fermentation) operated under optimum conditions identified through artificial neural network modeling, and secondly, a test fermentation incorporating 35 kHz sonication at a 20% duty cycle with otherwise identical conditions. The central objective of this study was to reconstruct the complete intracellular flux network using experimentally measured metabolite fluxes at steady state. For this purpose, a dedicated in silico MFA model was developed, which enabled the systematic quantification of

intracellular fluxes and the evaluation of the robustness of critical branch points in the anaerobic fermentation of hexose sugar-rich food waste hydrolysate. By comparing flux distributions between the control and sonicated (test) systems, the study provides new insights into flux redistribution under ultrasound stimulation and its direct implications for biohydrogen yield from fermentation. In addition to characterizing these effects, the MFA framework developed in this study also offers predictive direction on possible genetic modifications and interventions that could further enhance hydrogen production in *Clostridium pasteurianum*, thereby combining experimental validation with model-driven innovation.

5.2 Materials, methods, and metabolic flux analysis (MFA) model

5.2.1 Pretreatment and enzymatic hydrolysis of food waste

Food waste was obtained from various food outlets present on the campus of I.I.T. Guwahati. The obtained food waste was dried in a hot air oven at 60°C for 72 hours. The dried material was then ground to a particle size of 0.85 mm using a Bajaj Pluto 500 W mixer grinder and stored at 25°C. Prior to enzymatic hydrolysis, the composition of the food waste was determined to be: carbohydrate 43% w/w, starch 42% w/w, protein 6.5% w/w, and lipid 3.2% w/w.

Glucoamylase enzyme (GLCM) derived from *Aspergillus niger* was procured from Sigma-Aldrich, while all other chemicals were obtained from HiMedia Pvt. Ltd., India.

The hydrolysis of food waste was performed in an incubator shaker by the GLCM enzyme under optimum conditions. Greater details of the enzymatic hydrolysis procedure have been reported in our earlier studies [11, 38]. The optimum parameters for enzymatic hydrolysis, derived through Box-Behnken design (BBD) statistical optimization (as described in Chapter 3), were as follows: temperature, 40°C; biomass loading, 10% w/v; hydrolysis time, 42 hours; pH, 5; and GLCM loading, 50 U/g. The resulting hydrolysate contained 245

mg of glucose per gram of food waste and 18.5 mg of maltose per gram of food waste. The hydrolysate consisted exclusively of hexose sugars and was used as the substrate for fermentation by *Clostridium pasteurianum* for bioH_2 production.

5.2.2 Microbial culture preparation

The microbial strain *Clostridium pasteurianum* MTCC 116 was sourced from the Microbial Type Culture Collection (MTCC) in Chandigarh, India. The strain was cultured in Reinforced Clostridial Medium (RCM) [11, 31, 39]. Sodium chloride (5 g), beef extract (10 g), peptone (10 g), yeast extract (5 g), glucose (5 g), sodium acetate (3 g), starch (1 g), L-cysteine hydrochloride (0.5 g), and agar (0.5 g) were the RCM composition in 1000 mL of distilled water. The pH of the medium was adjusted to 7 using 1 M NaOH. The medium was incubated for 24 h at 37°C and 180 rpm using a rotary incubator shaker. The culture was streaked onto an agar plate with the same growth medium composition, containing 15 g/L agar, and maintained at 37°C in a desiccator with an attached anaerobic gas pack. The microbial culture broth was sub-cultured and utilized as stock once a month.

5.2.3 Batch fermentation of food waste hydrolysate

The cells from a previously prepared culture were cultivated in fresh RCM medium before being introduced into anaerobic conditions. For batch experiments, 10% of the culture in the mid-log phase was transferred into 120 mL serum bottles with a working volume of 60 mL containing modified production media at pre-determined optimum conditions in our previous study: pH = 6.8, temperature = 36.8 °C, total reducing sugar (TRS) concentration in food waste hydrolysate = 10 g/L [11]. This medium contained 1 mL of L-cysteine HCl (3% w/v) as a reducing agent and 6 mL (10% v/v) of *Clostridium pasteurianum* inoculum. The modified production medium for bioH_2 production consisted of yeast extract (1 g/L),

sodium chloride (5 g/L), KH_2PO_4 (4 g/L), K_2HPO_4 (0.23 g/L), sodium acetate (3 g/L), and peptone (2 g/L). Additionally, 1 L of this production medium was supplemented with 10 mL each of vitamin solution and trace element solution. The details of the modified production media for bioH_2 fermentation and the statistical optimization of fermentation parameters are provided in our previous chapter. The pH of the medium was adjusted to 6.8 using 1 M NaOH. Before inoculation, the production medium was purged with 99.99% pure nitrogen gas for 15 minutes to remove any oxygen [11]. Rubber stoppers were used to seal the serum bottles, which were then crimped and autoclaved for 30 minutes at 121°C and 15 psi pressure. The serum bottles were then incubated at 36.8 °C with 180 rpm after being inoculated with a 10% v/v inoculum. To ensure the reproducibility of results, all experiments were conducted in triplicate. Fermentation broth samples were periodically withdrawn to assess TRS consumption and soluble metabolite formation, while gas phase samples were collected to quantify the bioH_2 and CO_2 content in the product gas. The initial pH of the fermentation mixture was 6.8, which was optimized using a statistical design of experiments. The pH changes during fermentation (comprising acidogenic and solventogenic phases). The pH of the fermentation mixture after completion of the fermentation was measured as 6.3. This clearly shows that the application of sonication during fermentation has a negligible effect on the pH.

5.2.4 Ultrasound-assisted food waste hydrolysate fermentation

The fermentation of food waste hydrolysate in the presence of sonication was conducted using an ultrasound bath (sonoshaker) (Transonic T-460 model; 2 L capacity; 35 kHz frequency; 35 W power input; Elma, Germany). Water served as the medium for ultrasound propagation [38]. Prior to fermentation experiments, the ultrasound bath was calibrated using calorimetry for acoustic energy dissipation and ultrasound pressure amplitude [40]. The acoustic intensity in

the bath was approx. 0.75 W/cm^2, and the corresponding ultrasound pressure amplitude was 1.4 bar. The fermentation experiments were executed in 120 mL serum bottles with a working volume of 60 mL, maintaining the exact composition of the fermentation medium as previously outlined. Positioned at the center of the ultrasound bath, the serum bottle was partially submerged in water (approximately 50% of its height), adhering to the methodology proposed in our earlier studies [41, 42]. The temperature of the water in the bath was consistently maintained at 37 ± 1 °C using a circulating water bath. Sonication was applied with a duty cycle of 20%, involving 2 min ON followed by 8 min OFF (mechanical shaking) cycle for every 10 min treatment.

5.2.5 *In silico* metabolic model construction

The *in silico* model of *C. pasteurianum*'s metabolic network was developed by integrating experimental findings, information from the KEGG metabolic pathways database, and data gathered from published scientific literature [20, 43]. The model was constructed using 21 intracellular metabolites and 26 reactions. It covers pathways like the pentose phosphate pathway, glycolysis, the TCA cycle, and the glyoxylate shunt. Although bioH_2 production (via NADH-linked ferredoxin reduction) was included in the model, it was omitted from the flux distribution figures for simplicity. It was assumed that the cellular structure of *Clostridium pasteurianum* (MTCC 116) was the same as that of other *Clostridial* species described in the literature [44–46]. The model incorporated biomass formation (growth flux) to represent the diversion of precursors and building blocks into biomass. Using this metabolic network, the fluxes of *Clostridium pasteurianum* during food waste hydrolysate fermentation were evaluated and compared with experimental data for analysis. These experiments focused on studying the anaerobic fermentation of hexose sugar by *Clostridium pasteurianum* for bioH_2 production, comparing it with conventional glucose metabolism. During the exponential phase

of batch fermentation, we quantified the specific rates of hexose sugar (Glc) uptake and the production of soluble metabolites, including butyrate, acetate, lactate, and succinate. These metabolites served as constraints or boundary conditions in the *in-silico* MFA. The specific bioH_2 production rate was the benchmark for evaluating the consistency between the *in-silico* MFA (calculated) and experimental (measured) values. MATLAB R2022b was used to design and solve the *in-silico* MFA model.

5.2.6 Metabolic flux analysis

Metabolic flux analysis (MFA) quantifies cellular fluxes using a stoichiometric model and mass balance of intracellular metabolites, offering insights into cell physiology and metabolic regulation across various microorganisms. Despite its widespread use, there has been a notable absence of quantitative investigations using MFA to understand bioH_2 production in *Clostridium pasteurianum.* The primary objective of this investigation was to determine the maximum bioH_2 yield attainable in *Clostridium pasteurianum*, while elucidating the specific carbon metabolic pathways associated with enhanced bioH_2 production. For this, batch experiments were conducted with variations in initial hexose sugar concentration, and the quantitative analysis of the major fermentation products was performed. Additionally, an *in silico* metabolic-flux model was developed to comprehensively examine the anaerobic hexose sugar metabolism of *Clostridium pasteurianum*, providing a detailed analysis of the model to enhance our understanding of the underlying metabolic mechanisms influencing bioH_2 production. MFA evaluates steady-state reaction rates of metabolic reactions in microorganisms, using intracellular reaction stoichiometry as input. Reaction rates (or metabolic fluxes) are calculated based on molar balances and assuming a pseudo-steady state for intracellular metabolite concentrations. Measured rates of extracellular metabolite production or consumption place restrictions on the solution. The dynamic mass balance

equation that relates intracellular concentrations, stoichiometry and reaction fluxes is represented as:

$$\frac{dX}{dt} = S.v \qquad (5.1)$$

where v is the $r \times 1$ reaction rate vector, X is the $m \times 1$ concentration vector, t is time, and S is the $m \times r$ stoichiometric matrix, where the stoichiometric coefficient of species i in reaction j yields the element of the i^{th} row and j^{th} column. The left-hand side of Eq. (1) becomes zero if the intracellular metabolites are assumed to be in a pseudo-steady state, which results in equation 5.2.

$$S \cdot v = 0 \qquad (5.2)$$

Since there are always more reactions (J) than intracellular metabolites (K), the degree of freedom (F) is equal to $J - K$. Therefore, in order to ascertain the remaining reaction rates, it is necessary to measure some of the elements in v. If precisely F fluxes are measured, the system becomes determined, and the solution is unique. To find the solution, measured rates in vector v can be gathered in a new vector, v_m, while the other components of v are grouped into another vector, v_c. Likewise, the stoichiometric coefficients in matrix S are partitioned by collecting those of the measured reactions in S_m and the remaining coefficients in matrix S_c. Equation 5.2 can be written as:[20, 43].

$$S_m \cdot v_m + S_c \cdot v_c = 0 \qquad (5.3)$$

Because precisely $F = J - K$ fluxes are measured, S_c is a square matrix (dimension $m \times m$), and if this matrix can be inverted, then v_c can be found from equation (5.4).

$$v_c = -(S_C)^{-1} \cdot S_m \cdot v_m \qquad (5.4)$$

There are 21 metabolites and 26 metabolic reactions in the current system of food waste hydrolysate fermentation. The metabolite reactions are presented in Table 5.1, and the corresponding steady-state mass balance equations for different species are listed in Table 5.2

[14, 20, 43, 46–48]. The stoichiometric matrix *S* for metabolic flux analysis (MFA) is provided in Appendix 5A (Table 5A.2).

Table 5.1. Reactions in the metabolic flux model of *Clostridium pasteurianum*

1. $Glc \xrightarrow{v_1} G6P$
2. $G6P \xrightarrow{v_2} F6P$
3. $F6P + ATP \xrightarrow{v_3} F16BP + ADP$
4. $F16BP \xrightarrow{v_4} GAP + DHAP$
5. $GAP + NAD^+ \xrightarrow{v_5} 1,3PG + NADH$
6. $1,3PG \xrightarrow{v_6} 3PG$
7. $3PG \xrightarrow{v_7} 2PG$
8. $2PG \xrightarrow{v_8} PEP$
9. $PEP \xrightarrow{v_9} PYR$
10. $PYR + NADH \xrightarrow{v_{10}} LAC + NAD^+$
11. $FdH_2 \xrightarrow{v_{11}} H_2$
12. $PYR \xrightarrow{v_{12}} ACCOA$
13. $ACCOA \xrightarrow{v_{13}} AC$
14. $ACCOA + 2NADH \xrightarrow{v_{14}} BA + 2NAD^+$
15. $PEP \xrightarrow{v_{15}} OAA$
16. $OAA + NADP^+ + NAD^+ \xrightarrow{v_{16}} \alpha - KG + NADPH + NADH$
17. $OAA + NADPH \xrightarrow{v_{17}} SUCC + NAD^+$
18. $G6P + 2NADP^+ \xrightarrow{v_{18}} Ru5P + 2NADPH$
19. $Ru5P \xrightarrow{v_{19}} X5P$
20. $X5P + R5P \xrightarrow{v_{20}} S7P + GAP$
21. $S7P + GAP \xrightarrow{v_{21}} E4P + F6P$
22. $E4P + X5P \xrightarrow{v_{22}} F6P + GAP$
23. $DHAP \xrightarrow{v_{23}} GAP$
24. $DHAP \xrightarrow{v_{24}} GLY$
25. $E4P \xrightarrow{v_{25}} F6P$
26. $0.0016\ G6P + 0.1788\ F6P + 0.5726\ R5P + 1.239\ 3PG + 1.3285\ \alpha - KG \xrightarrow{v_{26}} Biomass$
$+0.611\ PEP + 2.6666\ PYR + 20.29\ ACCOA + 1.4452\ OAA$
$+10.75\ NADH + 7.6152\ NADPH$

Table 5.2. Steady-state mass balances for different metabolic species

1. $G6P: \ v_1 - v_2 - v_3 = 0$
2. $F6P: \ v_2 - v_4 + v_{13} = 0$
3. $F1,6BP: \ v_4 - v_5 = 0$
4. $GAP: \ v_5 - v_6 + v_{24} + v_{14} + v_{12} - v_{13} = 0$
5 .1,3 $PG: \ v_6 - v_7 = 0$
6. $3PG: \ v_7 - v_8 = 0$
7. $DHAP: \ v_5 - v_{24} - v_{25} = 0$
8. $2PG: \ v_8 - v_9 = 0$
9. $PEP: \ v_9 - v_{18} - v_{15} = 0$
10. $OAA: \ v_{15} - v_{16} = 0$
11. $PYR: \ v_{18} - v_{19} - v_{21} = 0$
12. $FdH_2: \ v_{19} - v_{20} = 0$
13. $ACCOA: \ v_{19} - v_{22} - v_{23} = 0$
14. $\alpha - KG: \ v_{17} = 0$
15. $Ru5P: \ v_3 - v_{10} - v_{11} = 0$
16. $X5P: \ v_{10} - v_{12} = 0$
17. $R5P: \ v_{11} - v_{12} = 0$
18. $S7P: \ v_{12} - v_{13} = 0$
19. $E4P: \ v_{13} - v_{14} = 0$
20. $NADH: \ v_6 - v_{16} + v_{17} - v_{21} - 2v_{23} = 0$
21. $NADPH: \ 2v_3 + v_{17} = 0$

5.2.7 Analytical methods

High-Performance Liquid Chromatography (HPLC) equipped with a refractive index (RI) detector and a photodiode array (PDA) analyzer was used to quantify metabolite concentrations in samples collected from the fermentation broth. The HPLC system included a guard column (catalogue #1250140, 50 mm × 7.8 mm) and an HPX-87H column (BIO-RAD, USA). The mobile phase consisted of 0.01 M H_2SO_4 in ultrapure water, maintained at a flow rate of 0.6 mL/min [39]. The detailed protocols for sample preparation, equipment description and analysis were described in our previous study [11, 49]. To analyse the composition of the product gas from fermentation, a gas chromatograph equipped with a thermal conductivity

detector (TCD) and a Porapak Q column was used. Argon served as the carrier gas at a flow rate of 30 mL/min. The column oven was maintained at 45°C, while the injector and detector temperatures were set at 200°C. The total volume of gas produced over time was measured using the water displacement method [50]. Gas samples were collected (above the surface of fermentation broth) from serum bottles and analyzed to determine the molar or volumetric content of bioH_2 and CO_2 [20, 31].

5.3 Results and Discussion

5.3.1 Carbon mass balance (CMB) for fermentation

The assessment of the CMB in the hexose sugar fermentation process by *Clostridium pasteurianum* involved observing the time-dependent profiles of various metabolites, including lactate, butyrate, succinate, acetate, and carbon dioxide, during fermentation. The fermentation experiments were conducted using both control (mechanical shaking) and test (mechanical shaking with periodic sonication) protocols. Tables 5.3 and 5.4 present a comprehensive overview of the CMB for the control and test experiments, respectively. Notably, butyrate and acetate emerged as primary metabolites, which form through the conversion of pyruvate into acetyl-CoA and butyryl-CoA. According to the core metabolic pathway of anaerobic fermentation reported by Yu et al. [34], hydrogen generation in dark fermentation is linked to the central metabolic pathways that provide ATP and reducing equivalents for cell growth. During glycolysis (or glucose to pyruvate conversion) and subsequent pyruvate oxidation to acetyl CoA, excess reducing equivalents (mainly NADH) are reoxidized through the hydrogenase-mediated evolution of H_2. This suggests that hydrogen is not the primary metabolic product of the cells, but rather a tool to maintain redox balance while channeling carbon and energy into biomass formation. In this sense, biohydrogen can be regarded as a byproduct of microbial growth.

A comparison between Tables 5.3 and 5.4 reveals the significant impact of ultrasound on food waste hydrolysate fermentation. Sonication accelerates hexose sugar consumption by ~ 42%, with ~ 78% of the initial sugar being utilized within 12 h, compared to the 24 h required in control experiments. However, the production rates of all metabolites exhibit non–uniform improvement with the application of sonication, with the most notable increase observed in succinate production (73%), followed by butyrate (9%), acetate (~ 94%), and lactate (~ 22%). Moreover, sonication does not influence the extent of substrate (or carbon) utilization for biomass growth (23.6% in control experiments and 23.1% in test experiments). However, the rate of substrate (or carbon) utilization and biomass growth is much faster in test experiments. This study also highlights the significance of the acetate-to-butyrate ratio (A/B ratio) in bioH_2 generation [45, 46]. A higher A/B ratio or increased acetate yield is associated with increased bioH_2 generation, while lactate synthesis hinders bioH_2 production due to NADH consumption and a lack of re-oxidation [13, 51]. The A/B ratio increases due to sonication, resulting in a remarkable ~22 % increase in bioH_2 yield (1.95 mol H_2/mol hexose sugar) compared to control experiments (1.61 mol H_2/mol hexose sugar). Correspondingly, the experimental findings support stoichiometric predictions that suggest an increase in bioH_2 yield with an increased A/B ratio. In practice, high bioH_2 yields are associated with the mixed acid route, i.e., a mixture of acetate and butyrate as byproducts. Cheng et al.[52] and Han et al.[53] propose the following plausible explanations for these results:

(i) Increased bioH_2 yield at a greater A/B ratio due to the consumption of lactate and butyrate (under favorable thermodynamic conditions) for producing acetate and hydrogen gas.

(ii) A higher bioH_2 yield at a higher A/B ratio could also be the result of enhanced acetogenesis. During the metabolic shift from acidogenesis to solventogenesis, the redistribution of carbon flux can lead to a reduction in butyrate formation, accompanied by a concurrent increase in acetate formation. This shift cuts down the hydrogen consumption in the formation of butyryl-

CoA from acetyl-CoA (via the intermediate of acetoacetyl-CoA) [34].

It can be seen from Tables 5.3 and 5.4 that the carbon balances match better for the control case than for the test experiments. In both cases, the unaccounted carbon (in the range of 9 to 10%) is attributed to substrate utilization for cell maintenance and the dissolved CO_2 in the medium. Possible reasons for the relatively lower carbon balance in the test experiments (dark fermentation with sonication) could be higher stress on the microbial cells due to the high shear generated in the medium by sonication, which results in higher substrate utilization for maintenance, and possibly, small degradation of the glucose molecules due to transient cavitation generated during sonication.

Garcia- Depraect *et al*. [54] have reported bioH_2 production from tequila vinasse using mixed consortia comprising lactic acid bacteria and hydrogen-producing bacteria. *Clostridial* species had the largest abundance among the hydrogen-producing bacteria. The overall COD-based mass balance revealed that approximately 9% of the carbon source is unrecovered (or unaccounted for), which is expected to be utilized for cell maintenance. This result is in concurrence with the present study, as seen from the carbon balance shown in Table 5.3.

Table 5.3. CMB for food waste hydrolysate fermentation (control experiment with mechanical shaking) by *Clostridium pasteurianum*

Time (h)	TRS (mg)	Butyrate (mg)	Acetate (mg)	Lactate (mg)	Succinate (mg)	CO_2 (mg)	Biomass (mg)	Total carbon (mg)	Carbon balance[$] (%)
0	600.0	0	0	0	0	0	0	600.0	100.0
3	545.3±8.12	16.9±0.36	1.7±0.03	3.9±0.05	2.5±0.04	1.2±1.1	17.0±0.24	588.6	98.1
6	503.0±7.74	16.8±0.36	2.4±0.04	4.2±0.03	2.7±0.03	4.7±1.60	41.0±0.36	574.7	95.8
9	449.1±8.6	20.9±0.42	3.0±0.05	5.1±0.04	2.8±0.05	9.9±1.23	56.0±0.58	546.9	91.2
12	381.0±7.1	15.6±0.48	44.4±0.69	5.8±0.12	3.7±0.12	14.8±1.2	89.0±0.98	554.7	92.5
15	343.7±6.2	17.6±0.39	57.0±0.96	6.3±0.06	6.1±0.15	24.3±1.2	102.0±1.12	556.7	92.8
18	248.6±8.32	66.5±1.44	61.6±1.02	6.5±0.12	7.2±0.11	25.3±1.5	132.0±1.5	547.5	91.3
24	129.9±7.15	115.5±2.44	134.6±2.07	7.7±0.10	8.9±0.14	23.8±1.3	142.0±1.2	562.4	93.7
C (%)[#]	21.5	19.2	22.3	1.75	1.4	3.9	23.6		

- percentage distribution of the initial carbon in the substrate at the end of the experiment. $ - The residual carbon (100 – carbon balance) is expected to be utilized for cell maintenance.

Table 5.4. CMB for food waste hydrolysate fermentation by *Clostridium pasteurianum* (test experiment with ultrasound irradiation)

Time (h)	TRS (mg)	Butyrate (mg)	Acetate (mg)	Lactate (mg)	Succinate (mg)	CO_2 (mg)	Biomass (mg)	Total carbon (mg)	Carbon balance (%)
0	600.0	0	0	0	0	0	0	600.0	100
3	421.6±2.51	33.1±1.24	62±0.38	7.2±0.3	5.7±0.08	1.6±1.11	36±0.5	566.8	94.4
6	301.8±3.32	36.1±1.46	78±1.2	7.5±0.05	5.6±0.32	4.9±1.5	84.2±0.68	518.1	86.3
9	254.2±5.45	43.8±0.5	96±0.84	5.8±0.20	5.4±0.07	11.4±1.6	114±0.25	530.6	88.4
12	131.8±4.52	102.8±0.92	143±1.11	7.8±0.09	5.3±0.11	18.6±2.2	138.6±1.52	542.2	90.3
C (%)#	22	17.1	23.8	1.3	0.8	4.1	23.1		

- percentage distribution of the initial carbon in the substrate at the end of the experiment

Table 5.5. Experimental metabolic rates and constraints used in *in silico* MFA

Parameter	Component	Control		Test	
		Mechanical shaking		Ultrasound-assisted	
		Measured	Calculated	Measured	Calculated
Specific uptake rate (mmol/L/h)	TRS	3.77	--	5.55	--
Specific production rate (mmol/L/h)	Acetate	2.12	--	4.12	--
	Butyrate	2.31	--	2.5	--
	Lactate	0.18	--	0.2	--
	Succinate	0.027	--	0.10	--
	H_2	2.90	2.91	3.7	4.12
$BioH_2$ yield (mol/mol hexose sugar)		1.61	1.8	1.95	2.12
Specific growth rate (h^{-1})		0.12	0.16	0.23	0.35

5.3.2 Metabolic flux analysis

The reaction scheme provided in Table 5.1 was used to develop the *in silico* metabolic network of *Clostridium pasteurianum*. A metabolic network and experimentally determined rates of specific hexose sugar uptake and production of four metabolites (succinate, lactate, butyrate, and acetate) were used to calculate intracellular fluxes of *Clostridium pasteurianum* during the exponential phase of food waste hydrolysate fermentation. To solve the pseudo-steady-state metabolic flux balance described in Eq. 2, these measured rates served as limiting conditions or boundary conditions. The results of the MFA are depicted in Table 5.5, which indicates an excellent match between experimental (measured, control case: 2.90 mmol/L·h, test case: 3.70 mmol/L·h) results and *in silico* (MFA model predicted, control case: 2.91 mmol/L·h, test case: 4.12 mmol/L·h) values for specific bioH_2 production rates. Due to the lack of detailed information on the cellular composition of *Clostridium pasteurianum in* previous literature, the biomass formation equation was derived using the cellular compositions of the closely related species *Clostridium acetobutylicum* and *Clostridium butyricum*, which share core fermentative physiology and lipid classes with *Clostridium pasteurianum*. A similar approach has also been adopted in previous literature [20, 39, 43, 46, 55, 56]. The results of MFA are depicted in Fig. 5.1 for both experiments. According to the results of MFA depicted in Fig. 5.1, flux through the Embden–Meyerhof (EM) pathway is approximately higher than that through the pentose-phosphate (PP) pathway. This suggests a predominant metabolism of hexose sugars (Glc) via the EM pathway, leading to the production of pyruvate. Conversion of pyruvate either into lactate or acetyl-CoA is accompanied by the co-generation of reduced ferredoxin. BioH_2 is then produced directly from reduced ferredoxin through the activity of the hydrogenase enzyme. MFA was carried out for both control and test experiments to get insight into how sonication or ultrasound irradiation affects the distribution of carbon flux in the metabolism of *Clostridium pasteurianum*. The application of sonication affected metabolic fluxes at three critical points:

phosphoenolpyruvate (PEP), pyruvate (PYR), and acetyl-CoA (ACCOA), as shown in Fig. 5.1. The effect of sonication at the respective nodes can be explained as follows:

(a) At the phosphoenolpyruvate (PEP) node, a greater fraction of carbon flux was directed towards oxaloacetate (OAA) than pyruvate (PYR). The remarkable increase (0.12 to 0.24 mmol/L·h) in metabolic flux towards OAA during the test experiments may be attributed to structural modifications in the PEP carboxylase enzyme induced by intermittent sonication, which enhanced its affinity for the substrate PEP.

(b) At the pyruvate (PYR) node, the carbon flux towards acetyl-CoA (ACCOA) and bioH_2 was higher than that towards lactate. Previous studies have confirmed that a lower flux towards lactate favors bioH_2 production [20, 55]. With the application of sonication, the carbon flux towards lactate increased by ~22% (0.18 to 0.22 mmol/L·h). However, this flux remains significantly lower than the combined flux (8.26 mmol/L·h) directed towards bioH_2 and acetyl-CoA.

Three enzymes, such as pyruvate dehydrogenase, pyruvate ferredoxin oxidoreductase, and lactate dehydrogenase, compete for pyruvate as a substrate at the pyruvate node. The distribution of fluxes suggests that the majority of pyruvate is converted into reduced ferredoxin and acetyl-CoA, both of which are associated with maximum bioH_2 production.

(c) Sonication had a significant impact on the carbon flux distribution at the acetyl–CoA (ACCOA) node, as the flux towards acetate (AC) (2.12 to 4.12 mmol/L·h) increased by ~ 94%. While the metabolic flux towards butyrate (BA) (2.31 to 2.5 mmol/L·h) increased by ~9% in the test experiment, the significant increase in the metabolic flux towards acetate may have resulted from changes in the secondary structure of the acetate kinase enzyme caused by intermittent sonication.

Table 5.6 presents the yields of the primary products from the fermentation of food waste

hydrolysate. Experimental results showed a notable ~22% increase in bioH_2 yield. MFA indicates that an increased flux towards acetate and butyrate correlates with higher bioH_2 production during ultrasound-assisted fermentation of food waste hydrolysate or hexose sugars. This finding is further supported by a higher acetate-to-butyrate (A/B) ratio observed in the test experiments, as shown in Table 5.6.

Table 5.6. Product yields (mol/mol hexose sugar) in control and test experiments

	Acetate	Butyrate	Lactate	Succinate	CO_2	H_2	Acetate/Butyrate
Control	0.52	0.38	0.035	0.016	0.27	1.61	1.36
Test	0.89	0.48	0.032	0.027	0.20	1.95	1.87

5.3.3 Analysis

The theoretical production of bioH_2 through glucose fermentation is represented by the following equations for the acetic acid and butyric acid as final products [12, 55].

$$C_6H_{12}O_6 + 2\,H_2O \rightarrow 2\,CH_3COOH + 2\,CO_2 + 4\,H_2 \quad (5.5)$$

$$C_6H_{12}O_6 \rightarrow C_3H_7COOH + CO_2 + 2\,H_2 \quad (5.6)$$

It should be noted that the above chemical reactions represent the conceptual conversion of glucose into the products of acetic acid and butyric acid. However, in actual cell metabolism, the conversion of glucose into acid products occurs through several series and parallel reactions catalyzed by different enzymes. Thus, the actual yields of the side products of hydrogen and

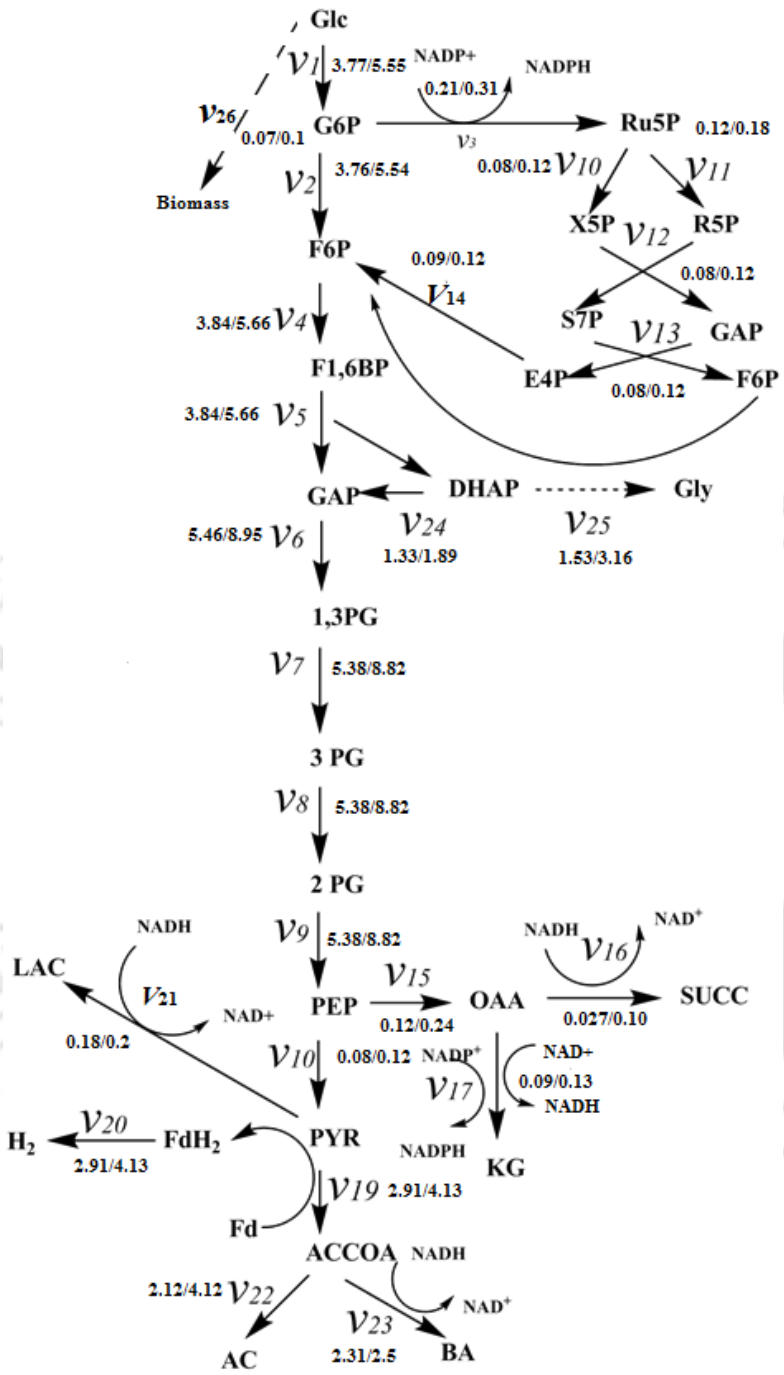

Fig. 5.1. MFA results of bioH₂ production from food waste hydrolysate fermentation using *Clostridium pasteurianum*. The flux values are depicted as: control case (mechanical shaking) / test case (mechanical shaking with sonication)

carbon dioxide is likely to be significantly different than the theoretical (or stoichiometric) yields shown by the above equations.

The decrease in bioH_2 yield during dark fermentation is mainly due to the accumulation of fermentation byproducts, particularly acetic acid and butyric acid, in the fermentation broth. The presence of these metabolites leads to acidification of the fermentation broth, triggering solventogenesis and subsequently lowering the bioH_2 yield. Notably, the primary metabolite, butyric acid, has been identified to have inhibitory effects on cell growth [57–60], further complicating the process optimization. As indicated by Eqs. 5.5 and 5.6, the stoichiometry of hexose sugar fermentation suggests a potential bioH_2 yield of 4 mol H_2 per mol of glucose when acetate is the sole product, and 2 mol of H_2 per mol of glucose when butyrate is the sole product. The butyrate formation pathway is a major competitor in bioH_2 production, consuming more NADH and diminishing the bioH_2 yield. However, as discussed in the preceding sections, experimental results reveal an increasing bioH_2 yield with the acetate/butyrate (A/B) ratio, presenting a notable agreement with the theoretical expectations. This also supports the conjecture that eliminating the butyrate pathway may lead to increased acetate production, resulting in a higher bioH_2 yield per unit of hexose sugar consumption.

Based on the above analysis, we propose two possibilities for genetic alteration of *C. pasteurianum* to further enhance bioH_2 yield in dark fermentation.

(a) Blocking the butyrate pathway in the *in silico* metabolic network: In this case, we set the flux from acetyl–CoA to butyrate (represented as v_{23}) and the butyrate concentration as zero (v_{23} = 0, BA = 0), while keeping all other concentrations of metabolites the same. For these conditions, the effect on bioH_2 flux was assessed using MFA. The MFA analysis depicted in Fig. 5.2 revealed a significant increase in flux toward bioH_2 (v_{20}), when v_{23} was nullified. Specifically, there was a ~41% rise (2.91 to 4.13 mmol/L·h) in v_{20} during control fermentation

(with mechanical shaking) and ~56% increase (4.13 to 6.13 mmol/L·h) in test fermentation (with sonication). The potential *in vivo* elimination of the butyrate pathway involves knocking out genes encoding enzymes in the butyrate formation pathway, including butyryl-CoA dehydrogenase (BCD), β–hydroxy butyryl–CoA dehydrogenase (BHBD), butyrate kinase (BK), 3–hydroxy–CoA dehydratase (CRT), and phospho–trans–butrylase (PTB).

(b) Increasing the substrate consumption rate: Genes encoding the enzymes glucokinase or hexokinase can be highly expressed *in vivo* to increase the substrate uptake (or consumption) rate. In this instance, the experimental value of the flux from hexose sugar (Glc) to G6P (v_1) was doubled. The previous data (or results) on metabolic flux analysis in the control and test fermentations were used to analyze the outcome of enhanced substrate consumption. The results of the MFA analysis are shown in Fig. 5.3. It can be seen that the carbon flux towards bioH_2 increases by approximately 3.5 times when the hexose sugar intake rate is doubled. This result is consistent for both control and test experiments. The values of different fluxes are reproduced here: substrate uptake flux = 11.1 mmol/L·h in the test fermentation, which resulted in bioH_2 flux (v_{20}) of 14.53 mmol/L·h, which is higher than flux in the control fermentation, viz., v_{20} = 4.13 mmol/L·h.

In essence, the two hypothetical strategies of eliminating the butyrate pathway or overexpressing genes to enhance hexose sugar or total reducing sugar uptake reveal significant enhancement of bioH_2 yield, and also provide valuable insights for genetic engineering *C. pasteurianum* mutants.

5.3.4 Comparison with previous literature

Several previous authors have employed metabolic flux analysis to study fermentative hydrogen synthesis using different substrates and microbial cultures. Sarma et al. [20] reported the MFA of ultrasound-assisted fermentation of crude glycerol by *Clostridium pasteurianum*,

showing that ultrasound enhanced glycerol consumption by ~ 50% and H_2 production by ~ 40%, with a maximum H_2 yield of 0.89 mol H_2/mol glycerol. Sonication influenced the carbon fluxes at the acetyl-CoA node in crude glycerol fermentation. Metabolic flux analysis of fermentation profiles revealed an enhanced flux towards butyrate with sonication, resulting in a higher butyrate-to-acetate ratio in the products and higher bioH_2 generation. Cheng et al. [46] applied MFA for the fermentation of glucose and lactate/acetate using *Clostridium tyrobutyricum* and found that increasing hydraulic retention time (HRT) improved H_2 production (< 3 mol H_2 /mol glucose) and reduced lactate formation. Niu et al. [61] employed MFA for analyzing glucose fermentation by *Klebsiella pneumoniae ECU-15* and reported an optimal H_2 flux at 5 g/L glucose, with a pH range of 7.0–7.5, and decreased substrate uptake at higher temperatures. Using MFA, Cai et al.[55] reported that for *Clostridium butyricum W5*, pH had a greater impact on H_2 production (H_2 yield of 0.79 mol/mol glucose) than the concentration of substrate glucose in the fermentation mixture. Similarly, based on flux comparisons of wild and mutant strains, Manish et al.[43] observed that in *E. coli*, ethanol and acetate were key to H_2 production, while lactate and succinate were less relevant. The results of metabolic flux analysis in the present study are consistent with previous literature, indicating that ultrasound influences the carbon flux at the acetyl-CoA node, resulting in a higher acetate/butyrate ratio, which is associated with increased bioH_2 production (H_2 yield: 0.17 mol/mol glucose). Moreover, the substrate uptake rate in the present study is also found to increase with sonication, as reported in previous literature.

In the present study, we have noted enhanced bioH_2 production by introducing ultrasound during hexose sugar fermentation; however, the resulting yield of 1.95 mol H_2/mol hexose sugar is approximately half of the maximum theoretical yield. The bioH_2 yield from food waste fermentation shows significant variance across previous literature. A direct quantitative comparison of the yields reported in previous literature is difficult due to variations

in the microbial strains used and the protocols followed for pretreatment/fermentation. Han et al. [14] reported a yield of 1.90 mol/mol hexose sugar from wheat flour hydrolysate, while Han et al. [62] achieved a slightly higher yield of 1.97 mol/mol hexose sugar from food waste hydrolysate. In contrast, Kim et al.[63] reported a significantly lower yield of 1.12 mol/mol hexose sugar from food waste fermentation. In the present study, the bioH_2 yield was 1.95 mol/mol hexose sugar from food waste fermentation, which is higher than that reported by Kim et al. [63] and Han et al. [53] but slightly lower than the yield obtained by Han et al. [62]. These variations highlight the influence of substrate composition and fermentation conditions on the efficiency of bioH_2 production. Gadhe et al. [28–30] have reported the effect of sonication on biohydrogen production from dark fermentation of dairy wastewater using an anaerobic digester sludge of hydrogen-producing microbes. Prior to fermentation, the dairy wastewater was also subjected to ultrasonic pretreatment. It was observed that ultrasonic pretreatment of dairy wastewater prior to fermentation increased the biodegradability of the wastewater, resulting in a 20-40% enhancement in bioH_2 production, with a H_2 yield of 15.33 mmol/g COD (specific hydrogen production rate of 31.38 mmol/g volatile suspended solid·day). The application of sonication during dark fermentation resulted in a nearly 2-fold increase in the bioH_2 yield.

Garcia-Depraect et al. [64] have reviewed the biohydrogen production from lactate during dark fermentation, highlighting the synergistic interactions between lactate-producing bacteria and hydrogen-producing bacteria. However, in the present study, the production of lactate is relatively minor, as indicated in Table 5.3. Hence, opportunities for enhancing bioH_2 production through lactate consumption by *Clostridium pasteurianum* are rather limited. In another study, Regueira-Marcos et al. [65] have reported biohydrogen production from household food waste via lactate-driven dark fermentation, integrating lactate production and its conversion to bioH_2. The process was carried out in a single stage (combining lactate

fermentation and dark fermentation) and in a two-stage process (separating lactate fermentation and dark fermentation). The two-stage operation yielded a higher hydrogen production rate of 4.4 L H_2/L·d, whereas the single-stage unit had a relatively lower bioH_2 production rate of 1.4 L H_2/L·d. The single-stage process has a hydrogen yield of 22.9 mL H_2/g volatile solid (VS) – corresponding to 1.02 mmol/g VS- and the two-stage process resulted in a hydrogen yield of 39.5 mL H_2 /g VS (corresponding to 1.76 mmol/g VS).

5.3.5 Practical feasibility of genetic modification in *Clostridium pasteurianum*

As evident from the MFA results presented in preceding sections, although the hypothetical genetic modifications of elimination of the butyrate pathway or enhancing the substrate uptake rates are potential strategies for bioH_2 yield, their effects on the redox balance of the cell and cell physiology need to be accounted for.

Knockout of the butyrate pathway would target the enzymes of *bcd* (butyryl-CoA dehydrogenase), *etf*A/B (electron transfer flavoprotein) and *bhbd* (3-hydroxybutyryl-CoA dehydrogenase). These enzymes are part of the central redox–balancing system. A complete disruption of the butyrate pathway could lead to reduced regeneration of NAD^+/$NADP^+$, reduced ATP yields and accumulation of toxic intermediates within the cell. All of these factors would adversely affect the cell growth and viability.

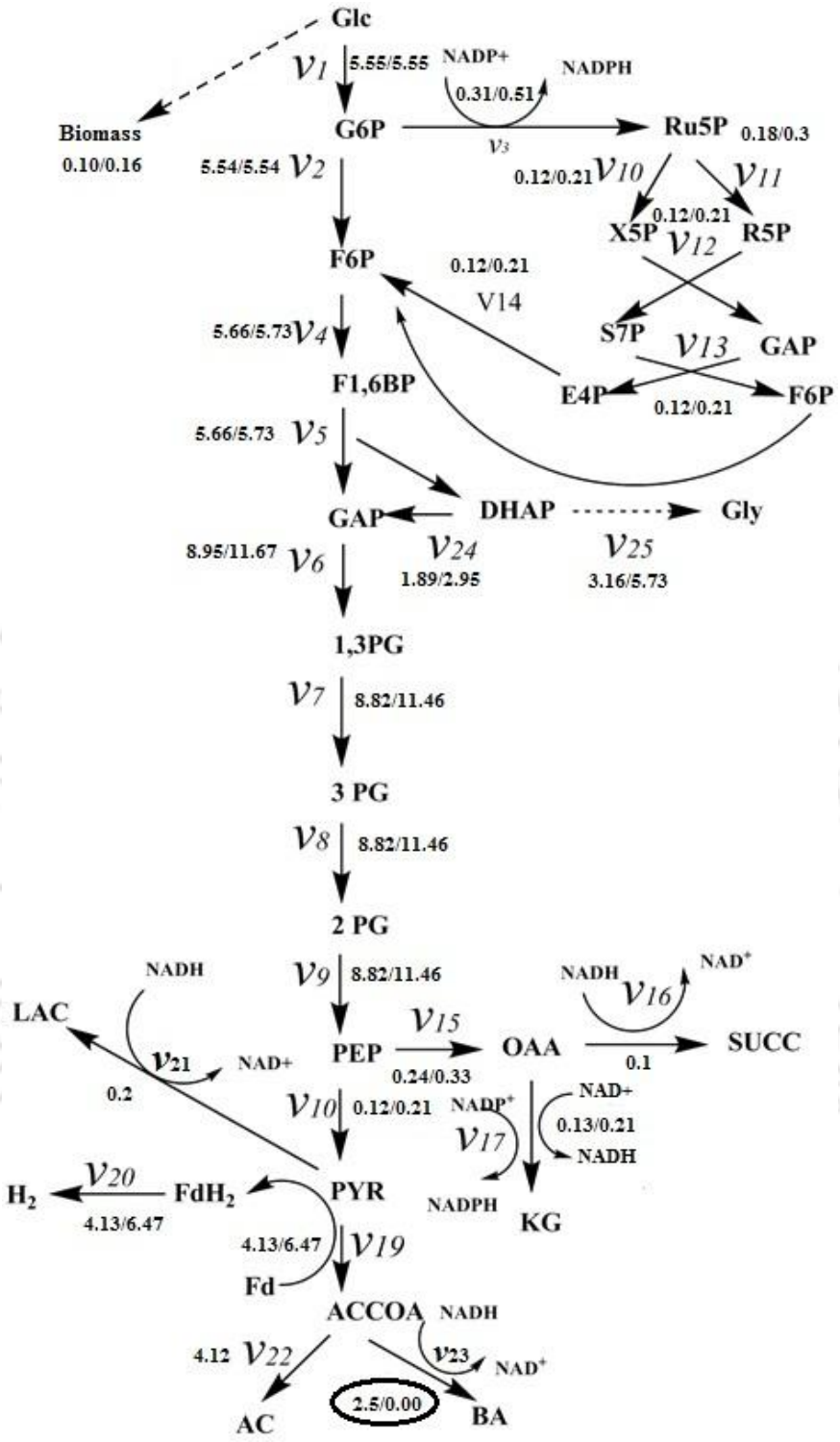

Fig. 5.2. MFA results of bioH₂ production from food waste hydrolysate fermentation using *Clostridium pasteurianum* for the hypothetical case v_{23} = 0, i.e., butyrate production assumed to be zero (encircled values). The flux values are depicted as: control case (mechanical shaking) / test case (mechanical shaking with sonication)

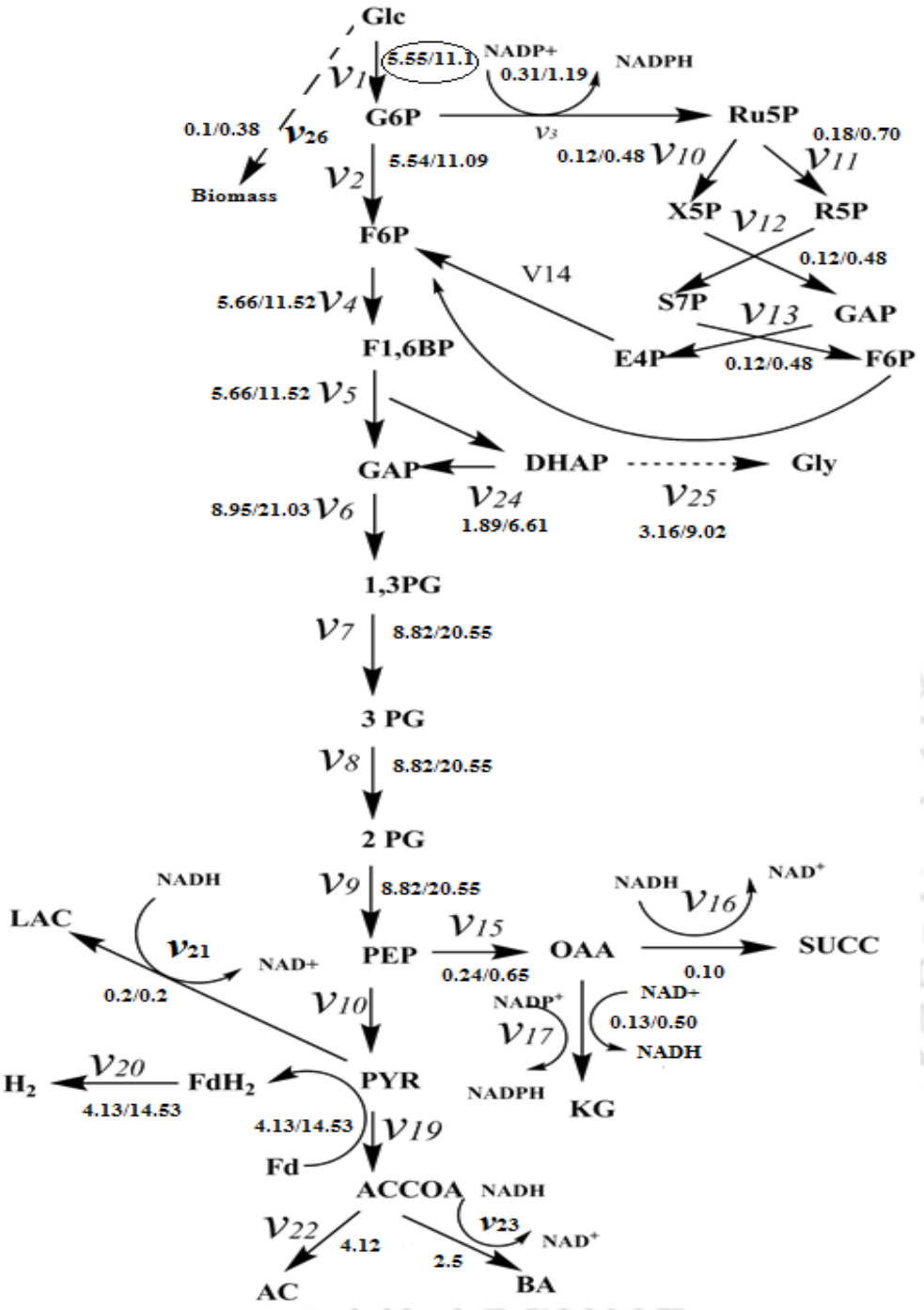

Fig. 5.3. MFA results of bioH_2 production from food waste hydrolysate fermentation using *Clostridium pasteurianum* for the hypothetical case $v_1 = 2\times$, i.e., hexose sugar uptake rate is doubled. The flux values are depicted as: control case (mechanical shaking) / test case (mechanical shaking with sonication)

Similarly, the hypothetical genetic modification of doubling substrate uptake is also associated with the limitation of saturating glucose transporter proteins and the energetics of transmembrane transport (i.e., the energy required to move molecules against their gradients using membrane proteins and ATP). Additionally, increased input carbon flux without balancing downstream metabolism can lead to overflow metabolism, resulting in the production of byproducts such as lactate, acetate, or ethanol. Higher substrate uptake could also lead to more osmotic stress and metabolic heat. In essence, the hypothetical genetic modifications suggested in this study require multi-layered optimization to be practically viable. A knockout of a metabolic pathway or enhancement of substrate flux must account for redox homeostasis, energy conservation and cellular health.

5.3.6 Practical implications of the MFA results for dark fermentation using mixed consortia

The present study is based on the metabolic pathway of *Clostridium pasteurianum*. Commercial-scale biohydrogen processes are likely to employ a consortium (or mixed culture) containing other bacterial species than *Clostridium pasteurianum*. However, the results of metabolic flux analysis in this study also apply to the mixed cultures, as all *Clostridium* species involved in biohydrogen production share many core metabolic features that govern the fermentation pathway. A few of these features are summarized as follows: (1) they utilize the Embden-Meyerhof-Parnas (EMP)pathway to convert reducing sugars into pyruvate – generating ATP and reduced cofactors (mainly NADH) for redox reactions; (2) oxidation of pyruvate to acetyl-CoA by pyruvate: ferredoxin oxidoreductase produces reduced ferredoxin – the key electron donor for hydrogen formation; (3) hydrogen formation is catalysed by [FeFe]-hydrogenases that oxidise reduced ferredoxin and regenerate oxidized cofactors; (4) acetate formation from acetyl-CoA (via phosphotransacetylase and acetate kinase) – which is a major

route associated with hydrogen generation and maintenance of redox balance while producing ATP; (5) formation of reduced products such as butyrate or ethanol consumes NADH, reducing the hydrogen yield. In addition, the genetic organization of key hydrogenase and fermentation-related enzymes also exhibits high homology among different *Clostridial* species [66, 67]. Due to these common metabolic features, the influence of ultrasound seen at different nodes of the metabolic pathway of *Clostridium pasteurianum* is also likely to occur for other hydrogen-producing species. However, the extent (quantitative) of this influence in altering metabolic fluxes may vary from species to species.

5.4 Conclusion

Metabolic flux analysis of the dark fermentation of food waste hydrolysate in the present study has provided clear insights into the effect of sonication on intracellular carbon flux and metabolism in *Clostridium pasteurianum*. Under statistically optimized conditions, the application of 35 kHz ultrasound at a 20% duty cycle increased the hexose uptake flux of the microbial cells by ~47%. Meanwhile, the intracellular fluxes of butyrate and acetate at the acetyl-CoA node of the metabolic pathway rose by ~9% and 94%, respectively. This redistribution of flux enhanced the bioH_2 yield by ~22% and increased the acetate-to-butyrate (A/B) ratio by ~37%. These findings clearly establish a direct link between flux redirection at the acetyl-CoA node and improved hydrogen production. Further, MFA-based simulations of hypothetical modifications in the cellular metabolism through genetic interventions (e.g., full diversion of butyrate flux to acetate or doubling of substrate uptake) revealed an opportunity for even greater hydrogen yields, thereby emphasizing the suitability of MFA for process optimization and intensification.

Beyond these mechanistic insights, the results of the present study also have practical implications. Ultrasound-assisted dark fermentation of inexpensive and waste substrates, such

as food waste, with enhanced substrate uptake and product yield, offers a straightforward and scalable approach for intensifying sustainable and green biohydrogen production. As demonstrated in the present study, this strategy is compatible with food waste hydrolysates and can be adapted to other waste-derived substrates. Moreover, the general framework of metabolic flux analysis established in this study provides a rational basis for extending the strategy to other solventogenic *Clostridium* strains with diverse fermentation pathways and products. In summary, these facets show the dual significance of our work: (1) advancing the fundamental understanding of metabolic flux redistribution in microbial cells under the influence of sonication, and (2) underscoring pathways for improving both the efficiency and the practical feasibility of sustainable large-scale biohydrogen processes. The mechanistic insights obtained from the present study using single-culture can lay the groundwork for developing more robust, mixed-culture based dark fermentation systems.

List of Abbreviations

Glc	hexose sugar or reducing sugar content in food waste hydrolysate
G6P	glucose 6–phosphate
F6P	fructose 6–phosphate
F1,6BP	fructose–1,6–bis phosphate
GAP	glyceraldehyde 3–phosphate
1,3 PG	1,3–bisphosphoglycerate
3PG	3–phosphoglycerate
2PG	2–phosphoglycerate
PEP	phosphoenolpyruvate
PYR	pyruvate
ACCOA	acetyl coenzyme A
AC	acetate
BA	butyrate
LAC	lactate

OAA	oxaloacetate
SUCC	succinate
Ru5P	ribulose 5–phosphate
X5P	xylulose 5–phosphate
R5P	ribose 5–phosphate
S7P	sedaheptulose 7–phosphate
E4P	erythrose 4–phosphate
DHAP	dihydroxyacetone phosphate
Gly	glycerol
NADPH	nicotinamide adenine dinucleotide phosphate (reduced form)
NADH	nicotinamide adenine dinucleotide (reduced form)
NAD^+	nicotinamide adenine dinucleotide
TRS	total reducing sugar or hexose sugar

CHAPTER 5: Appendix 5A

Table 5A.1. Summary of literature on metabolic flux analysis of biohydrogen production utilizing different substrates and microbial strains

Microorganism	Substrate	Salient features	Reference
Clostridium pasteurianum	Crude glycerol	The study aims to gain insight into ultrasound-induced enhancement in biohydrogen production from glycerol fermentation using metabolic flux analysis (MFA). A pseudo-steady-state metabolic flux network model was constructed and analyzed using experimentally measured glycerol uptake rates and fluxes of four metabolites, namely acetate, butyrate, succinate, and 1,3-PDO. Glycerol consumption increased under sonication	[20]
Clostridium tyrobutyricum	Glucose and lactate/acetate	The MFA methodology was applied to study the flux distribution during glucose and lactate/acetate metabolism, as well as the effect of HRT and initial substrate concentration. HRT showed a significant impact on H_2 production. An increase in HRT increased H_2 production and reduced lactate production	[46]
Rhodobacter capsulatus	Acetate, lactate, malate and CO_2	Study the flux distribution in the photoautotrophic metabolism of *R. capsulatus* for several substrates. Prediction of knockouts mainly by blockade of the Calvin cycle and reduction of formate, leading to an increase in H_2 yield using the constructed flux model.	[31]
Klebsiella pneumoniae ECU-15	Glucose	The MFA method was used to estimate the effects of various culture conditions (temperature, pH, initial glucose concentration) on the production and uptake of hydrogen flux. Higher temperature reduced the uptake of hydrogen and enhanced H_2 production. pH 7.0-7.5 was optimal for both the H_2 flux, and the producing H_2 flux was maximum at 5 g/L of initial glucose.	[61]
Clostridium butyricum W5	Glucose	Metabolic flux analysis (MFA) of fermentative hydrogen with variations in initial glucose concentration and operational pH. The results suggest that pH has a more significant effect on H_2 production than glucose concentration.	[55]

Microorganism	**Substrate**	**Salient features**	**Reference**
Synechocystis sp. PCC6803	Glucose	A metabolic model was implemented for analyzing hydrogen production under three conditions (heterotrophic, autotrophic, and mixotrophic) in terms of O_2 production and CO_2 fixation. Two conditions: anoxic maximum and anoxic photoreduction	[6]
Citrobacter amalonaticus Y19	Glucose	MetaFluxNet was employed for flux analysis of H_2 production with varying glucose concn. A high H_2 yield of 8.7 mol H_2/mol glucose was achieved when glucose metabolism is directed to the PP pathway and NAD(P)-linked hydrogenase is utilized to produce H_2.	[7]
Klebsiella pneumoniae	Glycerol	MFA of anaerobic glycerol metabolism for the production of 1,3-propanediol. Flux distribution revealed that the branch points of glycerol and dihydroxyacetone phosphate were rigid compared to the flexible node of pyruvate and acetyl-CoA under various environmental conditions.	[8]
Escherichia coli	Glucose	Evaluation and comparison of the metabolic network of wild and mutant (lacking lactate dehydrogenase) *E. coli* strain for H_2 production. Ethanol and acetate play significant roles in H_2 production, while lactate and succinate are not necessary.	[43]

Table 5A.2. Stoichiometric matrix S for metabolic flux analysis (MFA) analysis

Reaction number → / Species name ↓	v_1	v_2	v_3	v_4	v_5	v_6	v_7	v_8	v_9	v_{10}	v_{11}	v_{12}	v_{13}	v_{14}	v_{15}	v_{16}	v_{17}	v_{18}	v_{19}	v_{20}	v_{21}	v_{22}	v_{23}	v_{24}	v_{25}	v_{26}
G6P	1	-1	-1	0	0	0	0	0	0	0	0	0	0	0	0	0	0	0	0	0	0	0	0	0	0	–0.0016
F6P	0	1	0	-1	0	0	0	0	0	0	0	0	1	0	0	0	0	0	0	0	0	0	0	0	0	-0.1788
F1,6BP	0	0	0	1	-1	0	0	0	0	0	0	0	0	0	0	0	0	0	0	0	0	0	0	0	0	0
GAP	0	0	0	0	1	-1	0	0	0	0	0	1	-1	1		0	0	0	0	0	0	0	0	1	0	0
1,3 PG	0	0	0	0	0	1	-1	0	0	0	0	0	0	0	0	0	0	0	0	0	0	0	0	0	0	0
3 PG	0	0	0	0	0	0	1	-1	0	0	0	0	0	0	0	0	0	0	0	0	0	0	0	0	0	-1.239
DHAP	0	0	0	0	1	0	0	0	0	0	0	0	0	0	0	0	0	0	0	0	0	0	0	-1	-1	0
2 PG	0	0	0	0	0	0	0	1	-1	0	0	0	0	0	0	0	0	0	0	0	0	0	0	0	0	0
PEP	0	0	0	0	0	0	0	0	1	0	0	0	0	0	-1	0	0	-1	0	0	0	0	0	0	0	-0.661
OAA	0	0	0	0	0	0	0	0	0	0	0	0	0	0	1	-1	0	0	0	0	0	0	0	0	0	-1.4452
PYR	0	0	0	0	0	0	0	0	0	0	0	0	0	0	0	0	0	1	-1	0	-1	0	0	0	0	-2.666
FdH_2	0	0	0	0	0	0	0	0	0	0	0	0	0	0	0	0	0	0	1	-1	0	0	0	0	0	0
ACCOA	0	0	0	0	0	0	0	0	0	0	0	0	0	0	0	0	0	0	1	0	0	-1	-1	0	0	-20.29
α-KG	0	0	0	0	0	0	0	0	0	0	0	0	0	0	0	0	1	0	0	0	0	0	0	0	0	-1.3285
Ru5P	0	0	1	0	0	0	0	0	0	-1	-1	0	0	0	0	0	0	0	0	0	0	0	0	0	0	0
X5P	0	0	0	0	0	0	0	0	0	1	0	-1	0	0	0	0	0	0	0	0	0	0	0	0	0	0
R5P	0	0	0	0	0	0	0	0	0	0	1	-1	0	0	0	0	0	0	0	0	0	0	0	0	0	-0.5726
S7P	0	0	0	0	0	0	0	0	0	0	0	1	-1	0	0	0	0	0	0	0	0	0	0	0	0	0
E4P	0	0	0	0	0	0	0	0	0	0	0	0	1	-1	0	0	0	0	0	0	0	0	0	0	0	0
NADH	0	0	0	0	0	1	0	0	0	0	0	0	0	0	0	-1	1	0	0	0	-1	0	-2	0	0	-10.75
NADPH	0	0	2	0	0	0	0	0	0	0	0	0	0	0	0	0	1	0	0	0	0	0	0	0	0	-7.6152

List of abbreviations for metabolic species

Glc	hexose sugar or reducing sugar content in food waste hydrolysate
G6P	glucose 6–phosphate
F6P	fructose 6–phosphate
F1,6BP	fructose–1,6–bis phosphate
GAP	glyceraldehyde 3–phosphate
1,3 PG	1,3–bisphosphoglycerate
3PG	3–phosphoglycerate
2PG	2–phosphoglycerate
PEP	phosphoenolpyruvate
PYR	pyruvate
ACCOA	acetyl coenzyme A
AC	acetate
BA	butyrate
LAC	lactate
OAA	oxaloacetate
SUCC	succinate
Ru5P	ribulose 5–phosphate
X5P	xylulose 5–phosphate
R5P	ribose 5–phosphate
S7P	sedaheptulose 7–phosphate
E4P	erythrose 4–phosphate
DHAP	dihydroxyacetone phosphate
Gly	glycerol
NADPH	nicotinamide adenine dinucleotide phosphate (reduced form)
NADH	nicotinamide adenine dinucleotide (reduced form)
NAD^+	nicotinamide adenine dinucleotide

References

1. Shet K HN, Anand A, Moholkar VS (2025) Hydrogen Production Technologies: Pathways to a Sustainable and Cleaner Environment. In: Valera H, Agarwal AK (eds) Hydrogen as Emerging Fuel for De-Fossilizing Transport Sector. Springer Nature, Singapore, pp 129–165

2. Kaiwen L, Bin Y, Tao Z (2018) Economic analysis of hydrogen production from steam reforming process: A literature review. Energy Sources, Part B: Economics, Planning, and Policy 13:109–115. https://doi.org/10.1080/15567249.2017.1387619

3. Anand A, Umesh, Moholkar VS (2024) Chapter 3 - Biohydrogen production from microbial fermentation of organic wastes. In: Nanda S, Dalai AK, Goud VV (eds) Emerging Biofuels. Elsevier, pp 27–52

4. Pradhan AK, Goyal H, Patel P, Mondal P (2024) Bio-hydrogen production from crude glycerol: Optimisation through response surface methodology and artificial neural network approach. Biomass and Bioenergy 185:107243. https://doi.org/10.1016/j.biombioe.2024.107243

5. Li W, He L, Cheng C, et al (2020) Effects of biochar on ethanol-type and butyrate-type fermentative hydrogen productions. Bioresource Technology 306:123088. https://doi.org/10.1016/j.biortech.2020.123088

6. Patel K, Vashist M, Goyal D, et al (2025) From waste to resource: A life cycle assessment of biochar from agricultural residue. Env Prog and Sustain Energy 44:e14558. https://doi.org/10.1002/ep.14558

7. Li W, Cheng C, Cao G, Ren N (2020) Enhanced biohydrogen production from sugarcane molasses by adding Ginkgo biloba leaves. Bioresour Technol 298:122523. https://doi.org/10.1016/j.biortech.2019.122523

8. Chi Cheng, Teng Bao & Shang-Tian Yang (2019) Engineering Clostridium for improved solvent production: recent progress and perspective | Applied Microbiology and Biotechnology. https://link.springer.com/article/10.1007/s00253-019-09916-7. Accessed 18 Sep 2025

9. Sahoo A, Dwivedi A, Madheshiya P, et al (2024) Insights into the management of food waste in developing countries: with special reference to India. Environ Sci Pollut Res 31:17887–17913. https://doi.org/10.1007/s11356-023-27901-6

10. Das A, Verma M, Mishra V (2024) Food waste to resource recovery: a way of green advocacy. Environ Sci Pollut Res 31:17874–17886. https://doi.org/10.1007/s11356-023-27193-w

11. Anand A, Mahata C, Moholkar VS (2024) Biohydrogen synthesis from food waste hydrolysate: Optimization using statistical design of experiments (DoE) and artificial neural network (ANN). Biomass and Bioenergy 191:107452. https://doi.org/10.1016/j.biombioe.2024.107452

12. Gadkari S, Kumar D, Qin Z, et al (2021) Life cycle analysis of fermentative production

of succinic acid from bread waste. Waste Management 126:861–871. https://doi.org/10.1016/j.wasman.2021.04.013

13. Han W, Yan Y, Shi Y, et al (2016) Biohydrogen production from enzymatic hydrolysis of food waste in batch and continuous systems. Sci Rep 6:38395. https://doi.org/10.1038/srep38395

14. Han W, Wang X, Ye L, et al (2015) Fermentative hydrogen production using wheat flour hydrolysate by mixed culture. International Journal of Hydrogen Energy 40:4474–4480. https://doi.org/10.1016/j.ijhydene.2015.02.016

15. Paritosh K, Kushwaha SK, Yadav M, et al (2017) Food Waste to Energy: An Overview of Sustainable Approaches for Food Waste Management and Nutrient Recycling. BioMed Research International 2017:1–19. https://doi.org/10.1155/2017/2370927

16. Mahata C, Ray S, Das D (2020) Optimization of dark fermentative hydrogen production from organic wastes using acidogenic mixed consortia. Energy Conversion and Management 219:113047. https://doi.org/10.1016/j.enconman.2020.113047

17. Zhao X, Wang Z, Zhou X, et al (2019) Full length obtains of hydA and phylogenetic analysis of bio-hydrogen production new species of Clostridium based on efficient hydA degenerate primers. International Journal of Hydrogen Energy 44:29493–29499. https://doi.org/10.1016/j.ijhydene.2019.05.050

18. Gavahian M, Manyatsi TS, Morata A, Tiwari BK (2022) Ultrasound-assisted production of alcoholic beverages: From fermentation and sterilization to extraction and aging. Comprehensive Reviews in Food Science and Food Safety 21:5243–5271. https://doi.org/10.1111/1541-4337.13043

19. Malani RS, Umriwad SB, Kumar K, et al (2019) Ultrasound–assisted enzymatic biodiesel production using blended feedstock of non–edible oils: Kinetic analysis. Energy Conversion and Management 188:142–150. https://doi.org/10.1016/j.enconman.2019.03.052

20. Sarma S, Anand A, Dubey VK, Moholkar VS (2017) Metabolic flux network analysis of hydrogen production from crude glycerol by Clostridium pasteurianum. Bioresource Technology 242:169–177. https://doi.org/10.1016/j.biortech.2017.03.168

21. Xie M, Ma Y, An F, et al (2024) Ultrasound-assisted fermentation for antioxidant peptides preparation from okara: Optimization, stability, and functional analyses. Food Chemistry 439:138078. https://doi.org/10.1016/j.foodchem.2023.138078

22. Mamy D, Boateng ID, Chen X (2025) Metabolomic changes in Citrus reticulata peel after conventional and ultrasound-assisted solid-state fermentation with Aspergillus niger: A focus on flavonoid metabolism. Food Chemistry 467:142224. https://doi.org/10.1016/j.foodchem.2024.142224

23. Fonteles TV, Dos Santos AYS, Linhares MDFD, et al (2024) Metabolic responses of kombucha consortium fermentation upon ultrasound-processing. Food Chemistry Advances 4:100646. https://doi.org/10.1016/j.focha.2024.100646

24. Shokri S, Terefe NS, Shekarforoush SS, Hosseinzadeh S (2021) Ultrasound-assisted

fermentation for enhancing metabolic and probiotic activities of *LactoBacillus brevis*. Chemical Engineering and Processing - Process Intensification 166:108470. https://doi.org/10.1016/j.cep.2021.108470

25. Singh S, Agarwal M, Sarma S, et al (2015) Mechanistic insight into ultrasound induced enhancement of simultaneous saccharification and fermentation of Parthenium hysterophorus for ethanol production. Ultrasonics Sonochemistry 26:249–256. https://doi.org/10.1016/j.ultsonch.2015.02.011

26. Khanna S, Goyal A, Moholkar VS (2013) Mechanistic investigation of ultrasonic enhancement of glycerol bioconversion by immobilized Clostridium pasteurianum on silica support. Biotechnology and Bioengineering 110:1637–1645. https://doi.org/10.1002/bit.24839

27. Khanna S, Jaiswal S, Goyal A, Moholkar VS (2012) Ultrasound enhanced bioconversion of glycerol by *Clostridium pasteurianum*: A mechanistic investigation. Chemical Engineering Journal 200–202:416–425. https://doi.org/10.1016/j.cej.2012.06.040

28. Gadhe A, Sonawane SS, Varma MN (2015) Enhanced biohydrogen production from dark fermentation of complex dairy wastewater by sonolysis. International Journal of Hydrogen Energy 40:9942–9951. https://doi.org/10.1016/j.ijhydene.2015.06.098

29. Gadhe A, Sonawane SS, Varma MN (2014) Evaluation of ultrasonication as a treatment strategy for enhancement of biohydrogen production from complex distillery wastewater and process optimization. International Journal of Hydrogen Energy 39:10041–10050. https://doi.org/10.1016/j.ijhydene.2014.04.153

30. Gadhe A, Sonawane SS, Varma MN (2014) Ultrasonic pretreatment for an enhancement of biohydrogen production from complex food waste. International Journal of Hydrogen Energy 39:7721–7729. https://doi.org/10.1016/j.ijhydene.2014.03.105

31. Sarma S, Dubey VK, Moholkar VS (2016) Kinetic and thermodynamic analysis (with statistical optimization) of hydrogen production from crude glycerol using Clostridium pasteurianum. International Journal of Hydrogen Energy 41:19972–19989. https://doi.org/10.1016/j.ijhydene.2016.08.204

32. Li W, Cheng C, Ren N, et al (2022) Different feedback effects of aqueous end products on hydrogen production of *Clostridium tyrobutyricum*. International Journal of Hydrogen Energy 47:35156–35170. https://doi.org/10.1016/j.ijhydene.2022.08.120

33. Mermejo B da C, Bortolucci J, de Andrade AR, Reginatto V (2022) The Non-solventogenic Clostridium beijerinckii Br21 Produces 1,3-Propanediol From Glycerol With Butyrate as the Main By-Product. Front Sustain Food Syst 6:. https://doi.org/10.3389/fsufs.2022.848022

34. Yu Y, Shi Z, Li W, et al (2025) Application of exogenous electron mediator in fermentation to enhance the production of value-added products. Applied and Environmental Microbiology 91:e00495-25. https://doi.org/10.1128/aem.00495-25

35. Wang Y, Yang G, Sage V, et al (2021) Optimization of dark fermentation for

biohydrogen production using a hybrid artificial neural network (ANN) and response surface methodology (RSM) approach. Environmental Progress & Sustainable Energy 40:e13485. https://doi.org/10.1002/ep.13485

36. Ciranna A, Pawar SS, Santala V, et al (2014) Assessment of metabolic flux distribution in the thermophilic hydrogen producer Caloramator celer as affected by external pH and hydrogen partial pressure. Microb Cell Fact 13:48. https://doi.org/10.1186/1475-2859-13-48

37. Stephanopoulos G, Aristidou AA, Nielsen J (1998) Metabolic Engineering: Principles and Methodologies. Elsevier

38. Anand A, Kumar K, Khaire KC, et al (2024) Ultrasound-assisted hydrolysis of food waste using glucoamylase: Statistical optimization and mechanistic analysis with molecular simulations. Bioresource Technology Reports 27:101932. https://doi.org/10.1016/j.biteb.2024.101932

39. Kumar K, Jadhav SM, Moholkar VS (2024) Acetone-Butanol-Ethanol (ABE) fermentation with clostridial co-cultures for enhanced biobutanol production. Process Safety and Environmental Protection 185:277–285. https://doi.org/10.1016/j.psep.2024.03.027

40. Sivasankar T, Paunikar AW, Moholkar VS (2007) Mechanistic approach to enhancement of the yield of a sonochemical reaction. AIChE J 53:1132–1143. https://doi.org/10.1002/aic.11170

41. Moholkar VS, Huitema M, Rekveld S, Warmoeskerken MMCG (2002) Characterization of an ultrasonic system using wavelet transforms. Chemical Engineering Science 57:617–629. https://doi.org/10.1016/S0009-2509(01)00397-9

42. Bhasarkar J, Borah AJ, Goswami P, Moholkar VS (2015) Mechanistic analysis of ultrasound assisted enzymatic desulfurization of liquid fuels using horseradish peroxidase. Bioresource Technology 196:88–98. https://doi.org/10.1016/j.biortech.2015.07.063

43. Manish S, Venkatesh K, Banerjee R (2007) Metabolic flux analysis of biological hydrogen production by Escherichia coli. International Journal of Hydrogen Energy 32:3820–3830. https://doi.org/10.1016/j.ijhydene.2007.03.033

44. Cai G, Jin B, Monis P, Saint C (2011) Metabolic flux network and analysis of fermentative hydrogen production. Biotechnology Advances 29:375–387. https://doi.org/10.1016/j.biotechadv.2011.02.001

45. Cai G, Jin B, Saint C, Monis P (2010) Metabolic flux analysis of hydrogen production network by Clostridium butyricum W5: Effect of pH and glucose concentrations. International Journal of Hydrogen Energy 35:6681–6690. https://doi.org/10.1016/j.ijhydene.2010.04.097

46. Cheng H-H, Whang L-M, Lin C-A, et al (2013) Metabolic flux network analysis of fermentative hydrogen production: Using Clostridium tyrobutyricum as an example. Bioresource Technology 141:233–239. https://doi.org/10.1016/j.biortech.2013.03.141

47. Kuchenreuther JM, Stapleton JA, Swartz JR (2009) Tyrosine, Cysteine, and S-Adenosyl Methionine Stimulate In Vitro [FeFe] Hydrogenase Activation. PLoS ONE 4:e7565. https://doi.org/10.1371/journal.pone.0007565

48. Oh Y, Kim H, Park S, et al (2008) Metabolic-flux analysis of hydrogen production pathway in Citrobacter amalonaticus Y19. International Journal of Hydrogen Energy 33:1471–1482. https://doi.org/10.1016/j.ijhydene.2007.09.032

49. Anand A, Moholkar VS (2023) Analysis of Food Waste as Potential Substrate for Biohydrogen Production. In: Moholkar VS, Mohanty K, Goud VV (eds) Sustainable Energy Generation and Storage. Springer Nature, Singapore, pp 135–144

50. Yadav S, Singh V, Mahata C, Das D (2021) Optimization for simultaneous enhancement of biobutanol and biohydrogen production. International Journal of Hydrogen Energy 46:3726–3741. https://doi.org/10.1016/j.ijhydene.2020.10.267

51. Santiago SG, Morgan-Sagastume JM, Monroy O, Moreno-Andrade I (2020) Biohydrogen production from organic solid waste in a sequencing batch reactor: An optimization of the hydraulic and solids retention time. International Journal of Hydrogen Energy 45:25681–25688. https://doi.org/10.1016/j.ijhydene.2019.11.224

52. Cheng H-H, Whang L-M, Wu C-W, Chung M-C (2012) A two-stage bioprocess for hydrogen and methane production from rice straw bioethanol residues. Bioresource Technology 113:23–29. https://doi.org/10.1016/j.biortech.2011.12.103

53. Han W, Wang X, Ye L, et al (2015) Fermentative hydrogen production using wheat flour hydrolysate by mixed culture. International Journal of Hydrogen Energy 40:4474–4480. https://doi.org/10.1016/j.ijhydene.2015.02.016

54. García-Depraect O, Rene ER, Diaz-Cruces VF, León-Becerril E (2019) Effect of process parameters on enhanced biohydrogen production from tequila vinasse via the lactate-acetate pathway. Bioresource Technology 273:618–626. https://doi.org/10.1016/j.biortech.2018.11.056

55. Cai G, Jin B, Saint C, Monis P (2010) Metabolic flux analysis of hydrogen production network by Clostridium butyricum W5: Effect of pH and glucose concentrations. International Journal of Hydrogen Energy 35:6681–6690. https://doi.org/10.1016/j.ijhydene.2010.04.097

56. González-Pajuelo M, Meynial-Salles I, Mendes F, et al (2005) Metabolic engineering of Clostridium acetobutylicum for the industrial production of 1,3-propanediol from glycerol. Metabolic Engineering 7:329–336. https://doi.org/10.1016/j.ymben.2005.06.001

57. Li W, Cheng C, Ren N, et al (2022) Different feedback effects of aqueous end products on hydrogen production of *Clostridium tyrobutyricum*. International Journal of Hydrogen Energy 47:35156–35170. https://doi.org/10.1016/j.ijhydene.2022.08.120

58. Zheng X-J, Yu H-Q (2005) Inhibitory effects of butyrate on biological hydrogen production with mixed anaerobic cultures. Journal of Environmental Management 74:65–70. https://doi.org/10.1016/j.jenvman.2004.08.015

59. Chen Y, Yin Y, Wang J (2021) Influence of butyrate on fermentative hydrogen production and microbial community analysis. International Journal of Hydrogen Energy 46:26825–26833. https://doi.org/10.1016/j.ijhydene.2021.05.185

60. Steven Van Ginkel and Bruce E. Logan (2005) Inhibition of Biohydrogen Production by Undissociated Acetic and Butyric Acids | Environmental Science & Technology. https://pubs.acs.org/doi/full/10.1021/es0510515. Accessed 18 Sep 2025

61. Niu K, Zhang X, Tan W-S, Zhu M-L (2011) Effect of culture conditions on producing and uptake hydrogen flux of biohydrogen fermentation by metabolic flux analysis method. Bioresource Technology 102:7294–7300. https://doi.org/10.1016/j.biortech.2011.05.001

62. Han W, Yan Y, Shi Y, et al (2016) Biohydrogen production from enzymatic hydrolysis of food waste in batch and continuous systems. Sci Rep 6:38395. https://doi.org/10.1038/srep38395

63. Kim JK, Nhat L, Chun YN, Kim SW (2008) Hydrogen production conditions from food waste by dark fermentation with Clostridium beijerinckii KCTC 1785. Biotechnol Bioproc E 13:499–504. https://doi.org/10.1007/s12257-008-0142-0

64. García-Depraect O, Castro-Muñoz R, Muñoz R, et al (2021) A review on the factors influencing biohydrogen production from lactate: The key to unlocking enhanced dark fermentative processes. Bioresource Technology 324:124595. https://doi.org/10.1016/j.biortech.2020.124595

65. Regueira-Marcos L, Muñoz R, García-Depraect O (2025) Biogenic hydrogen production from household food waste via lactate-driven dark fermentation: A comparative study of single-stage and two-stage configurations. Journal of Environmental Chemical Engineering 13:117672. https://doi.org/10.1016/j.jece.2025.117672

66. Boynton ZL, Bennett GN, Rudolph FB (1996) Cloning, sequencing, and expression of genes encoding phosphotransacetylase and acetate kinase from Clostridium acetobutylicum ATCC 824. Appl Environ Microbiol 62:2758–2766. https://doi.org/10.1128/aem.62.8.2758-2766.1996

67. Brüggemann H, Gottschalk G (2008) *Comparative Genomics of Clostridia*: *Link between the Ecological Niche and Cell Surface Properties*. Annals of the New York Academy of Sciences 1125:73–81. https://doi.org/10.1196/annals.1419.021

Indian Institute of Technology Guwahati

CHAPTER 6

Overview and suggestions for future work

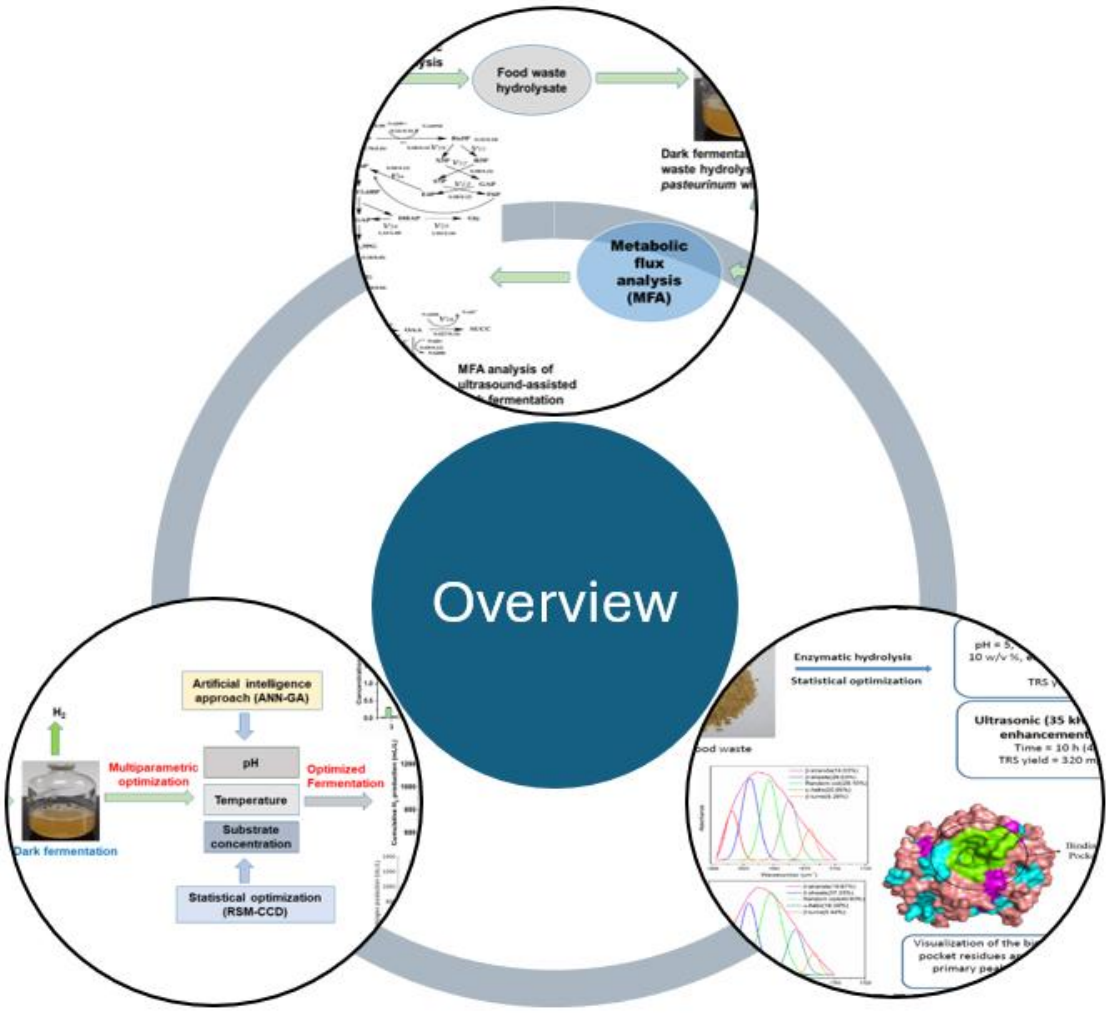

6.1 Overview

Biofuels hold promise as a sustainable alternative to fossil fuels, but developing technology for their large-scale economic production requires significant research and development activity. This thesis has addressed this issue by exploring the valorization of food waste for biohydrogen production, a process that converts waste into energy through microbial dark fermentation using *Clostridium pasteurianum*. Various chapters in this dissertation detail the research conducted to bridge knowledge gaps in this area. We present herewith a summary of the contents of each chapter and the major results obtained in each study.

Chapter 1 presented a general introduction to hydrogen synthesis through microbial fermentation. In this chapter, general biochemistry, physiology, metabolic pathways, and enzymes involved in the metabolism of microorganisms that result in bioH_2 production were discussed. Moreover, the docked structures of different hydrogenase enzymes in microbial cells were shown and discussed.

In **Chapter 2,** we presented a critical literature review in the area of biohydrogen production from renewable and waste resources such as lignocellulosic biomass (agro-residues), food waste, municipal solid waste, waste glycerol from the biodiesel industry etc. Based on the literature review, the major objectives of the thesis and approaches (or methodologies) for achieving these objectives were defined.

Chapter 3 investigated three facets of food waste hydrolysis using glucoamylase enzyme: (1) statistical optimization of physical parameters, (2) enhancement of hydrolysis kinetics with sonication, and (3) mechanistic investigation in sonication-induced kinetics enhancement with molecular docking and dynamics simulations. Statistical optimization of food waste hydrolysis resulted in a maximum TRS yield of 263.4 mg/g for the following optimized set of parameters: biomass loading = 10 % w/v, GLCM loading = 50 U/g, temperature = 40 ºC, pH = 5, time =

42 h. Further, an attempt was made to intensify the hydrolysis process with the application of sonication. Application of 35 kHz sonication at 20 % duty cycle resulted in a marked (4×) reduction in hydrolysis time (10 h) with a 22 % rise in TRS yield (320 mg/g biomass). Deconvolution analysis of the FTIR spectrum of ultrasound–treated GLCM showed major modifications in the secondary structure of the enzyme, viz., reduction in alpha helix content and rise in random coil content. Further, an attempt was made to gain biophysical insight into the sonication-induced intensification of the enzymatic hydrolysis using molecular simulations. The molecular docking simulation of the binding of amylotriose (representative food waste component) with GLCM revealed the presence of a majority of amino acid residues associated with the binding pocket in α-helix and random coil content of GLCM. The sonication of the enzyme essentially widened the binding pocket of the enzyme, providing easier transport of substrate/product to/from the binding pocket, which manifested in 4× faster hydrolysis with a significant rise in TRS yield. This effect translated into faster kinetics of enzymatic food waste hydrolysis.

Chapter 4 presented a study of the valorization of food waste to biohydrogen (bioH_2) through dark fermentation using *Clostridium pasteurianum*. The optimization of the fermentation of the food waste hydrolysate was carried out with two approaches: (1) statistical design of experiments, and (2) artificial neural network. The optimization of fermentation parameters using response surface methodology (RSM) with central composite design (CCD) resulted in bioH_2 yield = 1039 mL/L (1.58 mol/mol hexose sugars) for the conditions: pH = 6.5, temperature = 36 °C, TRS concentration = 10 g/L. An artificial neural network coupled with a genetic algorithm (ANN-GA) predicted the optimum parameter set as pH = 6.8, temperature = 36.8 °C, TRS concentration = 10.85 g/L. A bioH_2 yield of 1108 mL/L (1.73 mol/mol hexose sugar) was obtained for these conditions. The modified Gompertz model revealed a maximum

bioH_2 production rate of 185.34 mL/L·h for ANN-GA conditions, as compared to 153.74 mL/L·h for RSM-CCD predicted conditions. Fermentation at ANN-GA-predicted conditions revealed a greater shift of metabolic intermediates towards the acetic acid/ butyric acid pathway, resulting in higher bioH_2 production. The ratio of acetic to butyric acid increased from 0.9 to 0.94, indicating a metabolic shift favoring bioH_2 production. Analysis of bioH_2 profiles using a modified Gompertz model revealed higher H_2 production potential at ANN-GA-predicted fermentation conditions. The profiles of metabolic intermediates shifted towards the acetic acid/ butyric acid pathway at ANN-GA-predicted conditions, which resulted in higher H_2 production. These results demonstrated the superior efficacy of the ANN-GA methodology for simulating and predicting the behaviour of a nonlinear system like the metabolic pathway of *C. pasteurianum* in dark fermentation.

***Synergistic effect of TRS, pH, and temperature*:** The interaction between TRS concentration, pH, and temperature created optimal conditions for specific metabolic pathways that favored hydrogen production. For example, some pathways could have been more active at slightly acidic pH levels and moderate temperatures, leading to higher bioH_2 yield when TRS levels are sufficient. High TRS concentrations ensured ample substrates for metabolism, along with optimum pH and temperature that maximized the conversion efficiency. The optimum pH also helped minimize the production of inhibitory by-products (soluble metabolites) that could suppress hydrogen production. This synergy ensured effective sugar utilization and higher hydrogen yield.

Chapter 5 presented an investigation into the intensification of food waste hydrolysate fermentation using sonication. Moreover, the cellular-level mechanism of the sonication-induced intensification of the fermentation was analyzed with metabolic flux analysis (MFA) model. Control (with mechanical shaking) and test (with sonication) fermentation experiments

were conducted using *Clostridium pasteurianum* at optimized conditions to measure the flux of extracellular metabolites. A metabolic flux model was devised to determine fluxes of intracellular metabolites using the concentrations of extracellular metabolites. This analysis revealed the effect of sonication (at a duty cycle of 20%) on intracellular metabolic fluxes in test experiments. Hexose sugar (TRS) uptake increased from 3.77 to 5.55 mmol/L·h (~ 47% rise) with sonication, while butyrate and acetate fluxes at the acetyl-CoA node rose from 2.31 to 2.5 mmol/L·h, and 2.12 to 4.12 mmol/L·h (i.e., a rise of ~9% and ~94%, respectively). Sonication improved bioH_2 yield by ~22% (1.61 mol H_2/mol hexose sugar to 1.95 mol/mol hexose sugar), and the acetate-to-butyrate (A/B) ratio by ~ 37%. These results pointed out that bioH_2 production is linked to carbon flux at acetyl-CoA node. Higher flux towards the acetate route (than the butyrate route) enhances the hydrogen yield. A hypothetical MFA analysis was also conducted under sonication conditions for two situations, viz., complete redirection of carbon flux at acetyl-CoA node to acetate route and, secondly, doubling the uptake flux of hexose sugars. For the first case, bioH_2 enhanced from 4.13 to 6.47 mmol/L·h, while for the second case, a bioH_2 flux of 14.53 mmol/L·h was predicted by the MFA model.

To summarize, this thesis has attempted to develop a lab-scale upstream process for bioH_2 synthesis from the sustainable resource of food waste. The work presented in this thesis has addressed the upstream section of the bioH_2 process that includes pretreatment and hydrolysis of food waste, followed by dark fermentation. The processes of enzymatic hydrolysis and dark fermentation have been optimized using a statistical design of experiments. Further, an attempt is made to intensify the processes using a physical technique of sonication. This technique does not require any external addition of chemicals or catalysts for enhancing the kinetics and yield of the process. The net bioH_2 yield from 1 kg of food waste under statistically optimized conditions was 5.1 g per kg of food waste, which further improved to

5.73 g per kg of food waste under sonication. The present thesis has also made contributions to fundamental issues related to ultrasound-assisted bioH_2 synthesis in terms of the establishment of the basic mechanisms of the effect of sonication on enzymatic hydrolysis and dark fermentation using molecular docking and dynamics simulations and metabolic flux analysis.

The bioH_2 yield of 5.73 g per kg food waste (or 5.73 kg per ton of food waste) is rather low from the viewpoint of large-scale implementation. Moreover, for large-scale processes, the collection of food waste from different outlets is also going to add to the total cost. The biomass loading used in the hydrolysis step in the present study is 10% w/v. This is also a crucial parameter from the viewpoint of large-scale processes. This essentially means that it will require 10,000 litres of water for processing 1 ton of food waste, which will produce approx. 6 kg of hydrogen. Thus, effective water recovery and recycling are essential and important aspects to make such a process viable.

6.2 Suggestions for future work

This dissertation has clearly demonstrated the potential of bioH_2 production from food waste. To begin with, the food waste hydrolysis was optimized using the statistical design of experiments. Next, the hydrolysis kinetics and yield were intensified using sonication. Further, the fermentation of the food waste hydrolysate was optimized using two techniques, viz., statistical design of experiments and artificial neural network. Finally, the food waste hydrolysate fermentation was intensified using sonication and this intensification was analyzed using metabolic flux analysis. In essence, this thesis has provided a lab-scale process know-how of biohydrogen production from food waste. However, for the transformation of this

know-how into a commercial-scale process, further research and development are needed. Some suggestions in this direction are given below:

(a) Use of recombinant enzymes for higher hydrolysis yield: The food waste used in this work consisted of starch (42% w/w), carbohydrate (43% w/w) and proteins (6.5% w/w). The glucoamylase enzyme used in this study mainly hydrolyzed the starch portion of the food waste. New recombinant enzymes can be used for even more efficient hydrolysis of other components of food waste, such as carbohydrates. This will obviously enhance the specific productivity of bioH_2 from food waste.

(b) Efforts for sonication for larger volumes of fermentation mixture: For application of sonication in a commercial-scale dark fermentation process for bioH_2 production, significant research and development are required for high-power amplifiers operating at ultrasound-range frequencies (> 20 kHz). Multi-transducer systems will be required to dissipate the high power into the fermenter. Fabrication of such system is a significant technical challenge.

(c) Downstream processing: A thorough study of the downstream section of the process is also essential. The *Clostridial* (ABE) fermentation can be taken to completion for complete conversion of the substrate to acetone, butanol and ethanol solvents. Recovery of these valuable metabolite products from the fermentation broth is essential for the economy of the overall process. The final emissions from the process need to be analyzed. These include solid waste (unhydrolyzed food waste and other solid residues from the process), liquid waste (the net discharge of liquid residue from the process after recovery and recycle of water from the fermentation broth) and gas emissions (CO_2 emissions from the process). The biohydrogen produced in the process needs to be compressed to high pressure before storage. The life cycle analysis (LCA) and life cycle impact assessment (LCIA) are mandatory before commercial implementation of the process.

(d) Genetic engineering and metabolic engineering: Blocking the pathways of other metabolites is one of the essential methods to redirect the pathway toward the production of a particular product and increase the bioH_2 yield. This is possible by knocking out the corresponding genes, such as solvent and acid-associated genes in *C. pasteurianum*, which could help in further improvement of bioH_2 yield.

भारतीय प्रौद्योगिकी संस्थान गुवाहाटी
Indian Institute of Technology Guwahati

List of Publications

Journal publications

1. A. Anand, K. Kumar, K.C. Khaire, K. Roy, V.S. Moholkar, Ultrasound-assisted hydrolysis of food waste using glucoamylase: Statistical optimization and mechanistic analysis with molecular simulations, Bioresource Technology Reports 27 (2024) 101932. https://doi.org/10.1016/j.biteb.2024.101932

2. A. Anand, C. Mahata, V.S. Moholkar, Biohydrogen synthesis from food waste hydrolysate: Optimization using statistical design of experiments (DoE) and artificial neural network (ANN), Biomass and Bioenergy 191 (2024) 107452. https://doi.org/10.1016/j.biombioe.2024.107452.

3. A. Anand, V.S. Moholkar, Analysis of Food Waste as Potential Substrate for Biohydrogen Production, in: V.S. Moholkar, K. Mohanty, V.V. Goud (Eds.), Sustainable Energy Generation and Storage (Proceedings of NERC 2022), Springer Nature, Singapore, 2023: pp. 135–144. https://doi.org/10.1007/978-981-99-2088-4_11.

4. A. Anand, V.S. Moholkar, Ultrasound-assisted enhancement in biohydrogen production from food waste hydrolysate: a metabolic flux analysis, *Bioprocess Biosyst Eng* (2025). https://doi.org/10.1007/s00449-025-03265-8.

Book chapters

1. A. Anand, Umesh, V.S. Moholkar, Chapter 3 - Biohydrogen production from microbial fermentation of organic wastes, in: S. Nanda, A.K. Dalai, V.V. Goud (Eds.), Emerging Biofuels, Elsevier, 2024: pp. 27–52. https://doi.org/10.1016/B978-0-323-99547-4.00011-3.

2. A. Anand, K. Kumar, V.S. Moholkar, Various Routes for Hydrogen Production and Its Utilization for Sustainable Economy, in: C.R. Soccol, S.K. Brar, K. Permaul, K. Pakshirajan, J.C. de Carvalho (Eds.), Biohydrogen - Advances and Processes, Springer Nature Switzerland, Cham, 2024: pp. 503–527. https://doi.org/10.1007/978-3-031-49818-3_20.

3. K. Kumar**, A. Anand**, V.S. Moholkar, Molecular Hydrogen (H2) Metabolism in Microbes: A Special Focus on Biohydrogen Production, in: C.R. Soccol, S.K. Brar, K. Permaul, K. Pakshirajan, J.C. de Carvalho (Eds.), Biohydrogen - Advances and Processes, Springer Nature Switzerland, Cham, 2024: pp. 25–58. https://doi.org/10.1007/978-3-031-49818-3_2.

4. Shet K, H.N., **Anand, A**., Moholkar, V.S. (2025). Hydrogen Production Technologies: Pathways to a Sustainable and Cleaner Environment. In: Valera, H., Agarwal, A.K. (eds) Hydrogen as Emerging Fuel for De-Fossilizing Transport Sector. Energy, Environment, and Sustainability. Springer, Singapore. https://doi.org/10.1007/978-981-96-6620-1_5

Collaborative publications

1. Divyansh Adha, **Avinash Anand,** Arjita Roy, and Vijayanand Suryakant Moholkar Valorization of Polycarbonate Waste by Ultrasound-Assisted Methanolysis: Optimization Using an Artificial Neural Network and Kinetic Investigation, *ACS Sustainable Resour. Manage.*2025, https://doi.org/10.1021/acssusresmgt.5c00474

2. Piyush Hasani, **Avinash Anand**, Vijayanand S. Moholkar "Ultrasound-assisted synthesis of isopropyl lactate using ion-exchange resin catalyst: Statistical optimization and mechanistic analysis" (**under review)**

3. Diwakar Rai Srivastava, **Avinash Anand**, Vijayanand S. Moholkar "Enzymatic Synthesis of Perlauric acid and its intensification with ultrasound" (**under review**)

Awards

1. Avinash Anand and Vijayanand S. Moholkar "Optimization of biohydrogen production from food waste hydrolysate and its process intensification". Oral presentation in the 8th International Conference on Corporate Social Responsibility and Sustainable Development (CSR), June 16-17, 2025, Ho Chi Minh City, Vietnam. **(Best Paper Award)**

2. Awarded with "**Swachta Sarathi Fellowship (SSF)" under the waste to wealth mission (GOI**) (2022-2023)

3. Piyush Hasani**, Avinash Anand** and Vijayanand S. Moholkar**,** "Synthesis of Isopropyl Lactate using solid (ion-exchange resin) catalyst and its intensification using ultrasound." Oral presentation in **RIC 2024** at IIT Guwahati. **(Best Paper Award)**

Conferences presentations

1. Avinash Anand and Vijayanand S. Moholkar "Analysis of food waste as a potential feedstock for biohydrogen production" oral presentation in North east research conclave (NERC 2022) at IIT Guwahati.

2. Avinash Anand and Vijayanand S. Moholkar **"**Enzymatic saccharification of food waste for biohydrogen production: A response surface methodology based optimization and molecular simulation approach" Poster and flash paper presentation in International Conference on Biotechnology for Sustainable Bioresources and Bioeconomy (BSBB-2022**)** at IIT Guwahati.

3. Avinash Anand and Vijayanand S. Moholkar "Ultrasound-assisted biohydrogen production from food waste hydrolysate by using metabolic flux analysis" oral presentation in an international conference in CHEMCON 2023.

4. Avinash Anand and Vijayanand S. Moholkar **"**Enzymatic saccharification of food waste for biohydrogen production: A response surface methodology based optimization and molecular simulation approach" Oral presentation in International Conference on Biotechnology for Sustainable Bioresources and Bioeconomy (ISEES-2023**)** at MNIT JAIPUR.

5. Avinash Anand and Vijayanand S. Moholkar **"**Optimization of biohydrogen production from food waste and its process intensification" Oral presentation in international conference on Environmental challenges" Enviornment 2024"

6. Avinash Anand and Vijayanand S. Moholkar "Biohydrogen synthesis from food waste hydrolysate optimization using Response surface methodology(RSM) and artificial neural network (ANN)". Oral presentation in International Conference on International Conference on Advances in Sustainable Solutions for Energy Transitions (ASSET 2025).

7. Avinash Anand and Vijayanand S. Moholkar "Biohydrogen synthesis from food waste hydrolysate optimization using Response surface methodology(RSM) and artificial neural

network (ANN)". Poster presentation in Japan-NER Sustainable Technologies Cooperation Symposium 2025.

8. Avinash Anand and Vijayanand S. Moholkar "Optimization of biohydrogen production from food waste hydrolysate and its process intensification". Oral presentation in 8th International Conference on Corporate Social Responsibility and Sustainable Development (CSR, June 16-17, 2025) at Ho Chi Minh City, Vietnam.